

This item was submitted to Loughborough University as a PhD thesis by the author and is made available in the Institutional Repository (<https://dspace.lboro.ac.uk/>) under the following Creative Commons Licence conditions.



For the full text of this licence, please go to:
<http://creativecommons.org/licenses/by-nc-nd/2.5/>



Department of Materials

**SUBSURFACE AND BULK MECHANICAL PROPERTIES
OF POLYURETHANE NANOCOMPOSITE FILMS**

By

Kamal Yusoh

A doctoral thesis submitted in partial fulfillment of the requirement for

the award of

Doctor of Philosophy of Loughborough University

2010

Supervisor: Professor Mo Song

Department of Materials

Loughborough University

© Kamal Yusoh, 2010

ACKNOWLEDGMENTS

All praise and gratitude be to Allah, the Mighty and the Majestic for enabling me to reach this stage of my research study.

I wish to acknowledge and express my sincere thanks and gratitude to my Supervisor, Prof Mo Song, for his invaluable supervision, encouragement, suggestions, and help throughout this endurance research study. Thanks must also be extended to our research group, Drs J Jin and Cai for their continuous support and encouragement.

My thanks also go to the entire staff and research students of Department of Materials for their cooperation and constant help during my study. Thanks must also be extended to my numerous friends especially in Masyarakat Melayu Loughborough (MML) for their support and encouragement.

My appreciations also go to the Ministry of Higher Education, Malaysia and the University of Malaysia Pahang for supporting my PhD study financially.

Finally, I wish to express my love and appreciation to my wife, Husniyati Mohd Zubir and my daughter Nur Fatihah, Nur Farihah, and Nur Adni for their constant love, devotion and patience. Also to my father, Hj. Yusoh Salleh and my late mother who preserved and offered their warm encouragement and help over the past years.

Abstract

A series of exfoliated and intercalated polyurethane (PU) organoclay nanocomposites, polyurethane-graphite oxide (GO) and polyurethane carbon nanotubes (single-walled (SWNT) and multi-walled carbon nanotubes (MWNT)) were prepared by in situ polymerization. It is believed that the preparation of polymer/clay or polymer/CNTs nanocomposites with homogeneous dispersion of nanofillers in the matrices is a crucial step to developing high-performance polymer nanocomposites. The effects of various organoclays and carbon nanotubes (CNTs), polyol types and dispersion situation i.e. intercalation or exfoliation on viscosity were investigated. The interactions between the polyol and nanofillers and the mixing temperature play an important role in the occurrence of exfoliation and intercalation in polyurethane nanocomposite. The mechanism of exfoliation of clay was proposed based on the rheological data. The surface mechanical properties of the polyurethane nanocomposite films were investigated by means of nanoindentation. The results showed that the hardness and elastic modulus of the nanocomposites dramatically increased with the incorporation of nanofillers. This improvement was dependent on the content of nanofillers as well as the formation structure of organoclay in the polyurethane matrix. At 3wt% clay content, the hardness and elastic modulus of intercalated nanocomposites increased by approximately 16% and 44%, respectively, compared to the pure PU. For the exfoliated clay/PU nanocomposites, the improvement in these properties was about 3.5 (hardness) and 1.6 (modulus) times higher than the intercalated ones. For the polyurethane graphite oxide (GO) nanocomposites both the hardness and the elastic modulus were enhanced as a function of GO concentration. With incorporation of 4wt% GO, the hardness and modulus increased nearly ~400% and ~350%, respectively. Upon incorporation of only 1wt% SWNT, the hardness of polyurethane was greatly improved by about 150% from 3 MPa to 7.8 MPa and the modulus was improved by about 50% from 12MPa to 18.5 MPa. For only 1wt% MWNT, the hardness of polyurethane was improved by about 50% and the modulus is just slightly improved by about ~5%. The creep behaviour of bulk and sub-surface of the polyurethane nanocomposites were investigated by means of uniaxial conventional creep testing and nanoindentation, respectively. The results showed that the creep resistance of the PU was significantly improved by incorporation of nanofillers. The enhancement of creep resistance was

dependent on the filler. With 1wt% clay, the creep resistance increased by approximately 50% for the intercalated system and 67% for the exfoliated system, respectively, compared to the pure PU. The elastic-viscoelastic (EVE) model was employed to examine the effect of organoclay loadings on the creep performance of PU nanocomposites. Results showed the model was in good agreement with the experimental data. A similar results were also noticed in polyurethane with GO and CNTs. The creep deformation decreases when the GO content increases, as expected from the addition of a rigid reinforcement of GO and CNTs into a polyurethane matrix. In scratch test, the results pronounced that with incorporation of nanofillers the scratch depth of polyurethane matrix was dramatically reduced.

TABLE OF CONTENT

Thesis access form	i	
Title page	ii	
Certificate of originality	iii	
Acknowledgement	iv	
Abstract	v	
Table of Content	vii	
List of Tables	xi	
List of Figures	xii	
Chapter 1	Background of the research	
1.1	Introduction	1
1.2	Aims of the research	3
	References	4
Chapter 2	Chemistry and physical properties of polyurethane and polyurethane nanocomposites	
2.1	Introduction	8
2.2	Polyurethane	
	2.2.1 Synthesis of polyurethane	10
	2.2.2 Side reactions	13
	2.2.3 Physical properties of polyurethane	15
	2.2.4 Applications of polyurethane	16
2.3	Nanofillers	
	2.3.1.1 Layered silicate organoclay	17
	2.3.1.2 Structure of layered silicate	17
	2.3.1.3 Organically modified layered silicate	21
	2.3.2 Graphene Oxide	23
	2.3.3 Carbon Nanotube (CNT)	24
	2.3.3.1 Synthesis of CNTs	26
2.4	Structure of polymer nanocomposites	28

2.5	Preparation of polymer nanocomposites	30
2.5.1	Solution method	30
2.5.2	Melt processing	33
2.5.3	In situ polymerization	36
2.6	Physical and mechanical properties of polyurethane nanocomposites	
2.6.1	Polyurethane-organoclay nanocomposites	42
2.6.2	Polyurethane graphene nanocomposites	48
2.6.3	Polyurethane-CNT nanocomposites	49
2.7	Conclusions	52
	References	53
Chapter 3	Experimental	
3.1	Introduction	64
3.2	Raw materials	
3.2.1	Isocyanates	64
3.2.2	Polyols	65
3.2.3	Chain extender	66
3.2.4	Catalysts	66
3.2.5	Nanofillers	67
3.3	Preparation of polyurethane nanocomposites	
3.3.1	Polyurethane – organoclay	68
3.3.2	Polyurethane – grapheme oxide (GO)	69
3.3.3	Polyurethane - carbon nanotubes (CNTs)	69
3.4	Characterization	
3.4.1	Wide angle x-ray diffraction (WAXD)	70
3.4.2	Transmission electron microscopy (TEM)	71
3.4.3	Scanning electron microscopy (SEM)	72
3.4.4	Viscometer	73
3.4.5	Creep test by dynamic mechanical analyzer (DMA)	74
3.4.6	Surface mechanical properties studied by indentation	74
3.4.7	Creep test by nanoindentation	76
3.4.8	Scratch test by nanoindentation	77
	References	78

Chapter 4	Rheological behaviour of polyol/nanofillers mixtures	
4.1	Introduction	79
4.2	Rheological behaviour of polyol/organoclay Mixtures	81
4.3	Mechanism of exfoliation of organoclay	86
4.4	Rheological behaviour of polyol/CNT mixtures	92
	Conclusions	95
	References	96
Chapter 5	Subsurface mechanical properties of polyurethane nanocomposite thin films studied by nanoindentation	
5.1	Introduction	99
5.2	Fundamental knowledge of nanoindentation	101
5.3	Polyurethane-clay nanocomposites	105
	5.3.1 Influence of holding time on the values of hardness and modulus	110
	5.3.2 Influence of loading rate on the values of hardness and modulus	114
5.4	Polyurethane-GO nanocomposites	117
	5.4.1 Influence of holding time on the values of hardness and modulus	119
	5.4.2 Influence of loading rate on the values of hardness and modulus	121
5.5	Polyurethane-CNTs nanocomposites	122
	Conclusions	126
	References	126
Chapter 6	Bulk and subsurface creep behaviour of polyurethane nanocomposites	
6.1	Introduction	131
6.2	Theoretical of creep behaviour	132
6.3	Indentation creep test	134
6.4	Conventional creep test	134

6.5	Creep behaviour of polyurethane-organoclay nanocomposites	135
6.6	Comparison to bulk creep behaviour of PU-organoclay nanocomposites	142
6.7	Creep behaviour of polyurethane-graphene nanocomposites	146
6.8	Creep behaviour of polyurethane-CNTs nanocomposites	149
	Conclusions	154
	References	154
Chapter 7	Scratch behaviour of polyurethane nanocomposites studied by nanoindentation	
7.1	Introduction	157
7.2	Polyurethane-clay nanocomposites	
	7.2.1 Scratch depth profile	161
	7.2.2 Relative scratch resistance	164
7.3	Polyurethane-GO nanocomposites	
	7.3.1 Scratch depth profile	165
	7.3.2 Relative scratch resistance	167
7.4	Polyurethane-CNTs nanocomposites	
	7.4.1 Scratch depth profile	169
	7.4.2 Relative scratch resistance	176
7.5	Polyurethane with different hard-segment	
	7.5.1 Scratch depth profile	177
	Conclusions	181
	References	181
Chapter 8	Conclusions and future work	
8.1	Conclusions	184
8.2	Future work	187
	List of Publications	188

List of Tables

Table 2.1: Structure and molecular masses of selected diisocyanates

Table 2.2: Clay mineral (phyllosilicate) classification

Table 2.3: Chemical formula and characteristic parameter of commonly used 2:1 phyllosilicate

Table 3.1: Properties of Hydrogenated MDI

Table 3.2: Properties of Modified MDI

Table 3.3: Properties of polypropylene glycol

Table 3.4: Properties of 1-4-butanediol

Table 3.5: Properties of cloisite C20

Table 3.6: Properties of cloisite B30

Table 4.1: Shear thinning parameter, n , obtained by Herskel-Bulkley models

Table 4.2: The fitted n and f value for polyol-SWNT and polyol-MWNT dispersions

Table 5.1 Effect of organoclay on the plastic depth

Table 5.1: Effect of hold time on the values of hardness and modulus of the pure polyurethane

Table 6.1: Parameters obtained based on Equation 1 for the pure PU with different percentages of hard-segments

Table 6.2: Parameters obtained based on Equation 1 for the PU-clays nanocomposites

Table 6.3: Parameters obtained based on Equation 1 for the pure PU with different percentages of GO

Table 6.4: Parameters obtained based on Equation 1 for the PU with different percentages of CNTs

List of Figures

- Figure 2.1:** Schematic structure of segmented polyurethane
- Figure 2.2:** Structure of 2:1 phyllosilicate
- Figure 2.3:** Hierarchy of montmorillonite clay particles
- Figure 2.4:** Types of carbon nanotube
- Figure 2.5:** Schematic structure of CNTs after graphite sheet folding
- Figure 2.6:** Schematic illustration of three polymer layered silicate nanocomposites
- Figure 2.7:** Synthetic procedures for polyurethane-urea/MWNT composites
- Figure 2.8:** Schematic illustration of the intercalation process between a polymer melt and an OMLS
- Figure 2.9:** Schematic illustration of polymer chains intercalated in organosilicate
- Figure 2.10:** SEM images of the surfaces for pure PU (A), and PU composites fibres containing 5.6, 9.3 and 17.7wt% MWNTs (B) – (D), respectively
- Figure 2.11:** Schematic illustration for synthesis of Nylon-6/clay nanocomposite
- Figure 2.12:** SEM images of cross section of PU-MWCNTs composites (a) Method 1, (b) Method 2, and (c) Method 3
- Figure 2.13:** Schematic illustration for the synthesis of PU grafted SWCNTs through a two-step process (A: PolyTDI; B: PCL)
- Figure 2.14:** Illustration for the functionalization of MWCNTs and possible chemical structure for nanocomposites prepared by in-situ method
- Figure 2.15:** Stress-strain curves for (A) the pristine polyurethane and (B) as a polyurethane-clay nanocomposite prepared from C18A-SWy montmorillonite (5 wt%)
- Figure 2.16:** Log E' for (a) NPU0, (b) NPU4, (c) NPU20, (d) NPU40
- Figure 2.17:** Stress-strain plots for (a) NPU0, (b) NPU4, and NPU20.
- Figure 2.18:** Plot of d spacing versus elongation
- Figure 2.19:** TEM images of thermoplastic polyurethane/FSG

Figure 3.1: Principle of Transmission Electron Microscope

Figure 3.2: Principle of Scanning Electron Microscope

Figure 3.3: Schematic of the nano-test system

Figure 3.4: A typical indentation load-displacement curve. P_{\max} and H_{\max} are the maximum load and displacement, respectively. S^* is the slope of the tangent to the maximum load on the unloading curve

Figure 3.5: Schematic diagram of the creep experiment by nanoindentation

Figure 4.1: Temperature and shearing rate-dependent of viscosity of polyol4000+C20

Figure 4.2: Temperature and shearing rate-dependent of viscosity of polyol6000+C20

Figure 4.3: Temperature and shearing rate-dependent of viscosity of polyol4000+B30

Figure 4.4: Temperature and shearing rate-dependent of viscosity of polyol6000+B30

Figure 4.5: Flow behaviour index (n) of polyol/C20 as a function of mixing temperature

Figure 4.6: Flow behaviour index (n) of polyol/B30 as a function of mixing temperature.

Figure 4.7: Mixing time-dependent of viscosity of polyol4000+B30

Figure 4.8: Mixing time-dependent of viscosity of polyol6000+B30

Figure 4.9: Mixing time-dependent of viscosity of polyol4000+C20

Figure 4.10: Mixing time-dependent of viscosity of polyol6000+C20

Figure 4.11: XRD pattern for polyurethane-C20 organoclay nanocomposites

Figure 4.12: XRD pattern for polyurethane-B30 organoclay nanocomposites

Figure 4.13: Schematic mechanism of exfoliation of organoclay in a polymer matrix

Figure 4.14: Variation of viscosity for polyol, polyol with 1wt% of SWNT and MWNT as a function of shearing rate.

Figure 4.15: Variation of viscosity of polyol-SWNT and polyol-MWNT dispersions with CNT concentration.

Figure 4.16: TEM photographs of (a) PU/1wt% MWNT and (b) PU/1wt% SWNT

Figure 5.1: Schematic of tips used in instrumented indentation. (a) A sharp pyramidal tip is often modelled as a cone with $\theta = 70.3^\circ$, (b) A spherical tip is defined by its radius R, and a characteristic strain may be defined as a/R . (c) SEM image of a diamond Berkovich indenter

Figure 5.2 (A) and (B) Typical indentation load-displacement curves for pristine PU and PU nanocomposite thin films

Figure 5.3: Hardness for intercalated and exfoliated PU nanocomposite thin films as a function of organoclay loading.

Figure 5.4: Elastic modulus of intercalated and exfoliated PU nanocomposite thin films as a function of organoclay loading

Figure 5.5 Hardness and modulus for pristine PU as a function of hard segment

Figure 5.6: Comparison of load-displacement curves for different hold periods at maximum load for PU

Figure 5.7: Comparison of load-displacement curves for different hold periods at maximum load for PU/C20 clay nanocomposite.

Figure 5.8: Comparison of load-displacement curves for different hold periods at maximum load for PU/B30 clay nanocomposite

Figure 5.9: Hardness of PU/ C20 clay nanocomposite as a function of loading rate

Figure 5.10: Modulus of PU/ C20 clay nanocomposite as a function of loading rate

Figure 5.11: Hardness of PU/ B30 clay nanocomposite as a function of loading rate

Figure 5.12: Modulus of PU/ B30 clay nanocomposite as a function of loading rate

Figure 5.13: Typical load-unloading curves of neat PU and PU/GO nanocomposites.

Figure 5.14: Hardness and modulus for the PU/GO nanocomposites as a function of GO concentration.

Figure 5.15: Depth change ratio at different holding time on polyurethane and polyurethane graphite oxide nanocomposites.

Figure 5.16: Effect of holding time on hardness of polyurethane and polyurethane graphite oxide nanocomposites.

Figure 5.17: Effect of holding time on modulus of polyurethane and polyurethane graphite oxide nanocomposites.

Figure 5.18: Variation of the hardness of PU and its GO nanocomposites as a function of loading rate.

Figure 5.19: Variation of the modulus of PU and its GO nanocomposites as a function of loading rate.

Figure 5.20: Typical load-unloading curves of neat PU and PU/SWCNT nanocomposites

Figure 5.21: Typical load-unloading curves of neat PU and PU/MWCNT nanocomposites

Figure 5.22: Hardness of the PU/CNTs nanocomposites as a function of SWCNTs and MWCNTs concentration.

Figure 5.23: Modulus of the PU/CNTs nanocomposites as a function of SWCNTs and MWCNTs concentration

Figure 6.1: Schematic conventional creep curve showing the three creep regimes (A) primary creep region; (B) secondary creep region; (C) tertiary creep region

Figure 6.2: Schematic indentation creep curve showing the two regimes (A) primary creep region; (B) secondary creep region

Figure 6.3: Creep strain versus time for PU nanocomposites with different B30 organoclay loadings. Open points are experimental data and the solid lines are fitting results by Eq. 6.1.

Figure 6.4: Creep strain versus time for PU nanocomposites with different C20 organoclay loadings. Open points are experimental data and the solid lines are fitting results by Eq. 6.1.

Figure 6.5: Creep strain of pure PU with different percentages of hard segment. Open points are experimental data and the solid lines are fitting results by Eq. 6.1.

Figure 6.6: A generalized Kelvin model in viscoelastic study [27]

Figure 6.7: Bulk creep compliance of exfoliated PU nanocomposites *versus* time

Figure 6.8: Bulk creep compliance of intercalated PU nanocomposites *versus* time

Figure 6.9: Bulk creep compliance of pure PU with different hard segments

Figure 6.10: Effect of exfoliation degree (ED%) on the creep behaviour of PU nanocomposites.

Figure 6.11: (a) Creep strain versus time for PU nanocomposites with different GO loadings. Open points are experimental data and the solid lines are fitting results by Eq. 1.(b) Comparison of creep strain after 70s of creep time

Figure 6.12: (a) Creep strain versus time for PU nanocomposites with different SWNT loadings. Open points are experimental data and the solid lines are fitting results by Eq. 1.(b) Comparison of creep strain after 70s of creep time

Figure 6.13: (a) Creep strain versus time for PU nanocomposites with different MWNT loadings. Open points are experimental data and the solid lines are fitting results by Eq. 1.(b) Comparison of creep strain after 70s of creep time

Figure 7.1: Schematic representations of the polymeric material responses to scratching: (a) ductile response; (b) ductile and brittle response; (c) brittle response; and (d) elastomeric response

Figure 7.2: Typical scratch plot using indentation scratch test

Figure 7.3: Nanoscratch depth profiles for PU and its nanocomposites (A) $3\mu\text{m/s}$ (B) $5\mu\text{m/s}$

Figure 7.4: Relative scratch resistance as a function of organoclay concentration

Figure 7.5: Nanoscratch depth profiles for PU and its GO nanocomposites at $3\mu\text{m/s}$

Figure 7.6: Nanoscratch depth profiles for PU and its GO nanocomposites at $5\mu\text{m/s}$

Figure 7.7: Relative scratch resistance as a function of GO concentration

Figure 7.8: (a) TEM image of the GO/DMF dispersion; (b) SEM image of the PU; (c) SEM images of 4wt% GO/PU composite

Figure 7.9: AFM images and cross-sectional high profiles of scratches made at various normal loads on the epoxy and its SWCNT reinforced samples: (a) and (b) pure epoxy; (c) and (d) 1 wt% SWCNT; (e) and (f) 3 wt% SWCNT; and (g) and (h) 5 wt% SWCNT [17]

Figure 7.10: Nanoscratch depth profiles for PU and its SWCNT nanocomposites at $3\mu\text{m/s}$. (a) After 100 μm and (b) After 25 μm of scratch length

Figure 7.11: Nanoscratch depth profiles for PU and its MWCNT nanocomposites at $3\mu\text{m/s}$. (a) After 100 μm and (b) After 25 μm of scratch length

Figure 7.12: Nanoscratch depth profiles for PU and its SWCNT nanocomposites at $5\mu\text{m/s}$. (a) After 100 μm and (b) After 30 μm of scratch length

Figure 7.13: Nanoscratch depth profiles for PU and its MWCNT nanocomposites at 5 $\mu\text{m/s}$. (a) After 100 μm and (b) After 30 μm of scratch length

Figure 7.14: Relative scratch resistance as a function of SWCNT & MWCNT concentrations

Figure 7.15: Nanoscratch depth profiles for PU with different hard segment contents at 3 $\mu\text{m/s}$

Figure 7.16: Nanoscratch depth profiles for PU with different hard segment contents at 3 $\mu\text{m/s}$ after 25 μm scratch length

Figure 7.17: Nanoscratch depth profiles for PU with different hard segment contents at 5 $\mu\text{m/s}$

Figure 7.18: Nanoscratch depth profiles for PU with different hard segment contents at 5 $\mu\text{m/s}$ after 40 μm scratch length

Chapter 1

Background of the Research

1.1 Introduction

Interest in polymer nanocomposites has exploded over the last 15 years. The field flourished after the publication of a paper by the Toyota Central Research Group [1,2] regarding unusual physical property improvements in a nylon 6/clay nanocomposite with a low filler loading. The ultimate polymer nanocomposites are formed when individual nanofillers are completely dispersed into a polymer matrix and well interaction between nanofiller and polymer matrix were established [3]. This scenario is referred to the exfoliation system which yields the maximum improvement in properties. However, in many cases, the nanocomposites reported are intercalated or partially exfoliated where the insertion of polymer chains into the layered silicate occurs in a crystallographically regular fashion, regardless of the clay to polymer ratio [4]. The increment of clay gallery and also the well-defined arrangement of clay/polymer were observed in these systems.

At present, development of nanocomposites has been widened into almost every engineering polymer including polypropylene [5], polyethylene [6], polystyrene [7-9], polyvinylchloride [10], acrylonitrile butadiene styrene [11], polymethylmethacrylate [12], polyethylene terephthalate [13], ethylene-vinyl acetate copolymer [14], polyacrylonitrile [15], polycarbonate [16], polyethylene oxide [17], epoxy resin [18], polyimide [19], polylactide [20-21], polycaprolactone [22-23], phenolic resin [24], poly p-phenylene vinylene [25], polypyrrole [26], rubber [27], starch [28], polyurethane [29-31], and polyvinylpyridine [32].

Nanocomposites consisting of a polymer matrix and layered silicate or other nanofillers at nanosize obtained by dispersion frequently exhibit remarkably improved mechanical, thermal, and optical properties compared to pristine polymers. Layered silicates have been more widely investigated probably because of clay minerals are easily available. The first study of enhancement of mechanical properties by Okada et al [33] derived from in situ polymerized nylon

6/montmorillonite. The study showed increment of tensile strength by 55%, tensile modulus by 91% and the heat distortion temperature by 134% with incorporation of 1wt% of clay. The work reported by Fornes et al. [34] on melt compounding of organoclay in various molecular weight of nylon 6 polymers also indicated that the improvement of tensile strength and tensile modulus almost by 26% and 59% compared to the pristine nylon 6. It is also similar to the finding by Hasegawa et al [35] where a tensile strength increased by 48% and tensile modulus increased by 71% with introduction of organoclay.

Polymer nanocomposites show promising in flame retardancy and thermal stability as shown in ethylene vinyl acetate nanocomposites [36], polydimethylsiloxane-clay nanocomposites [37], and polycaprolactum nanocomposites [37]. The thermal stability of a material is usually assessed by thermogravimetric analysis where the sample mass loss due to volatilization of degraded by-products is monitored. According to Gilman [38], this enhancement is due to barrier effect increases during volatilization owing to the reassembly of the reticular of the silicate on the surface. In addition, their uniqueness to promote flame retardancy at low filler content shown tremendous result through the formation of insulating and incombustible char [12].

Polymer nanocomposites also produced remarkable improvement in barrier properties. The effects of high aspect ratio characteristic of nanofillers are believed to increase this property by creating tortuous path that retards the progress of the gas molecules through the nanocomposite matrix. The polyimide nanocomposites with the small fraction of organic modified layered silicate exhibited reduction in the permeability of small gases [39]. The effect on water permeability of poly(imide) nanocomposites has been reported by Yano et al [40] as the length of the clay increases, the relative permeability decreased drastically.

In addition to the tensile, modulus, thermal and barrier properties, other properties improved by polymer nanocomposites are optical transparency [37], biodegradability [40], and ionic conductivity [41]. Vaia et al [42] reported that incorporation of Li-montmorillonite in poly(ethylene oxide) has shown to enhance

the stability of the ionic conductivity at lower temperature when compared to conventional mixture of PEO/LiBF₄.

Polyurethanes constitute one of the most versatile classes of polymeric materials today [43,44]. Hence, much attention has been given to synthesis the polyurethane and also polyurethane nanocomposites due to remarkable enhancement in mechanical properties such as tensile strength [45, 46] and thermal properties [47]. Recently the development of polyurethane nanocomposites was relatively established and many publications were released especially in preparing polyurethane nanocomposites. However, less attention was paid in study in the mechanism of the enhancement of polyurethane properties and also the effect of nanofillers on the surface mechanical properties of polyurethane nanocomposites. It is necessary to understand the effect of nanofillers on the viscoelastic behaviour of polyurethane.

1.2 Aims of Research

The aims of the project are to study the effect of organoclay, carbon nanotube and graphite oxide nanofillers on the mechanical properties of polyurethane by means of nanoindentation technique. The following aspects were focused in this research

1. To prepare polyurethane nanocomposites with different kinds of nanofillers.
2. To investigate the effect of nanofillers on the bulk viscosity of polyurethane.
3. To characterize the morphology of the polyurethane nanocomposites
4. To understand the exfoliation and intercalation mechanism of nanofillers in the polyurethane matrix.
5. To study the surface mechanical properties (hardness and modulus) of polyurethane nanocomposites by means of indentation technique.
6. To study the surface and subsurface creep behaviour of polyurethane nanocomposites
7. To understand the surface and subsurface scratch behaviour of polyurethane nanocomposites

References

1. Kojima, Y., Usuki, A., Kawasumi, M., Okada, A., Fukushima, Y., Kurauchi, T., Kamigaito, O. *J. Mater. Res.* 1993, 8, 1185-9
2. Kojima, Y., Usuki, A., Kawasumi, M., Okada, A., Kurauchi, T., Kamigaito, O. *J. Appl. Polym. Sci.* 1993, 49, 1259-64
3. Powell, C. E., Beall, G. W. *Curr. Opin. Solid State Mat. Sci.* 2006, 10, 73-80
4. Sinha, R. S., Okamoto, M. *Prog. Polym. Sci.* 2003, 28, 1539-1641
5. Kawasumi, M., Hasegawa, N., Kato, M., Usuki, A., Okada, A., *Macromolecules.* 1997, 30, 6333 – 6338
6. Bergman, J. S., Chen, H., Giannelis, E. P., Thomas, M.G., Coates, G. W., *Chem. Comm.* 1999, 21, 2179 – 2180
7. Fu, X., Qutubuddin, S., *Mater. Lett.* 2000, 42, 12-15
8. Akelah, A., Moet, A., *J. Mater. Sci.* 1996, 31, 3589 – 3596
9. Noh, M.W., Lee, D.C., *Polym. Bull.* 1999, 42, 619 – 626
10. Wan, C., Qiao, X., Zhang, Y., Zhang, Y., *Polym. Test.* 2003, 22, 453 – 461
11. Jang, L. W., Kang, C.M., Lee, D.C., *J. Polym. Sci. Part B: Polym. Phys.* 2001, 39, 719 – 727
12. Okamoto, M., Morita, S., Taguchi, H., Yong, H. K., Kotaka, T., Tateyama, H., *Polymer*, 2000, 41, 3887-3890
13. Zhang, G., Shichi, T., Takagi, K., *Mater. Lett.* 2003, 57, 1858 - 1862

14. Alexandre, M., Beyer, G., Henrist., Cloots, R., Rulmont, A., Jerome, R., Dubois, P., *Macromol. Rapid Commun.* 2001, 22, 643 – 646
15. Carrado, K. A., Xu, L., *Chem. Mater.* 1998, 10, 1440 – 1445
16. Huang, X., Lewis, S., Brittain, W.J., Vaia, R. A., *Macromolecules.* 2000, 33, 2000 – 2004
17. Krawiec, W., Scanlon. Jr, L.G., Fellner, J.P., Vaia, R.A., Vasudevan, S., Giannelis, E.P., *J. Power Sources.* 1995, 54, 310
18. Brown, J. M., Curliss, D., Vaia, R.A., *Chem. Mater.* 2000, 12, 3376 – 3384
19. Chang, J.-H., Park, K. M., *Polym. Eng. Sci.* 2001, 41, 2226 – 2230
20. Sinha, R. S., Maiti, P., Okamoto, M., Yamada, K., Ueda, K., *Macromolecules.* 2002, 35, 3104 – 3110
21. Ogata, N., Jimenez, G., Kawai, H., Ogihara, T., *J. Polym. Sci: Part B: Polym. Phys.* 1997, 35, 389 – 396
22. Hao, J., Yuan, M., Deng, X., *J. Appl. Polym. Sci.* 2002, 86, 676 – 683
23. Messersmith, P.B., Giannelis, E.P., *J. Polym. Sci. Part A Polym Chem.* 1995, 33, 1047 – 1057
24. Zhi, L., Zhao, T., Yu, Y., *Scripta Materialia*, 2002, 47, 875 – 879
25. Choi, M. H., Chung, I.J., Lee, J.D., *Chem. Mater.* 2000, 12, 2977-2983
26. Lee, H.-C., Lee, T-W., Lim, Y.T., Park, O.O., *Appl. Clay Sci.* 2002, 21, 287 – 293

27. Hong, S. H., Kim, K.W., Gontarz, R., Kudryavtsev, Y. V., *Curr. Appl. Phys.* 2001, 1, 447 – 450
28. Wu, Y. P., Zhang, L.Q., Wang, Y.Q., Liang, Y., Yu, D.S., *J. Appl. Polym. Sci.* 2001, 82, 2842 – 2848
29. Park, H.-M., Li, X., Jin, C.Z., Park, C.Y., Cho, W.J., Ha. C.S., *Macromol. Mater. Eng.* 2002, 287, 553 – 558
30. D. Cai, K. Yusoh, M. Song, *Nanotechnology*, 2009, 20, 085712
31. K. Yusoh, J.Jin, M.Song, *Prog. Org. Coat.* 2010, 67, 220 – 224
32. Chen, T.-K., Tien, Y.-I., Wei, K.-H., *Polymer.* 2000, 41, 1345-1353
33. Dhamodharan, R., Jeyaprakash, D., Samuel, S., Rajeswari, M.K., *J. Appl. Polym. Sci.* 2001, 82, 555 – 561
34. Okada, A., Usuki, A., *Mater. Sci. Eng.* 1995, C3, 109-15
35. Fornes, T. D., Yoon, P. J., Heskkula, H., Paul, D. R., *Polymer.* 2001, 42, 9929-40
36. Hasegawa, N., Okamoto, H., Kato, M., Usuki, A., Sato, N., *Polymer.* 2003, 44, 2933-7
37. Zanetti, M., Camino, G., Thomann, R., Mulhaupt, R., *Polymer.* 2001, 42, 4501-7
38. Alexandre, M., Dubois, P., *Mater. Sci. Eng. R.* 2000, 28, 1-63
39. Gilman, J. W., *Appl. Clay Sci.* 1999, 15, 31-49

40. Yano, K., Usuki, A., Okada, A., *J. Polym. Sci., Part A: Polym. Chem.* 1997, 35, 2289-94
41. Sinha, R. S., Yamada, K., Okamoto, M., Ueda, K., *Polymer*. 2003, 44, 857-66
42. Vaia, R. A., Vasudevan, S., Krawiec, W., Scanlon, L. G., *Adv. Mater.* 1995, 7, 154-6
43. Hepburn, C. *Polymer Elastomers*, Applied Science, London, 1982
44. Kresta, J.E., *60 Years of Polyurethane*, Technomic Publication, Lancaster, PA, 1998
45. Lan, T., Pinnavaia, T. J., *Chem. Mater.* 1994, 6, 2216
46. Yao, K. J., Song, M., Hourston, D. J., *Polymer*, 2002, 43, 1017-1020
47. Tien, Y., Wei, K. H. *Macromolecules*. 2001, 34, 9045

Chapter 2

Chemistry and Physical Property of Polyurethane and Polyurethane Nanocomposites

2.1 Introduction

In the last two decades, polymer materials reinforced by nano-fillers, such as layered silicate, graphite nanosheets, carbon nanotubes (CNTs), metal oxide nanoparticles and titanate, have received much attention from both the scientific and the industrial communities due to their significant enhancement obtained from relatively low nanofiller loading comparing to neat polymer [1-3]. In particular, polymer nanocomposites based on layered silicate have shown a number of impressive property enhancements, including increased tensile strength, modulus, hardness and fracture toughness [4-5], decreased gas permeability and flammability as well as improved thermal stability [6,7] and tunable biodegradability [8].

CNTs are ideal reinforcing fillers for polymers, because of their nanometre size, high aspect ratio, and, more importantly, excellent mechanical strength, and electrical and thermal conductivity [9-10]. CNT-filled polymer materials enjoy the additional functionality of exceptionally high electrical and thermal conductivity whilst maintaining the polymer matrix properties (including elasticity, strength and modulus) [11-12]. Other fillers such as graphene have also become the subject of intense study as reinforcement agents in polymer nanocomposites due to their good electron transport properties [13]. The main reason for these improvements is the strong interfacial interactions between the polymer matrix and nanofillers.

A variety of polymer/clay, polymer/graphene and polymer/CNT nanocomposites, including polyethylene [14,15], polystyrene [16], polyurethane [17, 18], epoxy [19], poly(methyl methacrylate) [20], poly(vinyl chloride) [21] and nylon [22], had been successfully synthesized so far. Such novel polymer nanocomposites open up

opportunities to new multi-functional materials with broad commercial and industry applications.

Polyurethane is one of the polymeric material with a wide range of physical and chemical properties. This broad property allows polyurethanes to be designed in various applications. In recent years, the development of polyurethane nanocomposites are attracted considerable attention [23-25]. For instance, polyurethane/clay nanocomposites have been widely used in a number of industry areas ranging from high barrier packaging for food and electronics purposes and heat resistant automotive components. Polyurethane/CNT and polyurethane graphene nanocomposites have been mainly used in the two major areas of electronics and automotives. In electronics, CNTs and graphene are used to dissipate the build up of unwanted static charges. This dissipative effect is achieved by thoroughly dispersing these nanofillers in the polymeric material to form an interconnecting network. In the automotive industry, CNTs have been applied as a conducting agent in electrostatic painting.

This chapter was focused on the review of the physical and chemistry of polyurethane and the preparation and properties of polyurethane nanocomposites with different kinds of nanofillers such as nanoclay, graphene and CNTs.

2.2 Polyurethane

Polyurethane is a unique material that offers the elasticity of rubber combined with the toughness and durability of metal [26]. The ability to be tailored into a specific application is one of the reasons for the increase in polyurethane demands. In early 1970, polyurethane was relatively very high cost polymer. However, the rapid development in the technology of processing, this situation is changing [27]. Because polyurethane has a special combination of unusual properties and the ability to be processed by almost all known manufacturing techniques, they can be applied in a very broad range of fields such as coatings, durable elastomers, high performance

adhesives, flexible and rigid foams, condoms, fibres, automotive industries and also in medical applications.

2.2.1 Synthesis of Polyurethane

The generally used reactants for producing polyurethanes are a diisocyanate, a polyol, and a chain extender. Polyurethanes can be considered as segmented, elastomer and thermoplastic multiblock copolymers, consisting of a hard and a soft segment as shown in **Figure 2.1** [28]. The hard segment originates from the diisocyanate, the most common diisocyanates are presented in **Table 2.1** and chain extender, whereas the soft segment usually is the polyol.

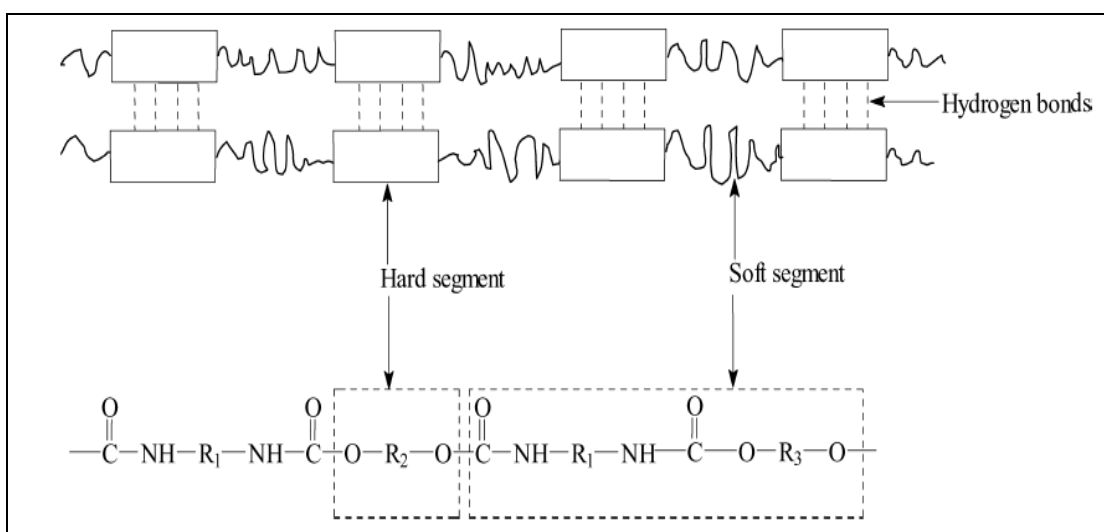
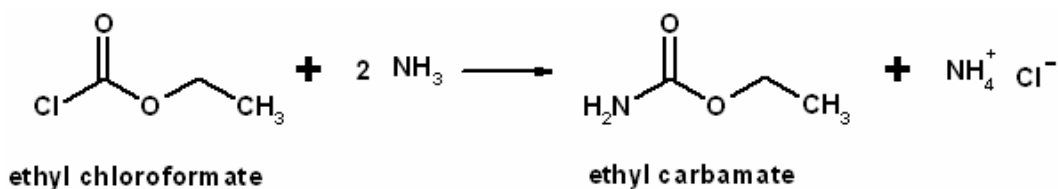


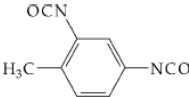
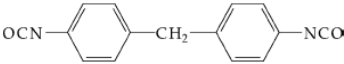
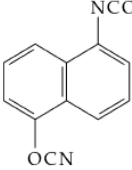
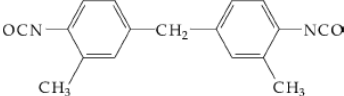
Figure 2.1: Schematic structure of segmented polyurethane [28]

Polyurethane is generally characterized by the urethane linkage. The urethane group may be obtained via such synthetic routes as a reaction of chloroformic esters with amines, or of carbamic esters with alcohols.

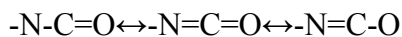


However, commercially, the reaction between isocyanates and alcohols is the only one of significance. In practice, polyurethanes may also incorporate a variety of other functional groups. Consequently, the chemistry of polyurethane is generally based on the ability of the isocyanate functional group to react with a compounds containing active hydrogen atom, i.e. compounds having hydrogen atoms which are replaceable by sodium [29].

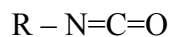
Table 2.1: Structure and molecular masses of selected diisocyanates [28]

Diisocyanate	Structural formula	Molecular mass (g/mol)
2,4 -toluene diisocyanate		175
4,4'-diphenylmethane diisocyanate		250
1,5-naphthalene diisocyanate		210
3,3'-dimethyl diphenylmethane-4,4'-diisocyanate		278
Hexane-1,6-diisocyanate	OCN(CH ₂) ₆ NCO	169

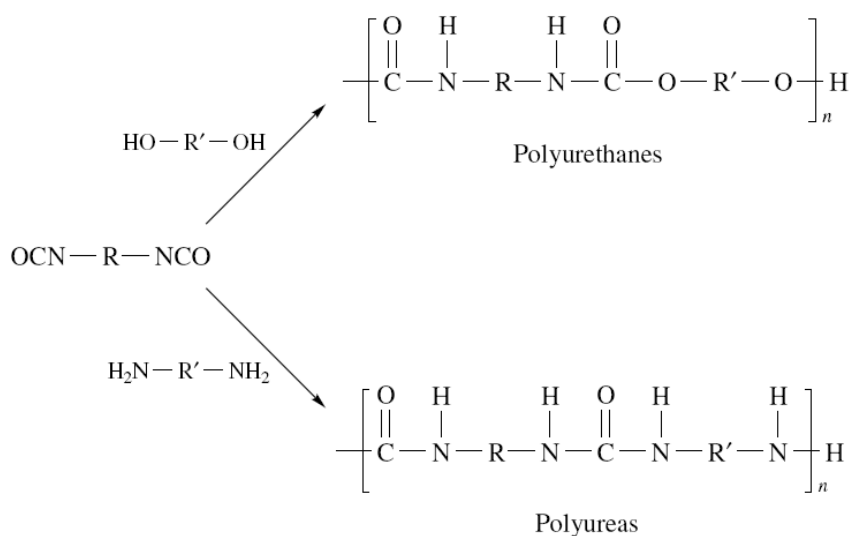
The reactivity of the isocyanate group with active hydrogen compound can be explained by the relative electronegativities of the group constituent atom and the resulting resonance structures [30].



These may be summarised by the general form shown below.

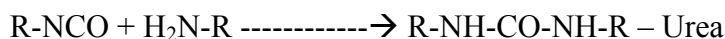
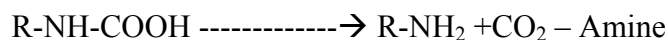


This structure indicates that the electron density is greatest on the oxygen atom and least on the carbon atom. Thus, the oxygen atom carries the greatest net negative charge and the carbon atom a net positive charge. The nitrogen atom carries an intermediate net negative charge. Reactions of isocyanates with active hydrogen compounds, therefore, proceed via an attack of nucleophilic centre on the electrophilic carbon atom. In such reactions, the active hydrogen compound acts as an electron donor. The electronegative substitutions in the active hydrogen compound tend to reduce electron density at the reactive site, so the rate of chemical reaction with isocyanate decreases. In contrast, electron-withdrawing substitutions in isocyanate compounds tend to increase the positive charge on the electrophilic carbon atom and cause increased rates with electrophilic groups [31].



The active hydrogen compounds which have the greatest importance for polyurethane technology are alcohol and amines [32]. They react with isocyanates to form urethanes or ureas, respectively. Urea derivatives are also produced as a result of the reaction of isocyanates with water. The carbamic acid changes into an amine, which reacts further with an isocyanate to form a symmetrically substituted urea and

gaseous carbon dioxide. This reaction is the basis of polyurethane flexible foam production.



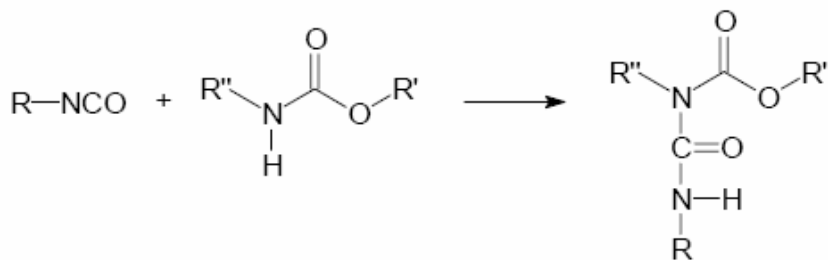
Organic acids react with isocyanates, also forming CO₂ and an amide structure.



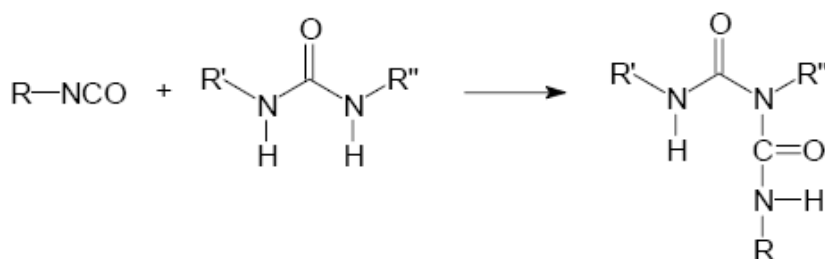
2.2.2 Side Reactions

The major reaction for the synthesis of polyurethanes is the reaction between a diisocyanate, chain extender and polyol which is supposed to give a linear polymer. It is also generally known that this type of polymerization is very sensitively to relative small changes in conditions which can greatly affect the final product. Several other reactions can occur during the synthesis of polyurethanes [26].

If di-or polyfunctional reagents are employed in any of these reactions, the formation of polymeric structures can occur. The use of purely difunctional compound leads to the formation of linear products, while higher functionality results in branched or crosslinked materials. Reactions of isocyanates with urethane, urea, and amide groups already introduced into polymeric systems are possible due to the fact that they also contain active hydrogen atoms. These reactions lead to chain branching and crosslinking and the formation of allophanates and biurets, respectively.

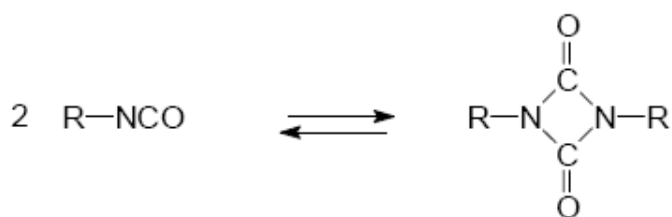


Allophanates



Biurets

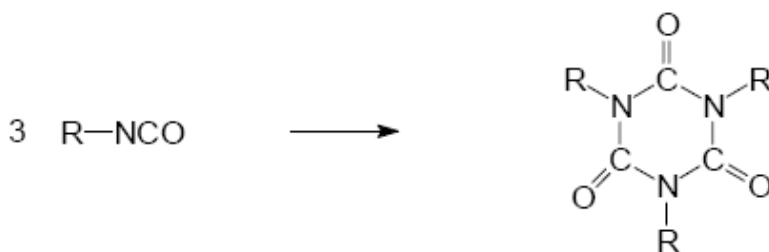
Other useful basic reactions of isocyanates are those which involve reactions with themselves. These can lead to the formation of dimmers, trimers, and polymeric structures. Dimerisation of isocyanates to form uretidiones provides a means to 'block' isocyanates, with dissociation leading to the isocyanate function becoming available at elevated temperature.



Isocyanates may also react with themselves to form carbodiimides and liberate carbon dioxide.



The trimerisation of isocyanates results in the formation of the isocyanate ring structure. In the case of diisocyanates, a trifunctional derivative is the product, which is capable of introducing chain branching and crosslinking into polyurethanes.



All these side reactions change the initial stoichiometry of the extension and thereby limit the final molecular weight and yield branched or even crosslinked polymers. The catalysts and solvents used for polymerization of polyurethanes or even catalysts or metal based impurities that are used or present during the synthesis of the reactants not only catalyze the chain extension, but will also catalyze these side reactions. This makes it very important to use high purity reactants in order to obtain high molecular weight linear polyurethanes with known catalysts.

2.2.3 Physical Properties of Polyurethane

Polyurethane can contain a high concentration of polar groups, in particular the urethane groups resulting from isocyanate-hydroxyl reactions, as well as ester, urea, and other groups. The interactions between these polar entities are of great importance in determining the final properties of polyurethane [33]. Generally, polyurethane contains hard and soft blocks which contribute to the versatility of this polymer. The hard or rigid segments in polyurethane particularly affect the modulus, hardness and tear strength, and determine the upper-use temperature by their ability to remain associated at elevated temperatures. However, in soft or flexible segment, primarily they influence the elastic nature of the polyurethane and its low-temperature performance, and they also make important contribution towards the hardness, tear strength and modulus.

The superior mechanical properties of polyurethanes are a result of microphase separation of the hard and soft domains. The hard segment acts as a filler and multifunctional crosslink and is very important for the mechanical properties of the material. Below the soft segment T_g , polyurethane are rigid. Above the hard segment T_g or melting temperature, the materials behave as amorphous, non-crosslinked liquids. Between these two transition temperatures, the materials behave as typical thermoplastic elastomers with their strength and modulus decreasing as temperature increases.

In general, the behaviour of these materials depends on the size and concentration of the hard segment domains, the strength of the hard segment aggregation, the ability of the segments to orient in the direction of stress and the ability of the soft segment to crystallize under strain [34]. The length of the soft segments also has a strong influence on the mechanical properties. Short soft segments ($M_n=800-1500$ g/mol) generally lead to rigid, high modulus materials while long soft segments (2000-5000g/mol) yield elastic materials which may show strain induced crystallization of the soft segments [35].

2.2.4 Application of Polyurethane

Polyurethane has been known as one of the major player in polymeric materials. With a wide range of properties, polyurethane is applied and increasingly established in areas such as medical, construction, automotive and aircraft coatings, and decorative and visual finishes. Changes in applications of this material need good technical knowledge and design approaches in creating high performance polyurethane.

Today, in coating technology, polyurethane easily dominates the coating material market. A detail review by Chattopadhyay and Ragu [36] regarding the structural engineering of polyurethane coating helps to explain the vital process in tailoring this material into coating technology application. In medical application such as in fabrication of extraoral prosthesis in dental material, polyurethane functions as

sealant to the porous silicone materials and improves the tear strength. As a result, it limits fungal growth often associated with silicon restorative materials [37]. Beside that, the softness of this material and advances in medical surgical technology make it one of the most selected materials in cardiovascular fields due to their good biocompatibility as well as their mechanical properties [38].

With increasing demands in nanotechnology material, the development of polyurethane nanocomposites could add a new value for this versatile material and it is intensively studied in every part of the globe in order to improve the material properties. Nanocomposites have been developed as an alternative to conventional filled polymer and homopolymer using a range of nanosize fillers.

2.3 Nanofillers

2.3.1 Layered Silicate Organoclay

(a) Structure of Layered Silicate

The clay used as layered silicate for the preparation of polymer layered silicate (PLS) nanocomposites belongs to the structural family known as the 2:1 layered or phyllosilicates. **Table 2.2** shows the clay classification [39]. Their crystal structure consists of layers made up of an octahedral sheet of alumina or magnesia sandwiched between two tetrahedral sheet of silica. **Figure 2.2** illustrates the structure of 2:1 phyllosilicates [40]. The layer thickness is ~ 1 nm and the lateral dimensions of these layers may vary from 30 nm to several micrometres and even larger depending on the particular layered silicate. The layers leads to organize themselves to form stacks with a regular van de Waals gap between the layers called the interlayer or gallery. In a pristine form, isomorphic substitution within the layers generates negative charges that are counterbalanced by alkali and alkaline earth cations (Na^+ , Li^+ , Ca^+) situated inside the galleries to maintain charge neutrality [39].

Table 2.2: Clay mineral (phyllosilicate) classification [39].

Type	Group	Groupoid	Species	Tetrahedron	Octahedron	Interlayer cation
2:1 Si ₄ O ₁₀ (OH) ₂	Pyrophyllite talc (x≈0)	di.	Pyrophyllite	Si ₄	Al ₂	–
		tri.	Talc	Si ₄	Mg ₃	–
	Smectite (0.25<x<0.6)	di.	Montmorillonite	Si ₄	(Al ₂ , Mg) ₂	Na, Ca, H ₂ O
		di.	Hectorite	Si ₄	(Mg ₂ , Li) ₂	Na, Ca, H ₂ O
		di.	Beidellite	(Si, Al) ₄	Al ₂	Na, Ca, H ₂ O
		tri.	Saponite	(Si, Al) ₄	Mg ₃	Na, Ca, H ₂ O
		di.	Vermiculite	(Si, Al) ₄	(Al, Mg) ₂	K, Al, H ₂ O
		tri.	Vermiculite	(Si, Al) ₄	(Mg, Al) ₃	K, Mg, H ₂ O
	Mica (x≈1)	di.	Muscovite	Si ₃ Al	Al ₂	K
			Paragonite	Si ₃ Al	Al ₂	Na
	Brittle mica (x≈2)	tri.	Phlogopite	Si ₃ Al	(Mg, Fe ²⁺) ₃	K
			Biotite	Si ₃ Al	(Fe ²⁺ , Mg) ₃	K
2:1:1 Si ₄ O ₁₀ (OH) ₈	Chlorite (large variation of x)	di.	Donbassite	(Si, Al) ₄	Al ₂	Al ₂ (OH) ₆
		di.–tri.	Sudoite	(Si, Al) ₄	(Al, Mg) ₂	(Mg, Al) ₃ (OH) ₆
		tri.	Clinochlore	(Si, Al) ₄	(Mg, Al) ₃	(Mg, Al) ₃ (OH) ₆
			Chamosite	(Si, Al) ₄	(Fe, Al) ₃	(Fe, Al) ₃ (OH) ₆
1:1 Si ₂ O ₅ (OH) ₄	Kaolin mineral serpentinite (x≈0)	di.	Kaolinite	Si ₂	Al ₂	–
			Halloysite	Si ₂	Al ₂	H ₂ O
		tri.	Chrysotile	Si ₂	Mg ₃	–
Needle	Sepiolite palygorskite (x≈0)	tri.	Sepiolite	Si ₁₂	Mg ₈	(OH) ₂ ·4H ₂ O
			Palygorskite	Si ₈	Mg ₈	(OH) ₂ ·4H ₂ O
Amorphous–low crystalline			Imogolite	SiO ₃ OH	Al(OH) ₃	–
			Allophane	(1–2)SiO ₂ ·(5–6)H ₂ O		
			Hisingerite	SiO ₂ –Fe ₂ O ₃ –H ₂ O		

x: degree of isomorphous substitution; di.: dioctahedral; tri.: trioctahedral.

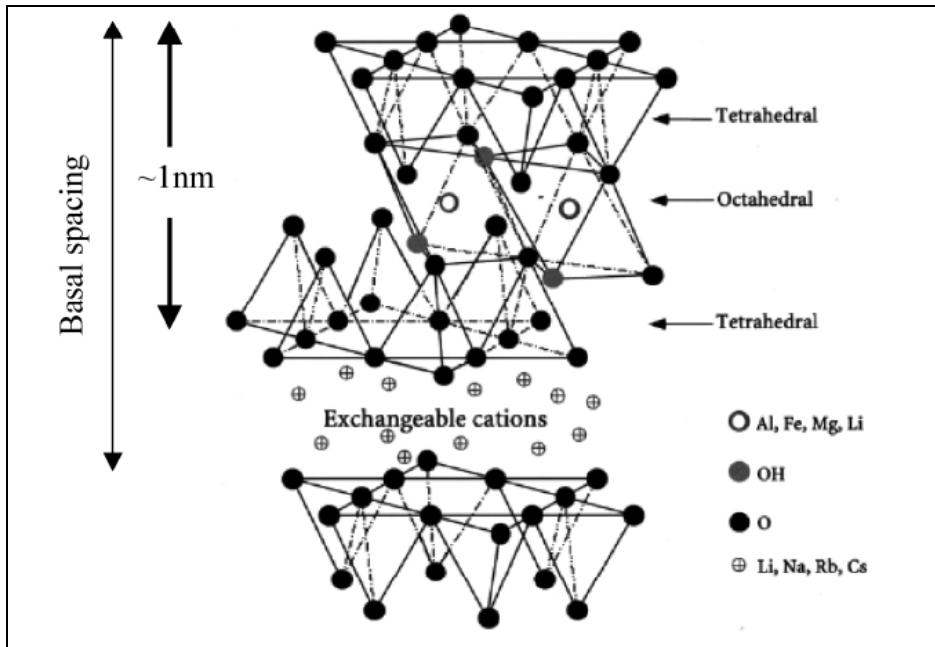


Figure 2.2: Structure of 2:1 phyllosilicate [40]

The type of clay can be characterised by a moderate surface charge known as the cation exchange capacity and generally expressed as mequiv/100gm and also using the layer morphology. Through the cation exchange capacity, the charge is not locally constant, but varies from layer to layer, and must be considered as an average value over the whole crystal [41].

The most commonly used layered silicate is montmorillonite, saponite and hectorite with different chemical formula respectively, shown in **Table 2.3** [42]. The smectite clays are the materials of choice for polymer nanocomposite design for two principal reasons. First, they exhibit a very rich intercalation chemistry, which allows them to be chemically modified and made compatible with organic polymers for dispersal on a nanometre length scale. Second, they are easy to find in nature and can be obtained in mineralogically pure form at low cost [43].

The layered silicate has two types of structure which are tetrahedral-substituted and octahedral-substituted. In the case of tetrahedrally substituted layered silicate, the negative charge is located on the surface of silica layers, and hence, the polymer

matrices can interact more readily with these than with octahedrally-substituted material [44].

Table 2.3: Chemical formula and characteristic parameter of commonly used 2:1 phyllosilicate [42]

2:1 phyllosilicate	Chemical formula	CEC (mequiv/100g)	Particle length (nm)
Montmorillonite	$M_x(Al_{4-x}Mg_x)Si_8O_{20}(OH)_4$	110	100 - 150
Hectorite	$M_x(Mg_{6-x}Li_x)Si_8O_{20}(OH)_4$	120	200 - 300
Saponite	$M_xMg_6(Si_{8-x}Al_x)Si_8O_{20}(OH)_4$	86.6	50 - 60

M, monovalent cation; x, degree of isomorphous substitution (between 0.5 and 1.3)

Beside these, other clays such as bentonite, and chlorite, are also used in preparing polymer layered silicate nanocomposite with specific properties [42]. Bentonite consists predominantly of montmorillonite with a minor portion of illite, a clay mineral with a dioctahedral structure and higher layer charge. The introduction of bentonite usually provides the nanocomposite with better mechanical and barrier properties than that of montmorillonite [42]. On the other hand, chlorite also has a basic 2:1 layer structure, but with a stable, positive charged octahedral sheet in the interlayer space. The positive charges of this octahedral sheet neutralize the negative charge of the 2:1 sheets. Because chlorite contains two octahedral sheets, it is called a 2:1:1 layer mineral. Sometimes, octahedral materials in chlorite neither totally fill the interlayer space between sheets nor completely neutralize the negative charge of the sheets. This unsatisfied charge is neutralized by various cations adsorbed to the particle surfaces from other materials. In other words, chlorite undergoes an ion-exchange process more readily than other clays with a 2:1 layer structure [45].

Two particular characteristics of layered silicate are generally considered for polymer layered silicate nanocomposites [46]. The first is the ability of the silicate particles to disperse into individual layers. The second characteristic is the ability to fine-tune

their surface chemistry through ion exchange reactions with organic and inorganic cations to form organophilic clay. These two characteristics are, of course, interrelated since the degree of dispersion of layered silicate in a particular polymer matrix depends on the interlayer cation.

(b) Organically Modified Layered Silicate

These clays are originally hydrophilic and only compatible with hydrophilic polymers, such as poly(ethylene oxide) (PEO) and poly(vinyl alcohol) (PVA). The organophilicity of the clay must be increased to improve its compatibility with many matrices of engineering polymers [47].

Generally, this can be carried out by ion exchange reactions with cationic surfactants including primary, secondary, tertiary, and quaternary alkyl ammonium or alkylphosphonium cations. Ion exchange reactions depend on the cation exchange capacity of the clay. The role of alkylammonium or alkylphosphonium cations in the organosilicates is to lower the surface energy of the inorganic host and improve the wetting characteristics and intercalation with the polymer matrix, and the results in a larger interlayer spacing [47]. Additionally, the alkylammonium or alkylphosphonium cations could provide functional groups that can react with the polymer matrix or in some cases initiate the polymerisation of monomers to improve the strength of interface adhesion between the clay nanolayers and the polymer matrix [48].

Whether organically modified or not, most layered silicates possess a hierarchical morphology as defined by three general levels of structure; crystallite (tactoid), primary particle and agglomerates. A general schematic of these is shown in **Figure 2.3** [49]. The crystallite is composed of as many as 100 individual layers stacked together. They are also commonly referred to as tactoids. The primary particles consist of compact face to face stacking or low angle intergrowth of individual tactoids. Finally weak agglomeration of these particles forms the powder that we

generally refer to as particles. In the polymer nanocomposite fabrication, disruption of the tactoids as well as primary particles and dispersion of the agglomerates are both important to achieve uniform nanoparticle distribution in the polymer matrix.

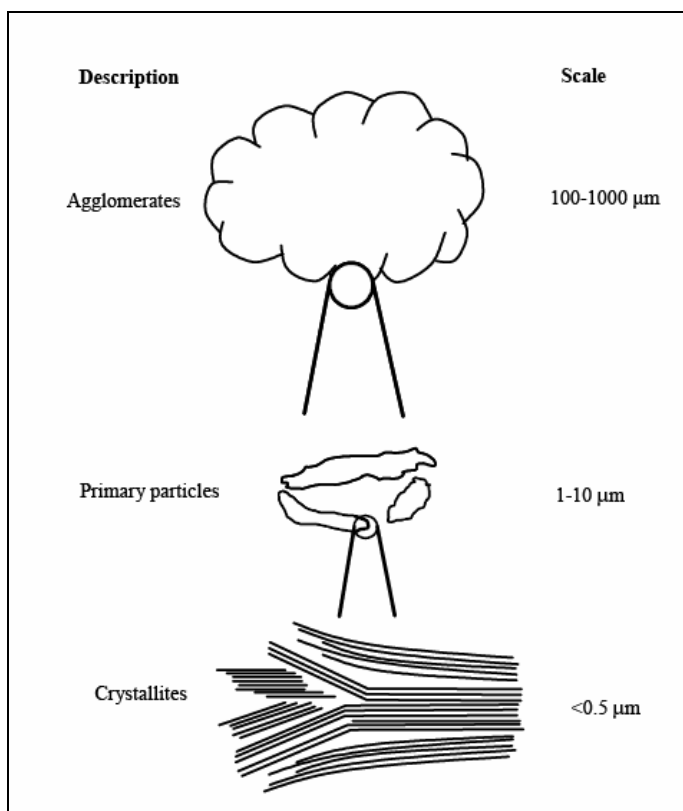


Figure 2.3: Hierarchy of montmorillonite clay particles [49]

2.3.2 Graphene Oxide

Graphene has been widely used as a filler in conducting polymer composites. Compared to CNTs, graphene is only recently been extensively investigated as an alternative filler to CNTs due to its cheaper in term of price, good electrical conductivity and it is a naturally abundant material [50]. In addition to these reasons, both theoretical and experimental results revealed that graphene is the strongest material developed so far [51].

In nature, graphene consists of an atom-thick and two-dimensional single layer of hexagonal carbon rings and the typical interlayer spacing between graphene layers is 3.35Å, and they are bonded to each other by van der Waals forces. A number of studies has demonstrated that graphene displays excellent electron transport properties which reflects to a good electrical conductivity [52-53]. However, due to the high cohesive energy of graphite, it is very difficult to strip graphene sheets from graphite, thus severely limiting the application of this material. To overcome this problem, Delgado et al [54] suggested two attractive routes to be applied in order to manipulate the full potential of graphite. Their suggestions are: (i) chemical modification of graphene obtaining by mechanical treatment of highly pyrolytic graphite such as micromechanical cleavage [55] and chemical vapour deposition (CVD) [56,57] or, (ii) chemical modification of monocrystalline graphite such as via graphite intercalation compound (GIC) [58] and oxidation of graphite [59].

Among these, the latter route by chemical treatment of natural graphite is most promising for fabricating graphenes in large quantities for industrial application [60]. Oxidation of graphite is among the popular modification process of graphene. Graphite oxide (GO) in layered form which is produced after the oxidation of graphite has strong oxygenated, hydroxyl and epoxide functional groups and the presence of these functional groups allows the exfoliation of graphite oxide in water [61]. However, owing to their hydrophilic nature, it has been found that GO cannot be exfoliated in most organic solvents.

Stankovich et al [59] used organic isocyanate to reduce the hydrophilic character of GO and this method is successful to produce isocyanate-derivatized GO in N,N-dimethylformamide (DMF). Haddon and coworkers [62] have recently reported an effective way to obtain graphene sheets functionalized with long hydrocarbon chain (G-ODA). Treatment of microcrystallize by oxidative treatment with acid produced oxidized graphite. The presence of acidic functionalities helps this material to be soluble in polar solvent and improve the processability of graphite.

Expandable graphite (EG) via GIC is another promising chemical treatment which is related to the process of expanding/intercalating the gallery of graphite by introducing sulfuric acid into natural flake graphite. Through this process, the gallery can expand up to a hundred times in volume at high temperature. Cai et al [63] disclosed that the GO prepared by oxidation of EG can be exfoliated into graphite oxide nanoplatelets (GNOPs) in DMF by assistance of ultrasound. Through this method, the preparation of GNOP/polymer composites seems to be easily with good dispersion of GNOPs in polymer matrix was successful achieved.

2.3.3 Carbon Nanotubes (CNTs)

Since the discovery of carbon nanotubes by Ijima [64] in 1991, the application of CNTs has attracted more and more attention due to their special structure, excellent mechanical properties, and good electrical and thermal conductivity. They are extremely small in size with the diameter of CNT is in range of nanometer. However, the strength is 20 times that of high strength steel alloys, and having current carrying capacities 1000 times that of copper in combination with superior thermal properties compared to diamond. As shown in **Figure 2.4**, CNTs can be considered as seamless cylinders rolled up by graphene sheets, which generally have a great length-to-diameter ratio [65].

According to the diameter of the cylinders, CNTs are classified as single-walled carbon nanotubes (SWCNT) and multi-wall carbon nanotubes (MWCNT). The SWCNTs typically have diameters ranging from 0.7 to 5.0 nm with thickness of 0.34 nm [65]. MWCNTs have a number of graphene sheet co-axially rolled together to form a cylindrical tube consisting of 2 to 50 nm of these tubes and has inner diameter of 1.5 to 15.0 nm and outer diameters of 2.5 to 30 nm. Depending on the angle at which the graphite sheet is rolled, CNTs can be categorized as “armchair”, “zig-zag”, and “chiral” nanotubes as shown in **Figure 2.5** [66].

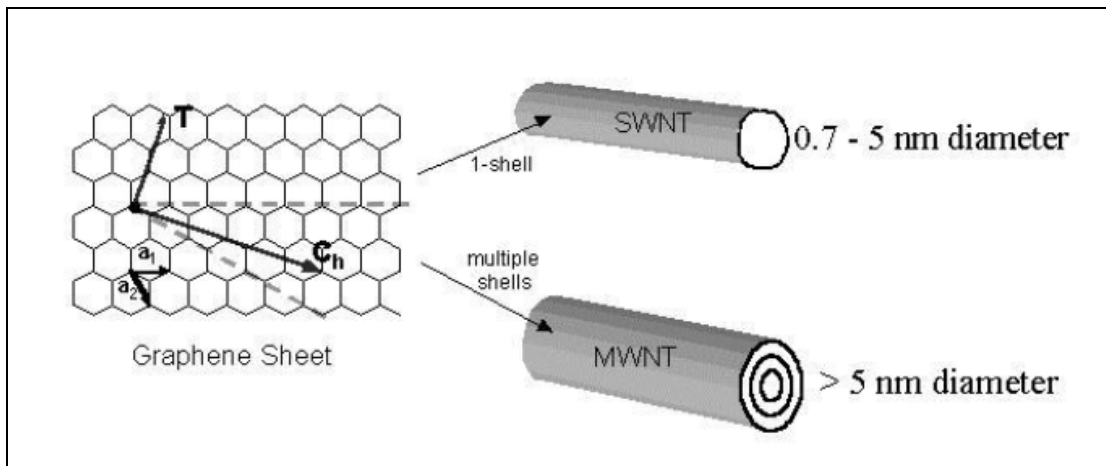


Figure 2.4: Types of carbon nanotube [65]

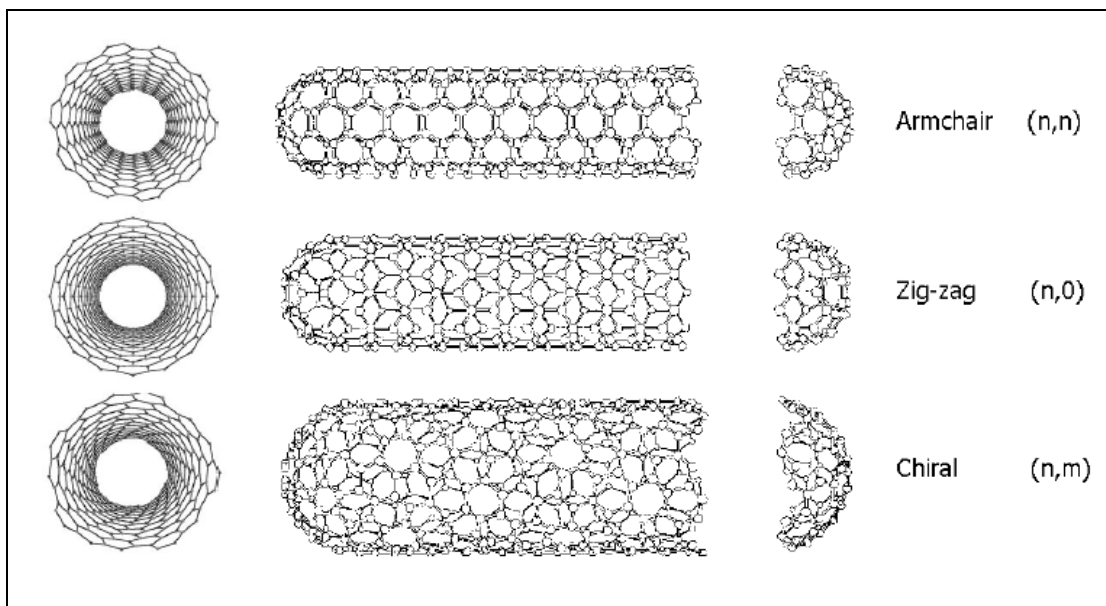


Figure 2.5: Schematic structure of CNTs after graphite sheet folding [66]

These intriguing structures have sparked much excitement in recent years and a large amount of research has been dedicated to their understanding and in developing novel CNT-based multi-functional materials. A huge number of papers were published to report the wide range application of CNTs such as sensor devices [67-68], emission

devices [69], biomedical and automotive application [70-71]. However, the cost and the difficulty in the dispersion of CNTs are the main disadvantages for commercial applications.

(a) Synthesis of CNTs

This part briefly reviewed the most popular techniques to synthesize CNTs, including arc-method, laser ablation and chemical vapour deposition.

(i) Arc-discharge

The carbon arc-discharge method refers to the growth of CNTs by arc-discharging graphite in inert gas [72], hydrocarbon, or hydrogen atmosphere [73]. This is the most common and perhaps the easiest way to produce CNTs. However, it is a technique that produces a complex mixture of components and requires further purification to separate the CNTs from the soot and the residual catalytic metals present in crude product.

In 1992, Ebbesen and Ajayan [72] firstly used arc-discharge technique to prepare high quality MWCNTs at the gram level. In following year, Bethune and a co-workers [74] reported a cobalt-catalysed growth of SWCNTs by using arc-discharge, in which electrodes were prepared by filling graphite rods with a mixture of powdered metals (Fe, Ni or Co) and graphite. Arc-discharge method is usually used to produce high quality and nearly perfect nanotube structure for scientific research.

(ii) Laser Ablation

Laser ablation is another useful method to produce CNTs with high quality and high purity. The technique was firstly invented by Samlley and co-workers in 1995 [75]. This technique involved direct vaporization of the mixture of graphite and transition metals by using a pulsed laser in a high temperature reactor with inert gas going

through the chamber. Compared with arc-discharge method, laser ablation showed greater control over growth, continuous operation, higher yield production and better quality. This technique is improved later by Yudasaka et al [76]. They used double-target laser ablation to massively produce SWNTs with higher purity compared to a single-target one. Afterward, much effort has been put in to optimize the growing process of CNTs, such as composition target [77], gas pressure [78-79], temperature and laser variations [80-81].

(ii) Chemical vapor deposition

Chemical vapor deposition (CVD) is a classical method to produce carbon materials such as carbon fiber, filament, and nanotube materials [82]. The CVD method involves synthesizing CNTs from hydrocarbon-containing feedstock on catalysts at high temperature (500-1000°C) in a tube furnace [83]. The choice of feedstock includes methane [83], ethylene [84], carbon monoxide [85] and benzene [86]. Transition-metallic nanoparticles formed on porous aluminum oxide with large surface areas are always used as a catalysts [87]. The growth mechanism of CVD method is commonly interpreted as follow [66]: (i) the dissociation of hydrocarbon molecules catalyzed by transition-metallic nanoparticles; (ii) the dissolution and saturation of carbon atoms in transition-metallic nanoparticles; (iii) the formation of tubular carbon solid in a sp^2 structure results from the precipitation of carbon from the saturated transition-metallic nanoparticles. Compared with above two methods, the CVD method has significantly attracted industry due to its advantage on large-scale production of CNTs from kilogram to ton level for commercial purpose.

2.4 Structure of Polymer Nanocomposites

In general, layered silicate has layer thickness on the order of 1 nm and a very high aspect ratio (eg 10 - 1000). A few weight percent of layered silicate that is properly dispersed throughout the polymer matrix creates much higher surface area for polymer/filler interaction as compared to conventional composites. The complete

dispersion or exfoliation of the clay layers in the monomer or polymer clay comprises up to three steps similar to the dispersion of powders in liquid, described by Parfitt [88]. The first step is wetting the surface of clay tactoids by monomer or polymer molecules. Secondly, intercalation or infiltration of the monomer or polymer takes place, followed by the third step, exfoliation of the clay layers. Thermodynamics controls the first and second steps, while mechanical and reaction driving forces determine the extent of the third step. Depending on the strength of interfacial interactions between the polymer matrix and the layered silicate (modified or not), three different types of PLS nanocomposites are thermodynamically achievable. **Figure 2.6** illustrate the three different types of polymer/layered silicate composites [89].

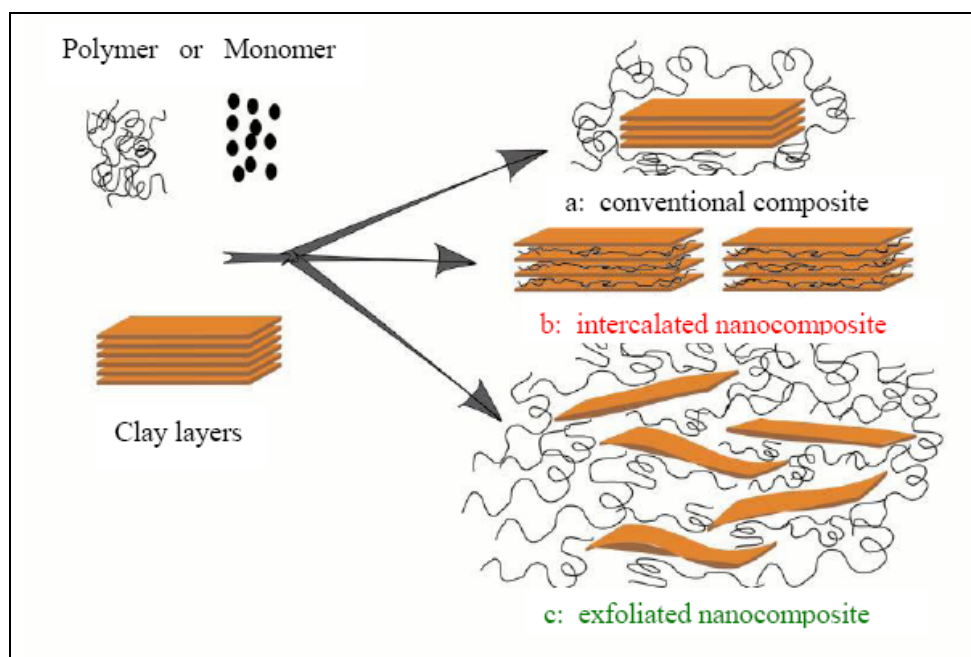


Figure 2.6: Schematic illustration of three polymer layered silicate composites [89]

The three different types of polymer layered silicate composites are (i) conventional composites, (ii) intercalated composites, and (iii) exfoliated nanocomposites [89]. In conventional composites, a phase separated composite is formed and the silicate acts as a conventional filler. There is no interaction (intercalated) between polymer and

silicate and the expected properties normally failed to achieve. The properties of conventional composite remained to that of polymer composite reinforced by microparticles. Meanwhile, an intercalated nanocomposite which is the insertions of a polymer matrix into the layered silicate structure occurs in a crystallographically regular fashion, regardless of the clay to polymer ratio. Normally in this type, the mechanism of interlayer by a few molecular layers of polymer and the properties is resembles those of ceramic materials. In contrast to others, an exfoliated nanocomposite is thermodynamically the individual clay layers are separated in a continuous polymer matrix by an average distance that depends on clay loading. Usually, the clay content of an exfoliated nanocomposite is much lower than that of intercalated nanocomposites [90].

Exfoliation is more appealing for the enhancement of certain properties of the material because of the high degree of dispersion and maximum interfacial area between polymer and clay. In reality, most nanocomposite systems fall between these two and showed mixed morphologies. Kinetic aspects associated with Brownian motion and shear alignment of layers [91], along with the processing history, will produce positional and orientational correlations between the plates.

2.5 Preparation of Polymer Nanocomposites

In order to produce polyurethane nanocomposites with the desired properties enhancements, it is necessary not only to compatibilize the silicate layers with the polyurethane matrix, but also to effectively mix and disperse them in order to take advantage of such compatibility. Failure to do either one of these things will result in a material whose properties are not optimal. In addition to that, failure to pay attention to the significance of materials preparation may result in an incorrect conclusion that the compatibilization strategy is to blame for poor silicate dispersion and/ or materials performance. Solution intercalation, melt intercalation and in situ

polymerization are the methods widely used to prepare polyurethane nanocomposites [92].

2.5.1 Solution Intercalation

In solution intercalation, a common solvent or solvent mixture is used to disperse the layered silicates and at the same time, dissolve the polymer matrix. Depending on the interaction of the solvent due to the weak van de Waals force to stack the layer together, polymer chains then can be adsorbed on to the delaminated individual layer.

Dai et al.[93], showed that the polyurethane/montmorillonite (MMT) nanocomposites can be prepared through this method by dispersing MMT into DMF solvent at 80 C and vigorously stirred until the solution became homogeneous. Then, MDI and PTMG at a molar ratio of 2:1 were dissolved in the aforementioned solution and stirred until the completion of reaction. The mechanism for the formation of nanocomposites by this technique involves two steps. First, the swelling of the clay layers by the solvent and second, an intercalation of the polymer chains into the expanded clay galleries by displacing the solvent molecules out of the gallery. After the solvent is completely displaced out of the galleries, the system is heated until all the solvent evaporates. Beside Dai and co workers, various other researchers such as Han et al [94], and Tien and Wei [123] also used this method.

However, there are some disadvantages of this method where they consumed a large amount of solvent, resulting in a higher cost and environmentally unfriendly, especially in a commercial point of view and in certain cases, upon solvent removal, the layers can reassemble to reform the stack with polymer chains sandwiched in between, forming a well ordered intercalated nanocomposites. In addition, it is believed that a small amount of solvent remains in the final product thus creating weaker interfacial interaction between the polymer and clay surfaces [95]. Moreover, the types of polymers that can be used to fabricate nanocomposite ultimately depend on the selection of proper solvent, limiting the applicability of this method.

Nevertheless, it is an attractive route in preparing water soluble polymer layered silicate nanocomposites because in this case most water soluble polymers are polar and hydrophilic enough to interact with the silicate surface. Therefore no cation exchange modification of the surface is needed. It is widely known that inorganic layered silicates are able to exfoliate in water and form colloidal particle.

Solution method is considered as perhaps the most common method to prepare the CNT/polymer nanocomposites [96], which mainly involve two steps: a) the dissolution of CNTs and polymers in solvents; and b) the evaporation of solvents. Mechanical stirring, shear mixing, and ultrasonification are generally used to disperse CNTs in solvents. The advantage of this method is that the mechanical agitation especially ultrasonication can effectively reduce the aggregation of CNTs.

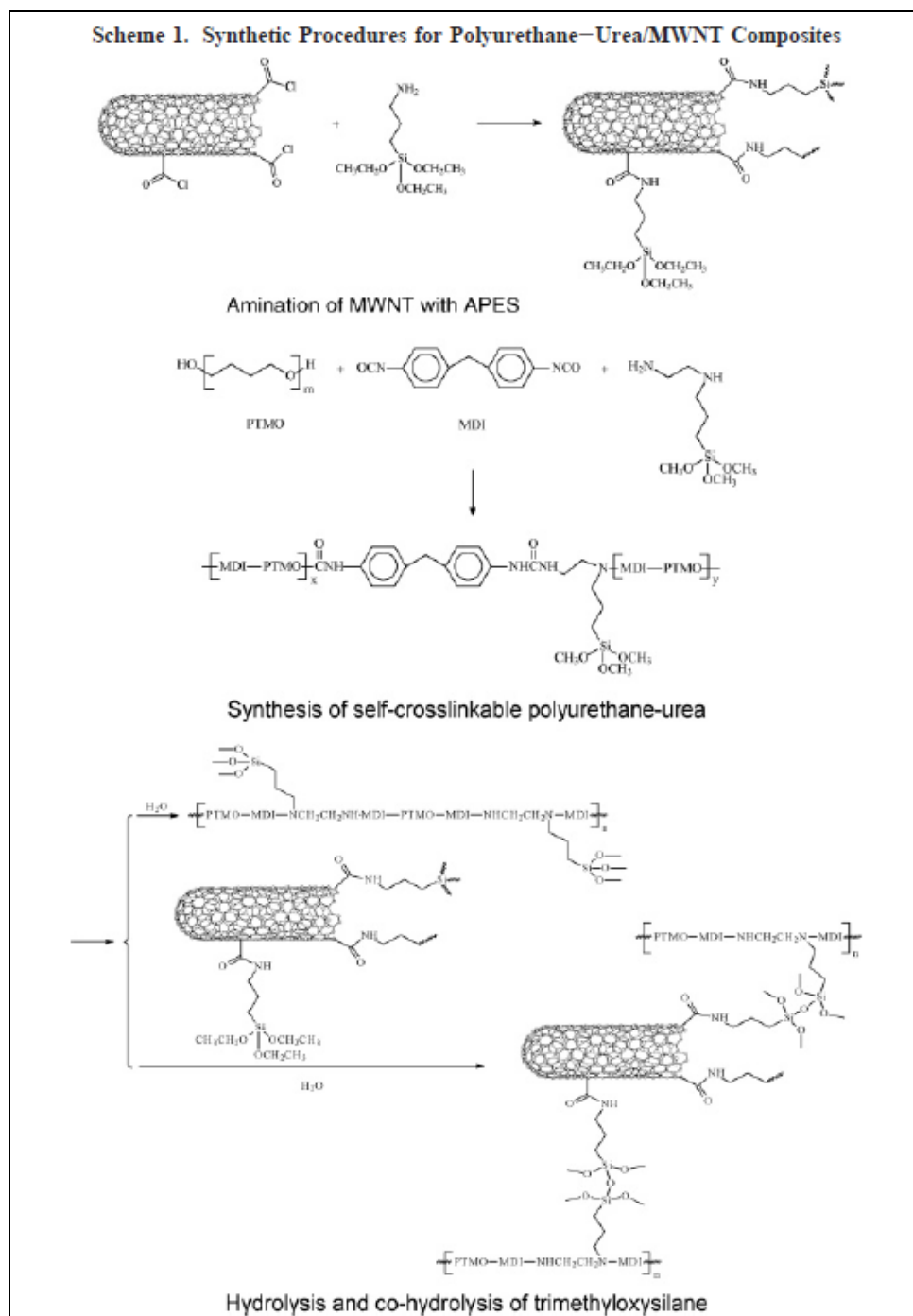


Figure 2.7: Synthetic procedures for polyurethane-urea/MWNT composites [97]

Xu et al [97] employed a typical solution method to prepare novel polyurethane-urea/MWCNTs composites. The synthesis routes of the polyurethane-urea samples are shown in **Figure 2.7**. A typical preparation was carried out as follows: i) PTMO was dissolved in DMF, followed by the addition of stoichiometric amounts of MDI and one drop of stannous octoate as catalyst; ii) the mixture was stirred by magnetic stirring for 3 hours and the extender (AEAPS) in DMF solution was added and the reaction was continued another 8 hours at 90 °C to ensure the completeness of reaction; iii) the addition of MWNTs and the mixture were stirred for another 48 hours in an oil bath at 100 °C under N₂ atmosphere. Afterward, the mixtures were cast to produce a thin film for testing. Chemical modification or surfactant wrapping of CNTs, in some cases, is used to improve the dispersion of CNTs in solvents. One of the most successful methods to incorporate CNTs into polymer latexes is colloidal physical method. There are several advantages using this method including minimizing the damages of CNTs properties by introducing a surfactant, improving electrical conductivity dramatically with low CNT concentration, and being more environmental friendly due to the use of water as medium instead of toxic solvent. Dufresne et al [98], Regev et al [99] and Grunlan et al [100] successfully used this method to incorporate CNTs into polymer latexes.

2.5.2 Melt Intercalation

Nowadays, the melt intercalation technique has become the standard for the preparation of polymer layered silicate nanocomposites [101, 102, 103]. This method is quite general and is broadly applicable to a range of commodity polymers, from essentially non-polar polystyrene to weakly polar poly(ethylene terephthalate) and to strong polar nylon. There are many advantages of using this method. It is environmentally benign and economical in term of cost because of the absence of solvent. In addition, it is highly open to a variety of polymer that is inaccessible before through the new hybrid process.

Direct melt intercalation involves annealing a mixture of the polymer and layered silicates above the softening point of the polymer, statically or under shear. While annealing, the polymer chains diffuse from the bulk polymer melt into the galleries between the silicate layers. A range of nanocomposites with structures from intercalated to exfoliated can be obtained, depending on the degree of penetration of the polymer chains into the silicate galleries. **Figure 2.8** shows the intercalation process between a polymer melt and organically modified layered silicates.

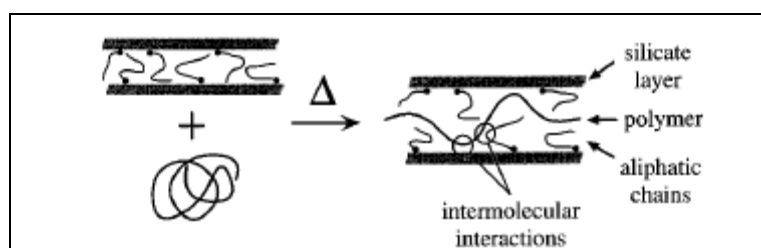


Figure 2.8: Schematic illustration of the intercalation process between a polymer melt and an OMLS [104]

Polystyrene with alkylammonium cation modified montmorillonite was the first polymer using this method. In the experiment, polystyrene was first mixed with the host organically modified layered silicate powder, and the mixture was pressed into a pellet, then heated under vacuum at 165°C which is well above the glass transition temperature of polystyrene to ensure the presence of a polymer melt. Meanwhile, the same authors also carried out an experiment to intercalate solution of polystyrene in toluene with the same organically modified layered silicate used for melt intercalation, but this resulted in intercalation of the solvent instead of polystyrene. Therefore, direct melt intercalation enhances the specificity for the intercalation of polymer by eliminating the competing host-solvent and polymer-solvent interactions [101]. Schematic illustration of the polymer chains intercalated in organosilicates is shown in **Figure 2.9**.

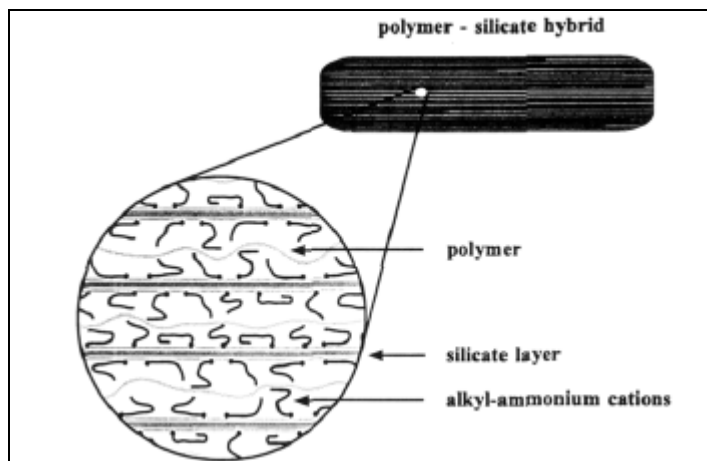


Figure 2.9: Schematic illustration of polymer chains intercalated in organosilicate [101].

By using high temperature and shear mixing, melting processing is particularly suitable for dispersing CNTs in thermoplastic polymers. In this method, CNTs are mechanically dispersed in melting polymers by some conventional processing methods such as extrusion, injection moulding and compression moulding. Due to the environmental issue and the toxicity of solvents, this method is considered as more widely accepted in industrial applications. However, the weaknesses in achieving homogenous dispersion of CNTs in a polymer matrix are the issue.

Chen et al [105] used chemical treatment on MWNTs by applying a mixture of nitric and sulfuric acids before blended with TPU in a Mini-lab twin-screw extruder. The use of chemical treatment CNTs is an effective mean to enhance the dispersion of CNTs in a polymer matrix and the interfacial interaction between CNTs and the polymer matrix. Results indicated that the homogeneous dispersion of MWNTs throughout PU matrix as shown in **Figure 2.10** and strong interfacial adhesion between oxidized MWNTs and the matrix were achieved.

In recent work by Zhang et al [106] produced conductive carbon nanotube/thermoplastic PU composites using this method. The desired amount of CNTs was mixed with PU at 190°C in nitrogen environment for 4 minutes at 50 rpm

using a DSM Xplore 15 ml mini extruder. The results demonstrated that dynamic percolation behaviour of the conductive PU/CNTs composites can be harnessed and used to lower the percolation threshold and improve the conductivity of the final product.

2.5.3 In situ Intercalation

In in-situ polymerization, the liquid monomer or a monomer solution was first swollen with layered silicates after which polymerization and intercalation took place. The polymerization can be initiated either by heat or radiation, by the diffusion of a suitable initiator or catalyst fixed through cation exchange inside the interlayer before the swelling step. Because of the low viscosity of monomer (compared to polymer), it is much easier to break up particle agglomerates using a high shear device, and achieve a more uniform mixing of particles in the monomer diffusion into the interlayer region. Furthermore, it is possible to control nanocomposite morphology through the combination of reaction conditions and clay surface modification.

In the area of polymeric layered silicate nanocomposites, it was firstly done by the team of Toyota researchers after reporting of a N6/ montmorillonite nanocomposite [107]. They prepared nylon 6 nanocomposites via in-situ polymerization, using ϵ -caprolactam as the monomer. They used a series of protonated amino-acid to modify the layered silicate surface. It was found that with the increase of chain length, the organic ammonium cations could change the orientation from monolayer, bilayer, to paraffin like structure with the tail inclined away from the silicate surfaces. When chain length is less than 8nm, the alkyl chain is parallel to the montmorillonite surface and radiates away from the surface. Then the chain can further leave away and adopts an orientation perpendicular to the silicate surface. This will allow more ϵ -caprolactam to intercalate into the gallery region. They then used protonated aminolauric acid (n=12) exchanged montmorillonite to prepare nylon 6 nanocomposites. The carboxyl group initiated the intralayer polymerization and

exfoliated nanocomposites were successfully prepared under appropriate conditions. A conceptual scheme for the synthetic method is presented in **Figure 2.11** [108].

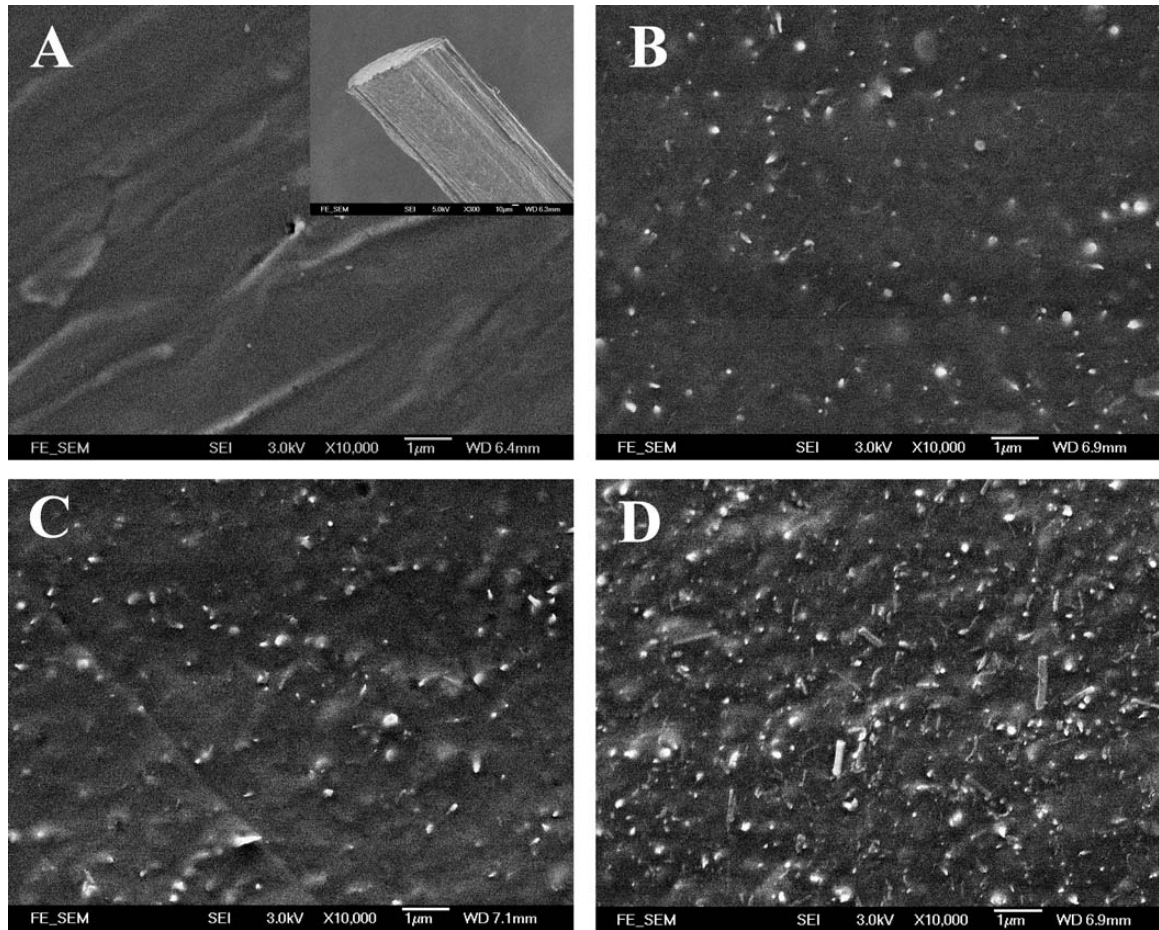


Figure 2.10: SEM images of the surfaces for pure PU (A), and PU composites fibers containing 5.6, 9.3 and 17.7wt% MWNTs (B) – (D), respectively [105]

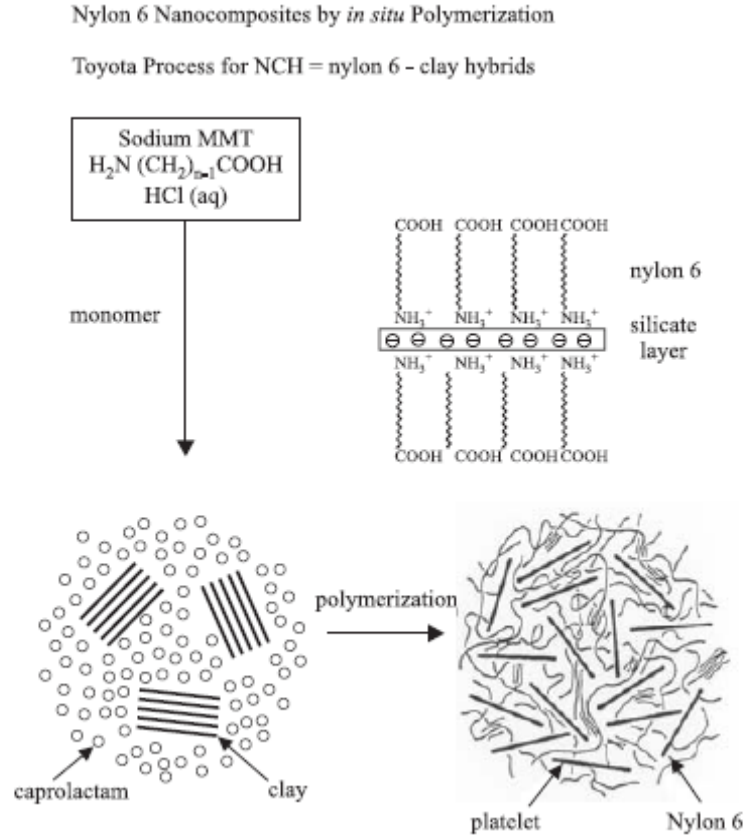


Figure 2.11: Schematic illustration for synthesis of Nylon-6/clay nanocomposite [108]

In polyurethane nanocomposites, *in situ* intercalation was widely used. The nanofiller was dispersed in polyols and the mixture was stirred vigorously. Then, it was reacted with diisocyanate together with chain extender and catalysts. Among the researchers using this method are Song et al [109,110,111], and Moon et al [112].

With regard to polyurethane-CNTs, Yoo et al [113] initially reported the achievement of the fabrication of well-dispersed CNT reinforce polyurethane via *in situ* polymerization. The authors used three methods of pre-polymer to prepare PU-MWCNT that include: 1) the prepolymer of MDI and PCL and subsequently a calculated amount of MWCNT and BD were added to the prepolymer solution; 2) the necessary weight fractions of MWCNT were first dispersed in PCL, followed by

MDI and BD were added into the mixture; 3) PU was first dissolved in DMF solution at room temperature, then the MWCNT were added into this solution and stirred for 24 hours. **Figure 2.12(a), (b), and (c)** show the SEM images of three different methods of PU/MWCNT preparations. The composites obtained by all three methods of in-situ polymerization showed enhanced mechanical properties as well as good electroactive shape memory.

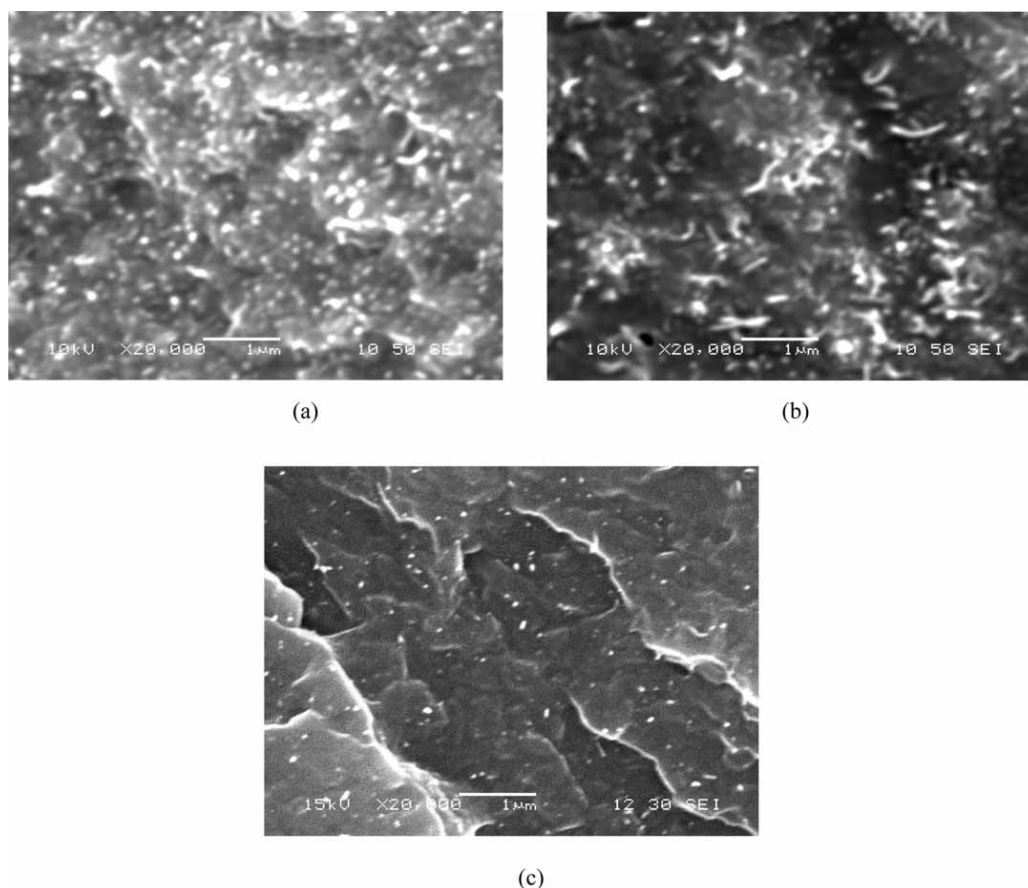


Figure 2.12: SEM images of cross section of PU-MWCNTs composites (a) Method 1, (b) Method 3, and (c) Method 2 [113]

Xia et al [114] also reported the fabrication of PCL/PU grafted SWCNTs using a hydroxyl functionalized SWCNT-OH via a two-step reaction. Schematic illustration for the synthesis of PU grafted SWCNTs through a two step process is shown in **Figure 2.13**. The process began with SWCNT-OH reacted with polyTDI, a kind of

highly active substance with $-NCO$ groups, to obtain the SWCNT-grafted-TDI. Then the mixture was reacted with PCL diol with molecular weight of ~ 2000 to produce the SWCNT-grafted-PU. The reactions were assisted by ultrasonic irradiation to assure well dispersed nanocomposites were prepared. In other work, Xia et al [115] revealed a two-step process in successfully preparing poly(propylene glycol)/PU-grafted MWCNT. The authors claimed that the grafted MWCNTs can improve the rheological behaviour of the polyol/MWCNT dispersion, and have a better reinforcing effect on the mechanical properties of PU.

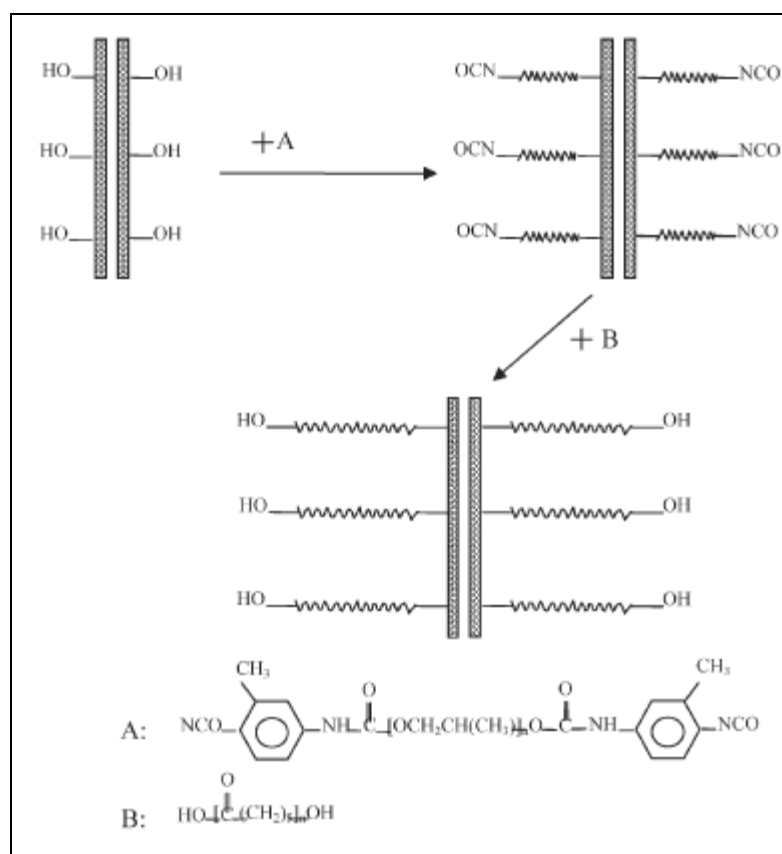


Figure 2.13: Schematic illustration for the synthesis of PU grafted SWCNTs through a two-step process (A:PolyTDI; B: PCL) [114]

Recently, Jana et al [116] reported a successful preparation of PCL-grafted-MWCNT by chemical modification of MWCNTs using HNO_3 and thionyl chloride (SOCl_2). Details of the process are shown in **Figure 2.14**. The grafting of PCL onto MWCNTs was confirmed by FTIR spectroscopy. The presence of PCL-g-MWCNTs made an important contribution to the enhancement of the mechanical and shape memory properties of polyurethane.

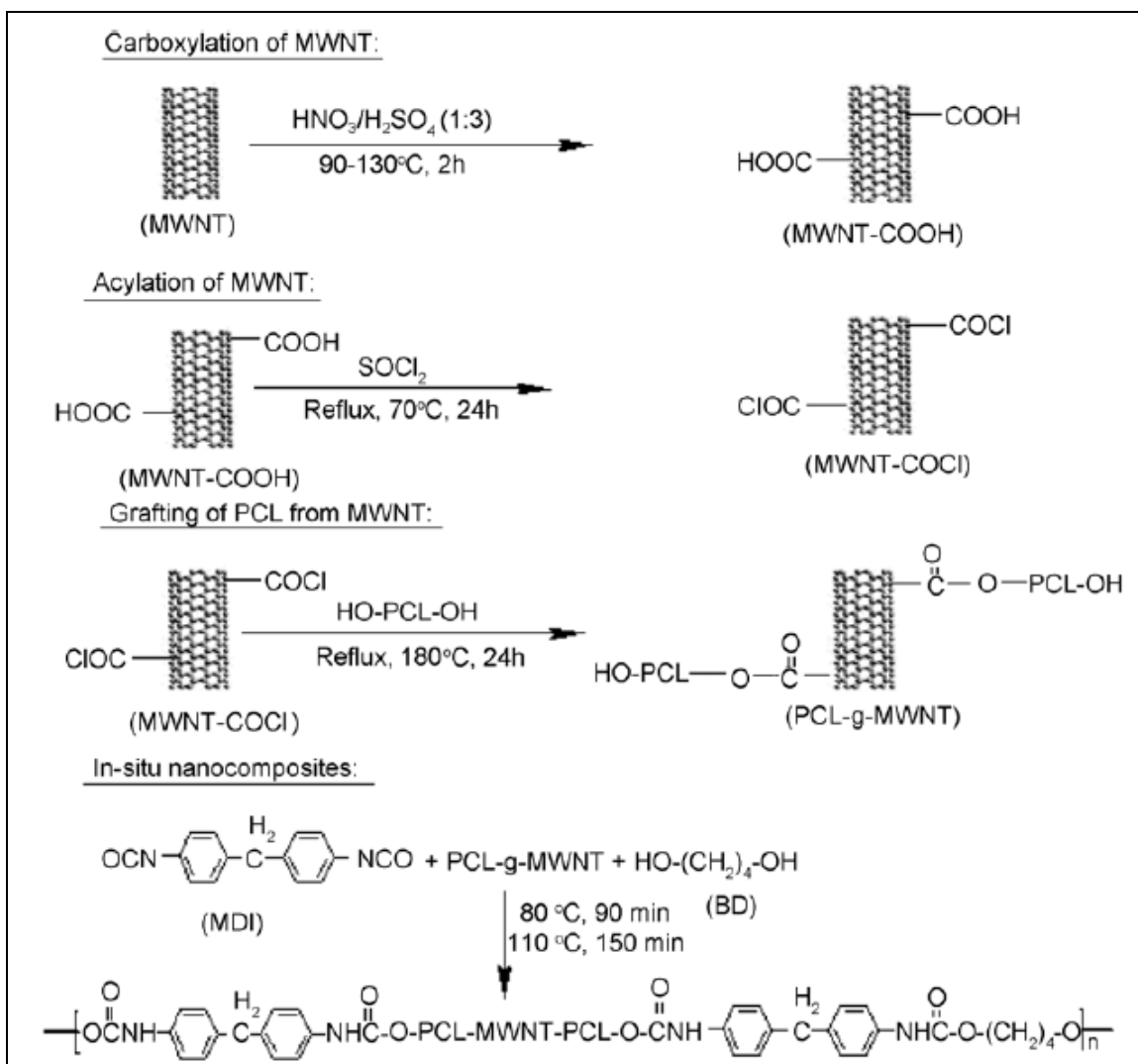


Figure 2.14: Illustration for the functionalization of MWCNTs and possible chemical structure for nanocomposites prepared by in-situ method [116]

2.6 Physical and Mechanical Properties of Polyurethane Nanocomposites

Polymer nanocomposites have recently received great attention from both academia and industry in exploiting the huge potential of reinforcement compared to conventional composites. The interest of material scientists in this kind of material is the result of the significant property enhancement obtained from relatively low nanofiller loading. After successful development of nylon 6 nanocomposites in 1990 [117], the development of polyurethane nanocomposites was drastically increased with the introduction of different kinds of nanofillers as reinforcement in matrix.

2.6.1 Polyurethane Organoclay Nanocomposites

Due to the nanometre-scale dimensions and the high aspect ratio of exfoliated or intercalated silicate layers, nanocomposites show different properties than traditional filled polymers. The huge interfacial interaction results in well dispersed layered silicate fillers into polymer matrixes lead to a significant improvement in polymer properties compared to microcomposites or neat matrixes.

The improvement in the mechanical properties was reported by Wang and Pinnavaia in 1998 [118]. They intercalated clay layers with various polyols before reacting with diisocyanate and the montmorillonite clay exchanged with long chain onium ions had a good compatibility with those polyols and expanded the clay galleries to some extent. The cross-linked polyurethane nanocomposites, formed by in-situ polymerization, showed clay particles in intercalated state with d-spacing of 5 nm, and with 10 wt% loading of montmorillonite modified with the longest onium ion a more than 100% increase in modulus, strength, and extensibility was exhibited as shown in **Figure 2.15**. This result suggested that onium ions acted as a plastisizer and improving the elasticity of the nanocomposite.

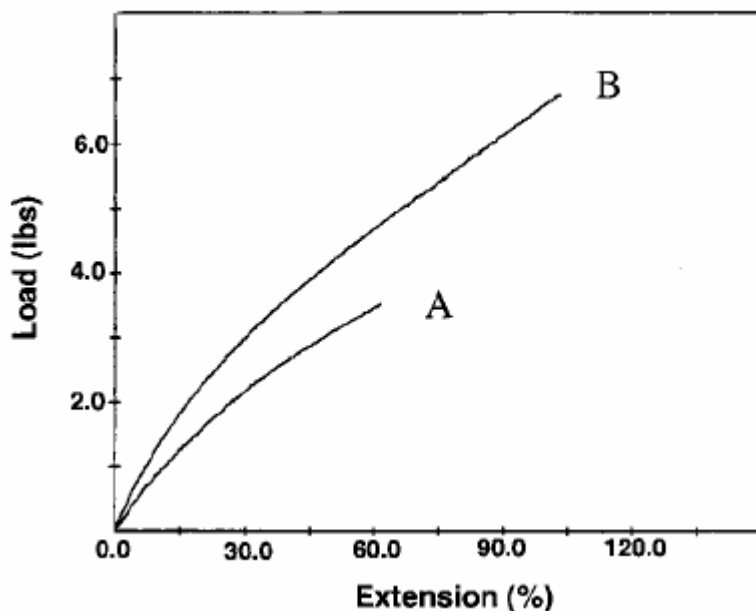


Figure 2.15: Stress-strain curves for (A) the pristine polyurethane and (B) as a polyurethane-clay nanocomposite prepared from C18A-SWy montmorillonite (5 wt%) [117]

Zilg et al [119] reported that polyurethane nanocomposites, containing synthetic fluoromica, exhibited enhanced tensile strength and elongation at break. Chen et al [120,121] synthesized a segmental polyurethane/clay nanocomposites, using poly(ϵ -caprolactone)/clay hybrid, whose mechanical properties increased with the hybrid content. However, the nanocomposites transformed from an elastomer to a plastic as the clay hybrid content increased. The number of new research in polyurethane nanocomposites with other nanofiller had dramatically increased.

Tien and Wei [122, 123] published a set of publication examining polyurethane/montmorillonite nanocomposites. In their study, polycaprolactone/montmorillonite prepolymer was prepared and substituted in a chain extender during polyurethane nanocomposites synthesis. Characterizations show that the clay was well dispersed within the polycaprolactone, and it helps the increment on the tensile strength of polyurethane nanocomposite. This group [124] also investigated the affect of clay swelling agents, 12-aminolauric acid (12COOH)

and benzidine. Although x-ray diffraction suggested that 12-aminolauric acid better exfoliated clay, the nanocomposites made using benzidine exhibited greater thermal stability, increased elongation, and drastically improved in tensile strength when compared to the pristine polyurethane.

Xu et al. [125] investigated a biomedical polyurethane system similar to one studied by Wei and co researchers. In their research, they found that at 20 wt% clay loading, the nanocomposite exhibited over 300% increase in initial modulus, 30% increase in strength, 50% in extensibility and 5-fold reduction in water vapour permeability when compared to pure polyurethane-urea. The silicates reduce the permeability of the polyurethane by forming the tortuous paths through which the water vapour molecules must diffuse. Consequently, the reduction in permeability was dependent upon the amount of clay added as well as the extent of its exfoliation.

Tortora et al. [126] studied the reinforcement effect of polyurethane nanocomposites containing poly (ϵ -caprolactone) as done by Wei and co researcher. However, they replaced di(ethylene glycol) and their results showed that the nanocomposite became more brittle with increased clay content. The storage modulus increased with clay loading, particularly at temperatures above the soft segment T_g , and resultantly the material flow temperature increased by 50°C at 20 wt% clay loading as shown in **Figure 2.16** and **Figure 2.17**. Furthermore, although the elastic modulus increased by over 5-fold at 20 wt% loading, there was a significant reduction in strain hardening slope which indicated that the clay disrupted the soft segment mobility and alignment, reducing the strength and toughness of the material.

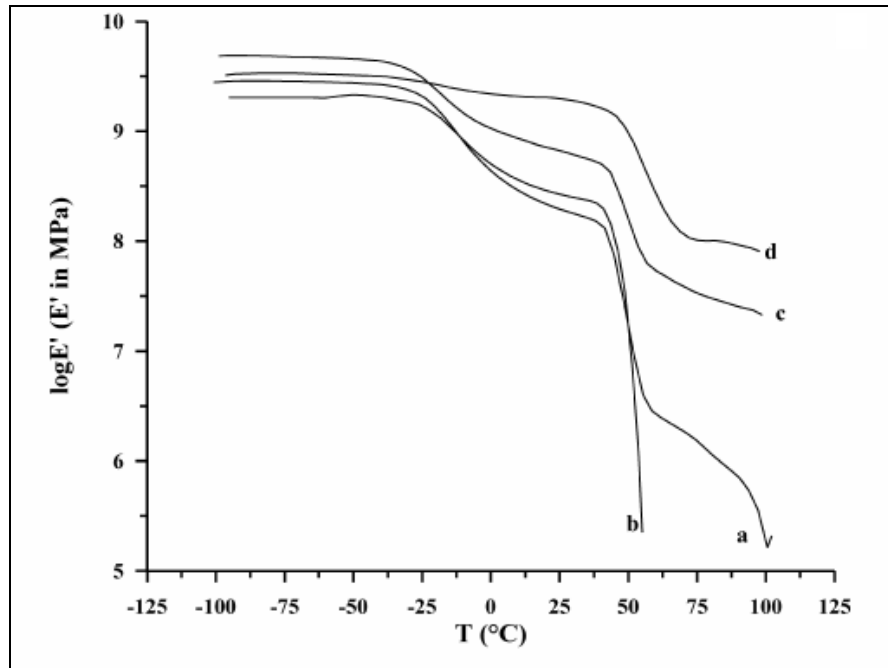


Figure 2.16: Log E' for (a) Pure Polyurethane (0%), (b) Polyurethane (4% of nanoclay), (c) Polyurethane (20% of nanoclay), (d) Polyurethane (40% of nanoclay) [126]

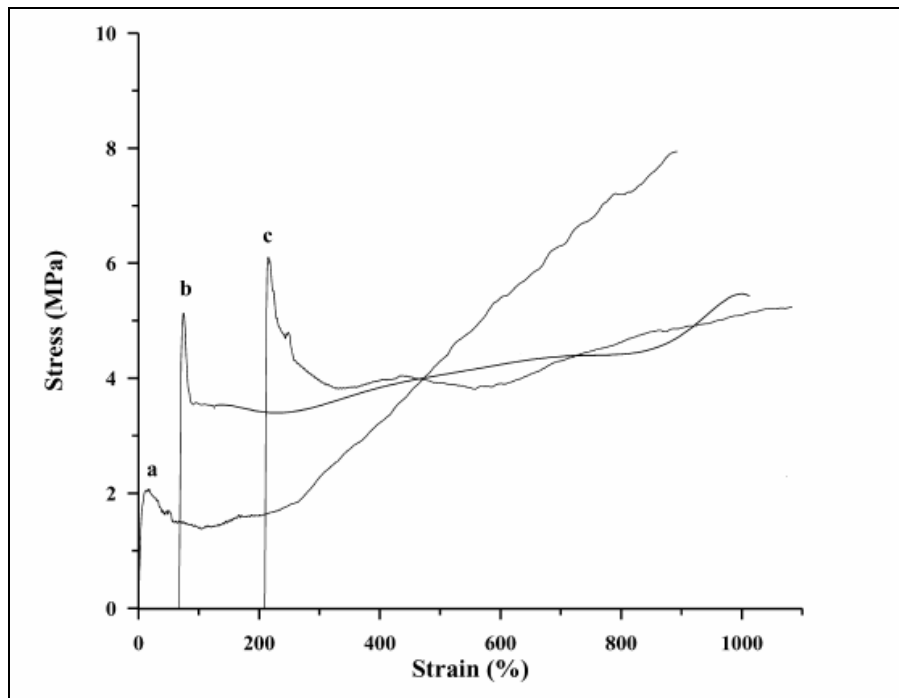


Figure 2.17: Stress-strain plots for (a) Polyurethane (0%), (b) Polyurethane (4% of nanoclay), and Polyurethane (20% of nanoclay). [126]

Osman et al [127] evaluated gas permeability of a polyurethane adhesive filled with montmorillonite modified by three ammonium ions. The montmorillonite was exchanged with organic cations that had either an aliphatic hydrocarbon nature, an aromatic moiety, or had a polarity that matched the polyurethane polarity. They found that water vapour permeability decreased by 40 – 50% at a 3 vol% clay loading for all three montmorillonite modifications. However, the oxygen permeability decreased by 30% at 3 vol% only.

Finnigan et al [128] studied the reinforcement effects of two different clay dispersal techniques which were melt and solution intercalation using a twin screw extruder. The polyurethane was synthesized using poly (tetramethylene oxide), 4,4'-methylene diphenyl diisocyanate, and 1,4-butanediol. Results showed that both of the techniques increased in the material stiffness and decreased the ultimate strength and extensibility.

In the same year, Song et al [110] published an interesting article in which they examined the evolution of the basal plane spacing of the clay or *d*-spacing in elastomeric polyurethane nanocomposite containing polypropylene glycol, methylene biscyclohexyl isocyanate, and 1,4-butanediol via wide angle x-ray diffraction during increasing cyclic mechanical deformations. They found that the *d*-spacing, the distance between the basal planes of the clay platelets, increased during deformation, but recovered to the original spacing upon release of the stretching force when the extent of deformation was within the elastic range. From the original state to ~ 200% strain the *d*-spacing of a 5 wt% filled nanocomposite increased from ~ 3.7 nm to ~ 4.4 nm. However, at strains greater than 200% the clay spacing exhibited less than a 0.2 nm increase as shown in **Figure 2.18**.

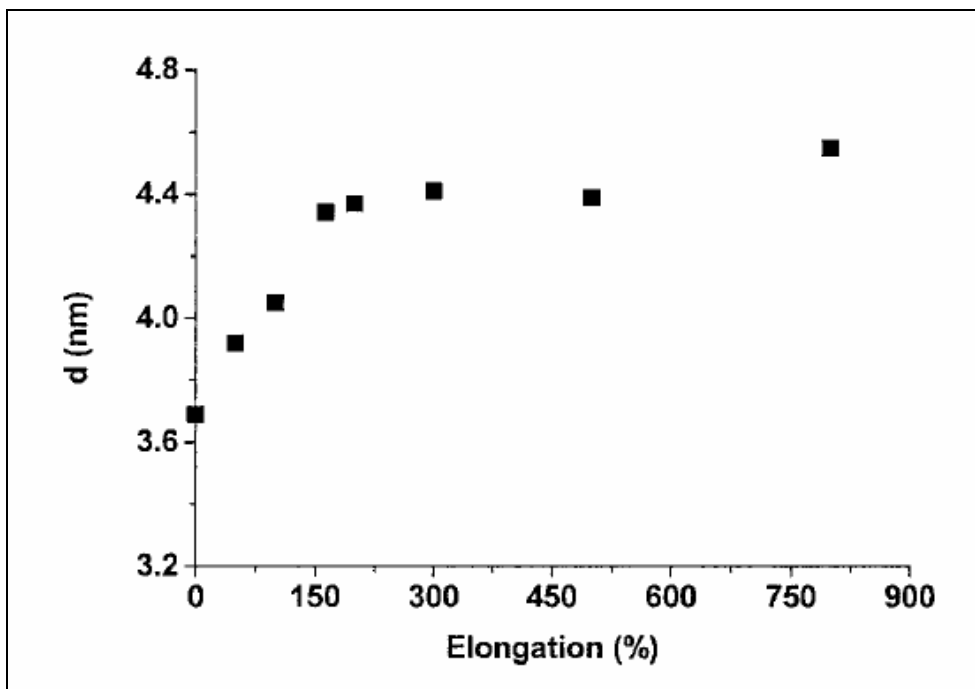


Figure 2.18: Plot of basal plane distance or d spacing versus elongation [110]

Song et al [110] also investigated the effect of organoclay on the morphology of PU using small-angle X-ray scattering and atomic force microscopy, they found that the inter-domain repeat distance decreased with the introduction of organoclay. The organoclay has a more significant effect on the inter-domain repeat distance at low hard segment content. Additionally, the hard segment, the inter-domain repeat distance and domain size increased markedly.

L. Song et al [111] investigated how the addition of montmorillonite in conjunction with melamine polyphosphate powder affects the flame retardance and mechanical properties of the polyurethane. Although the clay was intercalated, the tensile strength increased from 1.53 MPa to 3.85 MPa when 5 wt% clay was added with 6 wt% melamine polyphosphate. Thermogravimetric analysis on this same nanocomposite showed that the mass loss rate, the carbon monoxide, and carbon dioxide release amount, specific extinction area, and the heat release rate all decreased significantly, thereby increasing the material flame retardance.

2.6.2 Polyurethane Graphene Nanocomposites

(a) Electrical Conductivity

Electrically conducting composites produced by polymer and conductive fillers, such as graphite has been extensively studied in the past few decades. This kind of material can be introduced as antistatic coatings, electromagnetic shielding and various other applications. Nguyen et al [50] prepared a thermoplastic polyurethane (TPU)/functionalized graphene sheet (FSG) nanocomposite by suspended a mixture of TPU solution and FSG in methyl ethyl ketone (MEK). The FSG finely dispersed on nanoscale throughout the TPU matrix as shown in TEM images in **Figure 2.19**. A nanocomposite containing 2 parts of FSG per 100 parts of TPU had effectively enhanced an electrical conductivity by 10^{-4} Scm^{-1} , a 10^7 times increase over the pristine TPU. Ragu et al [129] used waterborne polyurethane (WPU) as a matrix with FSG and they found that WPU/FSG nanocomposite shows drastically improvement in the conductivity, about 10^5 times better than pristine WPU. Both of these results indicate that FSG is an effective filler that could be used in improving conductivity of polyurethane.

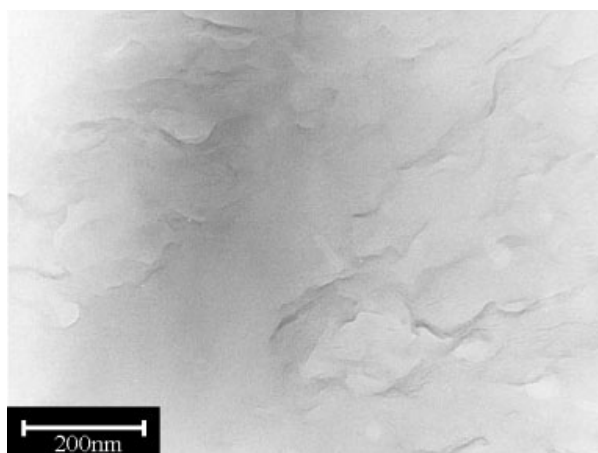


Figure 2.19: TEM images of thermoplastic polyurethane/FSG [50]

(b) Mechanical Properties

Incorporation of graphene into polymer matrix was successfully prepared. Cai et al [130] prepared graphite oxide nanoplatelets (GNOPs)/polyurethane composites using a solution method. With the incorporation of 4.4wt% of GNOPs, the Young's modulus and hardness of the PU were significantly increased by ~900% and ~327%, respectively. They concluded that the improvement in other properties such as scratch resistance made this material suitable as coating material.

Contrast to the findings by Ragu et al [129], at a small volume of FSG approximately less than 6wt%, the elastic modulus of WPU/FSG nanocomposites was found to be lower than the pristine WPU. They postulated the results were due to the softening effect of the reduced hard segment crystallinity in the presence of the FSG overwhelmed the reinforcing effect at a low FSG content. However at 6wt% of FSG, the modulus was higher than that of pristine WPU. In other polymer matrix, Yasmin et al [131] reinforced epoxy resin matrix with expanded graphite (EG) with concentration of 1-2wt%. They used a different processing technique in fabricating epoxy/EG nanocomposites in order to exfoliate EG in the epoxy matrix. It was found that after incorporating the EG in epoxy matrix, an elastic modulus showed dramatically to be improved compared to the neat epoxy and the shear mixing techniques provided the best exfoliation of graphite nanosheets in the matrix.

2.6.2 Polyurethane CNT Nanocomposites

(a) Electrical and Thermal Conductivity

Conductive fillers including carbon black and graphite have been used to enhance the electrical and thermal conductivities of polymers. Many reports showed that the addition of a small percentage of CNT to a polymer matrix greatly improves the thermal conductivity of the system [132,133]. Either by direct insertion or by

chemically functionalizing the CNT into polymer matrix [134], the systematic procedure was produced significant improvement in thermal properties of CNT/polymer nanocomposites. A percolation theory was created to explain the conductive mechanism of polymer composites, which reveals that the conductive pathway in polymer matrix formed by certain amount of conductive fillers can convert non-conductive polymers to be conductive. The critical amount of the fillers is called percolation threshold and this value is expected to be as low as possible to reduce the cost of the composites.

CNTs are highly conducting, and have a very low percolation threshold. Their conductivity has been shown to be a function of their chirality, the degree of twist as well as their diameter. Xu et al [135] fabricated PU foam by using water as blown agent in the presence of CNTs. In their work, the percolation threshold was valued by the density of the foam instead of filler concentration. The conductivity sharply increased with the increase of density from 0.03gcm^{-3} to 0.05gcm^{-3} . Xia et al [111] found that with the incorporation of 1 wt% SWNTs and MWNTs, the thermal conductivity of polyurethane improved by ~42% and ~21%, respectively.

(2) Mechanical Properties

The successful development of CNT/polymer-composites depends on many factors such as the type, size, and purity of CNTs. SWNTs have far better properties than MWNTs in term of high aspect ratio, modulus and strength.

There are two main issues of concern in gaining maximum potential and improvement of CNTs. These issues are the interfacial bonding and the dispersion of the individual CNTs in polymeric matrixes [136]. The former is related to the atomically smooth and non reactive surface of CNTs. The poor bonding extremely limits load transfer from CNTs to the matrix. Investigation focusing on the interfacial bonding has been performed by Wagner and co workers [137-138]. They performed pull-out experiments of individual carbon nanotubes embedded in a polymer matrix

with a specially developed test in order to evaluate the interfacial shear strength. The interfacial adhesion to the polymer can be enhanced by chemical functionalisation of the nanotube surface.

The dispersion of CNTs is another challenge for nanotube-reinforced polymers. CNT particles exhibit an enormous surface area which acts as interface for stress transfer. However, in certain situation, it is also responsible for the strong tendency to form aggregate into bundles of weakly interacting tubes by van de Waals attraction [139] which is absolutely harmful to the mechanical properties of composites. The aggregation of CNTs effectively reduces the aspect ratio of the reinforcement. Liao et. al. [140] overcomes this problem of aggregation by using tip sonication and addition of acetone. The mechanical properties of SWNT/SC-15 epoxy resin significantly improved by 50.8% in storage modulus. Li and co-workers [141], used a non-covalent functionalization method to produce “hybrid shish kebab” which is CNT periodically decorated with polymer lamellar crystals. This method seems to achieve homogeneous dispersion of CNTs without damaging their extraordinary properties.

Jana et al [116] reported on significant improvement of tensile strength and modulus with addition of MWNTs in polyurethane. However, elongation at break decreases as MWNTs were added, which could be due to additional physical entanglements between the polymeric chains and MWNTs that restrict the uncoiling of the chain. Xia et al [114] also reported huge improvement in mechanical properties after incorporating SWNTs into PU. SWNTs-g-PU has a remarkable effect on the Young’s modulus compared to pristine polyurethane. At 0.7wt% of SWNTs, the Young’s modulus of the nanocomposite was improved by ~278%. The remarkable reinforcing effects of SWNTs is related to better dispersion of SWNTs-PU and stronger interfacial interactions between the PU and SWNTs.

2.7 Conclusions

Although significant work has been done recently in synthesis and fabrication of polyurethane nanocomposites, the key method to achieve a good dispersion of nanofiller in polymer matrixes are still scientifically challenging. In an attempt to further understand the synthesis, processing, and the properties analysis of polyurethane nanocomposites, a selection of recent literature was chosen to highlight some of the issues related to the preparation, chemical and physical behaviour of composites with nano-sized reinforcement in comparison to traditionally micro-sized counterpart. However, comparative little information has emerged on this area especially on improving the dispersion of nanofiller in polymer matrix. The challenges are to determine the appropriate processing method as well as the good parameter i.e processing time, modifier, and suitable temperature that critically influences the interaction between nanofiller and matrix. This issue plays a major role and may offer an explanation to a significant improvement in mechanical properties of polymer nanocomposites.

References

1. Itagaki, T., Matsumura, A., Kato, M., Usuki, A., Kuroda, K., *J. Mater. Sci. Lett.* 2001, 20, 1483 – 1484
2. Xia, H., Shaw, S.J., Song, M., *Polym. Int.* 2005, 54, 1392 – 1400
3. Hussin, F., Hojjati, M., Okamoto, M., Gorga, R.E., *J. Compos. Mater.* 2006, 40, 1511 – 1575
4. Usuki, A., Kawasumi, M., Kojima, Y., *J. Mater. Res.* 1993, 18, 1174
5. Wetzel, B., Rosso, P., Hauptert, F., Friedrich, K., *J. Eng. Frac. Mech.* 2006, 73, 2375 – 2398
6. Schartel, B., Bartholmai, M., Knoll, U., *Polym. Adv. Technol.* 2006, 17, 772 – 777
7. Giannelis, E.P., *Appl. Organometal. Chem.* 1998, 12, 675 – 680
8. Sinha, R. S., Yamada, K., Okamoto, M., Ueda, K., *Polymer*, 2003, 44, 857 – 866
9. Lau, K.T., Hui, D., *Compos. B.* 2002, 33, 263 – 277
10. Thostenson, E.T., Ren, Z., Chou, T.W., *Compos. Sci. Technol.* 2001, 61, 1899 – 1912
11. Ajayan, P.M., Schadler, L.S., Giamaris, C., Rubio, A., *Adv. Mater.* 2000, 12, 750 – 753
12. Dalton, A.B., Collins, S., Munoz, E., Razal, J.M., Ebron, V.H., Ferraris, J.P., Coleman, J.N., Kim, B.G., Baughman, R.H., *Nature*, 2003, 423, 703 – 704
13. Vickery, J.L., Patil, V.J., Mann, S., *Adv. Mater.* 2009, 21, 2180 – 2184

14. Ivanyuk, A., Gerasin, V., Rebrov, A., Pavelko, R., Antipov, E., J. Eng. Phys. Thermophys. 2005, 78, 926 – 931
15. Zhong, Y., Janes, D., Zhang, Y., Hetzer, M., Kee, D.D., Polym. Eng. Sci. 2007, 47, 1101 – 1107
16. Shin, J., Kim, C., Geckeler, K.E., Polym. Int. 2009, 58, 579 – 583
17. Xia, H., Song, M., Polym. Int. 2006, 55, 229 – 235
18. Zeng, Q., Yu, A., Lu, G., Nanotechnology, 2005, 16, 2757 – 2763
19. Ganguli, S., Aglan, H., Dean, D., J. Elast. Plast. 2005, 37, 19 – 35
20. Ramanathan, T., Abdala, A.A., Stankovich, S., Dikin, D.A., Herrera-Alonso, M., Piner, R.D., Adamson, D.H., Schniepp, H.C., Chen, X., Ruoff, R.S., Nguyen, S.T., Aksay, I.A., Prud'homme, R.K., Brinson, L.C., Nature Nanotech. 2008, 3, 327 – 331
21. Gong, F.L., Zhao, C.G., Feng, M., Qin, H.L., Yang, M.S., J. Mater. Sci. 2004, 39, 293 – 294
22. Kim, H.S., Park, B.H., Yoon, J.S., Jin, H.J., Mater. Lett. 2007, 61, 2251 – 2254
23. K. Yusoh, J.Jin, M.Song, *Prog. Org. Coat.* 2010, 67, 220 – 224
24. D. Cai, K. Yusoh, M. Song, *Nanotechnology*, 2009, 20, 085712
25. Tien, Y., Wei, K. H. *Macromolecules*. 2001, 34, 9045
26. Hepburn, C., Polyurethane Elastomers, 1982, London, Applied Science Publishers

27. Pattanayak, A., Jana, S.C., *Polymer*, 2005, 46, 3275 – 3288
28. Njuguna, J., Pielichowski, K., *J. Mater. Sci.*, 2004, 39, 4081 – 4094
29. Sauder, J.H., Frish, K.C., *Polyurethanes chemistry and technology*, John Wiley & Sons, New York, 1964
30. Yao, K., *High performance polyurethane-organoclay nanocomposites*, PhD Thesis, Loughborough University, 2005
31. Aneja, A., *Structure-property relationship of flexible polyurethane foams*, PhD Thesis, Virginia Polytechnic Institute & State University, 2002
32. Oertel, G. *Polyurethane Handbook*, Hanser, New York, 1993
33. Chen, Y., Zhou, S., Yang, H., Gu, G., Wu, L., *J. Colloid. Inter. Sci.*, 2004, 279, 370 – 378
34. Szycher, M., *Szycher's handbook of polyurethanes*, CRC Press, Boca Raton, Florida, 1999
35. Lelah, M.D., Cooper S.L., *Polyurethanes in medicine*, CRC Press, Boca Raton, Florida, 1986
36. Chattopadhyay, D.K., Ragu, K.V.S.N., *Prog. Polym. Sci.* 2007, 32, 352 – 418
37. Grant, G.T., Taft, R.M., Wheeler, S.T., *J. Prosthet. Dent.* 2001, 85, 281 – 283
38. Lamba, N.M.K., Woodhouse, K.A., Cooper, S.A., *Polyurethanes in Biomedical Applications*. CRC Press, New York, 1998
39. Okamoto, M., *Mater. Sci. Technol.* 2006, 22, 756 – 79
40. Sinha, S.R., Okamoto, M., *Prog. Polym. Sci.* 2003, 28, 1539 – 1641

41. Sinha, S.R., Yamada, K., Okamoto, M., Ogami, A., Ueda, K., *Chem. Mater.*, 2003, 15, 1456
42. Krishnamoorti, R.K., Vaia, R.A., Gianellis, E.P., *Chem. Mater.*, 1996, 8, 1728
43. LeBaron, P.C., Wang, Z., Pinnavaia, T.J., *J. Appl. Clay Sci.*, 1999, 15, 11
44. Okada, A., Usuki, A., *Mater. Sci. Eng.: C3*, 1995, 109 – 115
45. Ogawa, M., Kuroda, K., *Chem. Rev.*, 1995, 95, 399
46. Koo, J.H., *Polymer nanocomposites, processing, characterization, and applications*, McGraw Hill, New York, 2006
47. Strawhecker, K.E., Manias, E., *Chem. Mater.*, 2000, 12, 2943 – 49
48. Ke, Y.C., Stroeve, P., *Polymer-layered silicate and silica nanocomposites*, Elsevier, Amsterdam, 2005
49. Gianellis, E.P., Krishnamoorti, R.K., Manias, E., *Advanced in polymer science, vol 138*, Springer Verlag, Berlin, 1999
50. Nguyen, D.A., Lee, Y.R., Raghu, A.V., Jeong, H.M., Shin, C.M., Kim, B.K., *Polym. Int.* 2009, 58, 412 – 417
51. Lee, C.G., Wei, X.D., Kysar, J.W., Hone, J., *Science* 2007, 321, 385 – 388
52. Avouris, P., Chen, Z.H., Perebeinos, V., *Nat. Nanotechnol.* 2007, 2, 605 – 615

53. Berger, C., Song, Z., Li, T., Li, X., Ogbazghi, A.Y., Feng, R., Dai, Z., Marchenkov, A.N., Conrad, E.H., First, P.N., de Heer, W.A., *J. Phys. Chem. B* 2004, 108, 19912 – 19916
54. Delgado, J.L., Herranz, M.A., Martin, N., *J. Mater. Chem.* 2008, 18, 1417 – 1426
55. Novoselov, K.S., Geim, A.K., Morozov, S.V., Jiang, D., Zhang, Y., Dubonos, S.V., Grigorieva, I.V., Firsov, A.A., *Science* 2004, 306, 666 – 669
56. Ando, Y., Zhao, X., Ohkohchi, M., *Carbon* 1997, 35, 153 – 158
57. Ebbesen, T.W., Ajayan, P.M., *Nature* 1992, 358, 220 – 221
58. Viculis, L.M., Mack, J.J., Kaner, R.B., *Science* 2003, 299, 1361
59. Stankovich, S., Dikin, D.A., Dommett, G.H.B., Kohlhass, K.M., Zimney, E.J., Stach, E.A., Piner, R.D., Nguyen, S.T., Ruoff, R.S., *Nature* 2006, 442, 282 – 286
60. Du, X., Yu, Z.Z., Dasari, A., Ma, J., Mo, M., Meng, Y., Mai, Y.W., *Chem. Mater.* 2008, 20, 2066 – 2068
61. Szabo, T., Szeri, A., Dekany, I., *Carbon* 2005, 43, 87 – 94
62. Niyogi, S., Bekyarova, E., Itkis, M.E., McWilliams, J.L., Hamon, M.A., Haddon, R.C., *J. Am. Chem. Soc.* 2006, 128, 7720 – 7721
63. Cai, D., Song, M., *J. Mater. Chem.* 2007, 17, 3678 – 3680
64. Iijima, S., *Nature*, 1991, 354, 56 – 58
65. Iijima, S., Ichihashi, T., *Nature*, 1993, 363, 603 – 605

66. Dai, H., *Acc. Chem. Res.*, 2002, 35, 1035 – 44
67. Kauffman, D.R., Star, A., *Chem. Inter. Ed.* 2008, 47 (35), 6550 – 70
68. Pradhan, B., Setyowati, K., Liu, H., Waldeck, D.H., Chen, J., *Nano Letters*, 2008, 8, 1142 – 1146
69. Li, Y.H., Zhao, Y.M., Roe, M., Furniss, D., Zhu, Y.Q., Silva S.R.P., Samll, 2006, 2 (8 – 9), 1026 – 30
70. Arami, H., Mazloumi, M., Khalifehzadeh, R., Emami, S.H., Sadrnezhaad, S.K., *Mater. Lett.* 2007, 61, 4412 – 15
71. Wang, Z., Xiao, H., *SAE IJMM*, 2009, 1, 631 – 640
72. Ebbesen, T.W., Ajayan, P.M., *Nature*, 1992, 358, 220 – 2
73. Zhao, X., Ohkohchi, M., Shimoyama, H., Ando, Y., *J. Crystal Growth*, 1999, 198/199, 934 – 8
74. Bethune, D.S., Klang, C.H., Devries, M.S., Gorman, G., Savoy, R., Vazquez, J., *Nature*, 1993, 363, 605 – 7
75. Guo, T., Nikolaev, P., Thess, A., Colbert, D.T., Smalley, R.E., *Chem, Phys. Lett.* 1995, 243, 49 – 54
76. Yudasaka, M., Komatsu, T., Ichihashi, T., Iijima, S., *Chem. Phys. Lett.* 1997, 278, 102 – 6
77. Yudasaka, M., Yamada, R., Sensui, N., Wilkins, T., Ichihashi, T., Iijima, S., *J. Phys. Chem. B*, 1999, 103, 6224 – 9
78. Yudasaka, M., Ichihashi, T., Iijima, S., *J. Phys. Chem. B*, 1998, 102, 10201 – 7

79. Gorbunov, A.A., Friedlein, R., Jost, O., Golden, M.S., Fink, J., Pompe, W., Appl. Phys. A: Mater. Sci. Process, 1999, 69, S593 – 6
80. Yudasaka, M., Komatsu, T., Ichihashi, T., Iijima, S., Chem. Phys. Lett. 1997, 278, 102 – 6
81. Dillon, A.C., Parilla, P.A., Alleman, J.L., Perkins, J.D., Heben, M.J., Chem. Phys. Lett. 2000, 316, 13 – 8
82. Tibbetts, G.G., Devour, M.G., Rodda, E.J., Carbon, 1987, 25, 367 – 75
83. Kong, J., Cassell, A.M., Dai, H., Chem. Phys. Lett. 1998, 292, 567 – 74
84. Hafner, J.H., Bronikowski, M.J., Azamian, B.R., Nikolaev, P., Rinzler, A.G., Colbert, D.T., Chem. Phys. Lett. 1998, 296, 195 – 202
85. Dai, H., Rinzler, A.G., Nikolaev, P., Thess, A, Colbert, D.T., Smalley, R.E., Chem. Phys. Lett. 1996, 260, 471 – 5
86. Cheng, H.M., Li, F., Su, G., Pan, H.Y., He, L.L., Sun, X., Appl. Phys. Lett. 1998, 72, 3282 – 4
87. Su, M., Zheng, B., Liu, J., Chem. Phys. Lett. 2000, 322, 321 – 326
88. Parfitt, R.L., Greenland, D.J., Clay Miner. 1970, 8, 305 – 315
89. Dennis, H.R., Hunter, D.L., Chang, D., Kim, S., White, J.L., Cho, J.W., Paul, D.R., Polymer, 2001, 42, 9513 – 9522
90. Ko, M.B., Jho, J.Y., Polym. Bull. 2001, 46, 315 – 322
91. Rao, Y.Q., Pochan, M., Macromolecules, 2007, 40, 290 – 296

92. Pinavaia, T.J., Beall, G.W., *Polymer – clay nanocomposites*, John Wiley & Sons, West Sussex, 2001
93. Dai, X., Xu, J., Guo, X., Lu, Y., Shen, D., Zhao, N., Luo, X., Zhang, X., *Macromolecules*, 2004, 37, 5615 – 23
94. Han, B., Cheng, A., Ji, S., Wu, S., Shen, J., *J. Appl. Polym. Sci.*, 2004, 91, 2536-2542
95. Jeon, H., Jung, H., Lee, S., Hudson, S., *Polym. Bulletin*, 1998, 41, 107 – 113
96. Koerner, H., Liu, W., Alexander, M., Mirau, P., Dowty, H., Vaia, R.A., *Polymer*, 2005, 46, 4405 – 20
97. Xu, M., Zhang, T., Gu, B., Wu, J., Chen, Q., *Macromolecules*, 2006, 39, 3540 – 45
98. Dufresne, A., Paillet, M., Putaux, J.L., Canet, R., Carmona, F., Delhaes, P., Cui, S., *J. Mater. Sci.*, 2002, 37, 3915 – 23
99. Regev, O., El Kati, P.N.B., Loos, J., Koning, C.E., *Adv. Mater.* 2004, 16, 248 – 251
100. Grunlan, J.C., Mehrabi, A.R., Bannon, M.V., Bahr, J.L., *Adv. Mater.* 2004, 16, 150 – 153
101. Vaia, R.A., Ishii, H., Gianellis, E.P., *Chem. Mater.* 1993, 5, 1694 – 6
102. Vaia, R.A., Gianellis, E.P., *Macromolecules*. 1997, 30, 8000 – 9

103. Vaia, R.A., Jandt, K.D., Kramer, E.J., Giannelis, E.P.,
Macromolecules, 1995, 28, 8080 – 5
104. Vaia, R.A., Giannelis, E.P., Macromolecules, 1997, 30, 7990 – 9
105. Chen, W., Tao, X., Liu, Y., Comp. Sci. Tech. 2006, 66, 3029 – 34
106. Zhang, R., Dowden, A., Deng, H., Baxendale, M., Peijs, T., Comp.
Sci. Tech. 2009, 69, 1499 – 1504
107. Usuki, A., Kawasumi, M., Kojima, Y., Okada, A., Kurauchi, T.,
Kamigaito, O., J. Mater. Res. 1993, 8, 1174 – 1178
108. Fornes, T.D., Paul, D.R., Polimeros: Ciencia e Tecnologia, 2003, 13,
212 – 217
109. Yao, K.J., Song, M., Hourston, D.J., Luo, D.Z., Polymer, 2002, 43,
1017 – 20
110. Song, M., Yao, K.J., Mater. Sci. Technol. 2004, 20, 989 -92
111. Song, L., Hu, Y., Tang, Y., Zhang, R., Chen, Z.Y., Fan, W.C., Polym.
Degrad. Stab. 2005, 87, 111 – 116
112. Moon, S.Y., Kim, J.K., Nah, C., Lee, Y.S., Eur. Polym. J. 2004, 40,
1615 – 21
113. Yoo, H.J., Jung, Y.C., Sahoo, N.G., Cho, J.W., J. Macromol. Sci. B.
Phys. 2006, 45, 441 – 51
114. Xia, H., Song, M., J. Mater. Chem., 2006, 16, 1843 – 1851
115. Xia, H., Song, M., Jin, J., Chen, L., Macromol. Chem. Phys. 2006,
207, 1945 – 1952

116. Jana, R.N., Yoo, H.J., Cho, J.W., *Fibers and Polymers*, 2008, 9, 247 – 254
117. Kojima, Y., Usuki, A., Kawasumi, M., Fukushima, Y., Okada, A., Kurauchi, T., Kamigaito, O., *J. Mater. Res.* 1993, 31, 2493 – 8
118. Wang, Z., Pinnavaia, T.J., *Chem. Mater.* 1998, 10, 1820 – 1826
119. Zilg, C., Thomann, R., Mulhaupt, R., Finter, *Adv. Mater.* 1999, 11, 49-52
120. Chen, T.K., Tien, Y.I., Wei, K.H., *J. Polym. Sci., Part A: Polym. Chem.* 1999, 37, 2225 – 33
121. Chen, T.K., Tien, Y.I., Wei, K.H., *Polymer*, 2000, 41, 1345-53
122. Tien, Y.I., Wei, K.H., *Macromolecules*, 2001, 34, 9045 – 52
123. Tien, Y.I., Wei, K.H., *Polymer*, 2001, 42, 3213-3221
124. Tien, Y.I., Wei, K.H., *J. Appl. Polym. Sci.* 2002, 86, 1741 – 48
125. Xu, R.J., Manias, E., Snyder, A.J., Runt, J., *J. Biomed. Mater. Res. Part A*, 2003, 64A, 114 -9
126. Tortora, M., Gorrasi, G., Vittoria, G., Galli, G., Ritrovati, S., Chiellini, E., *Polymer*, 2002, 43, 6147 – 57
127. Osman, M.A., Mittal, V., Morbidelli, M., Suter, U.W., *Macromolecules*, 2003, 36, 9851 – 9858
128. Finnigan, B., Martin, D., Halley, P., Truss, R., Campbell, K., *Polymer*, 2004, 45, 2249 – 2260
129. Raghu, A.V., Lee, Y.R., Jeong, H.M., Shin, C.M., *Macromol. Chem. Phys.* 2008, 209, 2487 – 2493
130. Cai, D., Yusoh, K., Song, M., *Nanotechnology* 2009, 20, 085917

131. Yasmin, A., Luo, J.J., Daniel, I.M., *Compos. Sci. Technol.* 2006, 66, 1182 – 1189
132. Zheng, Q., Jiang, Q., *Phys. Rev. Lett.* 2002, 88, 045503
133. Biercuk, M., *Appl. Phys. Lett.* 2002, 80, 2767 – 2769
134. Padgett, C.W., Brenner, D.W., *Nanoletters*, 2004, 4, 1051 – 1053
135. Xu, X.B., Li Z.M., Shi, L., Bian, X.C., Xiang, Z.D., *Small*, 2007, 3, 408 – 11
136. Fiedler, B., Gojny, F.H., Wichmann, M.H.G., Nolte, M.C.M., Schulte, K., *Comp. Sci. Tech.* 2006, 66, 3115 – 25
137. Wagner, H.D., Lourie, O., Feldman, Y., Tene, R., *Appl. Phys. Lett.* 1998, 72, 188 – 190
138. Barber, A.H., Cohen, S.R., Wagner, H.D., *Appl. Phys. Lett.* 2003, 82, 4140 – 42
139. Li, X., Gao, H., Scrivens, W.A., Fei, D., Xu, X., Sutton, M.A., Reynolds, A.P., Myrick, M.L., *Nanotechnology*, 2004, 15, 1416 – 23
140. Liao, Y.H., Tondin, O.M., Liang, Z., Zhang, C., Wang, B., *Mater. Sci. Eng. A* 2004, 385, 175 – 181
141. <http://meetings.aps.org/link/BAPS.2005.MAR.C1.196>

Chapter 3

Experimental

3.1 Introduction

In order to understand the effect of incorporation of nanofiller on the viscoelastic behaviour and the mechanical properties of polyurethane, a series of experiments were designed and conducted.

3.2 Raw Materials

3.2.1 Isocyanate

In this research, two types of isocyanate were used for the preparation of the polyurethane samples. One was HMDI, and the other was MDI. The details are shown in Table 3.1.

Table 3.1: Properties of Hydrogenated MDI

4,4'-methylene bis (cyclohexyl isocyanate)	
Commercial name	HMDI or Hydrogenated MDI
Molecular formula	OCN-C ₆ H ₁₀ -CH ₂ -C ₆ H ₁₀ -NCO
Molecular weight	262
Equivalent weight	262/2 = 131
Appearance	Colourless liquid
Density (at 20°C)	1.066 g/cm ³
Flash point	>110°C

The particular prepolymer used in the research was the addition product of modified MDI, to the prepolymer intermediate. The dihydric glycol must be linear and reacted with the MDI [1], which was commercially produced by hyperlast Ltd (UK). Its related parameters are shown in Table 3.2.

Table 3.2: Properties of Modified MDI

Appearance (25 °C)	Colourless liquid at 25 °C
NCO content (%)	23 %
Viscosity (25 °C)	120 – 180 mPas
Specific gravity (25 °C)	1.21-1.23

The MDI is much more environment's friendly, and has lower toxicity than toluene diisocyanate (TDI) and many other isocyanates.

3.2.2 Polyols

A polyol is an organic compound having more than one hydroxyl (-OH) group per molecule [2]. In the polyurethane industry, the term includes polymeric compounds containing alcoholic hydroxyl groups such as polyesters, and polyesters, used as reactants in polyurethane synthesis. In this experiment, a polyether polyol was chosen as a soft segment. The polyether polyol was supplied by Elastogran (UK) and the details are shown in Table 3.3.

Table 3.3: Properties of polypropylene glycol

Polypropylene glycol	
Commercial name	Lupranol 2090
Appearance	Colourless liquid
Molecular weight	6000
OHV	28 mgKOH/g
Viscosity (25 °C)	1125 mPa.s
Functionality	3
Structure	$\begin{array}{l} \text{CH}_2 - [\text{O} - \text{CH}_2 - \text{CH}(\text{CH}_3)]_m - \text{CH}_2\text{CH}_2 - \text{OH} \\ \\ \text{CH} - [\text{O} - \text{CH}_2 - \text{CH}(\text{CH}_3)]_n - \text{CH}_2\text{CH}_2 - \text{OH} \\ \\ \text{CH}_2 - [\text{O} - \text{CH}_2 - \text{CH}(\text{CH}_3)]_l - \text{CH}_2\text{CH}_2 - \text{OH} \end{array}$

3.2.3 Chain Extender

Some low molecular weight reactants are named as chain extenders in the polyurethane industry [1]. One of the most important chain extender is 1,4-Butanediol. The function of chain extender is to extend the chain of soft segment in polyurethane synthesis. In this experiment, the chain extender, 1,4-butanediol is used and was supplied by the Aldrich company. The details are shown in Table 3.4.

Table 3.4: Properties of 1-4-butanediol

1-4-Butanediol	
Commercial name	1-4-Butanediol
Appearance	Colourless liquid
Molecular weight	90
Equivalent weight	$90/2 = 45$
Melting point	16 °C
Flash point	230 °C
Structure	HO-(CH ₂) ₄ -OH

3.2.4 Catalysts

A catalyst is substance that cause, or accelerates, a chemical reaction when added to the reactants in a small amount, and it is not consumed in the reaction. There are two catalysts used in this research. One is DABCO-33LV which is the mixture of triethylenediamine and di(propylene glycol) and it was supplied by Air Products and Chemicals, Inc. The other is stannous-2-ethylhexanoate and was supplied by the Sigma Chemical.

3.2.5 Nanofillers

There are several kinds of nanofillers used in this research. The main nanofiller are organoclays (Cloisite C20 and Cloisite B30), graphite oxide, and carbon nanotubes (MWNTs and SWNTs). Both of these clays were supplied by the Nanocor Company (USA), Graphene was purchased from Chinese Qingdao Graphite Company, and commercialized CNTs were purchased from Chengdu Organic Chemistry Co. Ltd (China).

The details of organoclay used are shown in Table 3.5 and Table 3.6 [3].

Table 3.5: Properties of cloisite C20

Cloisite C20	
Commercial name	Cloisite 20A
Organic modified	Dimethyl, dehydrogenated tallow, quaternary ammonium (2M2HT)
CEC	95 meq/100g
Moisture	<2 wt%
Density	1.77 g/cm ³
Colour	Off white
X-ray data	d ₀₀₁ = 24.2Å
Structure	$ \begin{array}{c} \text{CH}_3 \\ \\ \text{CH}_3 - \text{N}^+ - \text{HT} \\ \\ \text{HT} \end{array} $ <p>HT – Hydrogenated Tallow</p>

Table 3.6: Properties of cloisite B30

Cloisite B30	
Commercial name	Cloisite 30B
Organic modified	methyl, tallow, bis-2-hydroxyethyl, quaternary ammonium (MT2EtOH)
CEC	90 meq/100g
Moisture	<2 wt%
Density	1.98 g/cm ³
Colour	Off white
X-ray data	d ₀₀₁ = 18.5Å
Structure	$ \begin{array}{c} \text{CH}_2\text{CH}_2\text{OH} \\ \\ \text{CH}_3 - \text{N}^+ - \text{T} \\ \\ \text{CH}_2\text{CH}_2\text{OH} \\ \\ \text{T} - \text{Tallow} \end{array} $

3.3 Preparation of polyurethane nanocomposite

(1) Polyurethane Organoclay Nanocomposites

Polyol dispersions containing 0, 1, 3 and 5 wt% of the organoclay was prepared by dispersing the corresponding amount of the clay in polyether polyol. The mixture of polyether polyol 2090 and the organoclay was, first, blended at 80°C and stirred for 4 hours. Then the mixtures were degassed under vacuum for 20 minutes. 100g of the mixture was blended with 2.25g of 1,4-butanediol, 0.75g of DABCO-33LV, 0.75g of stannous 2-ethyl hexanoate and 15.5 g of 4-4'-methylene bis (cyclohexyl isocyanate) at room temperature and stirred for 1 minutes and was vacuum degassed for 3-5 minutes. Then the viscous prepolymer was poured into an O-ring mould and cured at 50°C for another 24 hours to obtain a thin film. Finally, the sample was post-cured for a week at 80 °C [4].

(2) Polyurethane Graphite Oxide Nanocomposites

Graphite oxide was prepared using the oxidation of expandable graphite (EG) and it was conducted following the procedure. 2.5g EG was mixed with 57.5 ml concentrated H_2SO_4 in ice bath (0C) for half an hour. 7.5g $KMnO_4$ was slowly added into the mixture in order to keep the temperature of the mixture below 20°C. The mixture was then heated to 35°C and kept stirring for 30 minutes. Dropwise addition of 115ml distilled water caused the temperature increase to 98°C. The reaction was kept at this temperature for 15 minutes. Finally, the oxidation reaction was terminated by the addition of 350ml distilled water and 25 ml 30% H_2O_2 solution. Collection of the EGO by filtering and successive washing with 5% HCl aqueous solution was repeated by three times until there was no sulphate detected by $BaCl_2$ solution. The EGO was dried at 50°C under vacuum for one week. The exfoliation of 100 mg EGO in 10 g DMF was achieved using ultrasonication with a power of 300 W for 30 minutes at room temperature. 6 g PPG-4000, 1.5 g PPG-6000, 0.8 g BDO, 3.89 g MDI and 0.11 g DBTL (catalyst) were stirred in DMF at 60°C for 24 hours in a four-necked flask protected by N_2 , by which PU/DMF solution was finally obtained with 40 wt% solid content. Afterward, the calculated amount of the GNOP/DMF dispersion was mixed with the PU/DMF solution at 80°C for another 1 hour. The two-week drying at 50°C was the last step for the preparation of the GNOP/PU composites.

(3) Polyurethane CNT Nanocomposites

Both MWNTs and SWNTs were provided by Chengdu Institute of Organic Chemistry, Chinese Academy of Sciences. The as-grown MWNTs and SWNTs were produced by CCVD, in which CH_4 or C_2H_2 were converted into CNTs at 700 and 1000°C in presence of a Ni-La $2O_3$ catalyst. The diameter of MWNT and SWNT was at 8-15 nm, and 1-2 nm respectively. The product were washed with concentrated HCl to remove the catalyst and the carrier of catalyst, and then were purified with concentrated HNO_3 to remove the amorphous carbon particles. In preparation of stable polyol-CNTs dispersions, 194 g of polyol, 4 g of MWNTs or SWNTs and 2 g of dispersion agent BYK 9077 were blended and stirred at 600 rpm for 4 hours at 80C. Then to prepare the PU-CNTs nanocomposites, 20g of

polyol-CNT dispersion was blended with 0.89g of 1,4-butanediol, 5.93 g of MDI and 0.03 g of Dabco-33LV at room temperature for 2 minutes and was vacuum-degassed for 3-5 minutes to remove the bubbles. Then the viscous prepolymer was poured into an O-ring metal mould and cured at 50°C for 24 hrs and 80°C for one week to obtain PU-CNT nanocomposites.

3.4 Characterization

3.4.1 Wide angle X-ray diffraction (WAXD)

X-ray diffraction depends on to spacings between the scattering bodies and wavelength of the incident radiation. Bragg's law indicates that diffraction is only observed when a set of planes make a very specific angle with the incoming x-ray beam. This angle depends on the inter-plane spacing, d , which itself depends on the size of the molecules which make up the structure. Bragg equation gives rise to a maximum at a particular diffraction angle, θ . Positions of diffraction spots and Bragg's law give the size of the unit cell of the crystal being studied. The intensity maxima give the atomic positions within the crystal lattice.

Wide angle X-ray diffraction is a most straightforward method to evaluate the spacing between the clay layers [5,6]. From the experiments, the diffraction angle 2θ was obtained. According to Bragg's law, the gallery distance of the clay can be calculated as follow;

$$n\lambda = d \sin \theta \quad (3.1)$$

X-ray diffraction experiments were performed on sheet or powder sample using a Bruker X-ray diffractometer (AXS D8 Advance) using Cu K α ($\lambda = 0.154\text{nm}$) radiation. The organoclay powders were mounted on the sample holder with a large cavity and smooth surface was obtained by pressing the powders with a glass plate. The polyurethane nanocomposite sheets produced during a moulding process had a fairly smooth surface. Therefore, disc shaped specimens (50 mm in diameter, 2 mm thick) were cut from these sheet and were directly analyzed by WAXD. The samples were scanned at a rate 0.24 $^\circ$ /min from ca. 1 $^\circ$ to 25 $^\circ$ in the angle 2θ .

3.4.2 Transmission Electron Microscope (TEM)

TEM is an electron-optical microscope that uses electromagnetic lenses to focus and direct an electron beam as shown in Figure 3.1 [7]. Data collected from the beam after it passes through the sample. The reason for using an electron beam instead of a light beam is that electrons have a shorter wavelength than photons. Resolution and magnification of a microscope are related to the wavelength and the energy of the radiation. In general, the shorter is the wavelength, the better is the resolution. The source radiation is generated using an electron gun. The resulting beam of electrons is focused into a tight coherent beam by multiple electromagnetic lenses and apertures. The lens system is designed to eliminate stray electrons as well as to control and focus the electron beam.

Basically, the electron gun produces thermal electrons. These electrons are accelerated by applying high voltage to form an electron beam. The electron beam is then focused on penetrates the specimen. Additional electrostatic and/or electromagnetic lenses are used in order to form the image which can be observed on a fluorescent screen or recorded photographically.

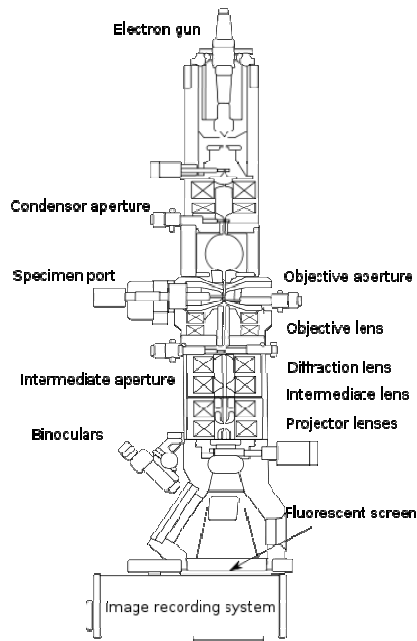


Figure 3.1: Principle of Transmission Electron Microscope [7]

TEM samples were cut from polyurethane nanocomposites blocks using an ultramicrotome with a diamond knife at liquid nitrogen conditions. Thin specimens were collected in a through filled with water and they placed on 400mesh copper grids. The analysis was conducted using a JEOL 2100 FX instrument.

3.4.3 Scanning Electron Microscope (SEM)

A schematic representation of the scanning electron microscope is shown in Figure 3.2 [7]. The electrons are accelerated in a potential difference typically of the order of 10-20 keV, and the magnetic lenses form an electron spot of a size of the order of a few nm. When the energetic electrons hit the surface under investigation, secondary electrons are emitted, some incident electrons are being backscattered, x-rays are emitted and a current is measured to the sample. The scanning electron microscope is a device which forms images of microscopic surface regions at magnification normally range of being x20 to x100000 depending on the type of specimen and the construction of the instrument. The principle of SEM includes there parts, 1) an electron gun and a means of focusing a beam of electron on the specimen, 2) a system of electron magnetic lenses used to demagnify the electron beam diameter to 5 – 10 nm across the specimen, and 3) a means of detecting the response from the specimen and a display system. For polyurethane nanocomposites, the SEM micrographs were taken using LEO 1530VP instrument. Samples were prepared from the fracture surfaces of the polyurethane nanocomposites. The room temperature fracture surfaces were investigated. These surfaces were sputted with gold to provide an electrically conductive layer, to suppress surface charge, to minimize radiation damage and to increase electron emission. The coating is intended to be a thin in-situ replica of the specimen surface. The thickness and the texture of the coating have to be minimized for fine surface texture and high resolutions.

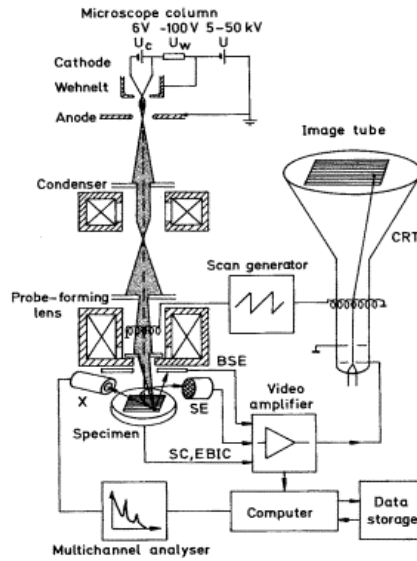


Figure 3.2: Principle of Scanning Electron Microscope [7]

3.4.4 Viscometer

The viscosity of raw materials is very important for processing. The viscosity of the liquid polyol-clay mixture was determined by a Haake VT500 instrument with a Haake K20 circulator. Shear rate was in the range from 4.45 s^{-1} to 266.7 s^{-1} [8]. Temperature for the measurement was in the range from 25°C to 80°C .

3.4.5 Creep Test

Creep test was performed at 30 C on a TA Instruments Thermal Analyzer DMA Q800. A small preload of 0.2 N was applied to make sure that the sample was taut. The samples were displaced at a stress of 0.2 MPa for 120 minutes and then were recovered for 60 minutes. The strain and creep compliance, $J(t)$ was recorded. The creep ratio was defined $(J_e - J_0) / J_0$, where $J_0 =$ the initial creep compliance, and $J_e =$ the equilibrium creep compliance.

3.4.6 Nanoindentation

Although significant progress in the reinforcement of nanofillers in polymer matrices has been made, their dispersion and load transfer mechanisms are still

very far from conclusions. The extremely tiny dimensions of nanofillers normally in the range of nanometre size and dimensions imposed a tremendous challenge for experimental equipment to characterize their functions in a polymer matrix. Conventional tensile tests have been extensively used to study the elastic/plastic deformation behaviour and mechanical properties of nanofiller reinforced polymer composites. However, because of the load and displacement resolution limitations of macroscopic tensile testers, the observations of the stress behaviour at the micro/nanoscale are relatively impossible [9]. In addition, fabrication of a tensile test specimen may introduce surface flaws and surface stress/strain concentration on the tensile specimen, making it difficult to study the mechanical properties and deformation behaviour at the micro/nano level [10]. It has been identified that the nanoindentation technique is the most accurate method for evaluation of the effect of nanofillers on the mechanical properties and deformation behaviour [9].

All nanoindentation experiments were performed using a fully calibrated Nano TestTM (Micro Materials, UK). A Berkovich (three sided pyramidal) diamond indenter tip manufactured by Micro Materials was used and a schematic diagram of the nanotest system is shown in Figure 3.3. The sample was cut with dimension of 10 mm x 5 mm x 1 mm. The specimen was mounted onto the nanoindentation sample stub using a suitable adhesive. All tests were conducted at room temperature. Typical experimental indentation parameters used for all measurements were as follows;

Initial load : 0.15 mN

Maximum load for all indents : 2.5 mN

Loading and unloading rate (strain rate): 0.05 mN/s

Dwelling time or holding time at maximum load : 180 s

The most common use of nanoindentation is for the measurement of elastic modulus and hardness as well as other mechanical parameters such as creep, residual stress and scratch. The basic concepts of indentation testing involve pressing a material with the indenter tip. During a typical nanoindentation test, force and displacement are recorded and the responses of interest are the load-displacement curves such as shown in Figure 3.4. The variation of load-

displacement usually reflects different mechanical properties of the materials. The hardness and modulus calculations were done according to Oliver and Pharr method [11].

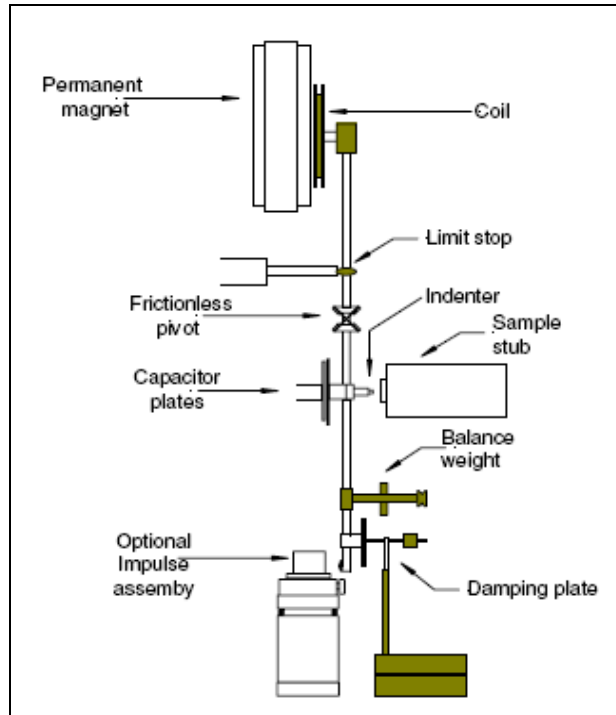


Figure 3.3: Schematic of the nanotest system [12].

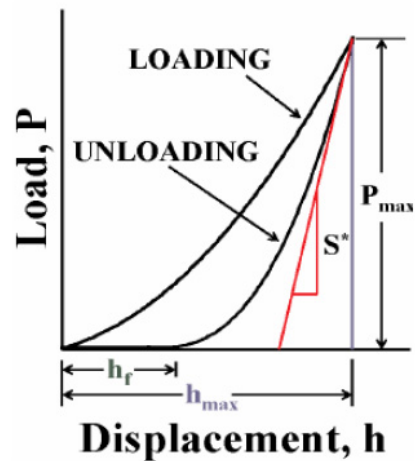


Figure 3.4: A typical indentation load-displacement curve. P_{\max} and H_{\max} are the maximum load and displacement, respectively. S^* is the slope of the tangent to the maximum load on the unloading curve [9].

3.4.7 Indentation Creep Test

The surface mechanical properties of the PU/organoclay nanocomposites were determined by Nano Test System from Micro Materials, UK. Measurements were accomplished by imposing a pendulum-based depth-sensing system with the sample mounted vertically and the load applied electromagnetically. The tests were carried out on cross-sections of the samples at initial load of 0.15mN to maximum load of 2.5mN. A loading rate of 0.5mN/s was maintained during the incremental increase of the load until the indenter reached the maximum depth into the surface. The load was then held for 180s in order to account for creep effects before the indenter was unloaded. The distance between the indentations was 250 μ m to avoid overlapping. **Figure 3.5** shows the schematic diagram of the nanoindentation procedure for creep experiment.

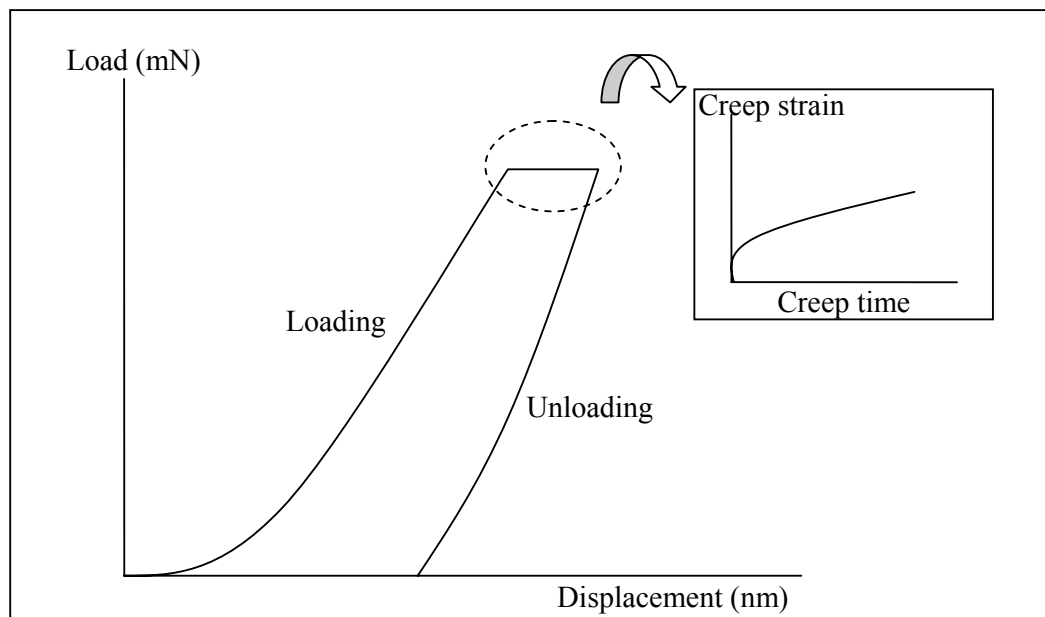


Figure 3.5: Schematic diagram of the creep experiment by nanoindentation

3.4.8 Nanoscratch Test

The nanoscratch test involves moving a sample (on sample stub) while being in contact with the diamond tip. All single-pass nanoscratch tests were performed over the square shaped sample surface with a thickness of ~1mm at ambient

temperature and using the same nanoindentation equipment with a Berkovich pyramidal diamond indenter of a tip radius of 50nm and an included angle of 60°C. In this test, the specimen was fixed on the sample stub and the scratch load and length were 5mN and 100µm at the various scratch rates and scratch velocities, respectively.

References

1. Hepburn, C., *Polyurethane Elastomers*, 1982, London, Applied Science Publishers
2. Szycher, M., *Szycher's Handbook of Polyurethanes*. 1999, Boca Raton, CRC Press
3. MSDS, from *www.scprod.com*
4. Yao, K.J., Song, M., Hourston, D.J., Luo, D.Z., *Polymer*, 2002, 43, 1017 – 1021
5. Kakudo, M., Kasai, N., *X-Ray Diffraction by Polymer*. 1972, Tokyo, Kodansha Ltd
6. Ward I.M., Hadley, D.W., *An Introduction the Mechanical Properties of Solid Polymers*. 1995, Chichester, John Wiley & Sons
7. Sperling, L.H., *Introduction to Physical Polymer Science*. 1992, New York, Jon Wiley & Sons Inc
8. Amerlinckx, S., van Dyck, D., van Landyt, J., van Tendeloo, G., (Eds). *Electron Microscopy: Principles and Fundamentals*. 1997, Amsterdam, Wiley-VCH
9. Dutta, A.K., Penumadu, D., Files, B., *J Mater Res*. 2004, 19, 158 – 164

10. Li, X., Gao, H., Scrivens, W.A., Fei, D., Xu, X., Sutton, M.A., Reynolds, A.P., Myrick, M.L., *Nanotechnology* 2004, 15, 1416 – 1423
11. Pharr, G.M., Oliver, W.C., *J. Mater. Res.* 1992, 7, 1565 – 1566
12. Dhakal, H. N., Zhang, Z. Y., Richardson, M.O.W., *Polymer Testing*. 2006, 846 – 852

Chapter 4

Rheological Behaviour of Polyol/Nanofiller Mixtures

4.1 Introduction

Polymer nanocomposites have attracted much attention in academic and industrial, as it is possible to achieve impressive enhancements of properties compared to pure polymer [1-3]. In general, the preparation of high performance polymer nanocomposites is very crucial stage especially in controlling the dispersion of the nanofillers when the filler is added in a polymer matrix. Homogeneous dispersion of nanofillers is not easily obtained. Several approaches have been studied such as surface modification of nanofillers through ion exchange reactions, and polymer grafting [4,5], mechanical-assisted processing such as ultrasonication [6], pre-polymerization of monomer in presence of nanofillers especially in in-situ polymerization [7-9], and colloidal-physics method [10-11] in order to overcome this problem. Among these approaches, pre-polymerization is very effective steps due to the polymerisation of the corresponding monomers especially in the galleries of the organoclay. The enthalpy evolved during the inter-gallery polymerisation provides an essential contribution to the exfoliation [12]. Pinnavaia discovered that a balance between the extent of the intra-gallery and extra-gallery polymerisation is a key factor [13]. It determines the structure of clay in an epoxy matrix [13]. Generally, in situ polymerisation includes two stages of process. First, the mixing of polymer precursor or monomer and nanofiller, and the second is in situ polymerisation in the presence of the nanofiller. In-situ polymerization is understood to be responsible for the exfoliation and intercalation of clay and CNTs in polymer nanocomposites. The viscosity of the polymer/nanofiller dispersions is important for the in-situ formation of polymer nanocomposites.

Much attention has been concentrated on the dispersing of nanofillers inside of a polymer matrix but the relationship between rheological behaviour (viscosity) and the dispersion (either exfoliation or intercalation) are still not very clear. Rheology is a semi-quantitative tool to characterize the interactions between nanofillers and polymer molecules in nanocomposites [14,15]. This study is very important as a

fundamental for understanding the nanomaterial processability, as well as the structure-property relations for polymer nanocomposites.

Depending on the degree of exfoliation of the filler in the polymer matrix, the morphology of the nanocomposites can be classified from intercalated to exfoliated structures. Intercalated structure is a form where one or more extended polymer chains are inserted into the clay gallery with fixed interlayer spacing. However, an exfoliated structure is obtained when the silicate layers are completely dispersed in a polymer matrix. Wide angle X-ray (WAXD) is a very powerful method to identify these structures, as well as the transmission electron microscopy (TEM). Owing to the costly method of TEM and also the WAXD signal in proving the formation of nanocomposites structure, the rheology study is necessary as alternative and pronouncing best option to demonstrate a semi-quantitative measure of the degree of exfoliation or intercalation. It has been shown [16-17], that there is a quantitative relation between the extent of shear thinning and the concentration of organoclay platelets.

To date, few papers were published related to this matter, however, the mechanism that the rule of clay dispersion upon which the enhanced physical properties are based is not always defined. In this chapter, the viscosity change during the first stage of in-situ polymerisation was investigated in order to understand the mechanism of the clay dispersion either intercalation or exfoliation and a mechanism was presented. The realization of exfoliation or intercalation during the first mixing stage has more advantages compared to the situation during the polymerization step. This gives better control on the degree of dispersion, and it is also easier to evaluate whether the material is intercalated or exfoliated before the formation of the products. The parameters such as polyol type, mixing time, shearing rate and effect of temperature were examined.

4.2 Rheological behaviour of polyol/organoclay mixtures

The effect of organoclay on the viscosity of polyol was investigated and the results are shown in Figures 4.1 – 4.4. The results revealed that, the polyol6000 with trifunctional group which has a higher molecular weight was significantly

better in clay dispersion than polyol4000 with linear group in both of the systems as indicating in increment of the viscosity. Molecular weight and architecture should be responsible for intercalation and exfoliation of clay layers as investigated by Xia et al [18]. In his work, three kinds of polyol with different molecular weights were studied. XRD results indicated that with higher number-average of molecular weight, the higher interaction of polyol/clay was occurred and the fully exfoliated structure was formed. However with other two kinds of polyols, just intercalated and partially exfoliated were formed. Meng et al [19] studied the ability of OMMT exfoliated into polyimide matrixes with different molecular weights, and they found that OMMTs can be exfoliated in polyimide matrixes with higher molecular weight, but OMMTs with lower adsorption level can be partially exfoliated with lower molecular weight. Similar finding was also reported by Fornes et al [20] when the nanocomposites based on nylon 6 with higher molecular weight prepared by melt mixing had higher degree of exfoliation due to higher melt viscosity. Beside that, Singh et al [21] found the polymer architecture has significant influences on the compatibility of polymer/clay using the self-consistent field calculations. The results provide guidelines for enhancing the intermixing of clay platelets and polymer matrix, as well as the exfoliation degree.

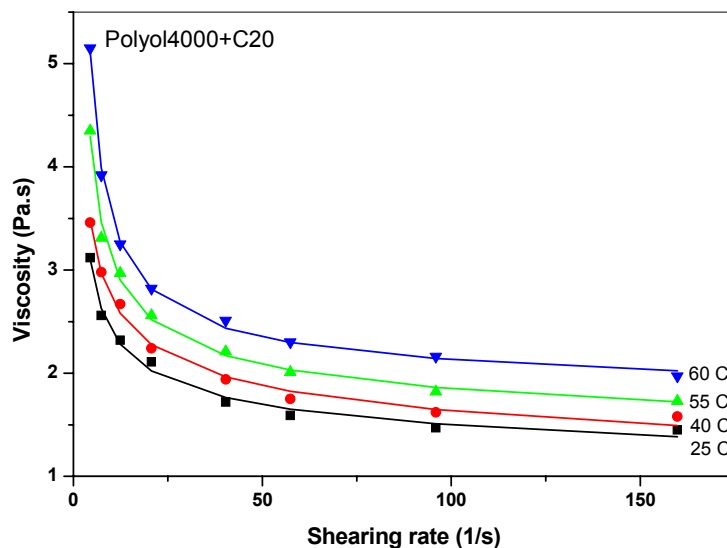


Figure 4.1: Temperature and shearing rate-dependent of viscosity of polyol4000+C20 (3wt%)

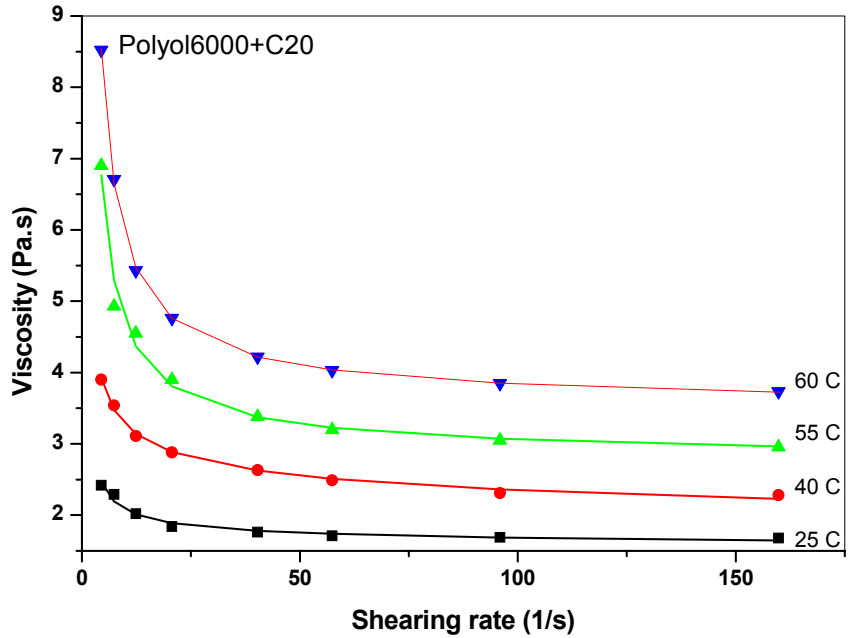


Figure 4.2: Temperature and shearing rate-dependent of viscosity of polyol6000+C20 (3wt%)

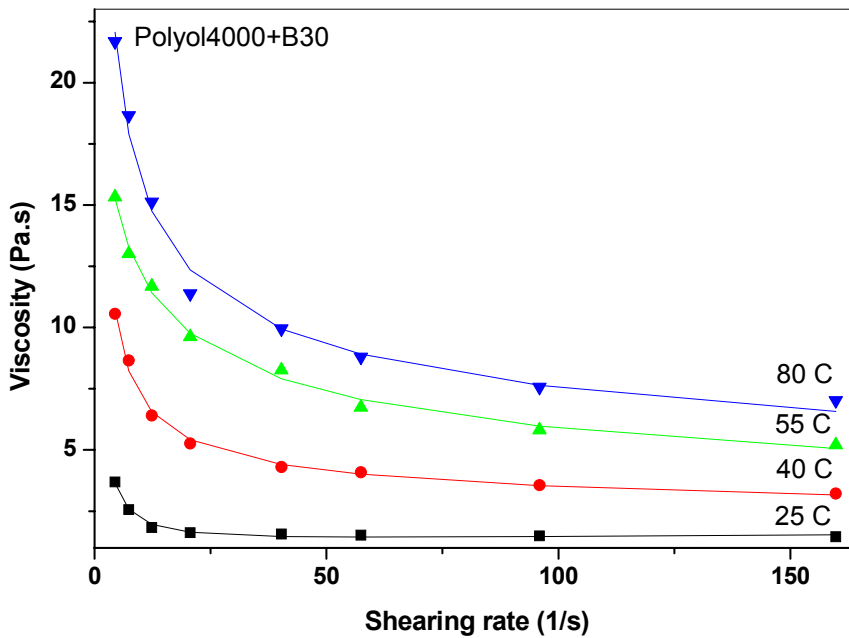


Figure 4.3: Temperature and shearing rate-dependent of viscosity of polyol4000+B30 (3wt%)

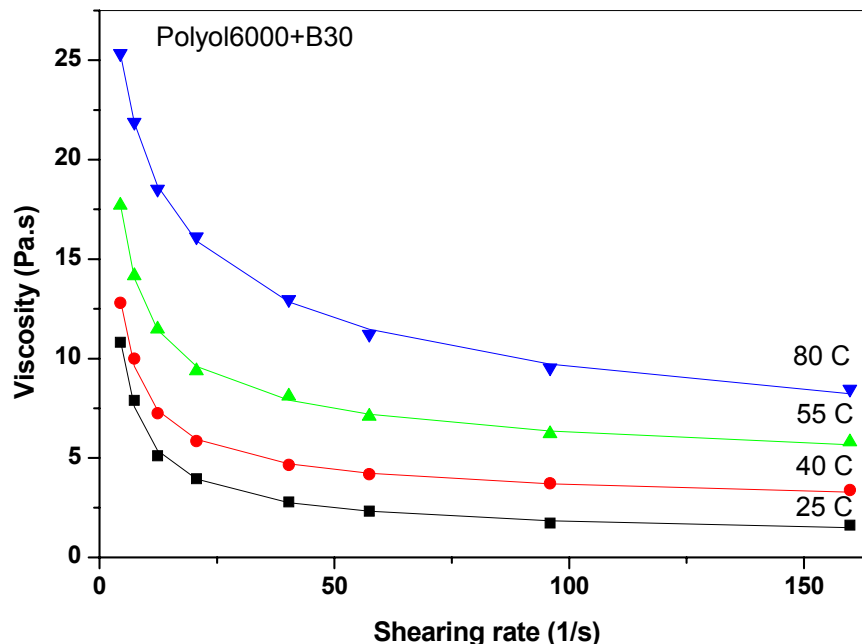


Figure 4.4: Temperature and shearing rate-dependent of viscosity of polyol6000+B30 (3wt%)

Figures 4.1 to 4.4 show the effects of temperature and shearing rate on the viscosity of organoclays with polyol4000 and polyol6000, respectively. The results revealed that temperature plays an important role in nanofiller dispersion. With increasing temperature the viscosity of the mixtures for both systems increased. However, with increase of shearing rate the viscosity of the mixtures reduced as the systems were exhibits a shear thinning behaviour. As shown in Figures 4.1 and 4.2, for the intercalated system, there was huge increase in viscosity on polyol6000+C20 mixture which is approximately 4 Pa.s when the temperature increases from 25 °C to 60 °C. However, in polyol4000/C20, the increase of viscosity is slightly lower than in polyol 6000+C20 approximately 2 Pa.s. For the exfoliation system (polyol4000+B30 and polyol6000+B30) shown in Figures 4.3 – 4.4, at low shearing rate, the viscosity of polyol6000+B30 system at 80°C is approximately 25 Pa.s and almost 10 Pa.s higher than that at 25°C. For polyol4000+B30 the results are nearly similar. Like other fillers such as carbon black, there is a hydrodynamic volume effect for the intercalated and exfoliated clay. The increase of viscosity as temperature increases could be attributed to this effect. This result is in agreement with the finding of Xia et al [18] at higher

temperatures, the dispersion of organoclays in the polymer matrix dramatically increased. In order to understand this phenomenon, the result was fitted with Herschel-Bulkley model [22] to investigate the shear thinning behaviour. This model was commonly used to describe materials such as mud, clay suspensions, oil, and drilling fluids. According to this model, the viscosity, η of Herschel-Bulkley suspensions can be calculated using equation 4.1;

$$\eta = \frac{\tau_o}{\gamma} + k\gamma^{n-1} \quad (4.1)$$

Where γ is the shear rate, τ_o and k are constant and n is the fluid behaviour index. When $n > 1$, the fluid exhibits a shear thickening behaviour, $n = 1$, the fluid exhibits a Bingham plastic behaviour, and $n < 1$, the fluid exhibits a shear thinning behaviour.

From the results shown in Figures 4.1 to 4.4, it can be seen that there are good correlation between the rheological data (in Figures 4.5 and 4.6), temperature and the dispersion behaviour of clay. As mention earlier, the shear thinning value, n , can be used to semi-quantitatively characterize the state of the clay platelet in the polymer matrix. When the clay layers were exfoliated, many separated platelets of clay formed. These exfoliated individual clay platelets with large surface formed a network gel structure, leading to a significant increase in viscosity. However, for the intercalated system, the increase of viscosity is can be explained due to the increase in clay tactoids and as a result of this, the interaction between clay and polyol become stronger.

The value of shear thinning behaviour, n , could express the ability of exfoliation of the organoclay in polymer matrix. With the low shear thinning behaviour, indicating the degree of exfoliation becomes better and if the n value is larger than 1, it seem no intercalation or exfoliation [18]. From the results shown in Figures 4.5 and 4.6, the shear thinning value, n for polyol+B30 system is smaller than that for polyol+C20 in all range of the temperature, showing that B30 is well exfoliated in polyol and for all polyol6000 systems show promising result compared to polyol4000 systems.

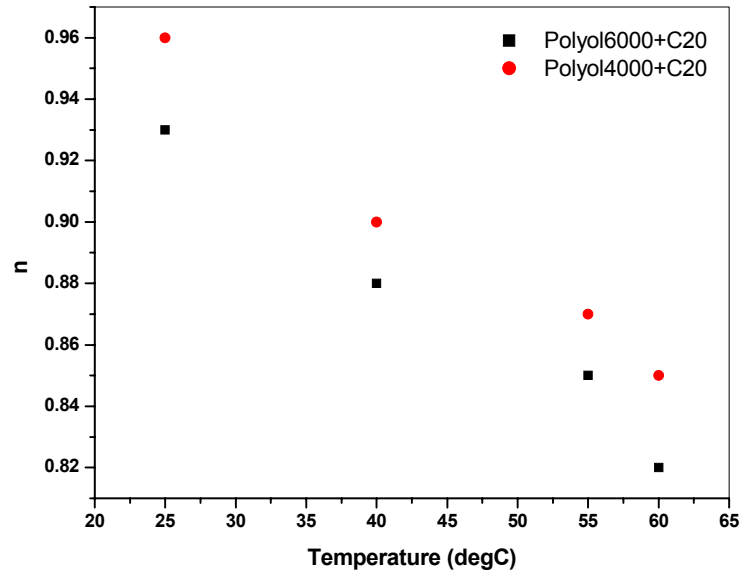


Figure 4.5: Flow behaviour index (n) of polyol/C20 (3wt% as a function of mixing temperature

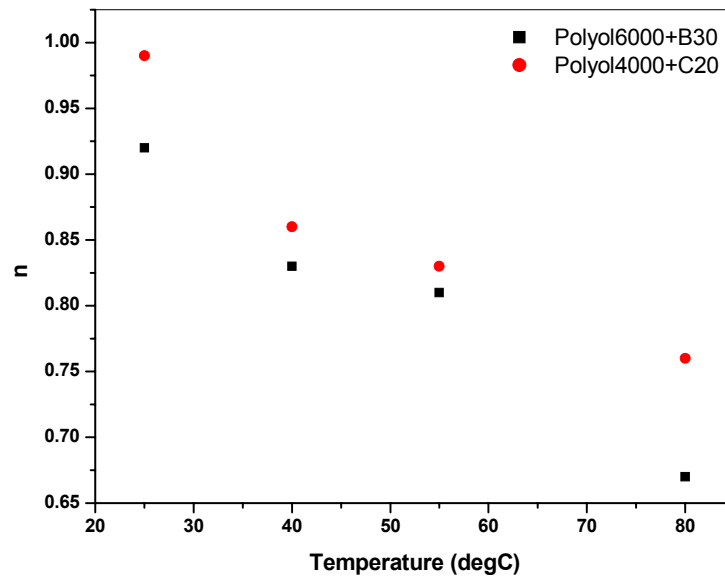


Figure 4.6: Flow behaviour index (n) of polyol/B30 (3wt%) as a function of mixing temperature.

4.3 Mechanism of exfoliation of organoclay

Generally, the interaction between polymer chains and organoclay, mixing time, the shear stress and molecular diffusion could be considered as important factors influencing the formation of well exfoliated nanocomposites. From the results shown in Figures 4.7 – 4.8, the viscosity drastically increases in the initial stage (30 minutes) of mixing for exfoliation system especially when the temperature is higher. For polyol6000+B30 system at 80°C, the increase of 3.5 Pa.s before becomes plateau at 7.1 Pa.s, however at 25 °C the increase is less than 0.2 Pa.s. The result is nearly similar for polyol4000+B30 system where for higher temperature at 80 °C, the viscosity increase almost 2.5 Pa.s after 30 minutes and nearly no increase at 25 °C, respectively. The rapid increase of viscosity in initial period of mixing could result from the rapid molecular diffusion of polyol chains into the galleries of organoclay due to the slippage of organoclay platelets driven by the shear force and it is attributed to the increase of exfoliated degree [23]. Beside that, when temperature increases, the motion of polyol chains become faster and it speeds up the insertion rate of polymer chains into clay galleries.

For the intercalation system shown in Figures 4.9 – 4.10, the polymer intercalated into organoclay platelets take a longer time. Therefore, until 200 minutes, there is still slight increase in the viscosity of the mixtures. This is because a small quantity of polymer molecules intercalated into clay C20 and the interaction become unfavourable. However it can be achieved with increasing mixing time and temperature. At 60°C the increase of viscosity is approximately 1 – 1.5 Pa.s for both of polyol4000+C20 and polyol6000+C20 systems. At 25°C, no intercalation occurred.

Beside that, when temperature increases, mixing time seems to reduce for achieving the plateau viscosity in both of intercalation and exfoliation. This effect is contributed by the increase of the chain motions. The polymer can diffuse easily into the organoclay at higher temperature, which results in higher viscosity rather than at lower temperature.

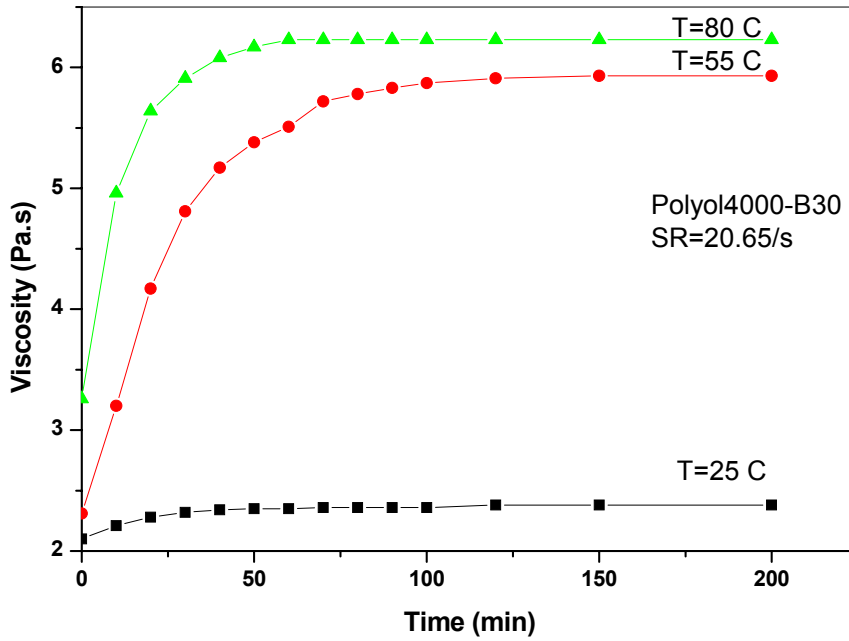


Figure 4.7: Mixing time-dependent of viscosity of polyol4000+B30 (3wt%)

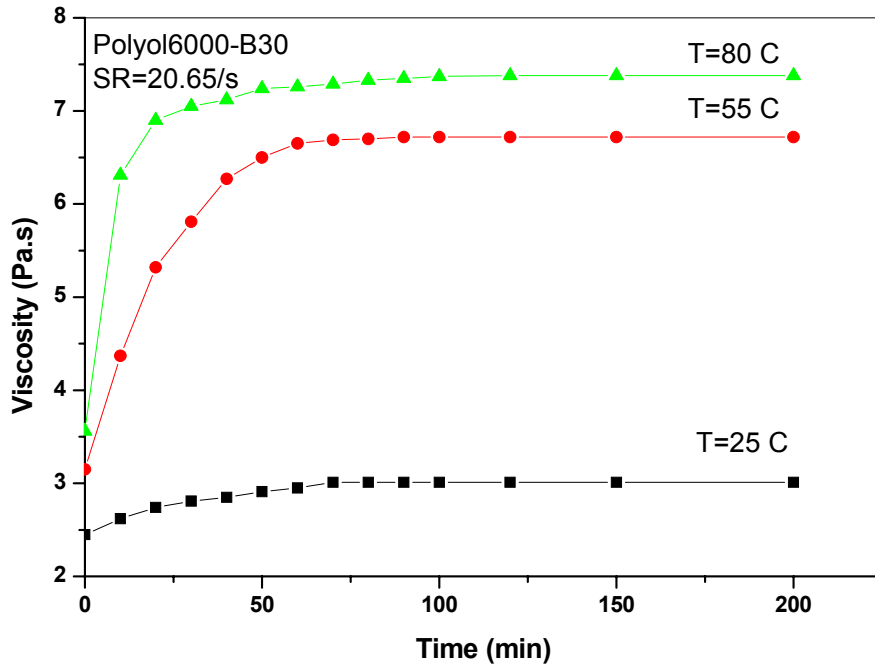


Figure 4.8: Mixing time-dependent of viscosity of polyol6000+B30 (3wt%)

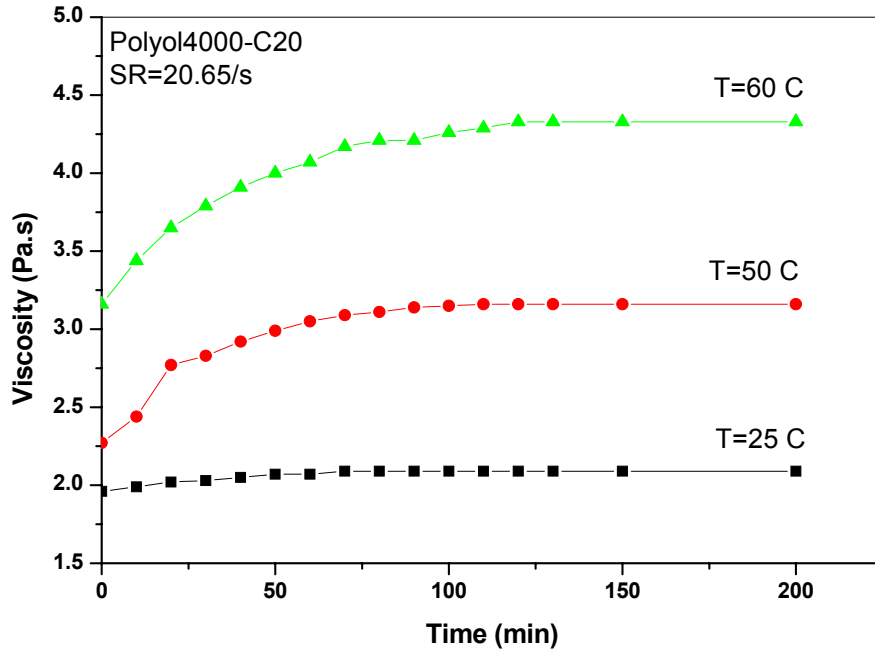


Figure 4.9: Mixing time-dependent of viscosity of polyol4000+C20 (3wt%)

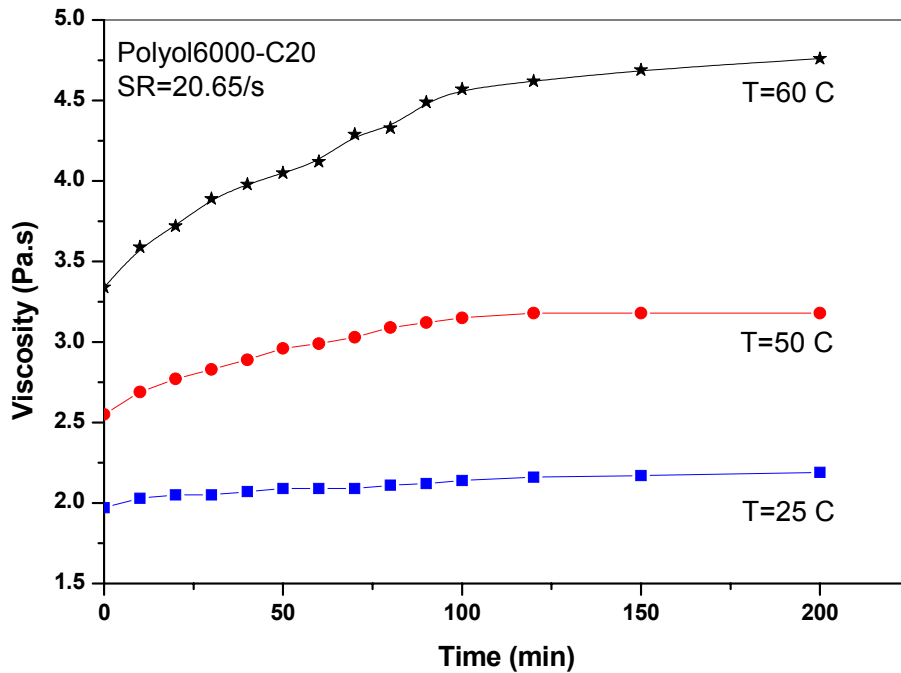


Figure 4.10: Mixing time-dependent of viscosity of polyol6000+C20 (3wt%)

The XRD results shown in Figures 4.11 – 4.12 illustrate that the exfoliation and intercalation B30 and C20 organoclay. As shown in Figure 4.11, when mixing time is increased, the peaks still appear, suggesting that significant intercalation

occurred in polyurethane-C20 nanocomposites. However, in polyurethane-B30 nanocomposites as shown in Figure 4.12, the exfoliated structure was obtained at higher temperatures. These results are in agreement with the result of viscosity study shown in Figures 4.7 – 4.8.

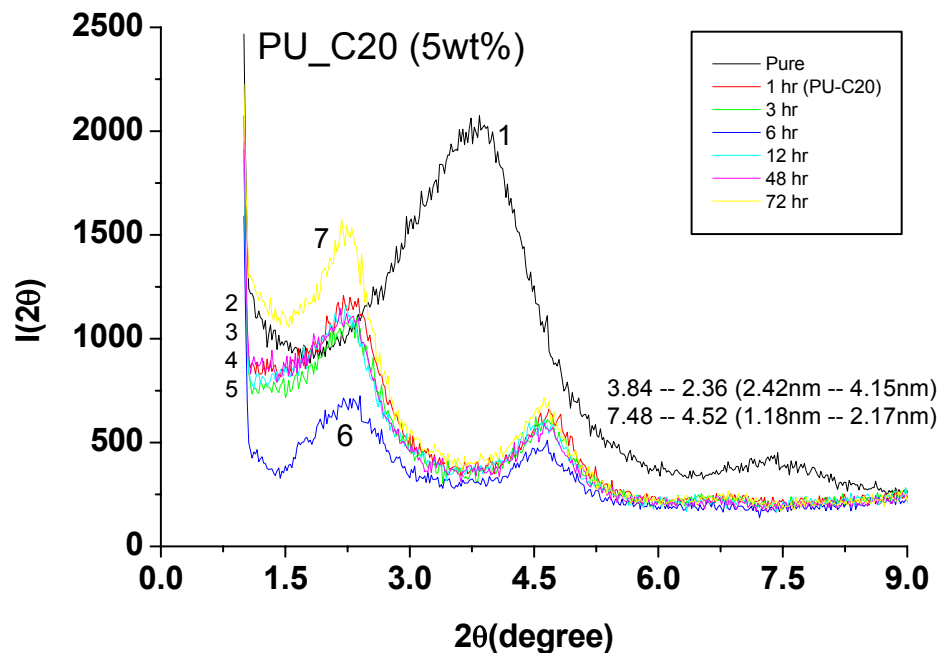


Figure 4.11: XRD pattern for polyurethane-C20 organoclay nanocomposites

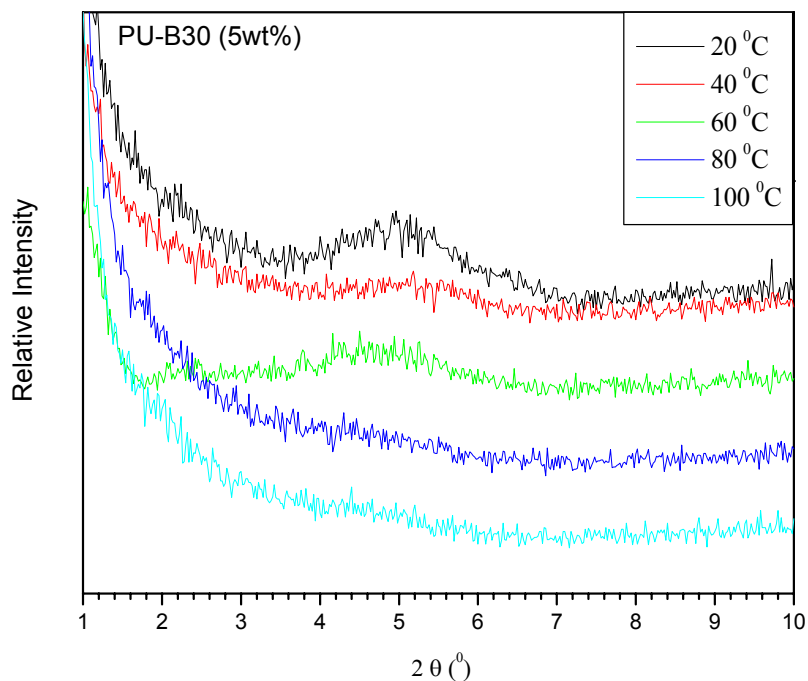


Figure 4.12: XRD pattern for polyurethane-B30 organoclay nanocomposites

From XRD and the rheological results, a possible exfoliation mechanism was proposed. It is believed that the exfoliation of platelets could be achieved through a combination of molecular diffusivity, destabilization of clay layers, and the external and internal forces. The mechanism is illustrated in Figure 4.13. It suggests that the process of exfoliation consists of two stages. The first stage is rapid insertion of polyol into clay galleries. In this stage, the process is sparked with the rapid diffusion of polyol chains into the clay galleries. This process will result in the rapid increase in viscosity as shown in Figures 4.5 – 4.6. Normally, this process depends on the ability of molecular diffusion and it could be promoted by increasing temperature.

In the second stage, the destruction or destabilization of the clay layers occurred. In this process, the rapid insertion of the polyol chains could disturb the attraction between two adjacent galleries and at the same time it could reduce the slippage friction because of the increase of interlayer distance. When the attraction force and slippage friction reduce, the slip of layers could become easier especially when shear force is applied. It worth to mention here, that the organic modifier

also plays a major role in this stage. The wrong selection of organic modifier, sometime retards the destabilization process due to the formation of bridge between organic modifier and clay layers [24]. The last step in this stage is cessation/exfoliation process through layer-by-layer. In this process, the outmost two layers in a stack will be pulled apart first and then next outmost two layers, and so on, until all the layers are separated. At some temperature, and under a certain shear force, thermal movement of polymer molecular chains and Brownian movement of clay particles could take different speeds and thus a pulling force between polymer matrix and outmost layer will be produced. When the interaction between the surface modifier and polymer is much stronger, the pulling force exerted by the polymer matrix will surpass the attractive force of the clay galleries, and the outer layers will be pulled apart. At higher temperatures, the motion of polyol chains increases, and thus lead to promote this stage become faster and state of exfoliation was achieved.

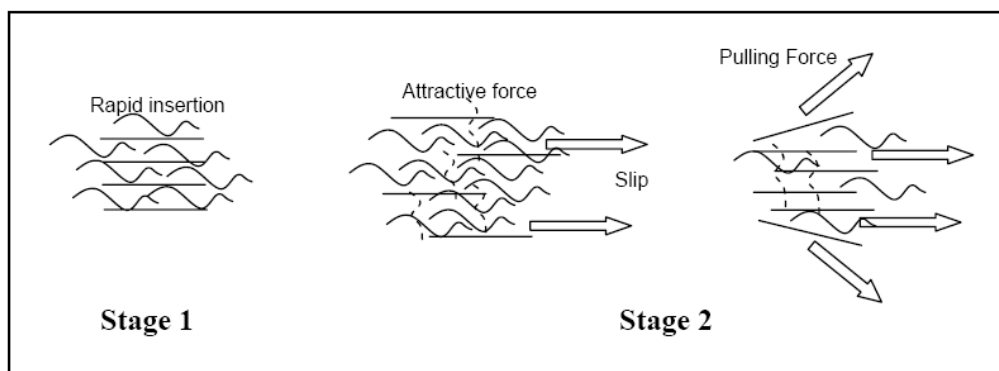


Figure 4.13: Schematic mechanism of exfoliation of organoclay in a polymer matrix

4.4 Rheological behaviour of polyol/CNT mixtures

Dispersion of polyol-CNT is one of the most important issues in preparing superior PU-CNT nanocomposites. Without properly control of the dispersion of CNT in polyol, desired final properties of PU-CNT is very hard to achieve. Due to its smaller size and strong van der Waals interaction, CNTs often aggregate to

form bundles [10,25-26] which is increase the difficulty in fabricating polymer nanocomposites. The rheological behaviour of polyol-CNT (SWNT and MWNT) dispersions as a function of shearing rate was investigated. The variation of viscosity of polyol-CNT dispersions with shearing rate was determined at 60°C as shown in Figure 4.14. The scatter points are the experimental data, and the solid lines are the fitted curves according to the Herschel Bulkley model [22]. The rheological curves show that all the systems exhibit shear-thinning behaviour. From Figure 4.14, it can be seen that, at low shear rates, the viscosity of the polyol with CNTs dispersion shows a noticeable enhancement. The result shows that that the viscosity for polyol/1wt% MWNT system was higher than that of polyol/1wt% SWNT.

The data can be fitted very well with the Herschel Bulkley model. The rheological data are shown in Table 4.1. It is believed that n , k , τ_0 values are related to the dispersion state of carbon nanotubes. Carbon nanotubes are one kind of filler with a high aspect ratio. If CNTs are in good dispersion, high shearing will make the nanotubes aligning with flow direction and a decrease in viscosity. If CNTs exist in an aggregation state, shearing thinning behaviour will be very weak. The better the dispersion of carbon nanotubes, the lower the shear thinning exponent, n . The results revealed that, for both polyol/SWNT and polyol/MWNT, with increasing shearing rate, the viscosities are decreased. Shearing thinning behaviour of MWNT-polyol is more apparent since they have a lower n value. If we consider the different dimension of SWNTs and MWNTs, one can infer that the SWNTs dispersion should have a more significant shearing thinning behaviour due to its high aspect ratio. However, this is not the case. The probable reason is that an individual dispersion of SWNTs is difficult to attain.

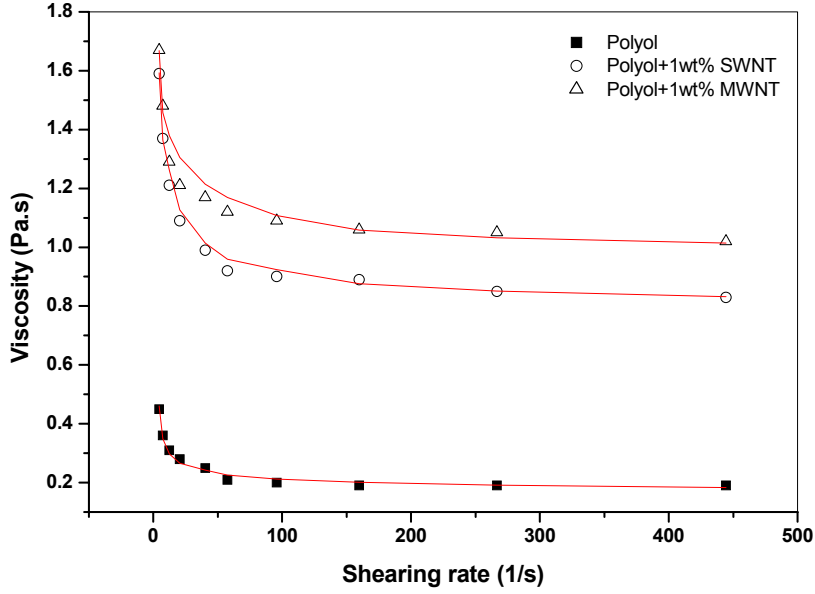


Figure 4.14: Variation of viscosity for polyol, polyol with 1wt% of SWNT and MWNT as a function of shearing rate.

Table 4.1: Shear thinning parameter, n , obtained by Herskel-Bulkley models

Sample	η_L (Pa.s)	η_H (Pa.s)	n
Polyol	0.45	0.19	0.99
Polyol + 1wt% SWNT	1.59	0.83	0.87
Polyol + 1wt% MWNT	1.67	1.02	0.86

For the SWNT and MWNT systems, with increasing the concentration of carbon nanotubes, the shearing thinning exponent decreased, which means a more significant shearing thinning behaviour. This is common features for SWNT-polyol and MWNT-polyol mixtures. In Figure 4.15, the variation of viscosity of SWNT-polyol and MWNT-polyol dispersions at a shear rate of 444.6 s^{-1} and at 60°C with CNTs concentration. The viscosity data is fitted with equation 4.2.

$$\eta = \eta_o \left(1 + 0.67 f \cdot C + 1.62 f^2 C^2 \right) \quad (4.2)$$

f is the shape factor, or the aspect ratio which is the ratio of the longest to shortest diameter of particles. η_o is the viscosity when CNTs concentration is zero. C is

the concentration of CNTs. The fitted parameters η_o and f value are listed in Table 4.2. Clearly, MWNTs have a much bigger f value than SWNTs. This result can be related to TEM observation in Figure 4.16. The f value is dependent on the CNT morphology in polyol. A better dispersion of CNTs leads to a high aspect ratio and thus a bigger f value. The rheological data including the viscosity, the fitted shearing thinning exponent and the shape factor gave an insight into the different reinforcing effects of MWNTs and SWNTs.

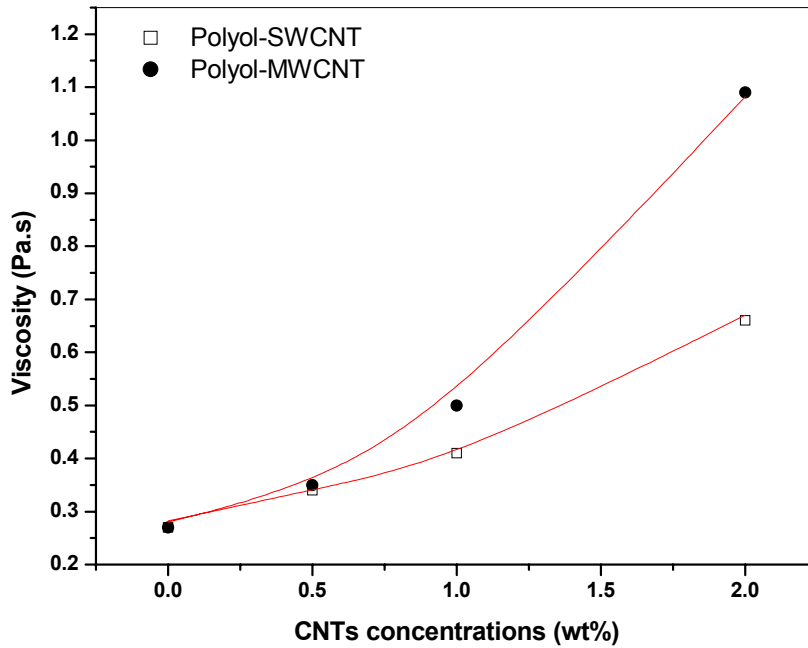


Figure 4.15: Variation of viscosity of polyol-SWNT and polyol-MWNT dispersions with CNT concentration.

Table 4.2: The fitted n and f value for polyol-SWNT and polyol-MWNT dispersions

Mixtures	n	f
Polyol-SWNT	0.279	30.49
Polyol-MWNT	0.276	46.28

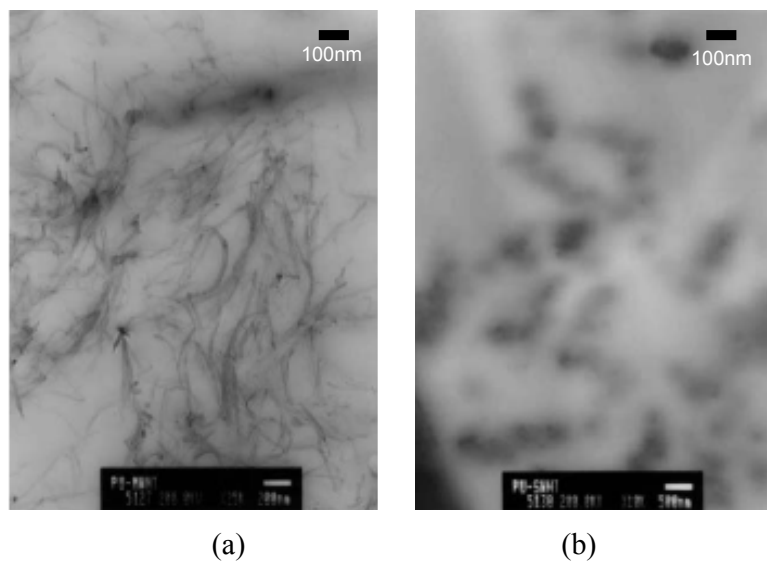


Figure 4.16: TEM photographs of (a) PU/1wt% MWNT and (b) PU/1wt% SWNT. The bar denotes 100nm (—)

Conclusion

The study of rheological behaviour of polyol/clay dispersion is essential in order to produce a well dispersion of nanofillers in polymer nanocomposites. The experiment results suggest that the interaction between polyol and clay either exfoliated or intercalated are occurred and influenced by the type of polyol, shearing rate and also the mixing temperature. The study shows that the trifunctional polyol with 6000 can produce a good dispersion. With B30 clay, the exfoliated system was successfully prepared. The relationship between rheological data (flow behaviour index) for polyol/clay dispersions and the intercalated or exfoliated state of clay was established. A possible exfoliation mechanism has been proposed. It is believed that the exfoliation of platelets could be achieved through a combination of molecular diffusivity, destabilization of clay layers, and the external and internal forces. For CNT systems, the results indicated that polyol/MWNT produced a lower shear thinning behaviour compared to polyol/SWNT. Thus, the better dispersion can be predicted using Herskel Bulkley model. In situ polymerisation is one of the methods to prepare polymer nanocomposite. The viscosity study during the first stage of this process which is the mixing of polymer precursor or monomer and nanofiller is crucial and the rheological data for polyol/clay and polyol/CNTs dispersion is a good

indicator of achieving the well dispersed nanofillers in preparing the polyurethane nanocomposites. This provides an efficient way to evaluate the final state of dispersion of nanofillers.

References

1. Ray, S.S., *J. Ind. Eng. Chem.* 2006, 12, 811 – 842
2. Ray, S.S., Okamoto, M., *Prog. Polym. Sci.* 2003, 28, 1539 – 1646
3. Yano, K., Usuki, A., Okada, A., Kuraichi, T., Kamigaito, O., *J. Polym. Sci. Part A: Polym. Chem.* 1993, 31, 2493 – 2496
4. Rehab, A., Salahuddin, N., *Mater. Sci. Eng. A* 2005, 399, 368 – 376
5. Frankland, S.J.V., Caglar, A., Brenner, D.W., Griebel, M., *J. Phys. Chem. B* 2002, 106, 3046 – 3048
6. Li, X., Gao, H., Scrivens, W.A., Fei, D., Xu, X., Sutton, M.A., Reynolds, A.P., Myrick, M.L., *Nanotechnology*, 2004, 15, 1416 – 1423
7. Xia, H., Shaw, S.J., Song, M., *Polym. Int.* 2005, 54, 1392 – 1400
8. Yao, K.J., Song, M., Hourston, D.J., Luo, D.Z., *Polymer*, 2002, 43, 1017 – 20
9. Viswanathan, G., Chakrapani, N., Yang, H., Wei, B., Chung, H., Cho, K., Ryu, C.Y., Ajayan, P.M., *J. Am. Chem. Soc.* 2003, 125, 9258 – 9259
10. Grossiord, N., Loos, J., Koning, C.E., *J. Mater. Chem.* 2005, 15, 2349 – 2355
11. Cai, D., Song, M., *Macromol. Chem. Phys.* 2007, 208, 1183 – 1189
12. Lagaly, G., *Appl. Clay. Sci.* 1999, 15, 1 – 9
13. Lan, T., Kaviratna, P.D., Pinnavaia, T.J., *Chem. Mater.* 1995, 7, 21144
14. Wagener, R., Reisinger, T.J.G., *Polymer* 2003, 44, 7513 – 7518

15. Seong, D.G., Kang, T.J., Youn, J.R., *e-Polymer*, 2005, no 005
16. Pinnavaia, T.J., Beall, G.W., *Polymer-clay nanocomposites*, John Wiley & Sons, West Sussex, 2001
17. Krisnamoorti, R., Ren, J., Silva, A.S., *J. Chem. Phys.* 2001, 114, 4968 – 4973
18. Xia, H., Song, M., *Polym. Int.* 2006, 55, 229 – 235
19. Meng, X., Wang, Z., Zhao, Z., Du, X., Bi, W., Tang, T., *Polymer*, 2007, 48, 2508 – 2519
20. Fornes, T.D., Yoon, P.J., Keskkula, H., Paul, D.R., *Polymer*, 2001, 42, 9929 – 9940
21. Singh, C., Balazs, A.C., *Polym. Int.* 2000, 49, 469 – 471
22. Matijašić, G., Glasnović, A., *Chem. Biochem. Eng. Q* 2002, 16, 165
23. Herschel, W.H., Bulkley, R., *Proc. Am. Test. Mater.* 1926, 26, 621
24. Zhulina, E., Singh, C., Balazs, A.C., *Langmuir*, 1999, 15, 3935 – 3943
25. Watts, P.C.P., Hsu, W.K., Chen, G.Z., Fray, D.J., Kroto, H.W., Walton, D.R.M., *J. Mater. Chem.* 2001, 11, 2482 – 2488
26. Kis, A., Csanyi, G., Salvétat, J.P., Lee, T.N., Couteau, E., Kulik, A.J., Benoit, W., Brugger, J., Forro, L., *Nat. Mater.* 2004, 3, 153 – 157

Chapter 5

Subsurface Mechanical Properties of Polyurethane Nanocomposite Thin Films Studied by Nanoindentation

5.1 Introduction

Polyurethane is very high performance polymeric material which applications including in areas such as coatings, adhesives, reaction injection molding, fibers, foams, thermoplastic elastomers and composites [1,2]. As a coating material, PU possesses a number of unique properties, including excellent surface mechanical properties, such as high strain, hardness, abrasion and scratch and wear resistant, effective chemical and weather resistance, and high temperature degradation [1-3]. Consequently, it is a principal candidate for a range of high-end applications: for example, PU coatings are applied to a variety of materials to improve their appearance, increase their lifespan, protect them against erosion and corrosion and enable them to meet the high-performance demands of specific environments such as the marine environment; with regards to automobiles, PU coatings satisfy the need for high, exterior gloss, enable good colour retention and improve scratch resistance; and in the construction industry, building floors, steel trusses and concrete supports are spray coated with PU coatings to make them more durable [3].

To meet the demands of any particular application, the properties of PU can be modified in two possible ways: changing PU microstructures or adding inorganic or organic fillers within continuous matrix. PU commonly consists of two phases. The hard-segment phase is made up of hydrogen bonded stiff segments that are formed by reaction of diisocyanate with a chain extender. The flexible soft-segment phase is composed of polyether or polyester diol. The composition of the segments, their length and the sequence of their length distribution, branching and crosslinking are all important factors that determine the morphology and physical properties in solid state of PU as well as its performance as a coating material [4-6].

Nanoparticles, at very low volume-fractions, often strongly influence the properties of composites. With improvements in coating technology and the availability of various kinds of synthesized nanopowders, nanostructured coatings with unique physical-chemical properties have attracted much interest recently. The incorporation of organoclay into a PU matrix can create an interface with high cohesive strength, good mechanical, thermal, barrier and flame-retardant properties, higher specific heat and electrical resistivity, and improved hardness and fracture toughness [7-10]. By reference to preparation methods and the selection of the organic modifier, two types of nanocomposites, which differ in the dispersion level achieved by the nanoparticles in the polymer matrix, can be produced. In intercalated nanocomposites, the unit cells of clay structure are expanded by the insertion of polymer into the interlayer spacing while the periodicity of the clay crystal structure is maintained. In exfoliated nanocomposites, the crystal structure of the clay is completely delaminated by individual dispersion of the clay layers into the polymer matrix. The difference in the micro-phase morphology of these two types of polymer/clay nanocomposites is a reason for differences in their physical properties [11, 12].

Exfoliated and intercalated PU/organoclay nanocomposites based on poly(propylene glycol), 4,4'-methylene bis(cyclohexyl isocyanate), 1,4-butandiol and organoclay have been fabricated in our research group by *in situ* polymerisation. Our previous studies have demonstrated that a wide range of PU properties can be improved by the incorporation of organoclay [11-18]. The intercalated PU/organoclay nanocomposites exhibited outstanding mechanical properties, in particular a 120% increase in tensile strength, a 100% increase in elongation at break and a 300% increase in fatigue durability, when only 3% organoclay had been introduced [12, 13, 16]. For exfoliated PU/clay nanocomposites, with increasing exfoliation, the tensile strength and modulus increased whereas the elongation and fatigue durability decreased [11]. Both nanocomposites have improved permeation-barrier properties and thermal properties [11, 15, 16]. Both the intercalated and exfoliated structures can lead to an increase in viscosity due to the relatively high aspect ratio of clay layers [19], which affected the viscoelastic nature of the nanocomposites [17]. These results

suggest that PU/organoclay nanocomposites with such improved properties have great potential for application as a coating material in the automotive industry, where surface mechanical properties such as hardness, modulus and scratch resistance are important to the application of a material as a coating material.

5.2 Fundamental knowledge of nanoindentation

In recent years, nanoindentation has been established as a standard method for probing mechanical properties of metal at submicron length scale and the application is increasingly being applied to polymeric materials. Many different indentation tests have been developed in an effort to measure the mechanical properties such as hardness and modulus especially with increased demand of nanomaterial technology that needs such a precise tool in measuring and interpreting those properties. Recent technological advances in instrumentation especially using computational power, have led to significant expansion in indentation interpretation not just in hardness and elastic modulus, but also creep and scratch properties directly from the load and displacement curves [20].

Nanoindentation is an advanced technique that is capable of providing a wealth of valuable quantitative information regarding the mechanical properties of a variety of materials at subsurface [21, 22]. This method relies on the local deformation phenomena of materials at small length and load scales using indenter by application of a load. The indentation depth variation is a combination of both visco and elastic contribution to the total indentation depth.

Figure 5.1 show three types of indenter tips commonly used in experiments and analyses. Sharp (Figure 5.1(a)) and spherical (Figure 5.1 (b)) indenters are, to the first order, suited for different types of experiments. For example, the self-similarity of a sharp tip makes it more favourable for analysis of ductile materials, simplifying the extraction of elastic-plastic properties. Conversely, the spherical tip has been more widely used for brittle materials, or more complex systems in which a small-strain elastic deformation is preferable for simpler analysis, but yet

has been used in extracting elastic-plastic properties as well. Figure 5.1(c) shows the example of spherical indenter under SEM image of Berkovich type.

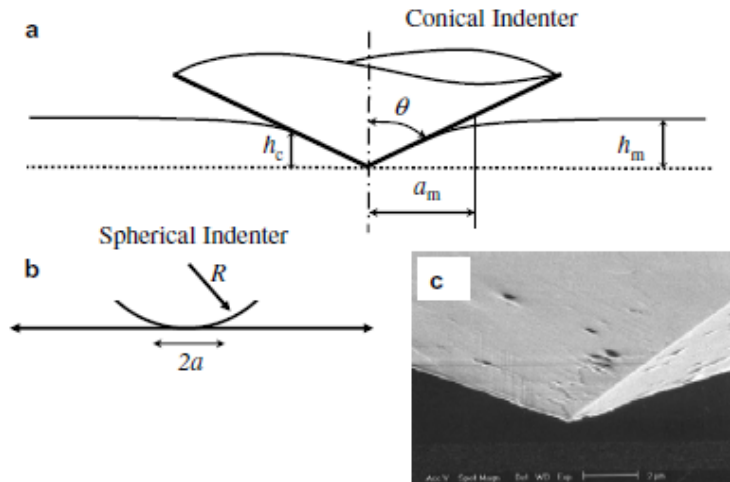


Figure 5.1: Schematic of tips used in instrumented indentation. (a) A sharp pyramidal tip is often modelled as a cone with $\theta = 70.3^\circ$, (b) A spherical tip is defined by its radius R , and a characteristic strain may be defined as a/R . (c) SEM image of a diamond Berkovich indenter [23]

During a typical nanoindentation test, load and displacement are recorded as the indenter tip is pressed into the test material's surface with a prescribed loading and unloading profile. Several models have been proposed to provide the mechanical properties using data from the indentation tests. For example, Doerner and Nix [24] have presented a method to calculate hardness from the loading curve and elastic modulus from the unloading curve, assuming that the contact area remains constant as the indenter is withdrawn and that the unloading curve is linear. Using dimensional analysis of nanoindentation experiments and finite element simulation, Cheng et al [25] have also described an approach to estimate the hardness and modulus of materials using the relationships between elastic modulus, contact area, and initial slope of the unloading curves. Oliver and Pharr [21] have refined the Doerner and Nix model to account for the fact that the indentation unloading curves are not linear even at the onset of unloading. The basic assumption of the Oliver and Pharr analysis is that the vertical displacement of the contact periphery can be described by models for indentation of a flat

elastic body by a rigid tip of simple geometry. The Oliver and Pharr approach has gone through numerous refinements and been adopted in commercial instruments.

The surface mechanical properties of the PU nanocomposites were determined by using Nano Test System from Micro Materials, UK. Measurements are accomplished by imposing a pendulum-based depth-sensing system with the sample mounted vertically and the load applied electromagnetically. The tests were carried out at initial load of 0.15mN to maximum load of 2.5mN. A loading rate of 0.05mN/s was maintained during the incremental increase of the load until the indenter reached the maximum depth into the surface. The load was then held for 180s in order to account for creep effects before the indenter was unloaded. This step is very important due to the nature of the polymer and related materials which is exhibiting viscoelastic property and that this behaviour can lead to overestimation of elastic modulus. In extreme cases of viscoelasticity, a “nose” appears in the unloading load-displacement curve. When the nose occurs, the stiffness at the unloading onset become negative and elastic modulus calculated by the Oliver and Pharr method may be unreasonable. The distance between the indentations was 250µm to avoid overlapping.

Hardness and elastic modulus can be determined using the method developed by Oliver & Pharr [20].

$$P = B(h - h_r)^m \quad (5.1)$$

Where P is the indentation load, h is the displacement, B and m are empirically determined curve-fitting parameters and h_r is the displacement after complete unloading. The initial unloading contact stiffness, S, is determined by differentiating Eq 1 at the maximum depth of penetration (h_{max}),

$$S = \frac{dP}{dh}(h = h_{max}) = mB(h_{max} - h_r)^{m-1} \quad (5.2)$$

The relationship between the projected area, A , of the indentation and the depth, h_p , beneath the contact is [22];

$$\begin{aligned} A &= 3\sqrt{3h_p^2 \tan^2 65.3} \\ &= 24.5h_p^2 \end{aligned} \quad (5.3)$$

in which, the effective hardness, H is

$$H = \frac{P_{\max}}{A} \quad (5.4)$$

The reduced modulus of the material can be analysed from the unloading curve and the relationships illustrated in Equation 5.5:

$$E_r = \frac{\sqrt{\pi}}{2} \frac{S_{\max}}{\sqrt{A}} \quad (5.5)$$

where, E_r is reduced modulus, S_{\max} is slope of the unloading curve at the point of maximum load.

The relationship between reduced modulus, E_r and elastic modulus, E_s , is shown in the Equation 5.6:

$$\frac{1}{E_r} = \frac{(1-\nu_s)^2}{E_s} + \frac{(1-\nu_i)^2}{E_i} \quad (5.6)$$

where, E and ν with subscripts 's' and 'i' are the elastic modulus and Poisson's ratios of the material and the indenter, respectively.

5.3 Results and discussion

5.3.1 Polyurethane Organoclay Nanocomposites

Indentation of the subsurface of a material with an indenter loaded with force results in a penetration depth of the indenter into the material. The data can be recorded as a function of time consisting of a single loading and unloading cycle curve and provides information regarding plastic, viscoelastic and elastic deformation behaviour of tested material [26].

Figure 5.2, (A) and (B), shows the typical indentation loading-unloading curves for PU with 26wt% hard segment and PU nanocomposites with 1%, 3% and 5wt% organoclay, respectively. The incorporation of organoclay into the PU matrix resulted in its film surface being more resistant to penetration by an indenter compared to that of the pure PU. For the pure PU, the maximum indentation depth at the maximum load of 2.5mN was 7787nm. When 3wt% C20 organoclay was introduced, the maximum depth was found to be about 6929nm. With the same load of B30 organoclay, the average maximum depth for the exfoliated PU nanocomposite was found to be about 6574nm, a reduction of nearly 15% compared to the pure PU. This means that the reinforcement effect of B30 organoclay is more effective.

The discontinuity in the unloading curves of the pure PU and the nanocomposites observed at approximately 0.15mN indicates a recovery in the material surface. In the case of a viscoelastic material, the change in plastic and elastic deformation corresponds to the total and residual indentation depths, as shown in Table 5.1. The results indicated that with the addition of clay, the stiffness of the PU increased.

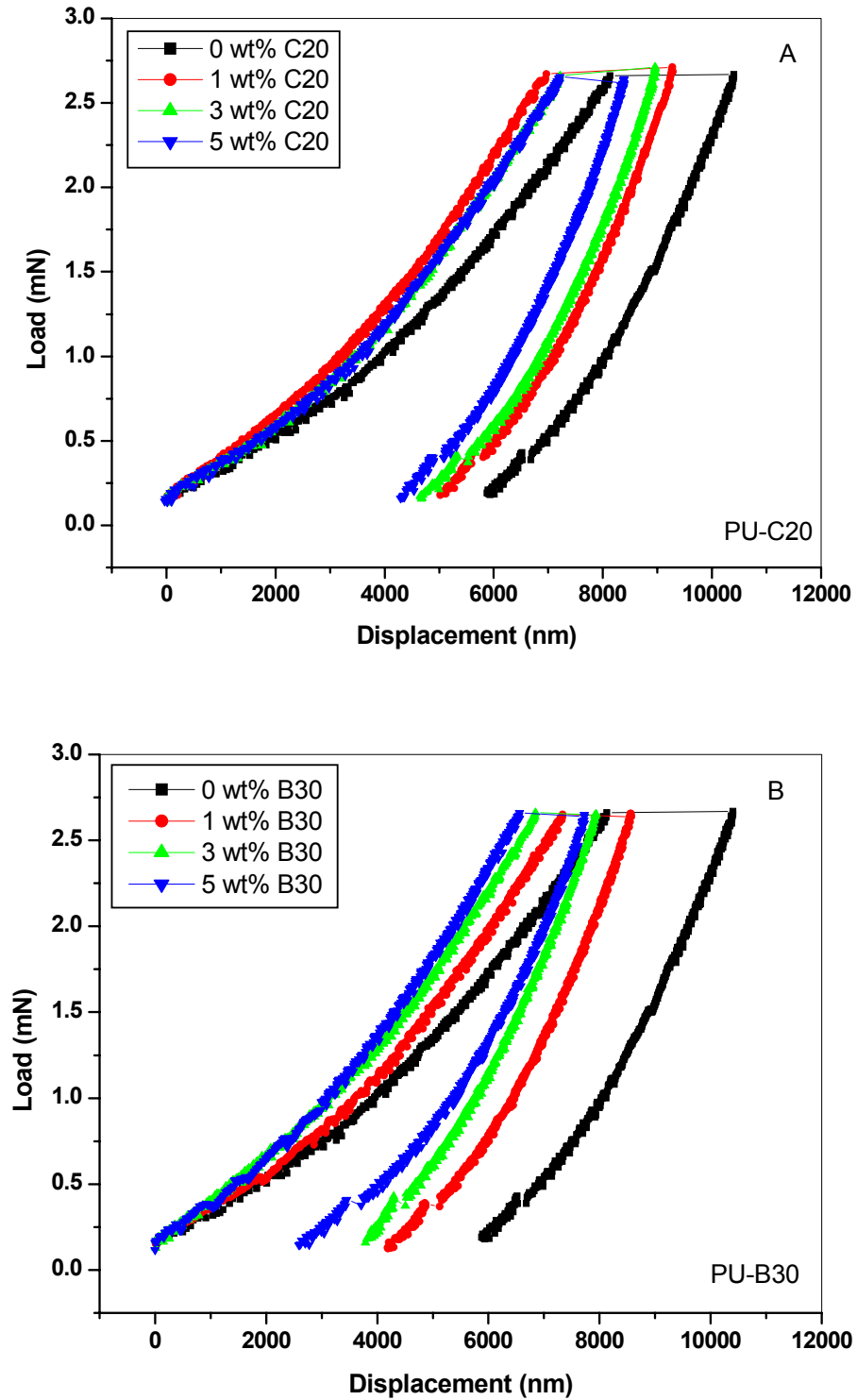


Figure 5.2 Typical indentation load-displacement curves for (A) pristine PU and (B) PU nanocomposite thin films

Table 5.1 Effect of organoclay on the plastic depth

% Clay	% Plastic deformation	
	<i>Intercalated</i>	<i>Exfoliated</i>
0	19.2	19.2
1%	37.5	39.9
3%	41.6	37.1
5%	42.4	21.2

The hardness value (H) represents the resistance of a material to local surface deformation. The elastic modulus (E) represents the overall stiffness of the polymer network. Using the obtained data, hardness and reduced modulus values were computed, and elastic modulus was then calculated using Equation 5.6. The average hardness and elastic modulus of all the samples were plotted against organoclay content shown in Figures 5.3 and 5.4, respectively. Clearly, the incorporation of organoclay into PU has a significant effect on mechanical properties: both hardness and elastic modulus steadily increased with increasing organoclay content. Furthermore, the improvements for the exfoliated PU/organoclay B30 nanocomposite systems were clearly much higher than those for the intercalated systems. With the addition of 3% organoclay, the hardness and the elastic modulus of the exfoliated PU nanocomposite film increased by approximately 55% and 70%, respectively. However, with the addition of the same amount of organoclay, these properties of the intercalated PU nanocomposite film only increased by approximately 16% and 44%. These results coincide with the maximum depth observation discussed above. With the addition of organoclay, polyurethane became stiffer.

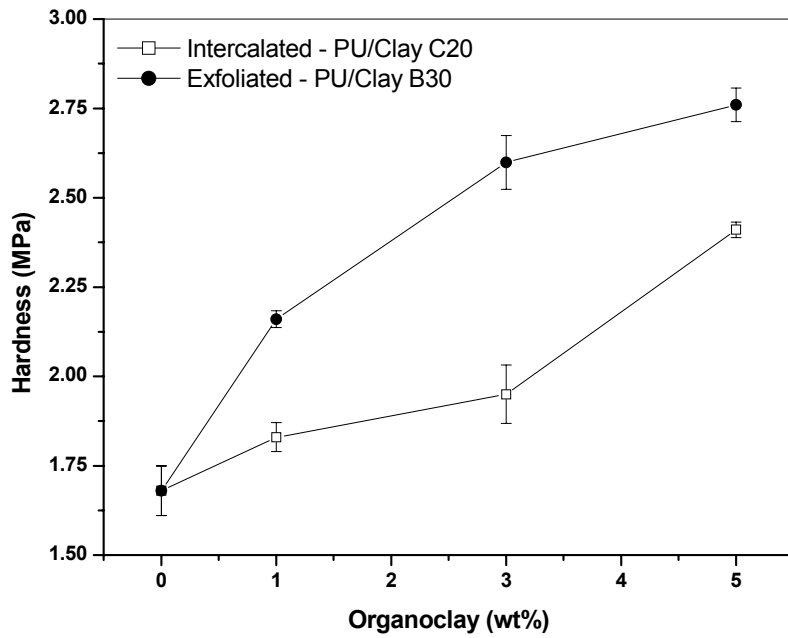


Figure 5.3: Hardness for intercalated and exfoliated PU nanocomposite thin films as a function of organoclay loading.

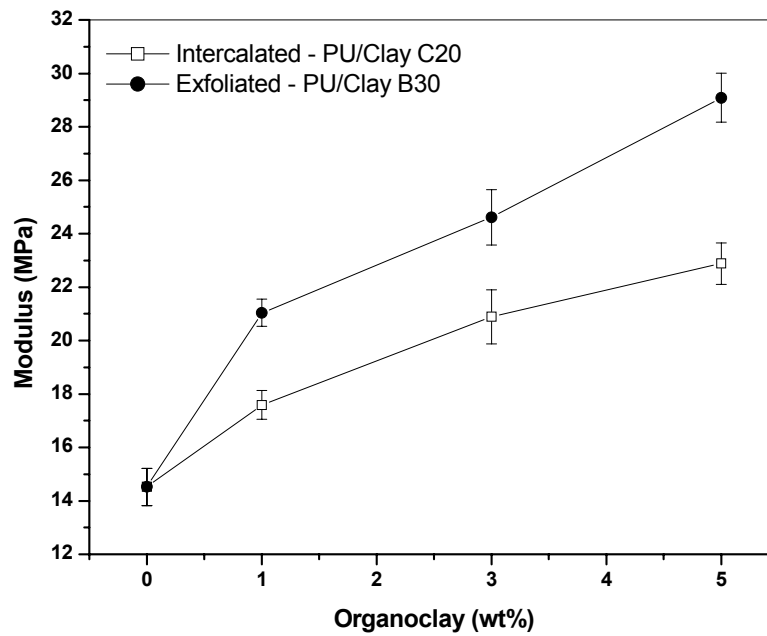


Figure 5.4: Elastic modulus of intercalated and exfoliated PU nanocomposite thin films as a function of organoclay loading

Segmented PU is a block copolymer with altering soft and hard blocks that, due to structure differences, separate into two phases or domains. The hard segment phase plays a vital role in determining the solid-state properties of the PU coatings [27]. The hard domains serve as physical cross-link and act as high modulus fillers, whereas the soft phases provide extensibility [1, 4]. The surface mechanical properties of pure PU prepared using different hard-segment contents were also investigated using nanoindentation tests. The hardness and elastic modulus values as a function of hard segment concentration are shown in Figure 5.5. As expected, as the hard-segment content increased from 18% to 36%, the hardness and elastic modulus increased from 0.59MPa to 3.52 MPa and from 7.83MPa to 64.14MPa, respectively. With Figures 5.3 and 5.4 in mind, it can be said that the effect of adding organoclay on the hardness and the elastic modulus of PU is similar to the increase in the hard-segment content.

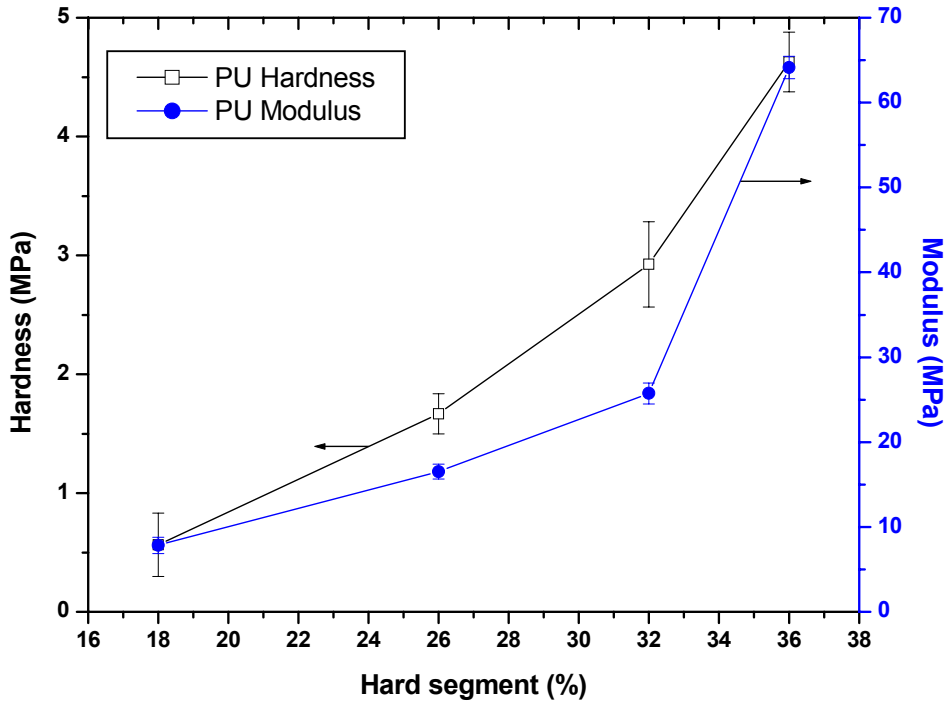


Figure 5.5 Hardness and modulus for pristine PU as a function of hard segment

5.3.1.1 Influence of holding time (creep time) on the values of modulus and hardness

The reliability of the indentation results depends on the observance of special measurement conditions and the elimination of undesired influences. From indentation experiments it is known that a further depth increase arises when the load is held constant after having reached the maximum load [28]. This behaviour is related to the creep behaviour and totally depends on the material and normally diminished to very low values within some times. The creep may reach values of several nanometers per second at the beginning of the hold period and reduces at the end of hold period. This behaviour is very crucial and not only influences the maximum depth but also the gradient of the upper part of the unloading curve which are used for the calculation of contact stiffness and modulus. If such behaviour is not considered, it can have a remarkable influence on the value of modulus and hardness and leads to inaccurate understanding especially in the modulus as it is determined from the tangent to the slope of the unloading curves at maximum load [29]. Chudoba et al [30] proposed an arbitrary definition to remove the bowing effect from unloading curves based on various metal films and inorganic substrates. They proposed that the hold period at maximum load has to be long enough such that the creep rate has decayed to a value where the depth increase in one minute is less than 1% of the indentation depth. However, they suggested that this method does not work well for materials with steady state or viscous creep. For polymeric materials, the bowing effect in the unloading curve were observed by Ngan et al [31] and Briscoe et al [32] and they tend to introduce only 10 seconds hold period in order to eliminate the bowing effect. For the amorphous polymeric materials such as PET and PMMA, Beake et al [33] found that 60s was deemed suitable to reduce significantly the effect of creep on the results. However, Liu et al [34] suggested that the selection of hold time should be long enough to erase the creep effect and it is in range of 10 to 800s and depend on the polymer matrix used.

In the following part, the particular influence of the hold time (creep effect) on the hardness and modulus results was investigated with the pure PU, PU with 3wt %

of C20 and B30 at the maximum load of 2.5mN, respectively. Figures 5.6 – 5.8 give a comparison of the load-displacement curves for five different holding times and including a zero hold period. After 180s of holding time, the penetration depth became more consistent for all samples. From these results, it is clear that it is possible to minimise the effect of creep in nanoindentation experiment if a proper correction of holding time can be managed. From Table 5.2 to 5.4, the change in hardness and modulus for difference holding times was calculated. For the pure PU, a dramatic decrease in hardness and modulus occurred approximately 0.42 MPa and 3.93 MPa, respectively, after 180s of holding time. Similar phenomena can be observed for the clay nanocomposites. For C20 and B30, it reduced nearly 0.31 MPa and 0.32 for hardness and 3.17 MPa and 4.94 MPa for modulus, respectively. In order to minimise the experimental error in the measurement of hardness and modulus due to creep, the holding time should be considered for 180s or more.

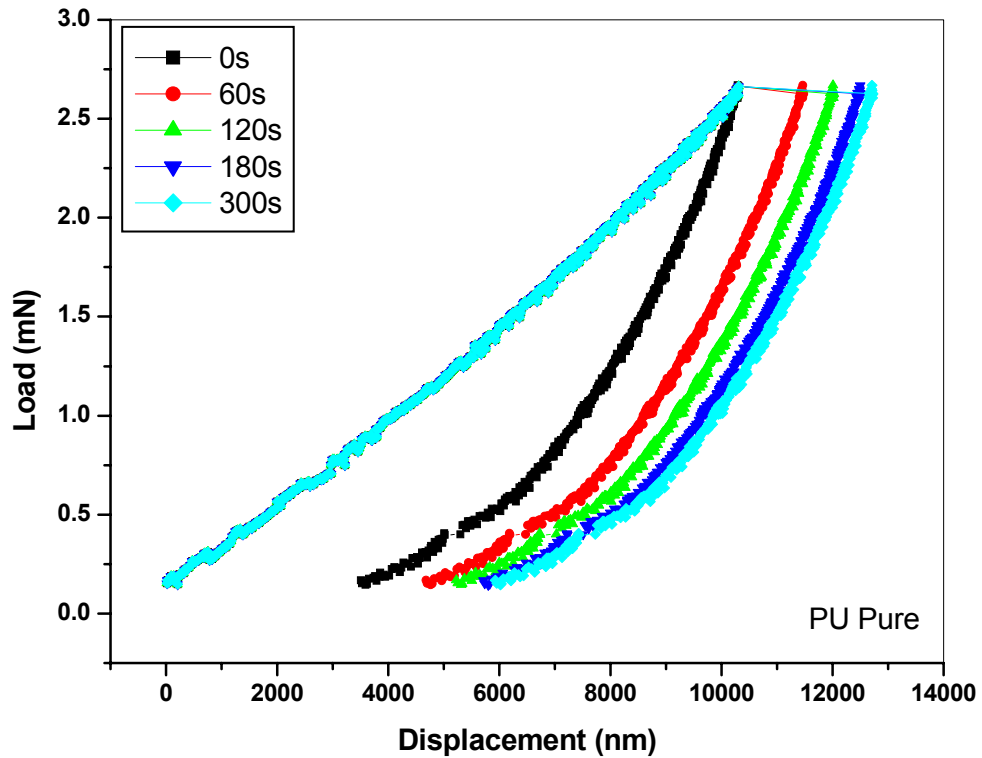


Figure 5.6: Comparison of load-displacement curves for different hold periods at maximum load for the pure PU

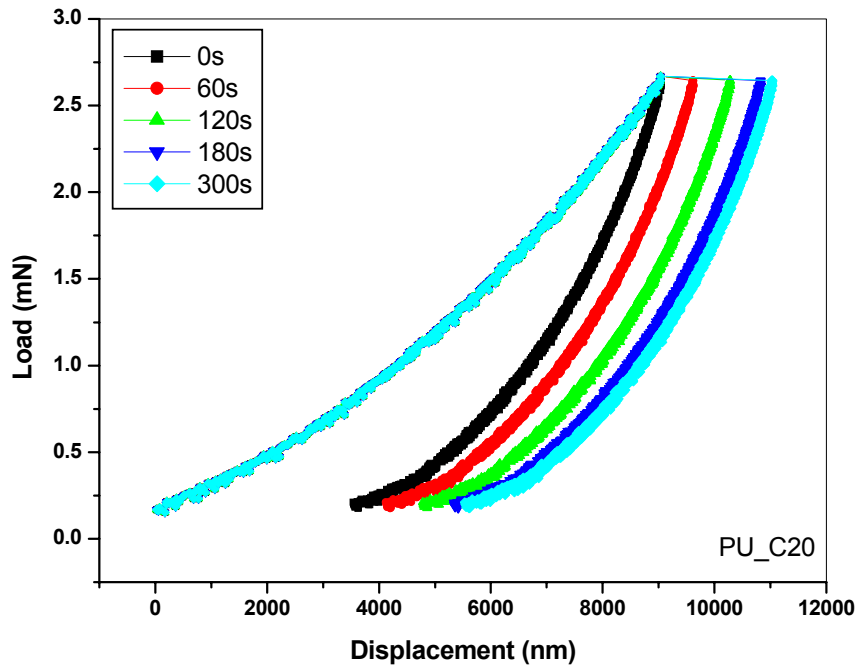


Figure 5.7: Comparison of load-displacement curves for different hold periods at maximum load for PU/C20 clay (3wt%) nanocomposite.

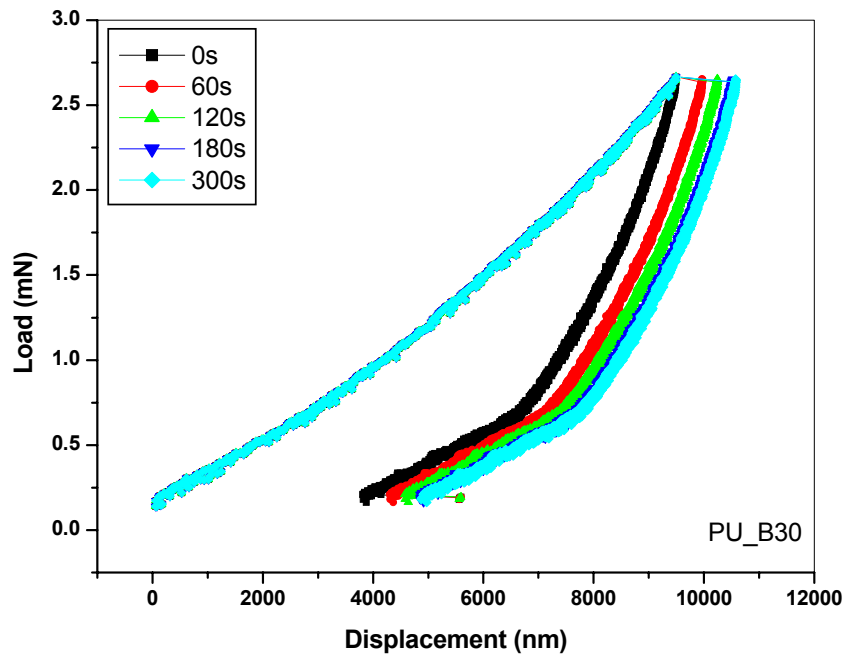


Figure 5.8: Comparison of load-displacement curves for different hold periods at maximum load for PU/B30 clay (3wt%) nanocomposite

Table 5.2: Effect of hold time on the values of hardness and modulus of the pure polyurethane

Hold Time (s)	Hardness (MPa)	Modulus (MPa)
0	2.09 ± 0.12	19.11 ± 0.66
60	1.81 ± 0.16	17.63 ± 0.79
120	1.76 ± 0.10	15.87 ± 0.23
180	1.67 ± 0.07	15.18 ± 0.61
300	1.62 ± 0.09	14.91 ± 0.61

Table 5.3: Effect of holding time on the values of hardness and modulus of PU-organoclay (3wt% of C20) nanocomposites

Hold Time (s)	Hardness (MPa)	Modulus (MPa)
0	2.26 ± 0.15	22.96 ± 0.73
60	2.14 ± 0.17	21.14 ± 0.80
120	2.01 ± 0.12	20.48 ± 0.94
180	1.95 ± 0.09	19.97 ± 0.85
300	1.92 ± 0.12	19.79 ± 0.97

Table 5.4: Effect of holding time on the values of hardness and modulus of PU-organoclay (3wt% of B30) nanocomposites

Hold Time (s)	Hardness (MPa)	Modulus (MPa)
0	2.81 ± 0.12	29.55 ± 0.75
60	2.61 ± 0.09	27.82 ± 0.99
120	2.55 ± 0.13	25.97 ± 1.00
180	2.49 ± 0.08	24.61 ± 1.16
300	2.47 ± 0.11	24.09 ± 0.87

5.3.1.2 Influence of loading rate on the values of modulus and hardness

The influence of loading rate which is related to the total loading-unloading time to the indentation cycle was investigated. The indentation response at three rates (0.20 mN/s, 0.10mN/s and 0.05mN/s) corresponding to loading segment time of 12.5, 25 and 50s were used for the pure PU and the clay nanocomposites at the maximum load of 2.5mN. The sensitivity of the loading rate was studied by Oyen et al [35] and Ma et al [36] and they found that the hardness was significantly influenced by the loading rate. Figures 5.9 – 5.12 give a comparison for the hardness and modulus values for three different loading times with a 180s hold period. The difference in the displacement rate during loading causes a difference in the maximum depth. The increase of the loading time reduces the penetration depth and this can be attributed to the rate dependent viscoelastic behaviour of the material. The hardness and the modulus are shown in Figures 5.9 to 5.12. The results exhibit some increment in both of the hardness and the modulus values for all samples after loading rate increased. However, the differences in the hardness value slightly larger in the pure PU as demonstrated in Figure 5.9 and Figure 5.11. In polyurethane nanocomposites, the hardness values slightly influence by loading rate especially in PU-C20. However, the modulus values seem to be quite stable and were nearly unchanged in both PU-B30 and PU-C20 systems. Normally for the higher loading rates, the unloading curve shows a ‘nose’ or bowing towards depth in the initial part of the unloading curve [30]. This affects influenced the calculation of modulus and lead to incorrect results. However, in this study, an introduction of a hold period of 180s before the unloading period minimised the measurement error. This is the recommended hold period for PU through experiments as the assumption that unloading is elastic during the initial portion of the unloading curve is incorrect and this creep behaviour needs to be taken into account [37].

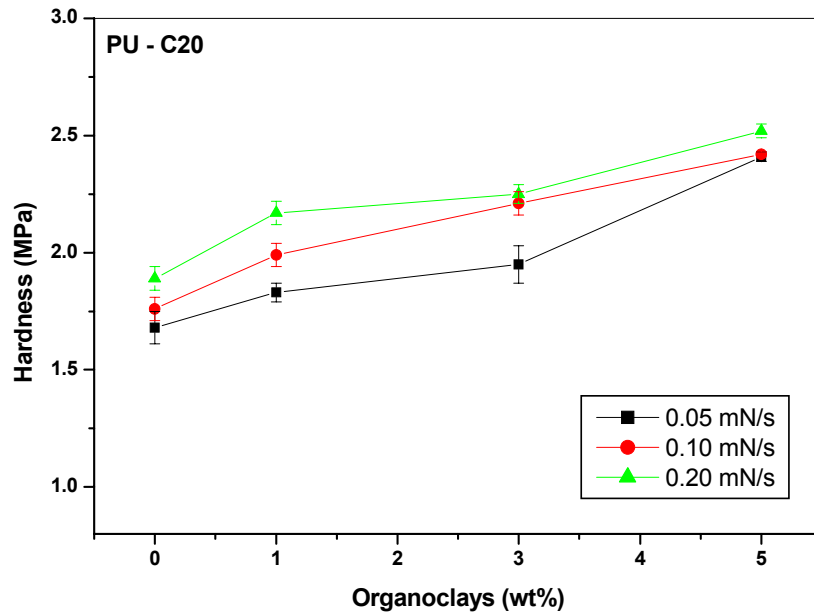


Figure 5.9: Hardness of PU/ C20 clay nanocomposite as a function of loading rate

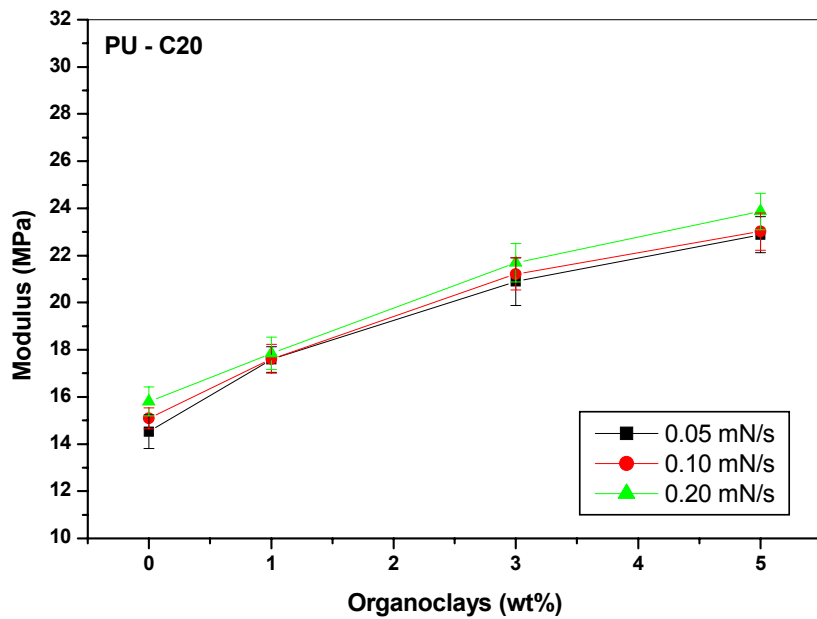


Figure 5.10: Modulus of PU/ C20 clay nanocomposite as a function of loading rate

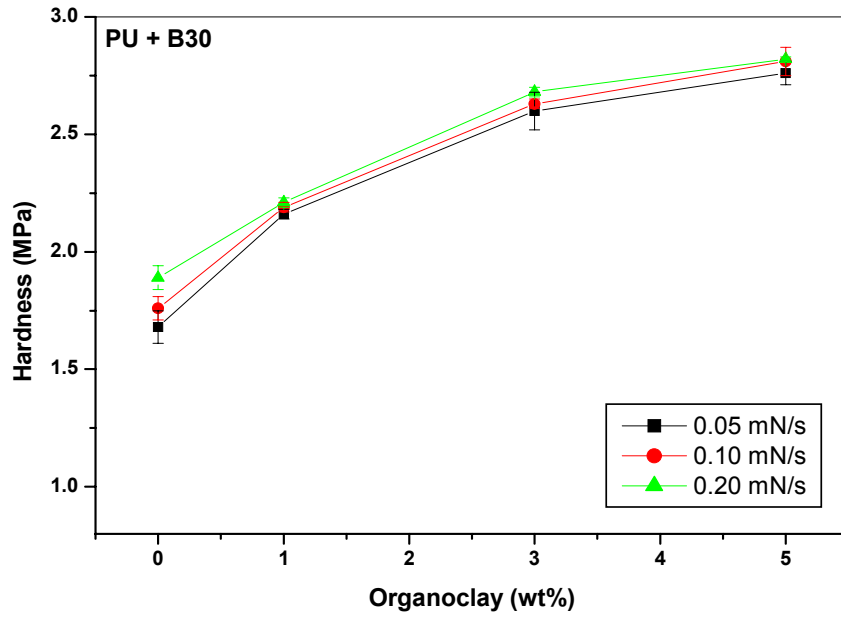


Figure 5.11: Hardness of PU/ B30 clay nanocomposite as a function of loading rate

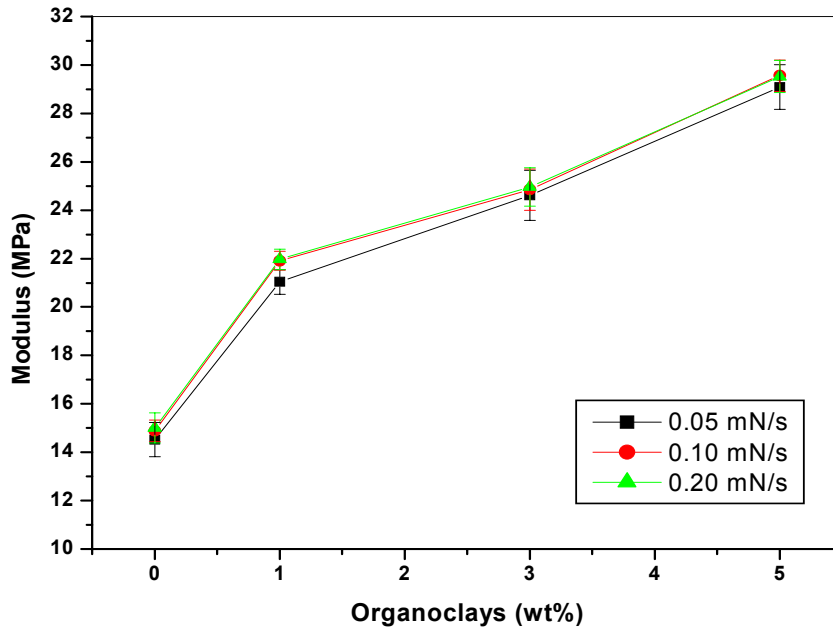


Figure 5.12: Modulus of PU/ B30 clay nanocomposite as a function of loading rate

5.3.2 Polyurethane Graphite Oxide (GO) Nanocomposites

Graphene is emerging as rising star in the field of material science because of its prominent intrinsic properties, which may rival or even surpass both the single and multiwall carbon nanotubes [38]. The extraordinary mechanical properties such as transport properties [39-40] offering strong opportunity as a nanofiller in producing the polymer nanocomposite. Recently, the addition of graphene as a nanofiller in polyurethane matrix demonstrated a unique mechanical properties for actuator application where graphene can work as photoactive energy transfer and PU can act as molecular switch units [38]. The latest results in our research group showed that the introduction of the graphene in polyurethane nanocomposites is strongly correlated with the ability to the dispersion of graphene in a polymer matrix [41,42].

Figure 5.13 shows the load-unloading indentation curves into the neat polyurethane and its nanocomposites as a function of graphite oxide (GO) content. It is clear that the mechanical response of the samples differs as shown in load-unloading curves in Figure 5.13. Again the loading curves are followed by a period of holding time at 180s at which the peak loads are 2.5mN. The curves steady shift on left with increasing the GO concentration, indicating that the nanocomposites' resistance to indentation dramatically increases with GO concentration. Again the depths represent the contributions from both elastic and plastic displacements.

Figure 5.14 shows the hardness and modulus plot with respect to the GO concentration, respectively, for neat PU and the nanocomposites. It can be seen that both the hardness and the elastic modulus are enhanced as a function of GO concentration, due to the addition of stiff GO fillers into the matrix. With incorporation of 4wt% of GO, the hardness and modulus increases nearly ~400% and ~350%, respectively. Cai et al [42] explained that this phenomena can be attributed by the efficient load transfer between the GO and PU matrix resulting from the physical crosslinks and chemical bonding.

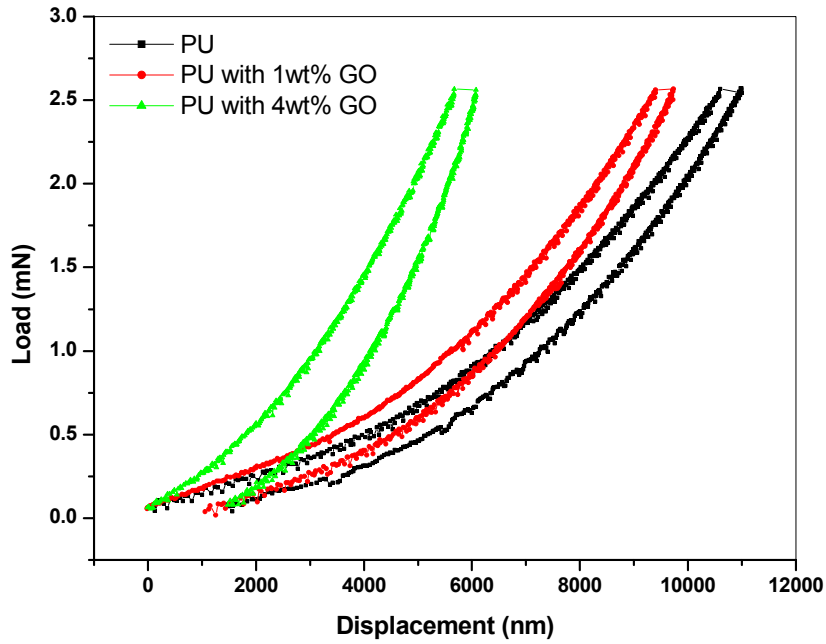


Figure 5.13: Typical load-unloading curves of neat PU and PU/GO nanocomposites.

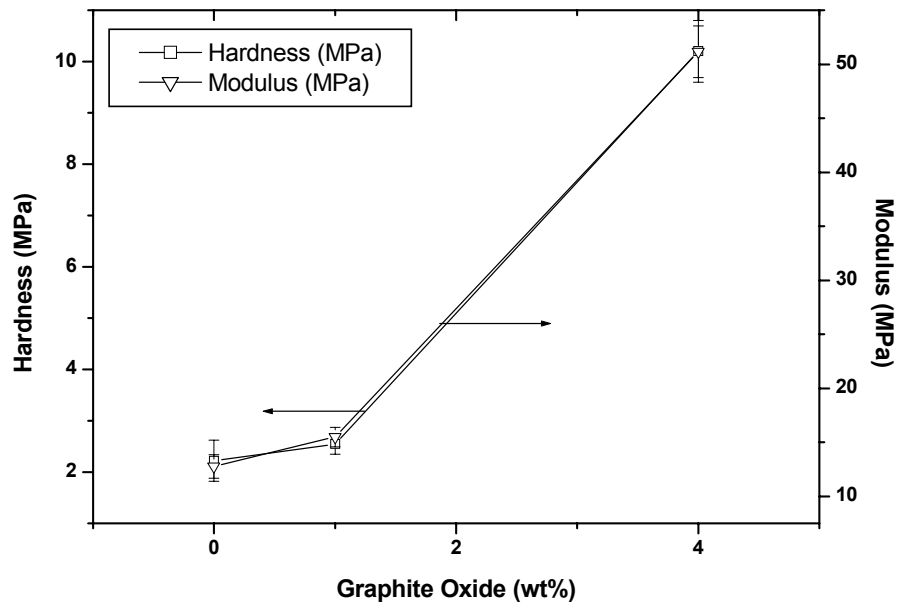


Figure 5.14: Hardness and modulus for the PU/GO nanocomposites as a function of GO concentration.

5.3.2.1 Effect of holding time on the values of hardness and modulus

The variation in hardness and modulus with loading rate and the creep during the holding time were investigated for determination of standard conditions. Figure 5.15 shows how the extent of depth varies with the dwell time at peak load. The ratio of displacement during hold vs. total displacement was fairly small for all samples between 180s and 300s of the holding time. Hardness and modulus values obtained from indentation to a peak load of 2.5mN at the loading rate of 0.05mN/s, with different holding times at peak load are shown in Figure 5.16 and 5.17. It is clear that there is a small decrease in both properties as the hold period was extended to 300s on pure polyurethane and sample with 1wt% GO. However, for the sample with 4wt% GO, the decrement is become smaller just after 180s of holding time. From the results shown in Figure 5.16 and 5.17, a 180s dwell time was deemed acceptable for the majority of the experiments, since this is sufficient to reduce significantly the effect of creep on the unloading data.

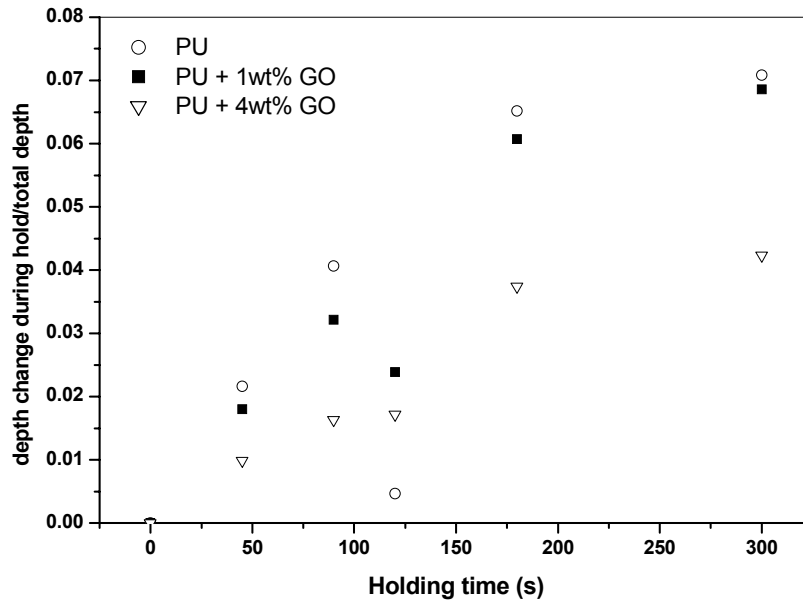


Figure 5.15: Depth change ratio at different holding time on polyurethane and polyurethane graphite oxide nanocomposites.

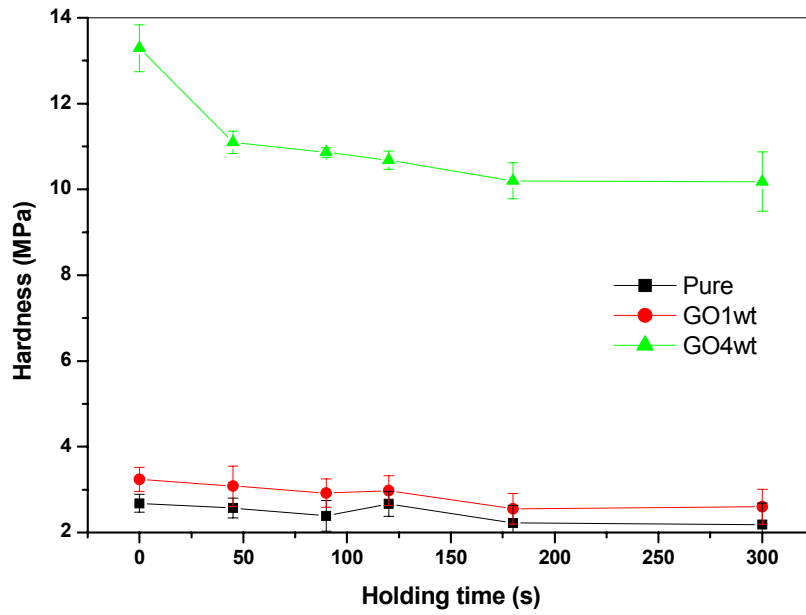


Figure 5.16: Effect of holding time on hardness of the PU and PU graphite oxide nanocomposites.

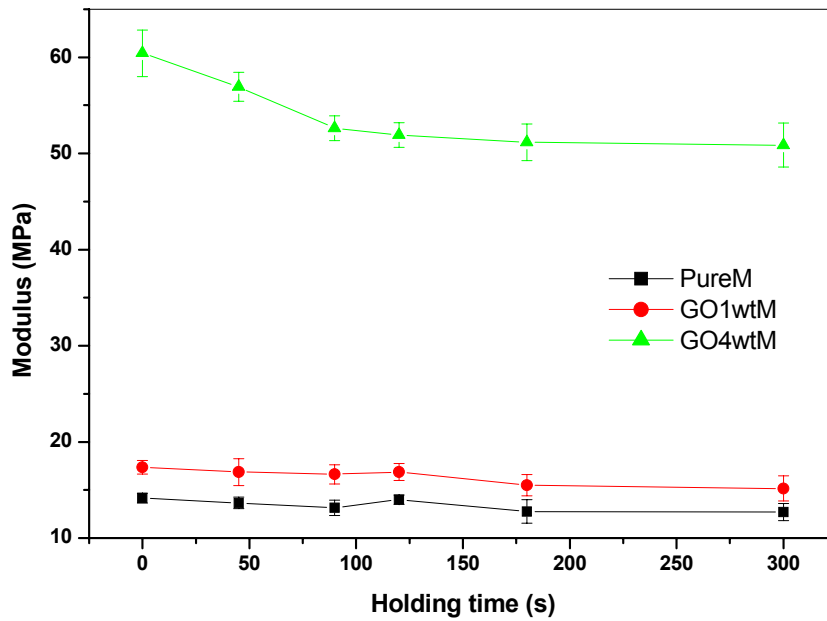


Figure 5.17: Effect of holding time on hardness of the PU and PU graphite oxide nanocomposites.

5.3.2.2 Effect of loading rate on the values of hardness and modulus

The variation in hardness and modulus with loading rate was examined over the range of 0.01 – 0.2 mN/s, while keeping the holding time constant (180s) for indentation to a peak load of 2.5mN. For this case, the unloading rate was kept at a constant of 0.05mN/s. Figure 5.18 – 5.19 illustrate that the hardness and modulus with loading rate. For PU and PU with 1wt% GO, there is a moderate rise (~10%) in the hardness and modulus as the loading rate increased from 0.01 to 0.2 mN/s. However, in PU with 4wt% GO, the hardness slightly increase in between 15 – 20%. The change in the hardness and modulus values due to the loading rate in polymer nanocomposites were studied by Chudoba et al [30], Beake et al [33], and Shen et al [43]. The authors contributed this phenomenon due to the increased viscoelastic recovery at the higher loading rates and the experimental conditions.

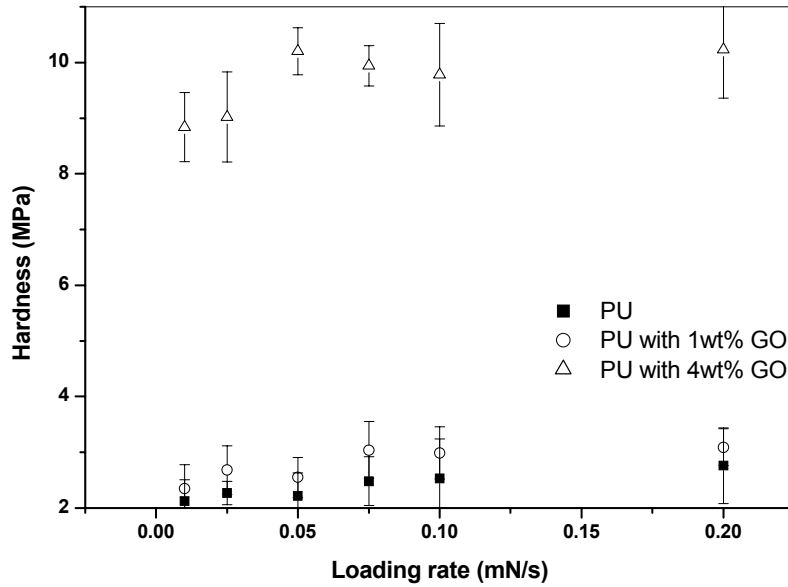


Figure 5.18: Variation of the hardness of PU and its GO nanocomposites as a function of loading rate.

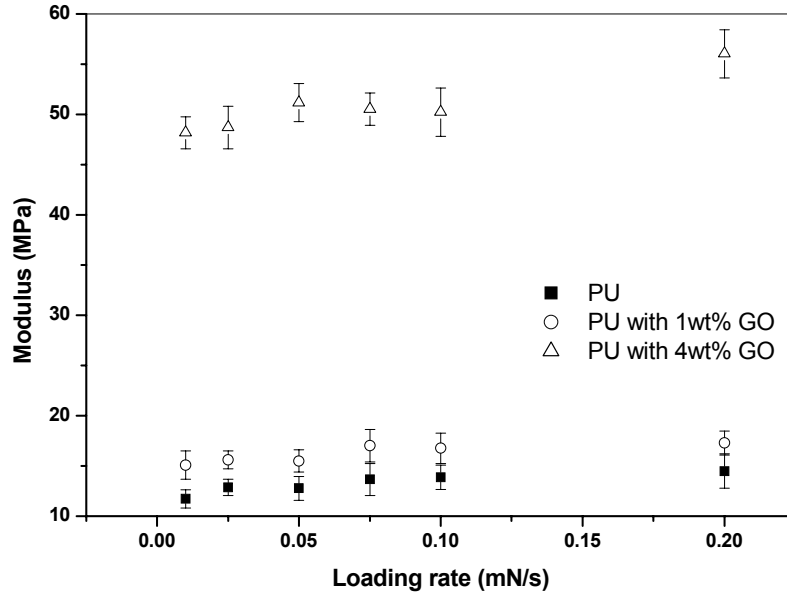


Figure 5.19: Variation of the modulus of PU and its GO nanocomposites as a function of loading rate.

5.3.3 Polyurethane-CNT nanocomposites

Carbon nanotubes (CNTs) has a unique combination of mechanical and electrical properties and were received a wide range of applications [44-45]. The dispersion of CNTs and the challenge in preparing CNT nanocomposite must be fully understood in order to fulfil their promises. The combination of high aspect ratio, small size, very low density, and more importantly, excellent physical properties such as high mechanical strength, stiffness, high electrical and thermal conductivity makes CNTs perfect candidates as reinforcing fillers in polymers [46]. In parallel with the high precision testing instrument, nanoindentation is one of the newest testing equipment that suitable in measuring the elastic modulus of PU-CNTs. To study the effect of CNTs in the polyurethane matrix, hardness and elastic modulus values were measured using indentation technique.

The indentation loading-unloading curves for the polyurethane and its CNTs (MWNTs and SWNTs) reinforced samples are presented in Figure 5.20 – 5.21. Ten indentation tests were carried out on each sample and the average values of hardness and elastic modulus are presented in Figure 5.22 – 5.23. It is clear that

the mechanical responses of neat PU and the composites were different considerably. As the weight percentage of CNTs increased, lower indentation depth and higher unloading slope were noted in Figures 5.20 - 5.21. It is immediately clear that the resistance of nanocomposite to indentation gradually increases with CNT concentration. These results can be interpreted by the homogenous dispersion of CNTs in the polyurethane matrix and strong interfacial interactions between CNTs and the polyurethane matrix. It can be seen that the hardness and modulus properties of CNT nanocomposites significantly increased with increasing the loading level of the nanotubes, as presented in Figure 5.22 and 5.23. Upon incorporation of only 1wt% SWNT, the hardness of PU was greatly improved by about 150% from 3 MPa to 7.8 MPa and the modulus is improved by about 50% from 12MPa to 18.5 MPa. For only 1wt% MWNT, the hardness of PU was improved by about 50% and the modulus was just slightly improved by about ~5%. For 2wt% SWNT, the improvement slightly unchanged in both hardness and modulus values which increased by only 5% as compared to 1wt% SWNT. However, for 2wt% MWNT the result showed remarkable enhancement especially in modulus by about 40%. The possibility of aggregation of SWNTs in PU matrix was predicted. However, in contrast with MWNT, the improvement became prominent. Clearly, both results in Figure 5.22 and Figure 5.23 indicated that the PU-SWNT nanocomposites showed better improvement as compared to PU-MWNTs. As we are concerned about the characteristic of SWNT-reinforced composites, this kind of nanotube could have a high interfacial strength and play a major role in delivering the stress transfer between the SWNT and the polymer matrix. However, due to their strong van der Waal forces, at high concentration, the SWNT tends to form aggregates which give some disadvantages to the final properties of the PU-SWNT nanocomposites.

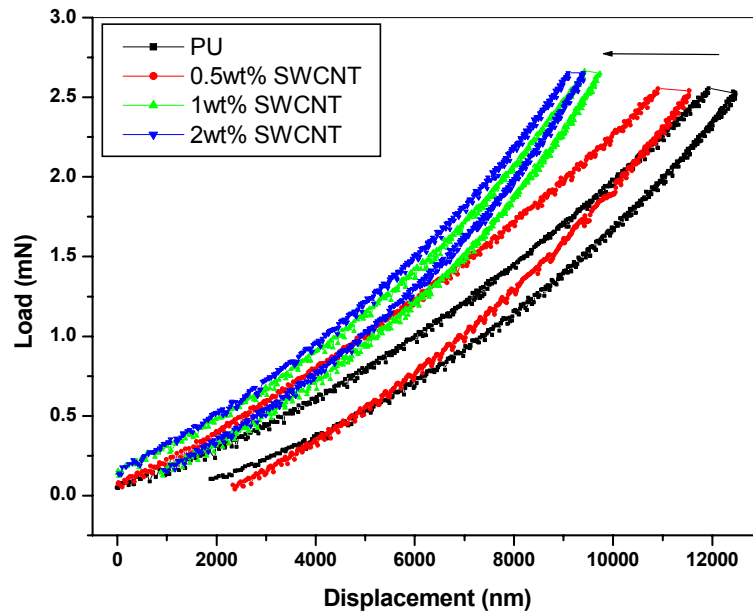


Figure 5.20: Typical load-unloading curves of neat PU and PU/SWCNT nanocomposites

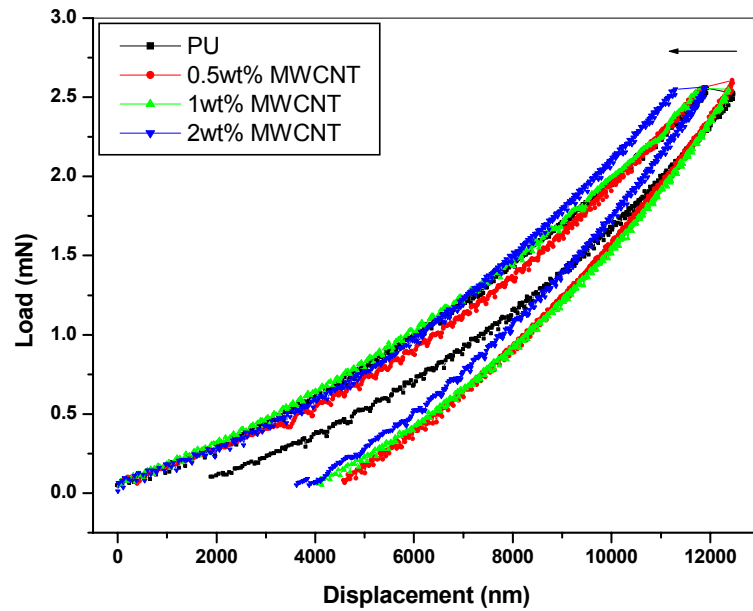


Figure 5.21: Typical load-unloading curves of neat PU and PU/MWCNT nanocomposites

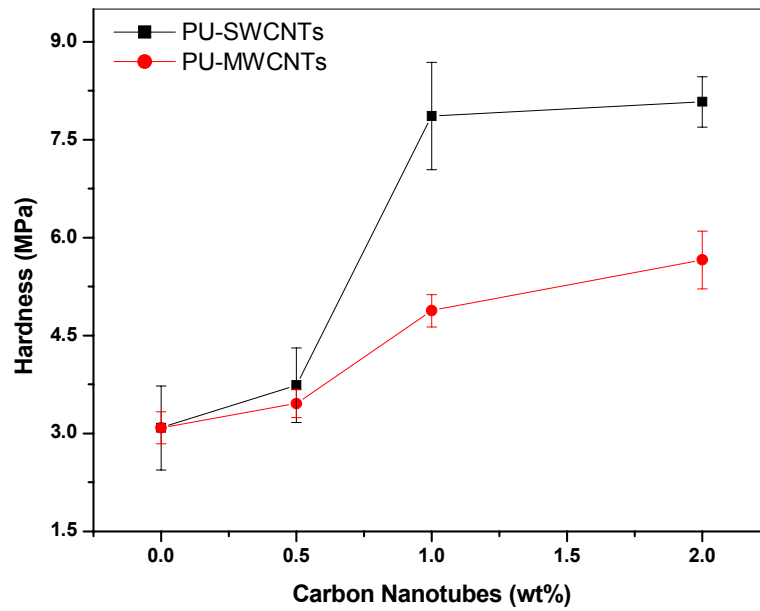


Figure 5.22: Hardness of the PU/CNTs nanocomposites as a function of SWCNTs and MWCNTs concentration.

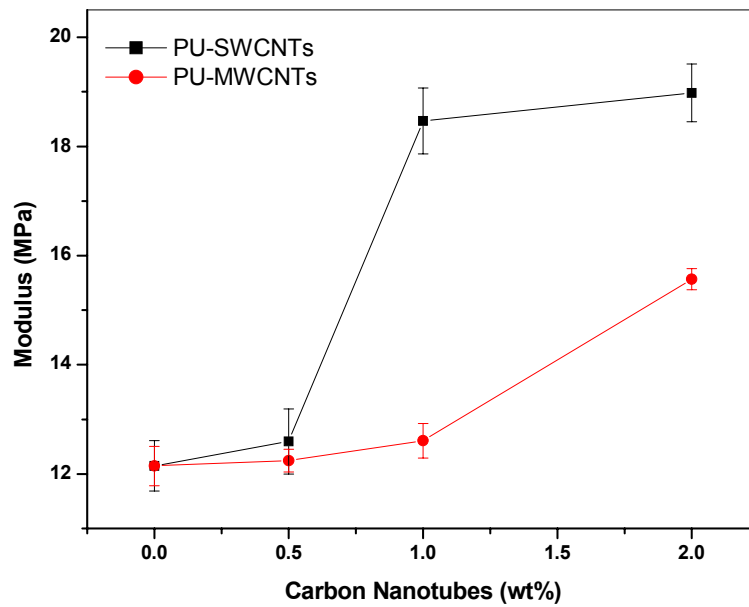


Figure 5.23: Modulus of the PU/CNTs nanocomposites as a function of SWCNTs and MWCNTs concentration.

Conclusion

The surface mechanical properties of PU nanocomposites with three different nanofillers were evaluated by nanoindentation. In PU clay nanocomposites, the effect of adding organoclay on the hardness and elastic modulus of PU significantly increased with increasing organoclay content. The improvement in these properties was determined by two factors: content of clay and structure of clay in the matrix. Exfoliated PU nanocomposites showed greater improvement than intercalated PU nanocomposites. For PU-GO nanocomposites, incorporation of GO into PU matrix leads to a significant increase in hardness and modulus due to the physical crosslinks and chemical bonding. In PU-CNT, the advantages and uniqueness of using CNTs as reinforcing nanofillers to make PU nanocomposites are obvious especially for SWCNT. Both the hardness and the modulus properties were improved after increased the concentration of CNTs. The study suggests that the loading rate and the holding time are crucial roles in producing a good result for the measurement of the hardness and the modulus in indentation test.

References

1. C. Hepburn, C., Polymer elastomers, 1982, London
2. Kresta, J.E., 60years of polyurethane 1998, Lancaster, PA, Technomic Publication.
3. Ulrich Meier-Westhues, 'Polyurethanes Coatings, Adhesives and Sealants' European Coating Tech Files, 2008
4. Paul, P.J., Nair, M.G.R., Koshy, P, Idage, B.B., J Appl. Polym. Sci. 1999, 74, 706 – 721
5. Pandya, M.V., Desphande, D.D., Hundiwale, D.G., J Appl. Polym. Sci. 1986, 32, 4959 – 4969
6. Blackwell, J., Nagarajan, M.R., Haitink, T.B., Polymer 1982, 23, 950 – 956
7. Gleiter, H., Prog. Mater. Sci. 1989, 33, 223 – 315
8. Baer, D.R., Burrows, P.E., El-Azab, A.A., Prog. Org. Coat. 2003, 47, 342 – 356
9. Chen, Y., Zhou, S., Yang, H., Gu, G., Wu, L., J. Coll. Inter. Sci. 2004, 279, 370 – 375
10. Finnigan, B., Martin, D., Halley, P., Truss, R., Campbell, K., Polymer 2004, 45, 2249 – 2254
11. Xia, H.S., Shaw, S.J., Song, M., Polym. Inter. 2005, 54, 1392 – 1400

12. Jin, J., Chen, L., Song, M., Yao, K.J., *Macromol. Mater. Eng.* 2006, 291, 1411 – 1421
13. Yao, K.J., Song, M., Hourston, D.J., Luo, D.Z., *Polymer* 2002, 43, 1017 – 1020
14. Song, M., Hourston, D.J., Yao, K.J., Toly, J.K.H., *Appl. Polym. Sci.* 2003, 90, 3239 – 3243
15. Song, M., Xia, H.S., Yao, K.J. Hourston, D.J. *Euro. Polym. J.* 2005, 41, 259 – 266
16. Yao, K.J., High Performance Polyurethane-organoclay nanocomposites, PhD Thesis, Loughborough University, 2005.
17. Jin, J., Chen, L., Song, M., (2008) Submitted for publication.
18. Jin, J., Song, M., Yao, K.J., Chen, L., *J. Appl. Polym. Sci.* 2006, 99, 3677 – 3683
19. Xia, H.S., Song, M., *Polym. Inter.* 2006, 55, 229 – 235
20. Gouldstone, A., Chollacoop, N., Dao, M., Li, J., Minor, A.M., Shen, Y.L., *Act. Mater.* 2007, 55, 4015 – 4039
21. Oliver, W.C., Pharr, G.M., *J. Mater. Res.* 1992, 7, 1564 – 1566
22. International Organisation for Standardisation, ISO 14577-1.2, 2001, 1 – 27
23. Pelletier, H., Mendibide, C., Riche, A., *Prog. Org. Coat.* 2008, 62, 162 – 178
24. Doerner, M.F., Nix, W.D., *J Mater Res.* 1986, 1, 601 – 609

25. Cheng, Y.T., Cheng, C.M., *Mater. Sci. Eng. R.* 2004, 44, 91
26. A. Flores, F.J. Balta Calleja, *Philos. Mag. A* 1998, 78, 1283 – 1297
27. Cooper, S.L., Tobolsky, A.V., *J. Appl. Polym. Sci.* 1996, 10, 1837 – 1844
28. Zhang, W., Joshi, A., Wang, Z., Kane, R.S., Koratkar, N., *Nanotechnology*, 2007, 18, 185703 (5pp)
29. Briscoe, B.J., Fiori, L., Pelillo, E., *J. Phys. D: Appl. Phys.* 1998, 31, 2395 – 2405
30. Chudoba, T., Richter, F., *Surf. Coat. Technol.* 2001, 148, 191 – 198
31. Ngan, A.H.W., Tang, B., *J. Mater. Res.* 2002, 17, 2604 – 2610
32. Briscoe, B.J., Fiori, L., Pelillo, E., *J. Phys. D: Appl. Phys.* 1998, 31, 2395 – 2405
33. Beake, B.D., Leggett, G.J., *Polymer* 2002, 43, 319 – 327
34. Liu, C.K., Lee, S., Sung, L.P., Nguyen, T., *J. Appl. Phys.* 2006, 100, 033503
35. Oyen, M.L., Cook, R.F., *J Mater Res.* 2003, 18, 139 – 150
36. Ma, Z., Long, S., Pan, Y., Zhou, Y., *J Mater Sci.* 2008, 43, 5952 – 5955
37. Klapperich, C., Komvopoulos, K., Pruitt, L., *J. Tribol.* 2001, 123, 624 – 629

38. Liang, J., Xu., Y., Huang, Y., Zhang, L., Wang, Y., Ma, F.Y., Li, F., Guo, T., Chen, Y., J. Phys. Chem. C. 2009, 113, 9921 – 9927
39. Stankovich, S., Dikin, D.A., Dommett, G.H.B., Kohlhass, K.M., Zimney, E.J., Stach, E.A., Piner, R.D., Nguyen, S.T., Ruoff, R.S., Nature 2006, 442, 282
40. Novoselov, K.S., Geim, A.K., Morozov, S.V., Jiang, D., Zhang, Y., Dubonos, S.V., Grigorieva, I.V., Firsov, A.A., Science 2004, 36, 666
41. Cai, D., Song, M., J Mater Chem. 2007, 17, 3678 – 3680
42. Cai, D., Kamal, Y., Song, M., Nanotechnology 2009, 085712 (5pp)
43. Shen, L., Wang, L., Liu, T., He, C., Macromol. Mater. Eng. 2006, 291, 1358 – 1366
44. Ajayan, P.M., Tour, J.M., Nature 2007, 447, 1066 – 1068
45. Wagner, H.D., Vaia, R.A., Material Today 2004, 7, 38 – 42
46. Liu, T., Phang, I.Y., Shen, L., Chow, S.Y., Zhang, W.D., Macromolecules 2004, 37, 7214 – 7222

Chapter 6

Bulk and Surface (sub-surface) Creep Behaviour of Polyurethane-Nanocomposites Studied by Means of Nanoindentation

6.1 Introduction

Polymer nanocomposite has been a topic of interest in recent years. A number of experimental reports have indicated that polymer nanocomposites exhibit greatly improvement in physical properties such as strength and modulus [1-3], heat resistance [4-5], energy dissipation [6] and gas permeability [7] compared to their neat counterparts. However, the improvement of the property depends on clay dispersion in the polymer matrix. Normally, nanocomposites can be obtained with structures ranging from an intercalated to a fully exfoliated state and these structures are influenced by preparation methods, type of nanofillers, and polymer chemical structure [1].

Numerous studies have focused on the mechanical properties and deformation behaviour of PU and its nanocomposites [8,9]. However, the viscoelastic behaviour including creep and stress relaxation is still not comparatively fully explored. In general, polymeric materials are viscoelastic materials which properties are deficient with time. Creep, for instance, is a time-dependent plastic deformation of a material that it subjected to a stress below its yield stress. The deformation process under load is strongly dependent on the mobility of the polymer chains. The chain mobility is not only temperature dependent, but also time dependent. The time dependent creep deformation will affect the applications of polymers [10].

There are few literatures concerning the study of viscoelastic behaviour of polymer nanocomposites especially in creep. Creep is much related to the service life and safety of materials and it should be one of the major concerns in developing the polymer nanocomposites. Incorporation of nanofiller into the polymer matrix could contribute the retardation of the process of creep or slow down the creep rate due to the restriction of polymer mobility and strong interface

interaction between the nanofiller and polymer chains. Nano-sized carbonitride significantly improved the creep strength of steel at high temperatures and reduced its creep rate [11].

Ranade et al. [12] studied polyethylene/MMT layer silicate films and found that the presence of small amount of rigid MMT contributed to the improved creep resistance of the polymers. The similar result was reported by Zhang et al. [13-14] that spherical nanoparticles with very low filler contents are able to enhance creep resistance of polyamide 66. Recently, Yang et al. [10] has demonstrated that the creep strain and creep rate of polypropylene nanocomposites were reduced by 46% and 80% respectively, and the service lifetime was extended by 330% by introduction of 1 vol% nanoparticles compared to the neat matrix. However, all of these findings usually implement tensile creep test which is reasonably well-developed for bulk materials. The ability to study the mechanical properties of materials at submicron scale is still not attainable. The implementation of depth-sensing indentation in creep test was proposed by Pollock et al [15] under the condition of constant load. Mayo et al [16] further implements a similar technique by using nanoindentation equipment. In this chapter, experimental approaches of creep property in bulk and subsurface of PU nanocomposites by using nanoindentation were presented as well as modelling.

6.2 Theoretical of creep behaviour

In the conventional creep test, the elongation of the specimen is measured as a function of duration and the test may not necessarily be continued to rupture of the sample. For each test, the creep strain (the increase in specimen length as a percentage of the initial length) is plotted as a function of the test duration to give the creep curve. Figure 6.1 is a schematic diagram of a typical tensile creep curve indicating the three regimes; a region of decreasing creep rate (primary creep), a region in which the creep rate is more or less constant (secondary creep), and a region in which the creep rate increases (tertiary creep) until rupture of the sample occurs. This is different from an indentation creep, in which the indentation load most likely leads only to the primary and secondary creep for polymeric materials.

Figure 6.2 shows a typical diagram of indentation creep. In general, the rupture cannot be observed during indentation experiments.

There are some differences between tensile and indentation creeps. Conventional tensile creep tests require many samples because each sample can be tested only at one temperature and under one stress. Owing to possible microstructure variations among samples, it is sometimes difficult to obtain consistent data. To avoid this difficulty, indentation creep is used in which a small indenter is forced into the surface of the specimen in a similar manner to the hardness test. However, unlike hardness tests in which the size of indent is measured, here the depth of penetration is measured under a constant external load imposed on the indenter. Another important advantage of indentation creep is the time consumed and it can be used to collect a lot of data in a short period [17].

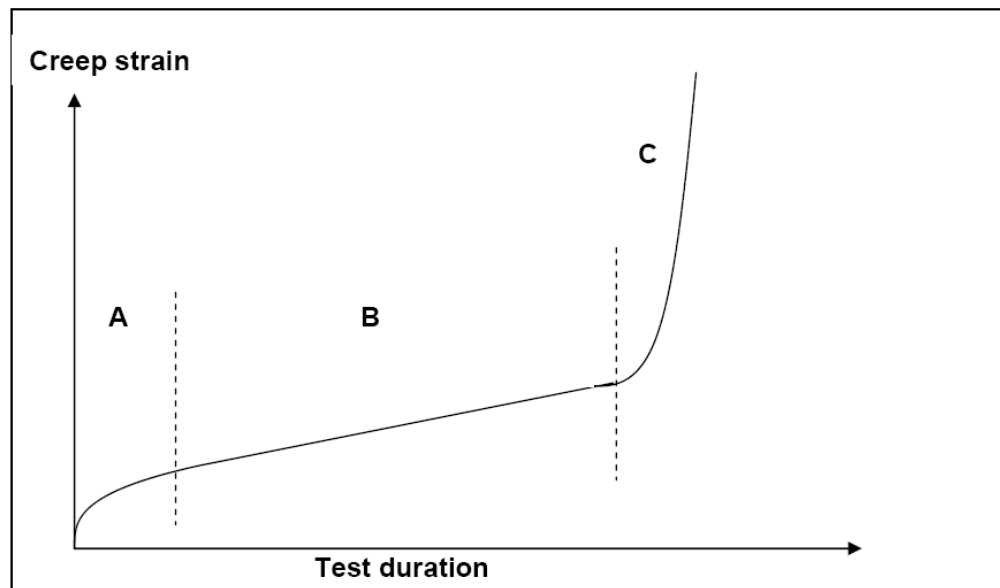


Figure 6.1: Schematic conventional creep curve showing the three creep regimes (A) primary creep region; (B) secondary creep region; (C) tertiary creep region

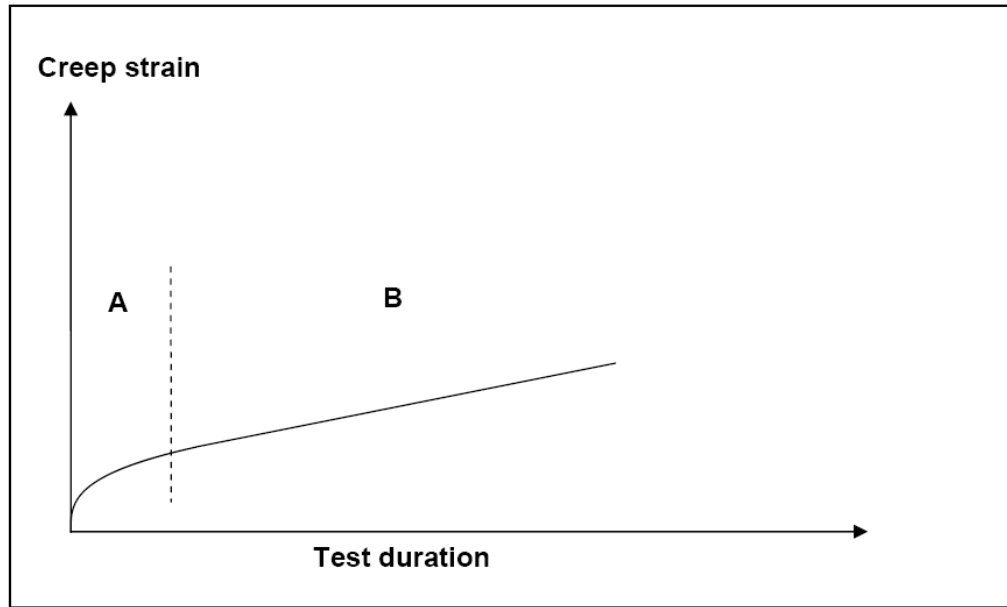


Figure 6.2: Schematic indentation creep curve showing the two regimes (A) primary creep region; (B) secondary creep region

6.3 Indentation creep test

The surface mechanical properties of the PU/organoclay nanocomposites were determined by Nano Test System from Micro Materials, UK [18]. Measurements are accomplished by imposing a pendulum-based depth-sensing system with the sample mounted vertically and the load applied electromagnetically. The tests were carried out on cross-sections of the samples at initial load of 0.15mN to maximum load of 2.5mN. A loading rate of 0.5mN/s was maintained during the incremental increase of the load until the indenter reached the maximum depth into the surface. The load was then held for 180s in order to account for creep effects before the indenter was unloaded. The distance between the indentations was 250 μ m to avoid overlapping. Figure 3.5 shows the schematic diagram of the nanoindentation procedure for creep experiment.

6.4 Conventional creep test

Creep test for the specimens (width, 4mm; thickness, 1-2 mm; length, 40 mm) was performed at 30°C on a TA Instruments Thermal Analysis DMA Q800. A small preload of 0.2 N was applied to make sure that the sample was taut. The samples were displaced at a stress of 0.2 MPa for 120 min and then were recovered for 60 min. The strain and creep compliance $J(t)$ was recorded.

6.5 Creep behaviour of PU-clays nanocomposites

A comparative evaluation of creep behaviour of bulk and subsurface PU nanocomposites using conventional and creep indentation was carried out. The creep performance of the pure PU and the PU nanocomposites can be characterized by the creep strain for creep indentation and by the creep compliance as a function of time in conventional creep test, respectively, under a constant stress. The creep behaviour of the PU nanocomposites with two different kinds of organoclays which are represent the different dispersion mechanisms were compared with the neat PU using indentation creep test.

In general, indentation creep strain versus time curve can be classified into two stages. Primary creep or stage one is reflect to region of decreasing creep rate owing to the slippage and reorientation of polymer chains under persistent load, and secondary creep or second stage is reflect to more or less constant creep rate and normally after a certain period, the creep rate reaches a steady state value [17]. For the exfoliated system as shown in Figure 6.3, the neat PU exhibits a particularly higher creep strain as compared with the other PU incorporates with different percentages of B30 organoclay at the same load after 180 seconds except for the sample with 5wt% of the filler. The introduction of organoclay into the neat PU shows a remarkably enhanced in their creep resistance as their creep strains were significantly reduced by 77% (1wt% B30) and 27% with 3wt% B30, respectively. The reduction in creep strain especially in secondary creep is speculated due to the restriction effect by the presence of small nanoparticles. Well dispersed nanofillers are producing huge interfacial areas that are

contributed to the change of curing degree and mobility of polymer chains [19]. This restriction, however, does not imply the creep resistance of the PU with 5wt% organoclay where the creep strain increases higher than the neat PU. The increment of the creep strain with 5wt% organoclay may be attributed by the formation of clay agglomerates which is not just obstructed the organoclay/PU matrix interaction, but in worst scenario, it even brought to the slippage layers of organoclay that resulting insignificant constraint creep resistance. Shen et al [20] investigated the creep behaviour of PA66 and its nanocomposites, and found that the enhancing effect of nanofillers was steadily decreased after a critical concentration of nanofillers. The adverse effect on creep behaviour could be due to the change of morphology or microstructure of the polymer matrix with incorporating nanoclay [20].

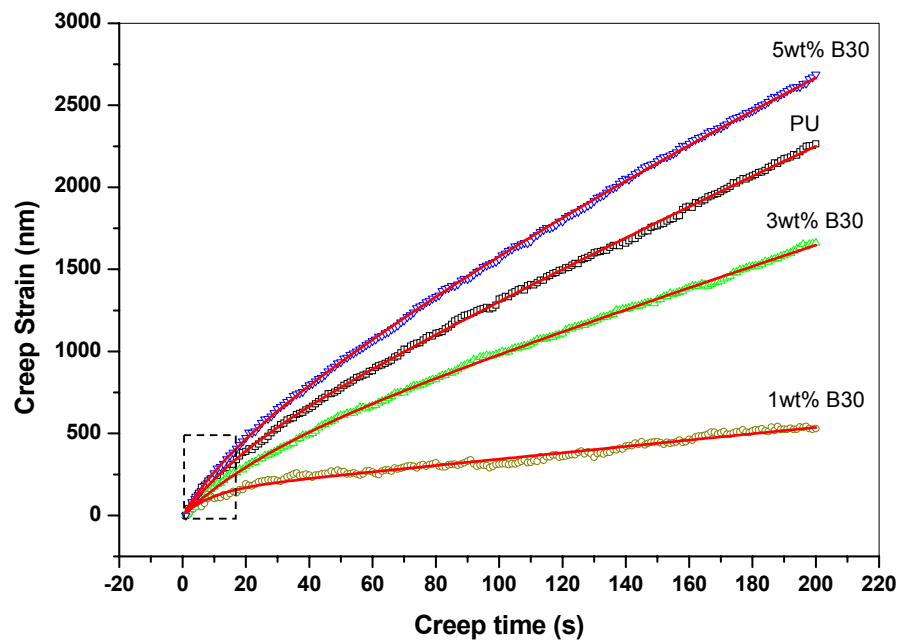


Figure 6.3: Creep strain versus time for PU nanocomposites with different B30 organoclay loadings. Open points are experimental data and the solid lines are fitting results by Eq. 6.1.

Figure 6.4 shows the creep behaviour of intercalated PU nanocomposites. It could be observed that all samples with presence of C20 organoclay, the creep strain is significantly decreased with respect to that of neat counterpart. The results show that the creep strains are decreased nearly by 50% for 1wt%, 16% for 3wt% and 57% for 5wt% organoclay, respectively. The reduction of the creep strain with increasing C20 organoclay content suggests that the development of clay layers that probably allow much PU chains to penetrate into the clay galleries and produced a maximum interaction between clay and matrix. As a consequence, it could retard and reduce the molecular mobility when the constant load is applied.

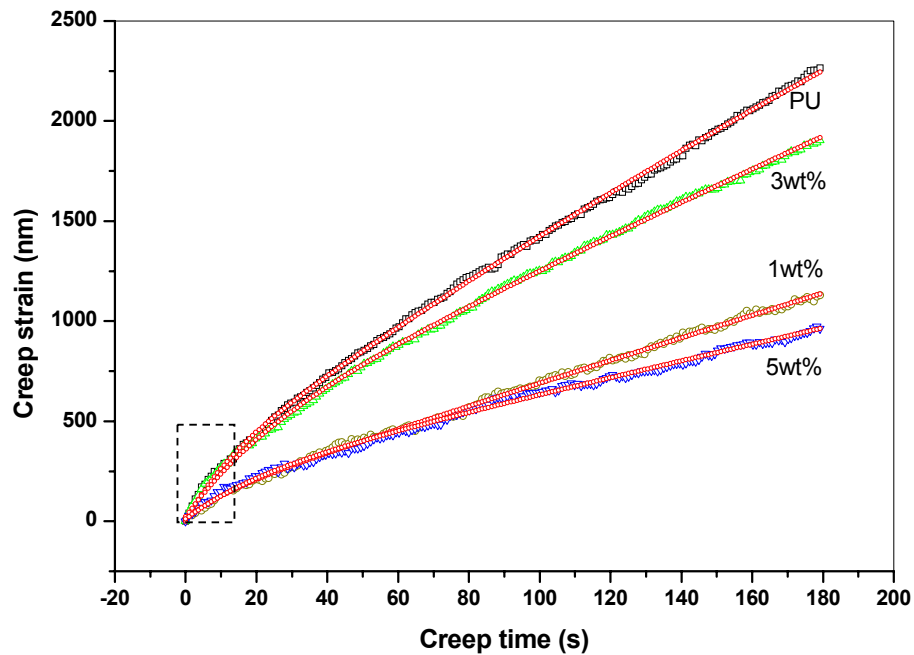


Figure 6.4: Creep strain versus time for PU nanocomposites with different C20 organoclay loadings. Open points are experimental data and the solid lines are fitting results by Eq. 6.1.

Segmented polyurethane is a block copolymer with altering soft and hard segments. The percentage of the hard segment significantly affects the final properties of PU [21]. The hard segments of PU normally serve as physical cross-links and act as high modulus fillers, whereas the soft segments provide extensibility characteristic [22]. The creep behaviour of the pure PU with different

hard segment contents was also investigated by creep indentation test. The results for creep strain as a function of hard segment concentration are shown in Figure 6.5. As expected, with the increase of hard segment content from 18% to 32%, the creep strain was reduced from 5000nm to 1000nm after 180s of creep time. As compared to the PU nanocomposites systems shown in Figures 6.3 and 6.4, it can be said that by incorporating only 1wt% organoclay B30 or C20 into the PU with 26% hard segment, the creep resistance is much higher than that of PU containing 32% hard segment.

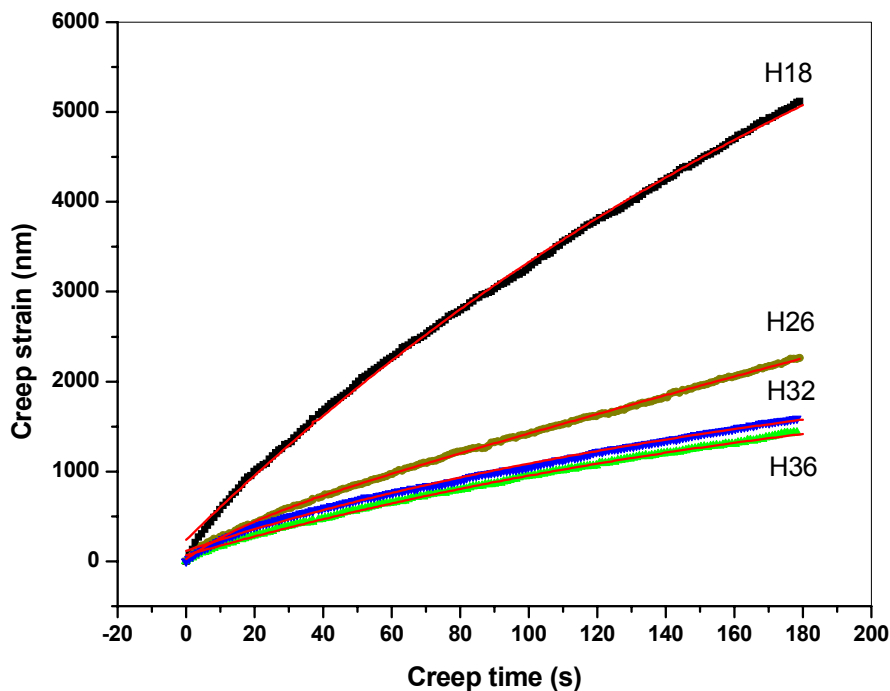


Figure 6.5: Creep strain of pure PU with different percentages of hard segment. Open points are experimental data and the solid lines are fitting results by Eq. 6.1.

It is worth to mention here, at low level of organoclay loadings (i.e less than 3wt %), the performance of an exfoliated system is significantly better than its intercalated counterpart (see Figures 6.3 and 6.4). Exfoliation of organoclay in polymer matrix clearly can produce significant improvement in creep resistance.

In order to obtain a deeper insight into the creep response of polyurethane to the nanofillers, the results were modelling using generalized elastic-viscoelastic (EVE) model which a slightly modified from EVEV model [23] generated from a generalized Kelvin model as illustrated in Figure 6.6. This model consists of a series of spring and dashpot in order to explain the total displacement during the indentation creep tests. According to this model, the creep deformation during indentation can be expressed as:

$$h = h_{in} \frac{P_o}{E_o A_o} + \sum_i^n \frac{P_o h_{in}}{E_i A_o} (1 - e^{-E_i t / \eta_i}) = h_e + \sum_i^n h_i (1 - e^{-t/\tau_i}) \quad (6.1)$$

where h is the indentation creep displacement. h_{in} is a virtual length which is used to define the indentation strain as $\varepsilon = h/h_{in}$ and its value is equal to the elastic-plastic displacement. P_o is the constant indentation load for the indentation creep experiments; E_o is the elastic modulus of the materials. A_o is the initial contact area at the beginning of the indentation creep experiment and can be determined by using the calibrated indenter area function. E_i and η_i are the elastic modulus and viscosity coefficient for the i th Kelvin unit in the model, respectively. The t is the creep time and n is the numbers of the Kelvin units, and the value of $n=3$ [23]. The equation demonstrates that an indentation creep should include two contributions to the deformation which are instantaneous displacement resulting from the elastic deformation of the materials during loading, and the viscoelastic deformation controlled by the exponential terms during creep.

This model can fit the indentation creep data of the polyurethane and polyurethane nanocomposites well. As shown in Figures 6.3 to 6.5 (solid lines), the model's approaches leads to a satisfactory agreement with the indentation creep experimental data of the neat PU with different percentages of hard-segments, and PU nanocomposites with different percentages of B30 and C20 organoclays, respectively.

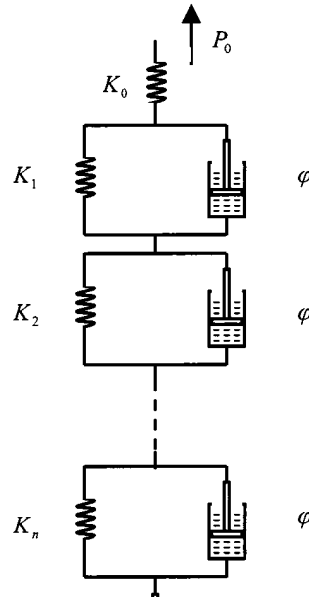


Figure 6.6: A generalized Kelvin model in viscoelastic study [23]

Table 6.1 lists the fitting results base on Equation 6.1 for the indentation creep experiments using a Berkovich indenter tip. The value of instantaneous displacement, h_e , which resulted from the elastic deformation, showed some decrement when the increase of hard-segment content in the pure polyurethane. The result indicates that the stiffness of polyurethane possibly retards the initial process of creep. In contrast, polyurethane nanocomposites showed the initial creep slightly increased by increasing the clay content. The increases of h_e , could be correlated with the aggregation of organoclays in the polymer matrix. Furthermore, at the initial stage of creep (illustrated as small boxes in Figure 6.3 and 6.4), intercalated nanocomposites showed better performance in creep resistant than exfoliated counterpart due to a lower value of h_e . It indicated that intercalation and exfoliation of organoclay in the polymer matrix could play major roles in controlling the creep at initial stage. The nanocomposites with lower loadings of organoclays show a much lower value of h_e , indicating a higher stiffness composites were developed. A further increase in clay content leads to an increase in elastic deformation especially in the exfoliated polyurethane nanocomposites system and induced a higher initial displacement at the early stage of creep.

For viscoelastic behaviour which is represented by h_1 , h_2 , and h_3 , the presence of organoclays showed some improvement on the creep performance by reduced depth penetration in both exfoliated and intercalated nanocomposites.

The results shown in Table 6.1 indicate that pristine polyurethane with lower hard-segment contents has longer retardation time, while in polyurethane nanocomposites with increasing organoclay content, the retardation times become longer, especially in τ_1 , as shown in Table 6.2. The increase of retardation time in the PU nanocomposites could result from clay-matrix interactions. The value of τ_1 is higher than that of τ_2 and τ_3 probably associated with the movement of polymer chains.

Table 6.1: Parameters obtained based on Equation 1 for the pure PU with different percentages of hard-segments.

Parameter	Pure PU			
	H18	H26	H32	H36
h_e (nm)	205	26	27	28
h_1 (nm)	6345	2321	1674	1473
τ_1 (s)	734	429	447	426
h_2 (nm)	6169	1968	1374	1321
τ_2 (s)	514	283	270	259
h_3 (nm)	3645	430	321	237
τ_3 (s)	279	214	128	114

Table 6.2: Parameters obtained based on Equation 1 for the PU-clays nanocomposites

Parameter	Materials					
	PU with B30			PU with C20		
	1wt%	3wt%	5wt%	1wt%	3wt%	5wt%
h_e (nm)	19	29	38	12	14	11
h_1 (nm)	375	2289	4048	1056	1817	1121
τ_1 (s)	105	396	503	235	291	355
h_2 (nm)	176	1103	2548	987	1755	950
τ_2 (s)	186	307	364	272	260	323
h_3 (nm)	98	310	449	104	191	101
τ_3 (s)	7	28	22	13	7	8

6.6 Comparison to bulk creep behaviour of PU nanocomposites

The bulk creep experiment was conducted using dynamic mechanical analyzer (DMA). The creep compliance for the polyurethane and its nanocomposites with 1, 3, 5wt% organoclay were determined as a function of time. Figure 6.7 and 6.8 display the creep compliance value for the pure polyurethane and its nanocomposites for exfoliated and intercalated systems. The shapes of the creep curves of the composites are very similar for all systems.

Figure 6.7 shows the creep compliance of polyurethane nanocomposites with B30 organoclay are remarkably reduced compare to the pure polyurethane in all ranges of nanofiller loadings. Interestingly, the result with the incorporation of 1wt% of B30 organoclay shows the best enhancement in creep compliance compared to 3wt% and 5 wt% loadings. With increasing the concentration of B30 organoclay, clay aggregation formed and increased which could act as stress concentrators and void formation. Thus, the mobility of polymer chains is encouraged resulting in dramatic increase in deformation. The result showed a similar trend with creep strain in indentation experiment (Figure 6.3). However, the results in intercalated system (see Figure 6.8) showed a contradictory finding compared to creep indentation shown in Figure 6.4. The improvement of creep resistance can only be achieved with a higher percentage of organoclay loading which leads to a

significantly reduced creep compliance. However, at small amount of organoclays (i.e 1 wt% and 3 wt%) seems to produce a worse result than that of the pure polyurethane.

The reason possibly comes from the testing methods. In bulk testing, the creep test was more likely in a uniaxial direction (uniaxial tension), whereas in creep indentation the load is applied in multiaxial directions. In intercalated nanocomposites, the penetration of matrix chains into the clay galleries caused the expansion of clay layers and facilitated stress transfer inside of the clay galleries. As a consequence, the possibility of the slippage of clay and matrix chains under persistent stresses is relatively high. However in creep indentation, the distributions of stresses during the indentation are in multiaxial direction and it is likely to reduce the possibility of clay slippage and restrict the realignment and motion of polymer chains.

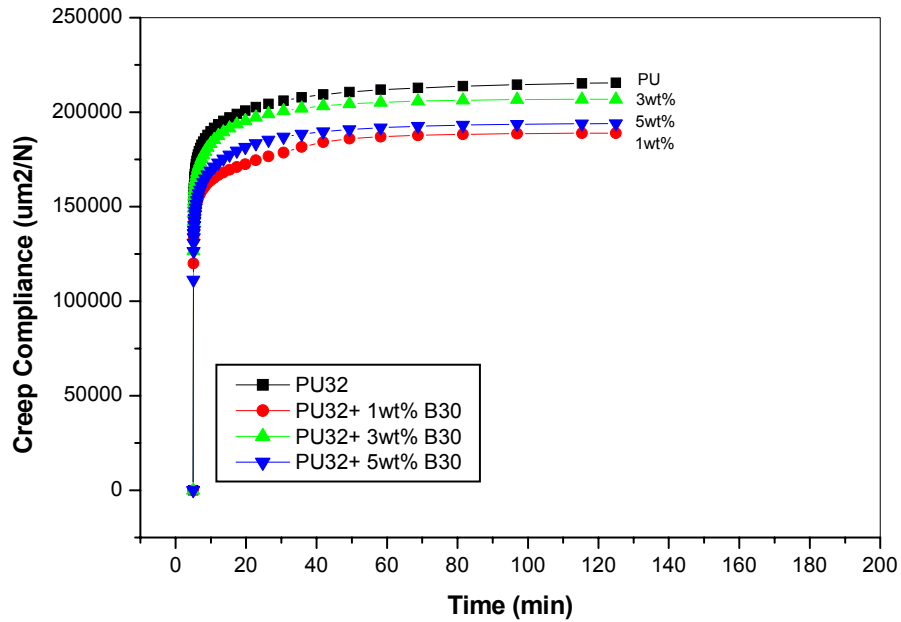


Figure 6.7: Bulk creep compliance of exfoliated PU nanocomposites *versus* time

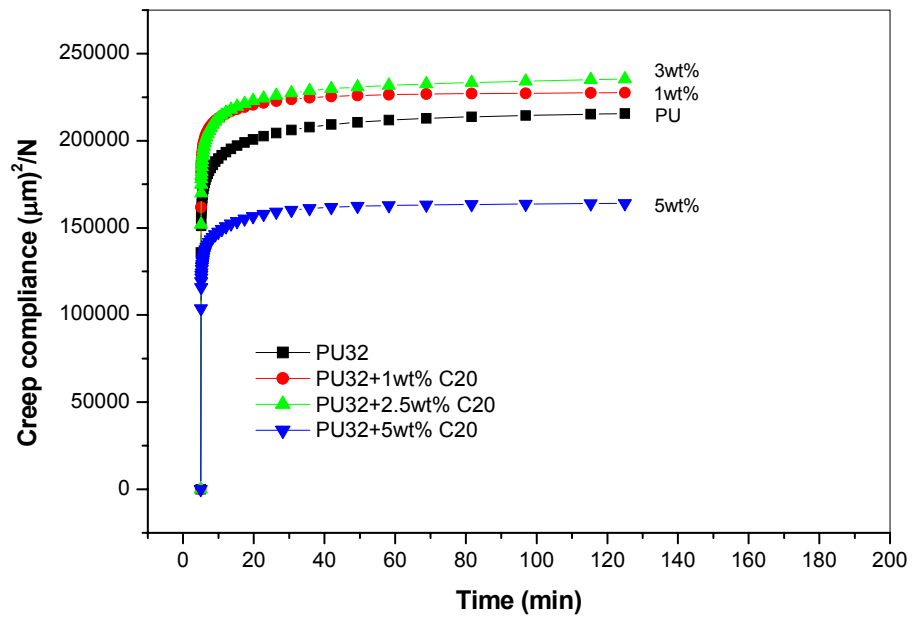


Figure 6.8: Bulk creep compliance of intercalated PU nanocomposites *versus* time

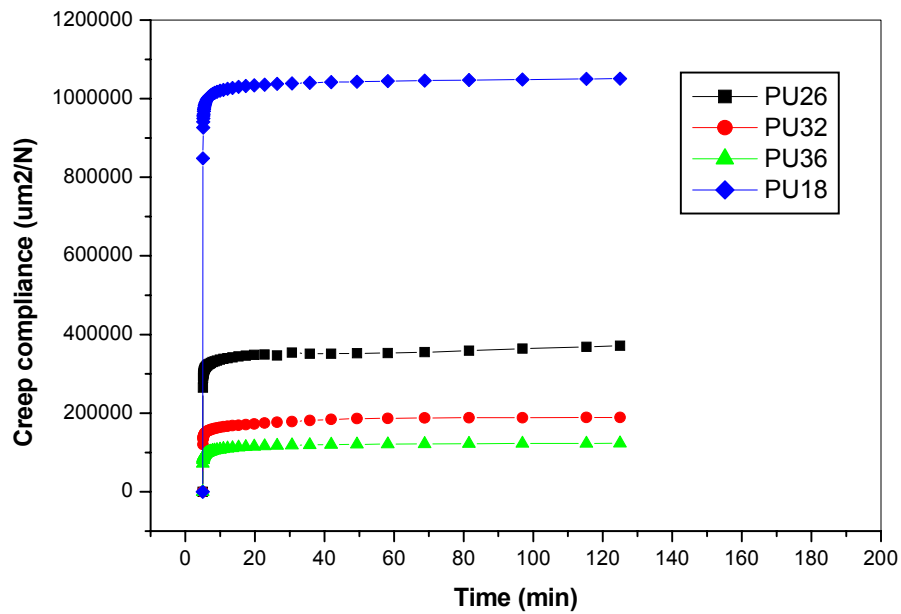


Figure 6.9: Bulk creep compliance of pure PU with different hard segments

In bulk creep tests, the trend of creep resistance of the pure polyurethane with different percentages of hard segments is consistent with the finding in creep indentation illustrated in Figure 6.5. By increasing hard segment, the creep compliance dramatically decreased as illustrated in Figure 6.9. Note that, the hard domain in pure polyurethane serves as physical cross-links and its act as high reinforce fillers in retarding the motion of the chains in matrix, thus preventing it from creeping.

Although many intercalated and exfoliated nanocomposites have been prepared, controlling of exfoliation degree still is a major challenge. In most cases, partial intercalated and partial exfoliated clay in polymer matrix exist. To provide some insight of both characteristics, model samples with different exfoliation degrees (ED) were prepared in this study. The weight ratio of intercalated C20/polyol and exfoliated B30/polyol dispersion was used to produce the polyol/organoclay mixtures with an exfoliation degree of 0% to 100%. The creep compliances of polyurethane nanocomposites with various exfoliation degrees are shown in Figure 6.10. Compared to the pure polyurethane, the creep resistance of polyurethane nanocomposites with more than 60% of exfoliation degree of clay was improved. In contrast, at less than 60% of exfoliation degree, the creep resistance of polyurethane nanocomposites was worse than that of the polyurethane. Creep resistance of polyurethane nanocomposite can be improved by incorporating the fillers with a high exfoliation degree. As the exfoliation degree increases, the aspect ratio of clay increases, and the interfacial interaction could be strengthened due to the increase in the contact area between polymer and the organoclay clay.

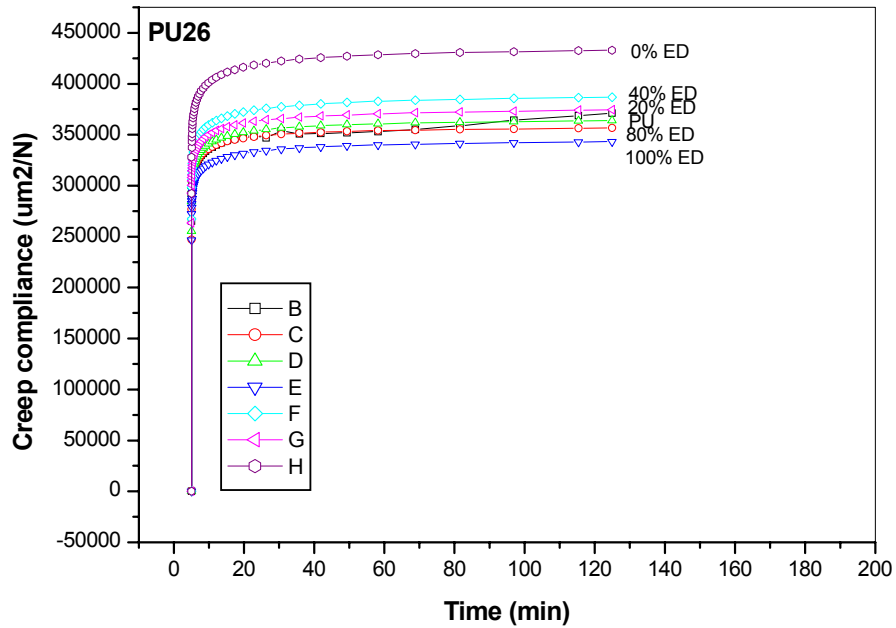
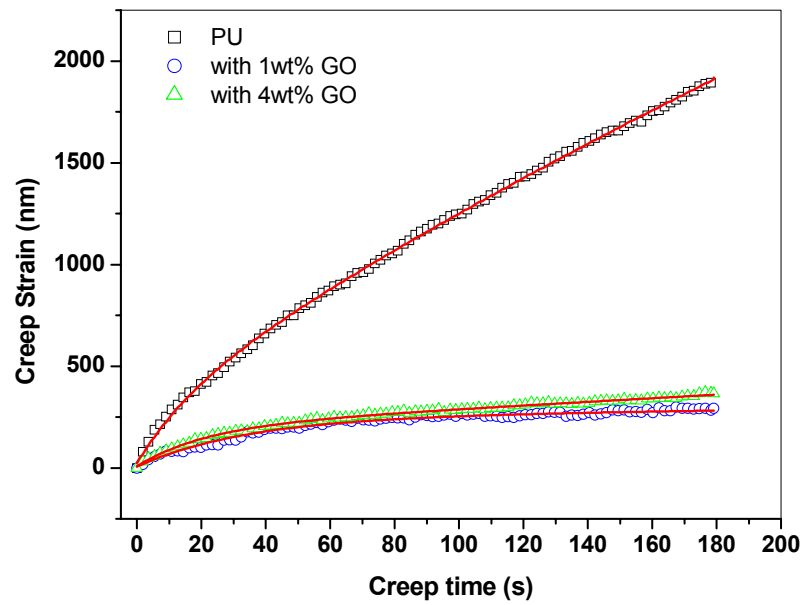


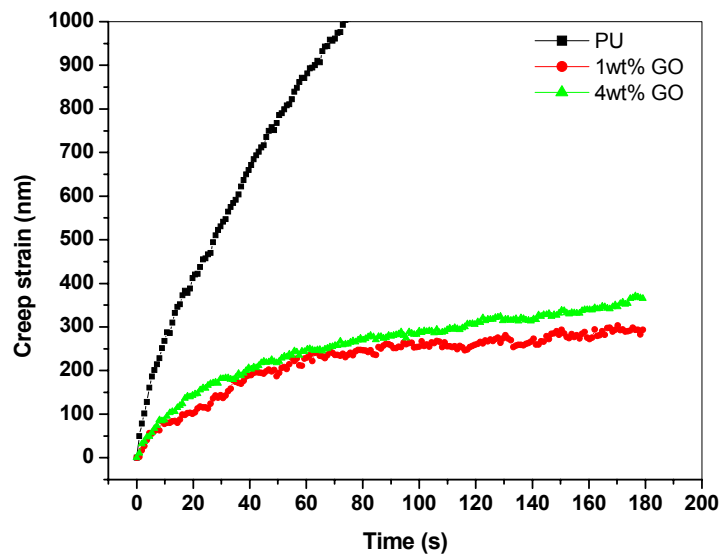
Figure 6.10: Effect of exfoliation degree (ED%) on the creep behaviour of PU nanocomposites.

6.7 Creep Behaviour of Polyurethane Graphene Nanocomposites

Figure 6.11 shows the creep strain results performed on the PU-GO composites prepared with different GO concentrations. It is noticed that the creep deformation (creep strain) decreases as the GO content increases, as expected from the addition of a rigid reinforcement of GO into a polyurethane matrix as shown in Figure 6.12(a). As GO content increases to 4wt%, the creep resistance only slightly improved. After 70s of creep time in Figure 6.12(b), the creep strain of 1wt% and 4wt% GO were reduced to 236nm and 257nm, respectively, as compared to the PU matrix. The increases in the resistance to creep could be contributed by the good interaction of PU matrix and GO and it is very pronounced with just 1wt% of GO.



(a)



(b)

Figure 6.11: (a) Creep strain versus time for PU nanocomposites with different GO loadings. Open points are experimental data and the solid lines are fitting results by Eq. 1. (b) Comparison of creep strain after 70s of creep time

Graphene has a large surface area as compared to other nanofillers such as SWCNTs and MWCNTs [24]. This property results in an increased interaction between the GO and the PU matrix. In the pure PU matrix, creep deformation is propagating as there are no obstacles for their chain movement. In contrast, the presence of GO in the composites could offer resistance for the creep by introduction of good mechanical interlocking and the presence of obstacles to the motion of matrix chains. This could be a reason for the enhancement in creep strain in PU-GO nanocomposites.

Table 6.3 lists the fitting results base on Equation 6.1 for the indentation creep experiments for PU-GO nanocomposites using a Berkovich indenter tip. The value of instantaneous displacement, h_e , which resulted from the elastic deformation, shows huge decrement when the addition of GO in the pure PU indicating a higher stiffness composites developed. The result indicates that an introduction of GO possibly helps the retardation of creep process at the initial stage due to elastic deformation. However, by further increase of GO content to 4wt% leads to an increase in elastic deformation and induces a higher initial displacement at the early stage of creep. The increases of h_e , maybe is correlated with the aggregation of GO in the polymer matrix and possibly some changes in the structure of the polymer chains. It indicates that the dispersion may play major roles in controlling the creep in initial stages.

Table 6.3: Parameters obtained based on Equation 1 for the pure PU and with different percentages of GO

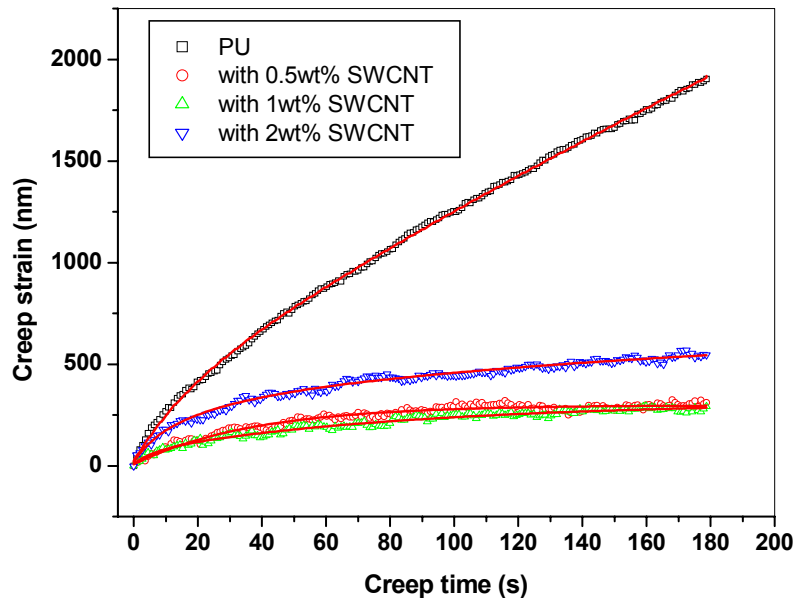
Parameter	PU	1wt% GO	4wt% GO
h_e (nm)	26	6	10
h_1 (nm)	2321	71	170
τ_1 (s)	489	35	24
h_2 (nm)	1968	67	95
τ_2 (s)	483	45	71
h_3 (nm)	430	78	107
τ_3 (s)	244	67	113

For viscoelastic behaviour which is represented by h_1 , h_2 , and h_3 , the presence of GO shows significant improvement on the creep performance in nanocomposites. In this result, the values of h_1 , h_2 , and h_3 in PU containing 1wt% GO show a lower viscoelastic deformation similar as an experimental results in Figure 6.12. The retardation times, τ_1 , τ_2 , and τ_3 are the response times indicating that with increasing GO content, the retardation time became longer, especially in τ_1 , as shown in Table 6.3. The increase of retardation time in the PU nanocomposites could result from GO-PU matrix interactions.

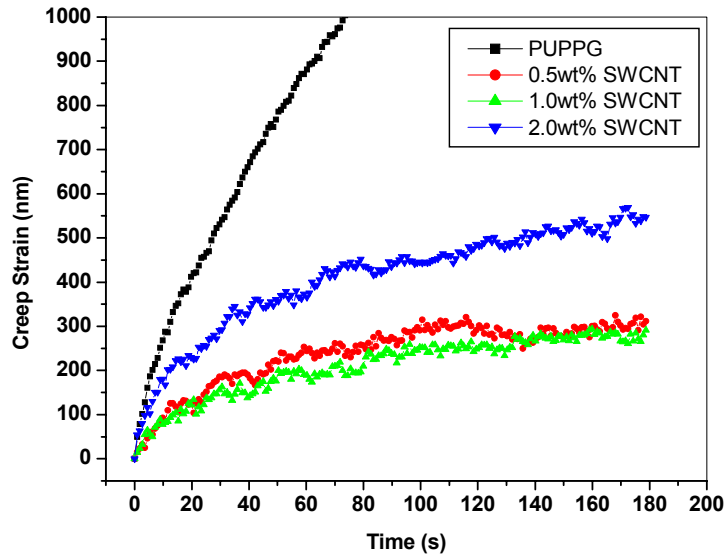
6.8 Creep Behaviour of Polyurethane CNT Nanocomposites

Figures 6.12 to 6.13 show the comparison of creep deformation (creep strain) data under constant load for the pure PU and PU with different percentages of CNTs nanofillers. As compared to the pure PU, with incorporation with only 0.5wt% of CNTs (SWCNT and MWCNT), the creep strain is significantly reduced from 1893nm to 311nm and 483nm for SWCNT and MWCNT, respectively, after 180s of creep time. However, with increase in CNTs content from 0.5wt% to 1wt% in both systems, the resulting creep resistance only slightly improved with such small decreasing in creep strain as noticed in Figures 6.12 – 6.13. This indicates the beneficial effects of reduced creep strain and its rate with increased weight percentage of CNTs. Dutta et al [25] showed that with incorporation with of 1wt% SWCNT in epoxy matrix, the creep deformation was dramatically reduced and they related this affect with the improvement of interface shear properties, straight morphology (instead of curve tubes) and good dispersion of SWCNT in epoxy matrix. Straight CNT tubes is very important and significantly improves the structural reinforcement to host polymer matrix as compared to curvature counterparts, as pointed out by Fisher et al [26]. In contrast, after incorporation with 2wt% of CNTs, the creep resistance for the samples shows a dramatic drop as creep strain increases. As shown in Figures 6.12(b) and 6.13(b), after 70s of creep time the creep strain was found to be about 413nm for 2wt% of SWCNT as compared to 261nm and 209nm for 0.5wt% and 1wt% of SWNT and was about 447nm for 2wt% of MWCNT as compared to 330nm and 302nm for 0.5wt% and

1wt% of MWCNT, respectively. This discrepancy can be explained by considering the possibility of aggregation of SWCNT that always impair the performance of nanocomposites after passing of certain amount in concentrations. As we are aware, high concentration of CNTs in polymer matrices is strongly attracts this kind of nanofiller to agglomerate as a results of van der Waals attraction [27,28], making load transfer difficult and thus, it deteriorated the resistance to creep deformation. In this study, the improvements of creep resistance for the PU with SWCNTs nanocomposites systems were clearly much higher than those of the PU with MWCNTs. The properties of the polymer matrix surrounded by individual (single-walled) tubules are different from those with multiwall tubes. With SWCNT the composite reinforcement strength is dominated by the huge interaction area than the multiwall tubes which is the inner concentric plays no role in increasing the effective cross-linking density within the nanocomposites [29]. Only the outside nanotubes can be strongly bonded to the polymer matrix and the inside nanotubes are weakly interacting by van der Waals attraction. Thus, this reason why the nanotubes with multiwall geometry can easily slide past each other and the shear modulus of the multiwall carbon nanotube is relatively low [29]. Therefore, for the same weight fraction of CNTs, SWCNTs will offer significantly higher creep resistance to the PU matrix than MWCNTs, as observed in experiments.

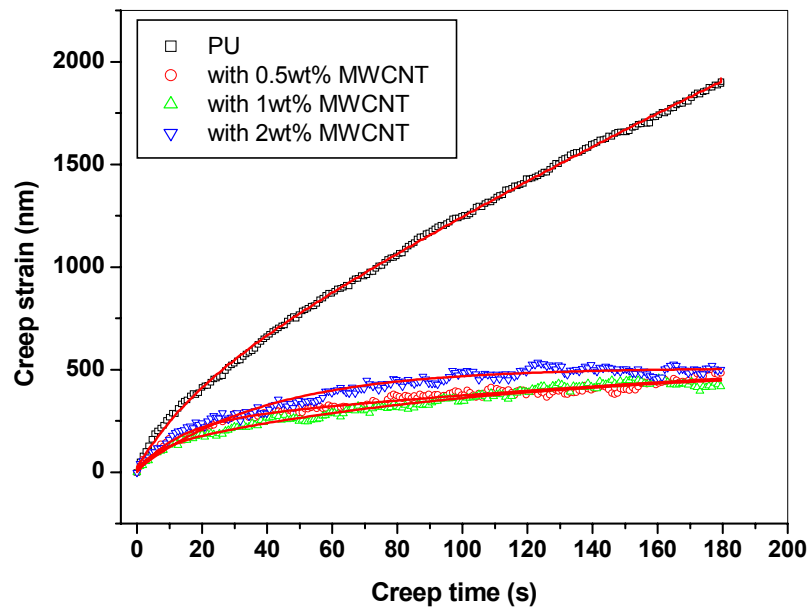


(a)

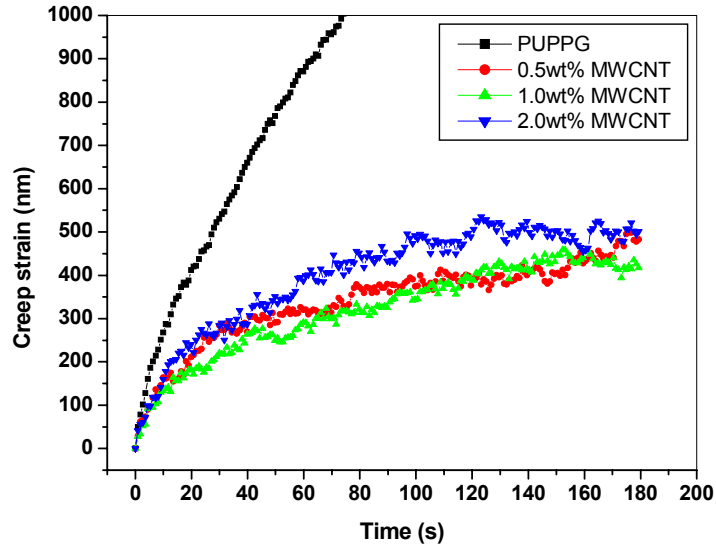


(b)

Figure 6.12: (a) Creep strain versus time for PU nanocomposites with different SWCNT loadings. Open points are experimental data and the solid lines are fitting results by Eq. 1.(b) Comparison of creep strain after 70s of creep time



(a)



(b)

Figure 6.13: (a) Creep strain versus time for PU nanocomposites with different MWCNT loadings. Open points are experimental data and the solid lines are fitting results by Eq. 1.(b) Comparison of creep strain after 70s of creep time

Table 6.4 lists the fitting results base on Equation 6.1 for the indentation creep experiments for PU-CNT nanocomposites using a Berkovich indenter tip. The value of instantaneous displacement, h_e , which resulted from the elastic deformation, shows some decrement when the increase of CNTs content in nanocomposites. The increases of h_e , maybe is correlated with the aggregation of CNTs in the polymer matrix and possibly some changes in the structure of the polymer chains.

Table 6.4: Parameters obtained based on Equation 1 for the PU and with different percentages of CNTs

Parameter	Materials					
	PU with SWCNTs			PU with MWCNTs		
	0.5wt%	1wt%	2wt%	0.5wt%	1wt%	2wt%
h_e (nm)	7	10	21	10	17	11
h_1 (nm)	74	99	210	167	142	126
τ_1 (s)	41	112	209	288	122	43
h_2 (nm)	71	88	183	142	132	126
τ_2 (s)	35	116	25	274	114	43
h_3 (nm)	61	69	101	232	108	126
τ_3 (s)	41	60	8	12	7	43

For viscoelastic deformation which is represented by h_1 , h_2 , and h_3 , the presence of CNTs showed dramatically improvement on the creep performance in both SWNT and MWCNT-PU nanocomposites compared to the pure PU. Again the performance of SWCNTs is outperforming the capability of MWCNTs in retard the viscoelastic deformation. The retardation times, τ_1 , τ_2 , and τ_3 are the response times indicating that the pure PU has the longest retardation time as shown in Table 6.3 compared to PU-CNT nanocomposites. For the PU nanocomposites, with increasing CNT content, the retardation time became longer, especially in τ_1 , as shown in Table 6.4. Again, the increase of retardation time in the PU nanocomposites could result from CNT-PU matrix interactions.

Conclusion

The bulk and subsurface creep behaviour of PU nanocomposites were studied by conventional and indentation creep testing. Indentation creep test revealed the creep resistance of subsurface of polyurethane can be improved by incorporating organoclays. The significant increment in creep resistance obviously occurred in exfoliated systems. With a higher percentage of organoclay, an improved creep resistance in intercalated systems also can be achieved. Exfoliated polyurethane nanocomposites showed greater improvement in creep resistance than intercalated ones. The creep resistance is significantly increased when the polyurethane were reinforced with graphene and CNT nanofillers. This indicates that the graphite oxide and CNTs could produce a strong interaction with the polyurethane matrix and its benefits to retard the creep deformation in nanocomposites.

References

1. Sinha, S.R., Okamoto, M., Prog. Polym. Sci. 2003, 28, 1539 – 1641
2. Kojima, Y., Usuki, A., Kawasumi, M., Okada, A., Fukushima, Y., Kurauchi, T., Kamigaito, O. J Mater. Res. 1993, 8, 1185 – 9
3. Alexandre, M., Dubois, P., Mater. Sci. Eng. 2000, 26, 1 – 5
4. Pinnavaia, T.J., Beall, G.W., *Polymer-clay nanocomposites*, John Wiley & Sons, West Sussex, 2001
5. Vaia, R.A., Giannelis, E.P., Macromolecules, 1997, 30, 8000 – 9
6. Jin, J., Song, M., Yao, K.J., Chen, L., J. Appl. Polym. Sci. 2006, 99, 3677 – 3683
7. Xu, R.J., Manias, E., Snyder, A.J., Runt, J., Macromolecules 2001, 34, 337 – 339

8. Doman, D.A., Cronin, D.S., Salisbury, C.P., *Experimental Mechanics*, 2006, 46, 367 – 376
9. Jin, J., Song, M., Yao, K.J., Chen, L., *J. Appl. Polym. Sci.* 2006, 99, 3677 - 3683
10. Messersmith, P.B., Giannelis, E.P., *J. Polym. Sci. Part A: Polym. Chem.* 1995, 33, 1047 – 1050
11. Yang, J.L., Zhang, Z., Friedrich, K., Schlarb, K., *Appl. Phys. Lett.* 2007, 91, 011901
12. Taneike, M., Abe, F., Sawada, K., *Nature* 2003, 424, 294 – 296
13. Ranade, A., Nayak, K., Fairbrother, D., D'Souza, N.A., *Polymer* 2005, 46, 7323 – 7333
14. Zhang, Z., Yang, J.L., Friedrich, K., *Polymer* 2004, 45, 3481 – 3485
15. Pollock
16. Mayo, M.J., Nix, W.D., *Acta Metall.* 1998, 36, 2183
17. Cahn, R.W. (Editor), *Concise Encyclopedia of Materials Characterization*, 2nd Edition, Elsevier, Oxford, 2005
18. *Manual of Nanotest System*. Micro Materials, UK
19. Ajayan, PM, Schadler, LS, Braun, PV., *Nanocomposites Science and Technology*, Wiley-VCH, Weinheim, 2003
20. Shen, L, Phang, IY, Chen, L., Liu, TX., Zeng, K. *Polymer* 2004, 45, 3341 – 3349

21. Cooper, S.L., Tobolsky, A.V. *J Appl. Polym. Sci.* 1996, 10, 1837 – 1844
22. Paul, P.J., Nair, M.G.R., Koshy, P., Idage, P.B.B., *J Appl. Polym. Sci.* 1999, 74, 706 – 721
23. Yang, S., Zhang, Y.W., Zeng, K., *J. Appl. Phys.*, 2004, 95, 3065 – 3666
24. Ramanathan, T., et al., *Nat. Nanotechnol.* 2008, 3, 327 – 332
25. Dutta, A.K., Penumadu, D., *J. Mater. Res.* 2004, 19, 158 – 164
26. Fisher, F.T., Bradshaw, R.D., Brinson, L.C., *Appl. Phys. Lett.* 2002, 80, 4647 – 4649
27. Li, X., Gao, H., Scrivens, W.A., Fei, D., Xu, X., Sutton, M.A., Reynolds, A.P., Myrick, M.L., *Nanotechnology*, 2004, 15, 1416 – 1423
28. Xia, H., Song, M., *Soft Matter* 2005, 1, 386 – 394
29. Zhang, W., Joshi, A., Wang, Z., Kane, R.S., Koratkar, N., *Nanotechnology*, 2007, 18, 185703 (5pp)

Chapter 7

Scratch Properties of Polyurethane Nanocomposites Studied by Nanoindentation

7.1 Introduction

Polymers and nanocomposites have been widely used in microelectronic packaging, coatings, aerospace, automotive, food packaging and biomedical applications because of their adequate strength, lightness, versatility, ease to processing and low cost [1]. In recent years, the developments of polymeric materials as coating materials has been gain more and more attention. However, polymer matrices are very sensitive to scratching and subjected to low scratch and wear resistance, and are unacceptable for most coating applications.

There are common efforts of improving the scratch resistance of polymeric materials. The first solution found to reduce this scratch sensitivity was to deposit a mineral coating on the surface of the polymer. This procedure experienced however little success, at least partly due to the large difference between the elastic strains domains of the substrate and coating [2]. A second generation of coatings used polysiloxane and acrylic materials, where the scratch resistance is given by the hardness of the coat and the coatings have elastic strain domains in the range as the substrate [2].

The new generation of protective coatings has employed nano-materials, in which an organic matrix is filled with nanosized particles of fillers or polymer nanocomposites [2]. The idea behind this strategy is to associate the large elastic domain of an elastomeric polymer with the hardness of the filler. As nanocomposites material, polymers are combined with hard nanofillers, in order to improve the materials properties of polymer. Polymer nanocomposites offer the advantage of favorable material properties and diminish their disadvantages.

Research on nanoscale scratching can help develop mechanical scratching into a promising nanofabrication process. Thus, whether it is aiming to improve the surface scratch resistance or to engineer polymer surfaces for more efficient nanofabrication process, knowledge on scratch and wear properties at the micro to nanoscale is crucial [1].

It has been suggested by various authors that the surface properties of polymers might be different from those of the bulk due to differences in molecular dynamics [3-4]. Conventional wear type tests, which focus on bulk properties, might not be appropriate for assessing the surface properties of polymer nanocomposites. In recent years, the rapidly expanding field of depth-sensing nanoindentation which uses a sharp tip sliding on the surface provides a quantitative method for studying the scratch and wear properties of the surface or subsurface region of polymeric materials [5].

The advent of newly developed depth sensing devices which use a sharp tip sliding on the surface to stimulate a single asperity contact has made possible characterization techniques, such as nanoscratch, that are sensitive enough to examine the surface properties for small scale and light loads [6]. Unlike an indentation process where the normal load is uniformly distributed beneath the indenter, scratching involves a high-friction-induced sliding process [7]. The indenter is fully supported by the specimen in the front and only partially by recovered material in the rear-half. The extent of recovery again depends on the stress-relaxation characteristics of the material in the contact zone. Figure 7.1 is a schematic of the most common types of material damage during scratching [7].

Research on surface roughness and scratch behaviour of polymer nanocomposites is very limited. In order to develop good understanding on interfacial phenomena in nanostructure materials, knowledge in scratch and wear on a nanoscale in a lightly loaded situation is essential to providing a bridge between surface science and engineering. Thus, in order to investigate the effect of nanofillers in polyurethane

nanocomposites, the nanoscratch test under certain scratching conditions was studied using the nanoindentation test. A typical profile depth of scratch test was recorded as shown in Figure 7.2. The profile depth is the penetrating depth of the tip into the material, influenced by the hardness of the scratched material. It also indicates the resistance of the material to the tip penetration. However, in this work the nanoscratch hardness cannot be measured due to the nature of the polyurethane itself where the scratch morphology is totally invisible after the scratch test. Normally, the scratch deformation can be measured using the scratch hardness and calculated using equation 7.1 [8]:

$$\text{Scratch hardness, } H_s = \frac{P}{A} = q \frac{4P}{\pi \cdot d_s^2} \quad (7.1)$$

where P is the applied normal load, A is the projected load supporting area, and d_s is the recovered scratch width. The parameter q is a measure of the material response, which is arbitrarily chosen as 1 [8].

In this part, the research focused on the scratch behaviour of polyurethane nanocomposites with different kinds of nanofillers. The depth profile was measured based on the constant load and the different scratch velocity and the results were correlated between the relative scratch resistance and the mechanical properties of the nanocomposites. Due to the problem to identify the scratch damage with the high depth recovery in PU, the scratch hardness was not measured. Thus, the study was only focused on the relative scratch depth using the depth profile of the nanoscratch and the relative scratch resistance.

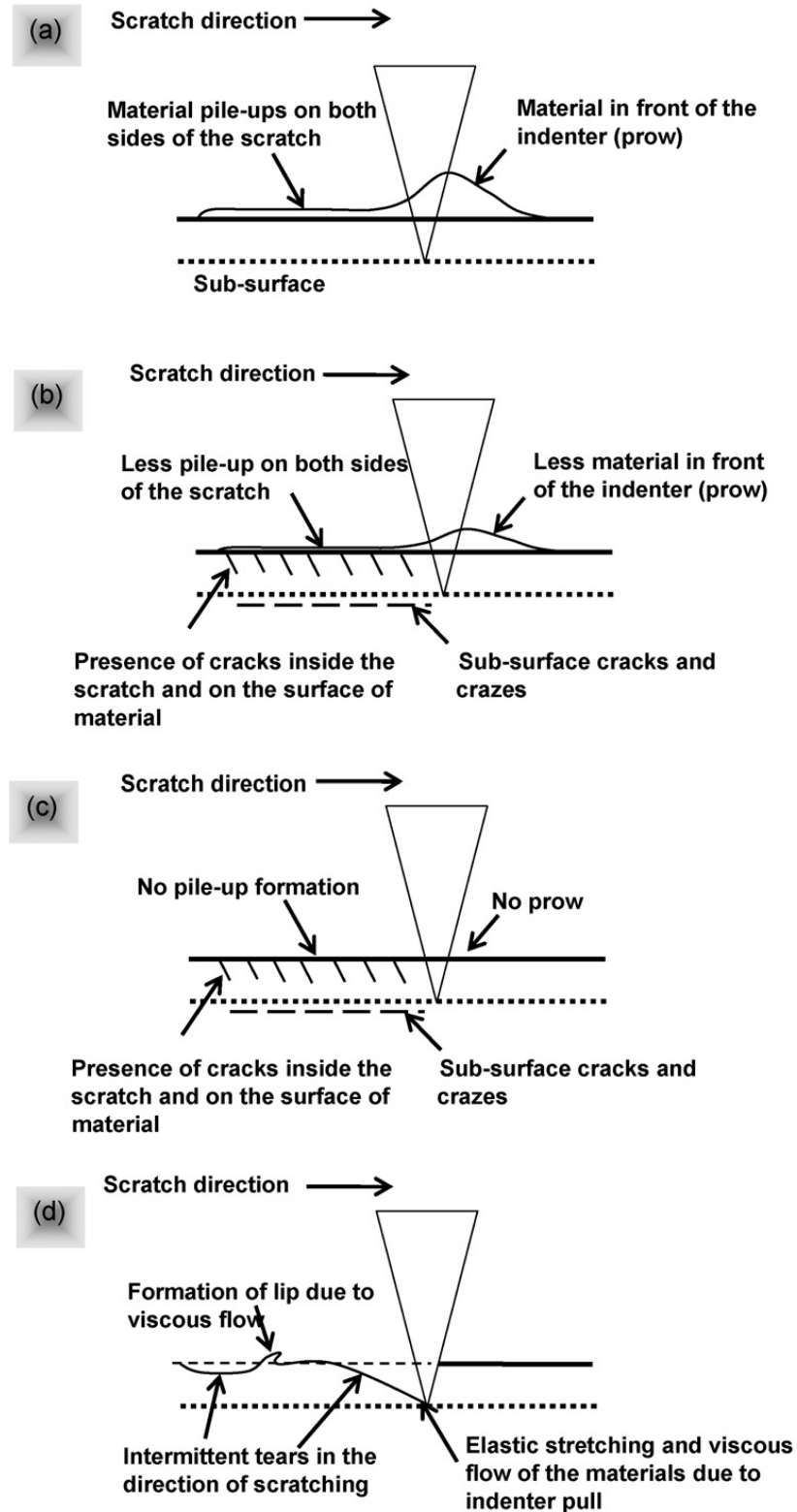


Figure 7.1: Schematic representations of the polymeric material responses to scratching: (a) ductile response; (b) ductile and brittle response; (c) brittle response; and (d) elastomeric response [7]

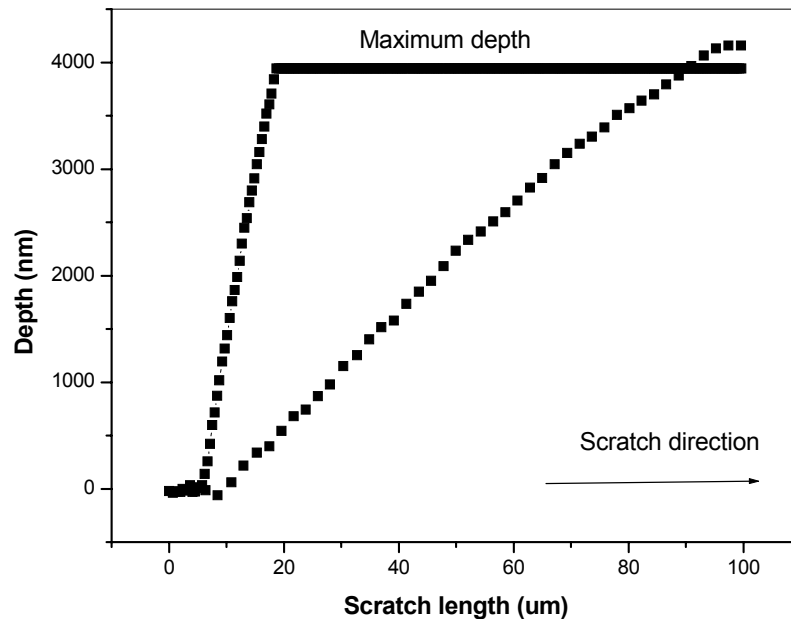


Figure 7.2: Typical scratch plot using indentation scratch test

7.2 Polyurethane clay nanocomposites

7.2.1 Scratch depth profiles

Since the surface properties of polymers maybe differ from those of the bulk, techniques using indentation scratch that focus on nanoscale surface damage were applied to correlate surface damage with material characteristics of polyurethane nanocomposites. Material characteristics influence the damage occurred when varying the penetration depth during the scratch test.

The intrinsic surface properties of a material, for example, hardness, strength, ductility and work hardening, are very important factors for wear/scratch resistance. The mechanism of wear/scratch is very complex. The conventional model for abrasive wear involves the removal of materials through scratching by an abrasive particle by protuberances on counterface. On a microscale, the scratching of a sharp indenter against the sample surface during a scratch test can be regarded as the wear of the material by a hard particle as occurs during normal wear [9]. In order to assess the wear resistance of PU nanocomposite films, nanoscratch tests were performed

over the sample surface with specified scratch length and at specified scratch rate. The depth of indenter penetration into the samples reflects the ability of the material's surface to resist scratching.

Figure 7.3, (A) and (B), shows the scratch depth profiles on the PU and the exfoliated and intercalated nanocomposite thin films with 3% organoclay at the scratch rates of $3\mu\text{m/s}$ and $5\mu\text{m/s}$, respectively. At the scratch length of $20\mu\text{m}$, the scratch depth on the PU surface was about 957nm but that of the intercalated nanocomposite film was merely about 448nm . With the hardness tests, surface scratch resistance was more enhanced in the case of exfoliated nanocomposites than in the case of the intercalated nanocomposites, as indicated by the lower scratch depths of the exfoliated nanocomposites. It can be seen from the scratch-depth values shown in Figure 7.3(B) that the reality of the film surface to resist the indenter scratch was strong at the high scratch velocity. These results revealed that the outcome of adding organoclay into a PU matrix system is beneficial for the PU's scratch resistance and suggest that this improvement is achieved more obviously for the exfoliation structured PU nanocomposite.

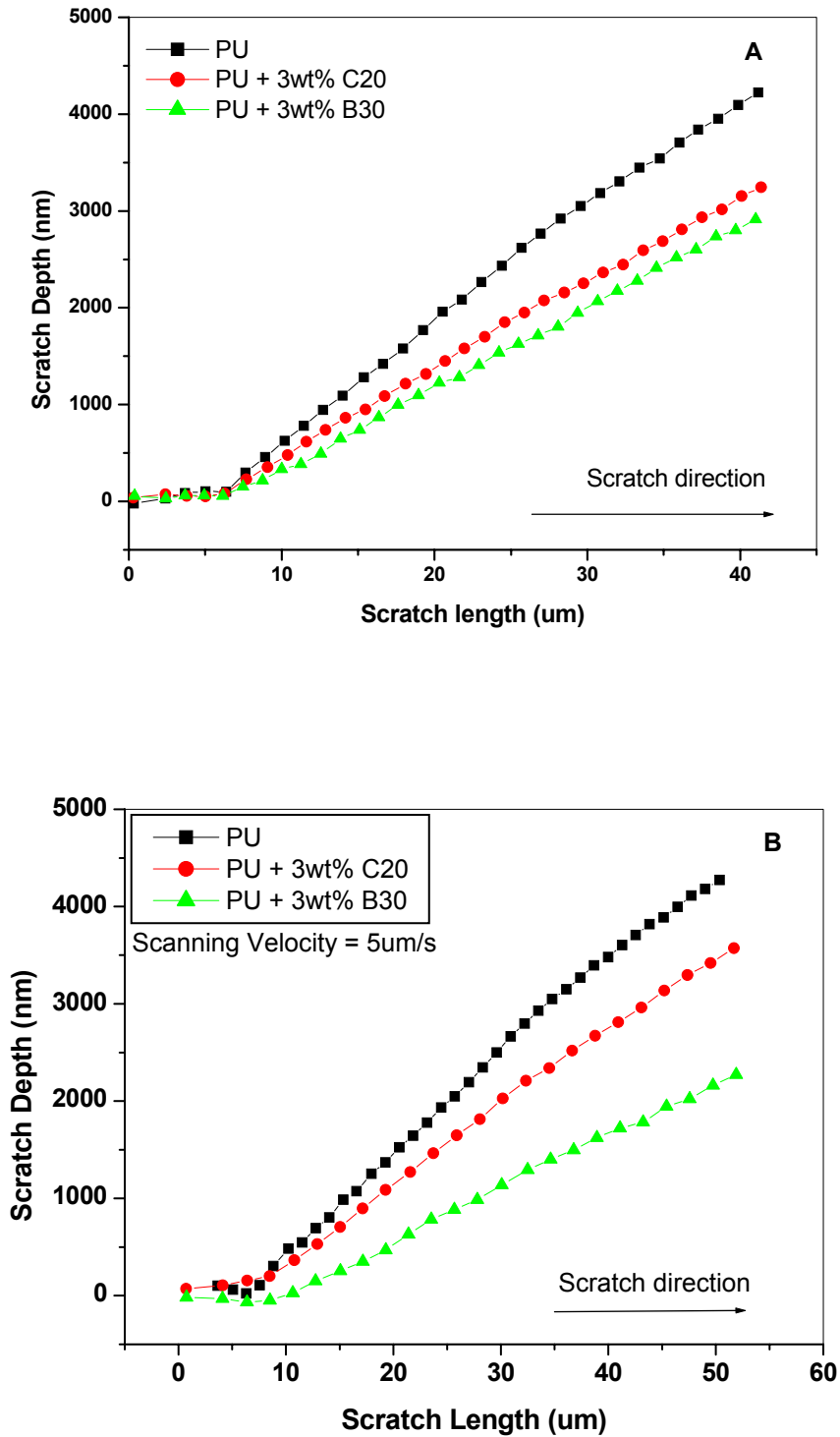


Figure 7.3: Nanoscratch depth profiles for PU and its nanocomposites (A) 3 μm/s (B) 5 μm/s

7.2.2 Relative scratch resistance

As stated above, the indenter scratch during a scratch test is similar to the abrasion of hard particle on the material surface during normal abrasive wear. Both are dominated by the mechanisms of micro-plowing and micro-cutting. It is, therefore, generally accepted that scratch resistance and wear resistance are closely related, that is, materials with high scratch resistance will have high abrasive wear resistance. In a conventional model for abrasive wear, the wear rate is linearly proportional to the applied load (P) and inversely proportional to the hardness (H) of the surface being abraded, that is $Q = k \times P/H$, where k is wear coefficient [9]. According to this equation, attempts can be made to establish a relationship between the relative scratch resistance (W) and surface hardness [10]. In our studies, given the factor of load can be eliminated as the same load was applied, the relative scratch resistance can be expressed as a ratio of the scratch rate for PU (Q_{PU}) and that for the nanocomposite ($Q_{PU/clay}$), which is proportional to the ratio of the hardness, that is, $W \propto H_{PU/clay}/H_{PU}$.

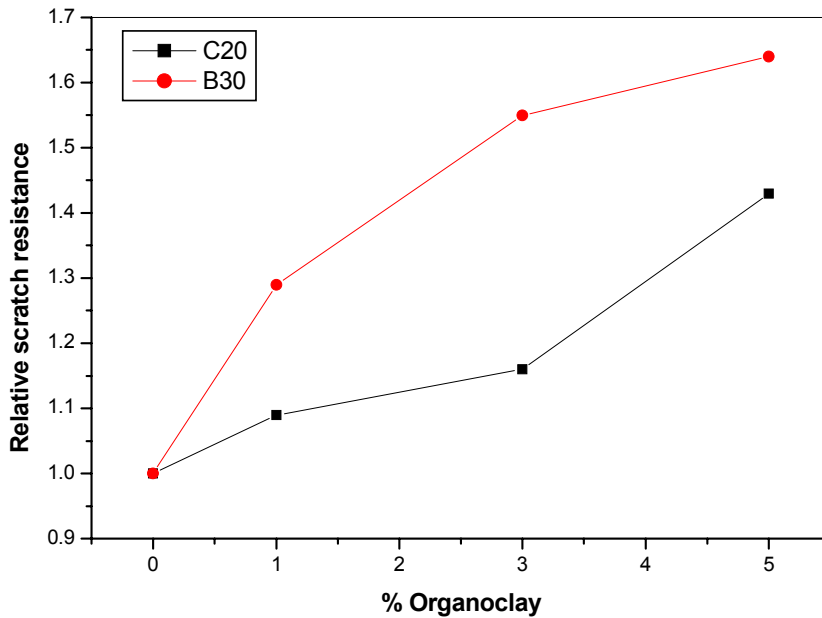


Figure 7.4: Relative scratch resistance as a function of organoclay concentration

The relative scratch resistance as a function of organoclay concentration is shown in Figure 7.4. Introduction of organoclay into the PU matrix increased in the surface hardness and enhanced the scratch resistance. Of the two types of PU nanocomposites, the exfoliated PU nanocomposites one had greater hardness and showed better scratch resistance. Generally speaking, two factors are principally responsible for the enhancement effect of the addition of organoclay to polymer. The first factor is dispersion or high aspect ratio nanoclay platelets, which usually results a remarkable increase in hardness and modulus of materials, as observed here. The second factor is exfoliation of organoclay. When the clay layers are completely and uniformly dispersed in a continuous polymer matrix, an exfoliated or delaminated structure is obtained as demonstrated by WAXD (see Figures 4.11 and 4.12). This structure makes the entire surface of clay layers available for the polymer and maximizes polymer-clay interactions. In such an environment, it leads to a dramatic increase in the interfacial bonding between the polymer matrix and the reinforcement [11, 12]. In nanoscratch tests, an indenter slides along the subsurface of the film where a number of clay platelets oppose to the indenter's movement. As between the two types of PU nanocomposites, with the same organoclay content, exfoliated PU nanocomposites have the larger number of clay platelets in the subsurface. The larger number of exfoliated organoclay in the matrix influences their surface's resistance to scratching. For surface protect, it is believed that exfoliated organoclay/PU nanocomposites are better than intercalated ones.

7.3 Polyurethane GO nanocomposite

7.3.1 Scratch depth profile

In the nanoscratch test, the scratch depth of the indenter in the sample was recorded along with the scratch length at a certain scratch rate, which reflects the ability of the surface coatings for the substrates. Figures 7.5 and 7.6 show the scratch depth profiles of the PU and its nanocomposites with 1wt% and 4wt% of GO against the scratch length. At a scratch rate of 3 $\mu\text{m/s}$ (Figure 7.5), the curve of the PU reveals that the scratch depth completely achieved a maximum value just after 40 μm of the scratch

length. However, incorporation with GO the maximum depth was delayed until 100 μm . Figure 7.5 (inlet) shows that at 40 μm of scratches, the scratch depth profiles of PU were reduced 37% for incorporation with 1wt% of GO (3501 nm to 2194 nm) and 51% for 4wt% of GO (to 1708 nm), respectively. Meanwhile, at a scratch rate of 5 $\mu\text{m/s}$ they seems to give a significant amount of scratch depth reduction as shown in Figure 7.6 (inlet). The incorporation of 1wt% of GO in the PU matrix resulted in nearly 21% (2666nm to 2099nm) reduction in scratch depths. For 4wt% of GO, such effect is apparent with a large reduction in scratch depth with 73% from 2666nm to 712nm. It is clear that an increase in the concentration of GO, the scratch resistance was dramatically improved. The improvement in PU-GO nanocomposites at higher concentration could be attributed through the strong interaction between GO and the PU matrix due to the chemical crosslinker for isocyanate-terminated PU by GO [13]. This phenomenon makes the PU/GO composites show strong potential in protecting metallic surface, such as airplanes and wind turbines.

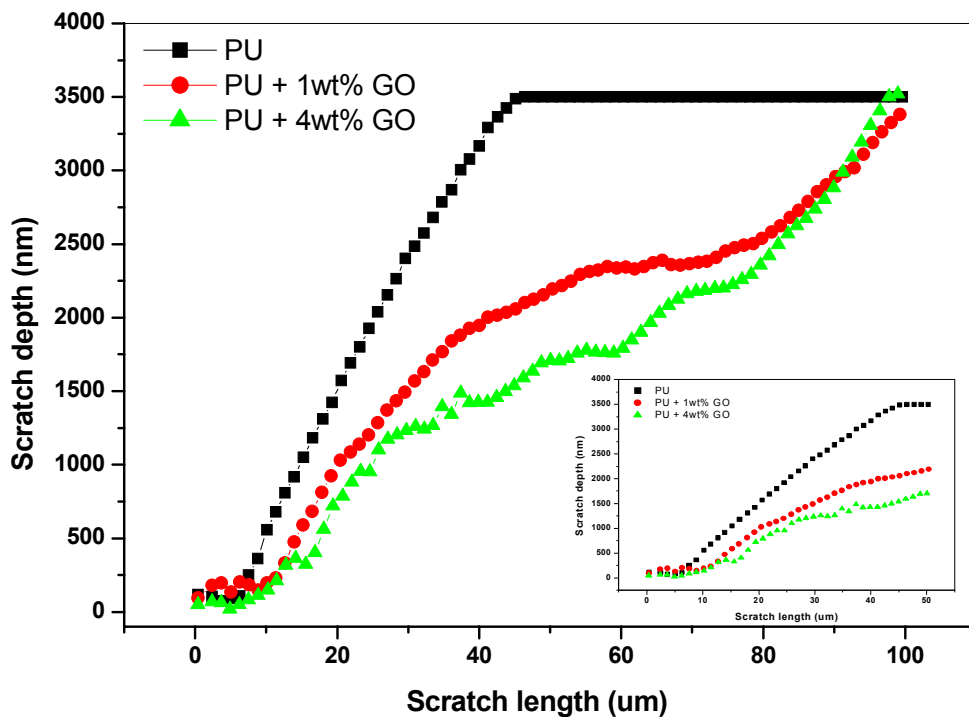


Figure 7.5: Nanoscratch depth profiles for PU and its GO nanocomposites at 3 $\mu\text{m/s}$

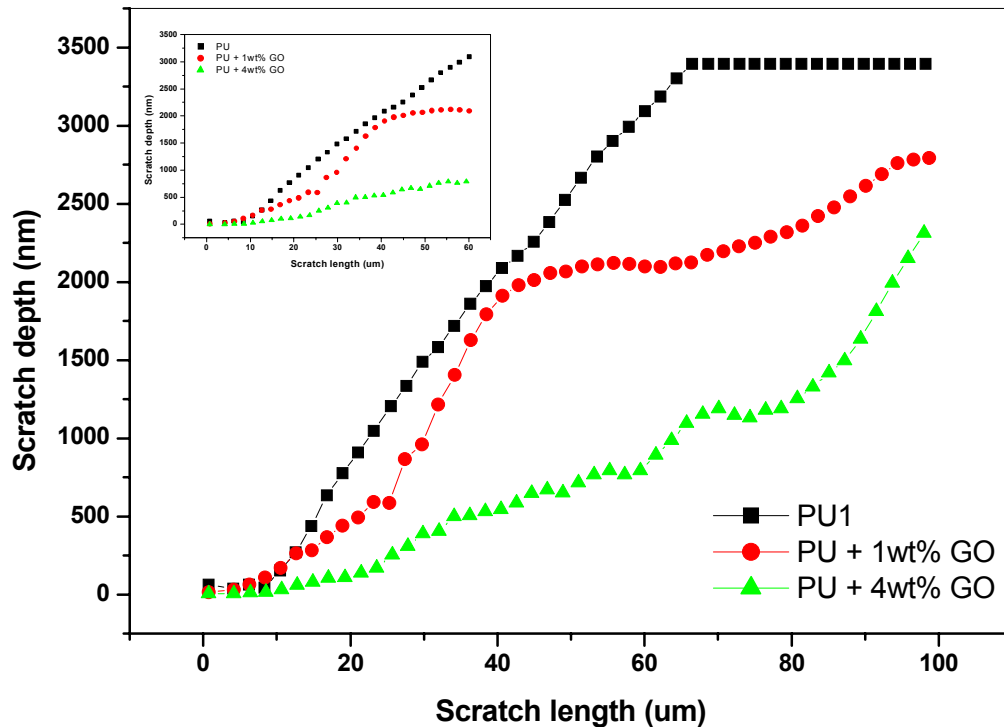


Figure 7.6: Nanoscratch depth profiles for PU and its GO nanocomposites at 5 μm/s

7.3.2 Relative scratch resistance

The relative scratch resistance as a function of GO concentration is shown in Figure 7.7. Introduction of GO into the PU matrix increased in the surface hardness and enhanced the scratch resistance. Figure 7.7 shows that with only 4wt% of GO the PU nanocomposites had greater hardness and showed better scratch resistance. Generally speaking, the main factor principally responsible for the enhancement effect of the addition of GO to polymer is the reduction in the phase separation of the PU matrix. The reduction of the phase separation caused by the GO is the function as a chemical cross-linker for isocyanate-terminated PU. The second factor is exfoliation of GO in the PU matrix. When the GO are completely and uniformly dispersed in a continuous polymer matrix, an exfoliated or delaminated structure was obtained demonstrated by TEM and SEM images in Figure 7.8 [13]. This structure makes the entire surface of GO available for the polymer and maximizes polymer-GO interactions.

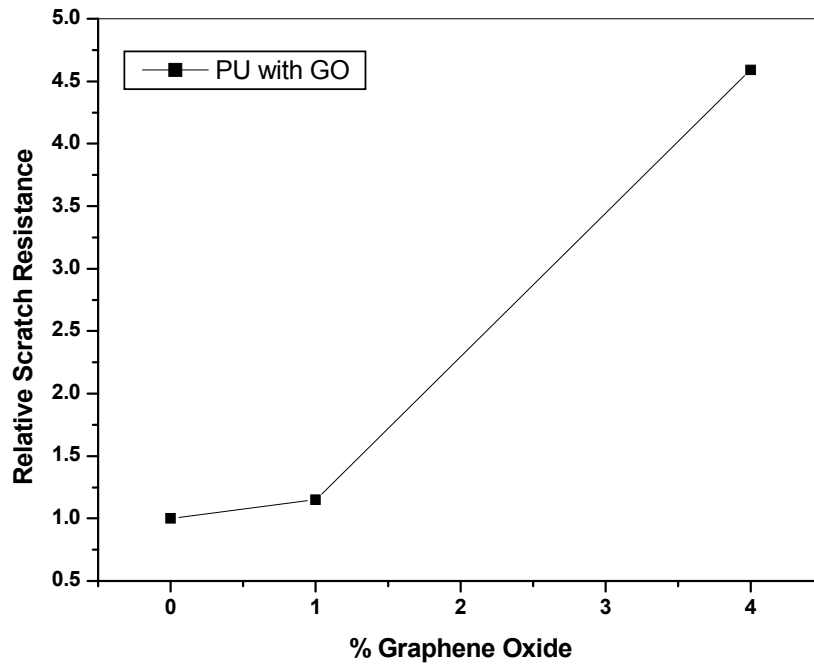
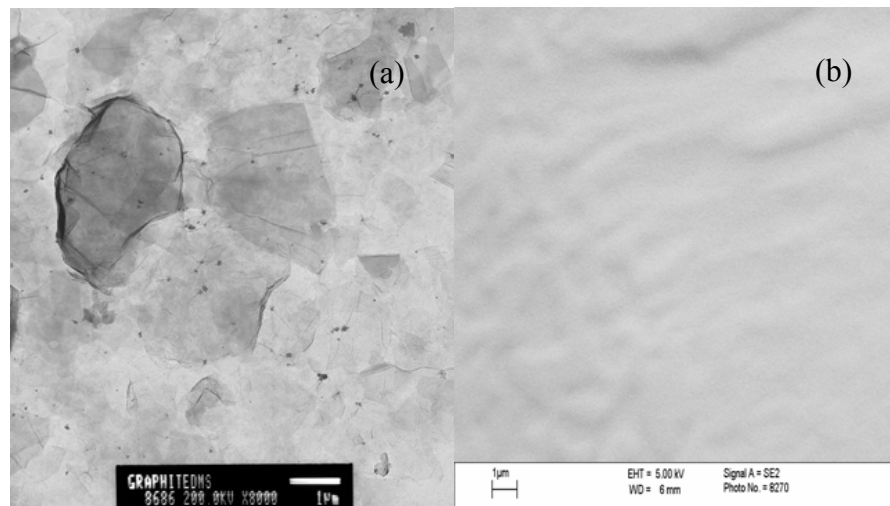


Figure 7.7: Relative scratch resistance as a function of GO concentration



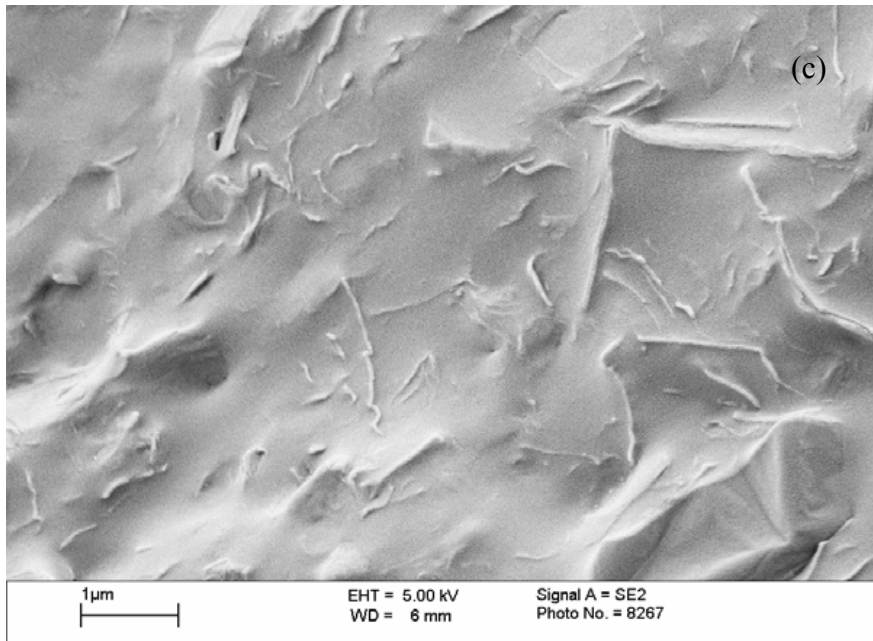


Figure 7.8: (a) TEM image of the GO/DMF dispersion; (b) SEM image of the PU; (c) SEM images of 4wt% GO/PU composite

7.4 Polyurethane CNT nanocomposites

7.4.1 Scratch depth profile

On the basis of their remarkable mechanical properties of carbon nanotubes (CNTs), the wide applications of CNTs in many engineering materials have been proposed. From tiny electronic devices to higher performance structures for aerospace industry, the applications of CNTs are widely accepted in many industrial applications. The combination of high aspect ratio, small size, very low density, and more importantly, excellent physical properties make them a perfect candidate to improve the polymer nanocomposites with new high performance materials [14,15,16]. The extensive development and use of polymer thin films in the hard coatings industry has stimulated the development of polymer nanocomposites in order to improve the scratch and wear resistance of neat polymer coatings in wide range of applications such as automobile industry, aerospace and decorative purposes.

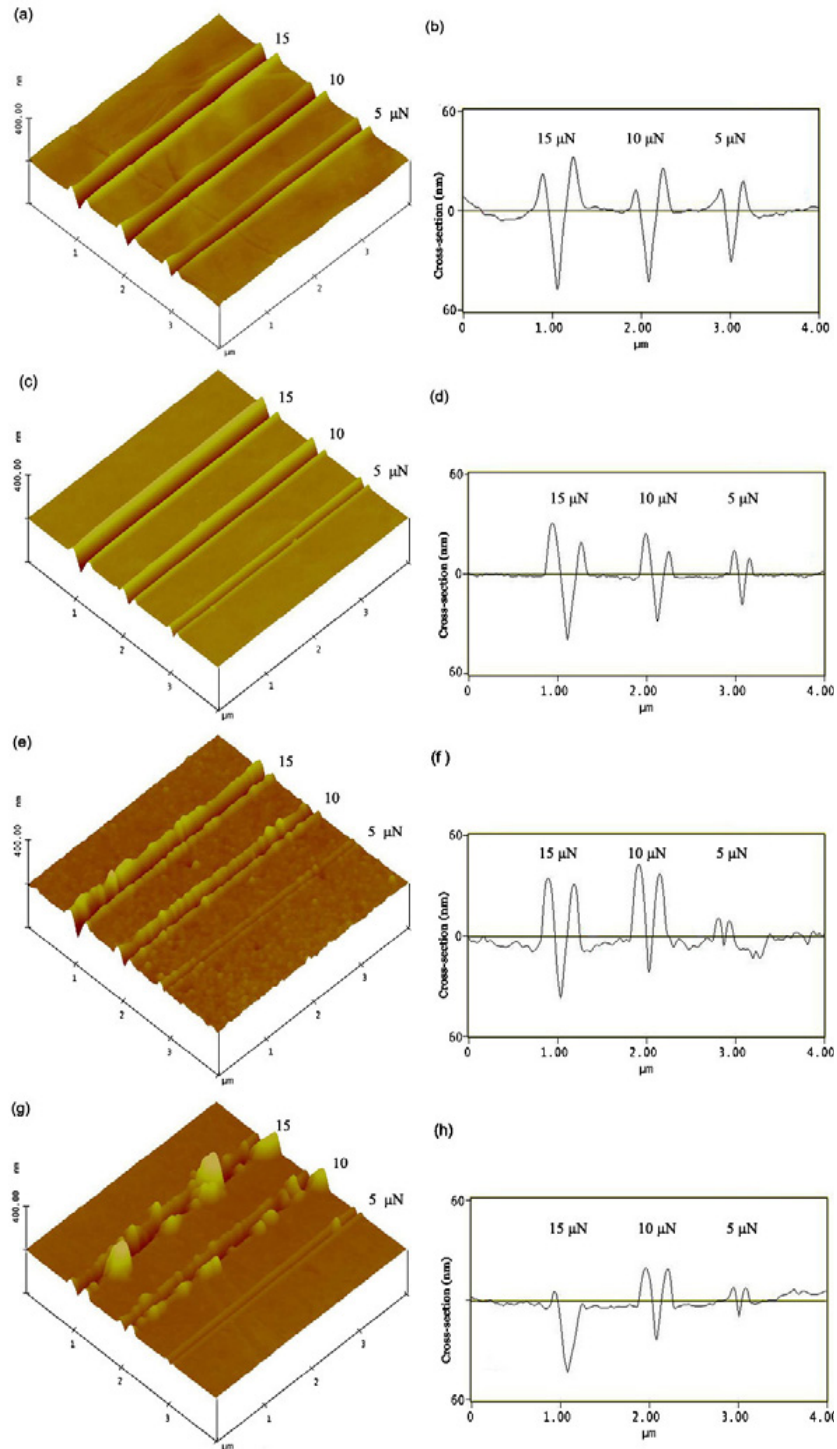
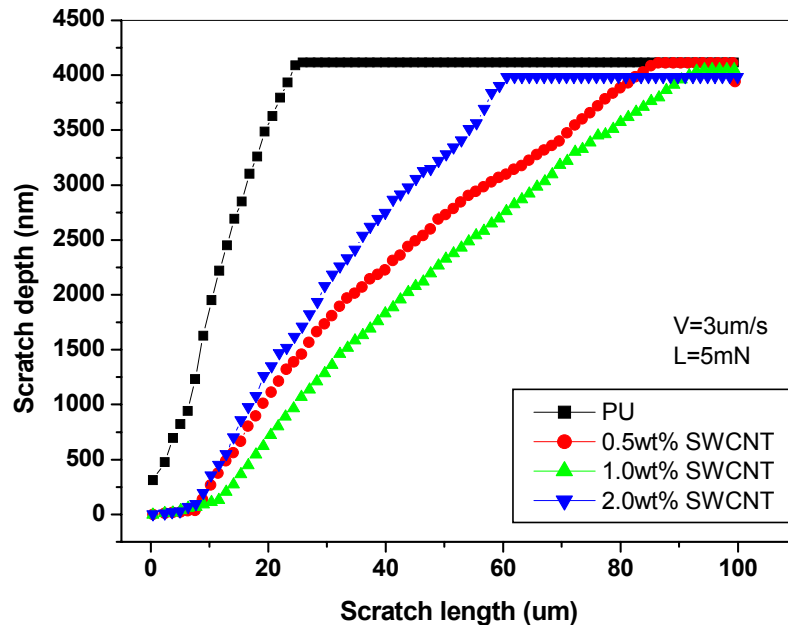


Figure 7.9: AFM images and cross-sectional high profiles of scratches made at various normal loads on the epoxy and its SWCNT reinforced samples: (a) and (b) pure epoxy; (c) and (d) 1 wt% SWCNT; (e) and (f) 3 wt% SWCNT; and (g) and (h) 5 wt% SWCNT [17]

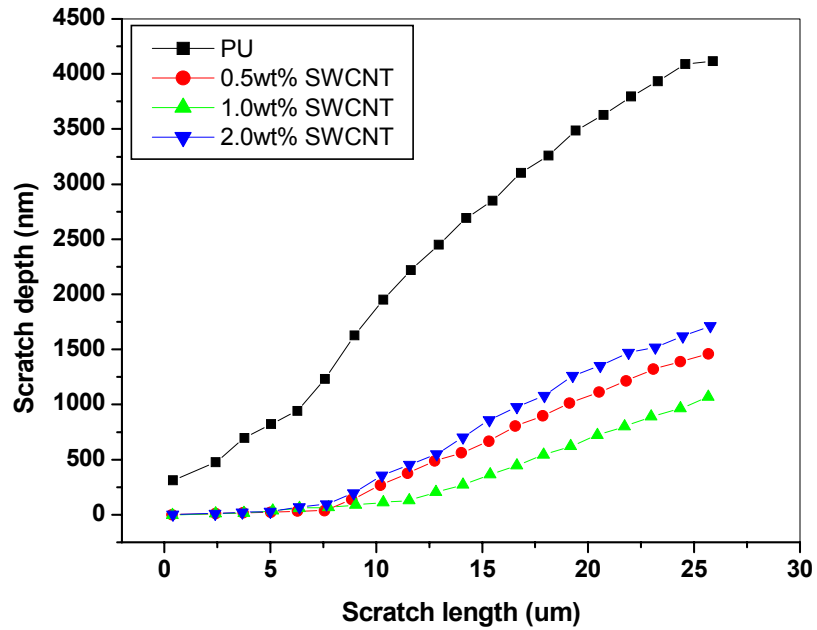
In a study on scratch profiles in epoxy CNT nanocomposites [17], it was shown that when SWCNT fillers were added, the scratch depth was became shallower as the weight percentage of nanotubes increased as shown in Figure 7.9. Besides that, AFM micrographs of scratched surfaces have also shown major differences between neat epoxy and SWCNT nanocomposite in term of crack and debris particles inside of the scratch tracks suggesting poor surface integrity of the neat epoxy. In recent study on the nanoscratch of polyamide 66/CNT nanocomposites, the authors indicated that the resistance to scratch penetration increases in the presence of finely dispersed CNTs even at a low weight percentage [18].

In the present research, two different polyurethane CNT nanocomposites were studied. Typical scratch depth profiles for PU and different CNT loadings are given in Figures 7.10 - 7.13. As expected, the scratch penetration for the PU with SWCNTs exhibited greater resistance to nanoscratch as evident from the depth profiles at all percentages of nanotubes as compared to MWCNTs. It can be seen that the scratch depth dramatically reduced with increasing the loading level of the nanotubes until 1wt%, as presented in Figures 7.10 – 7.11. In contrast, with 2wt% of SWCNT, the scratch resistance was slightly lower as compared to 0.5wt% and 1wt% counterparts. For PU-SWCNT, the addition of 1wt% of nanotube at 3 μ m/s showed a strong impact on scratch resistance and it was lower nearly 3000nm of scratch depth as compared to pure PU after 25 μ m of scratching. Similar phenomena with PU-MWCNT, at 1wt% of MWCNT the scratch depth was lowered almost 2800nm as compared to pure PU. In addition, the scratch penetration was less for PU-SWCNT composites than for the PU-MWCNT composites and it demonstrated as the time to achieve the maximum depth increased. This is consistent with PU-SWCNT composites being highly filler dispersion compare to the PU-MWCNT. Thus the higher modulus/hardness/weight % of nanofiller composites results in lesser depth of penetration among the PU-CNT samples.

The use of high velocity of scratch speed gives slightly reduction in depth penetration on the polymer scratch in all cases, as expected. The influence of the use of different scratch velocities is more striking for PU-MWCNT and PU-SWCNT as shown in Figure 7.12 and 7.13, respectively. A change of this speed from $3\mu\text{m/s}$ to $5\mu\text{m/s}$, each translates to a lesser amount of depth penetration. For PU-MWCNT, such effect is apparent with a large reduction in penetration as the maximum depth took a long time to achieve. For 1wt% of MWCNT at $5\mu\text{m/s}$, after $100\mu\text{m}$ of scratching, the penetration still not achieve the maximum depth as compared to 1wt% of MWCNT at $3\mu\text{m/s}$ which is need only $65\mu\text{m}$ of scratching to reach the maximum depth.

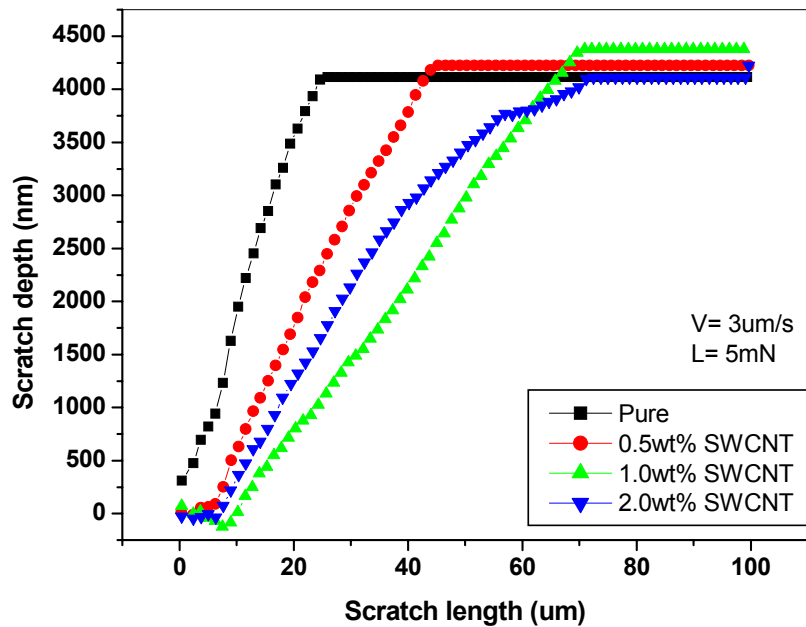


(a)

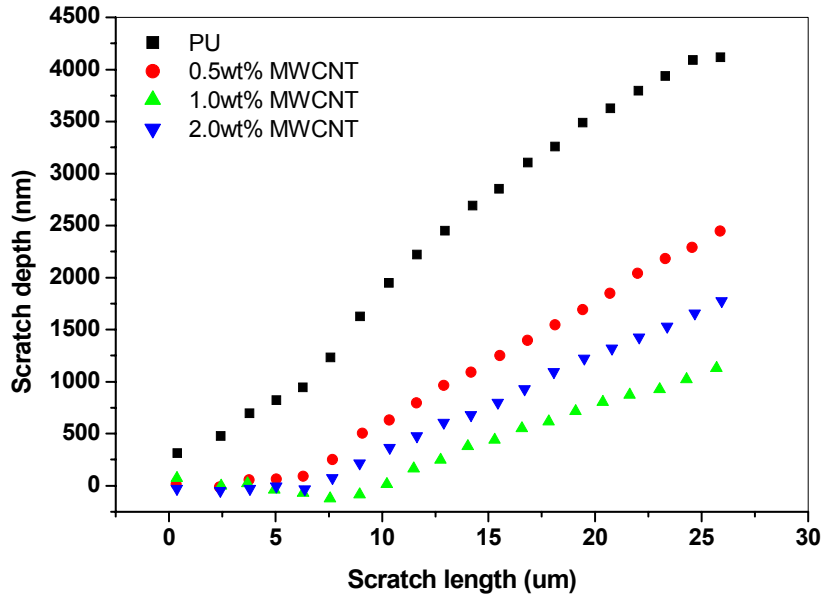


(b)

Figure 7.10: Nanoscratch depth profiles for PU and its SWCNT nanocomposites at 3 μm/s. (a) After 100 μm and (b) After 25 μm of scratch length

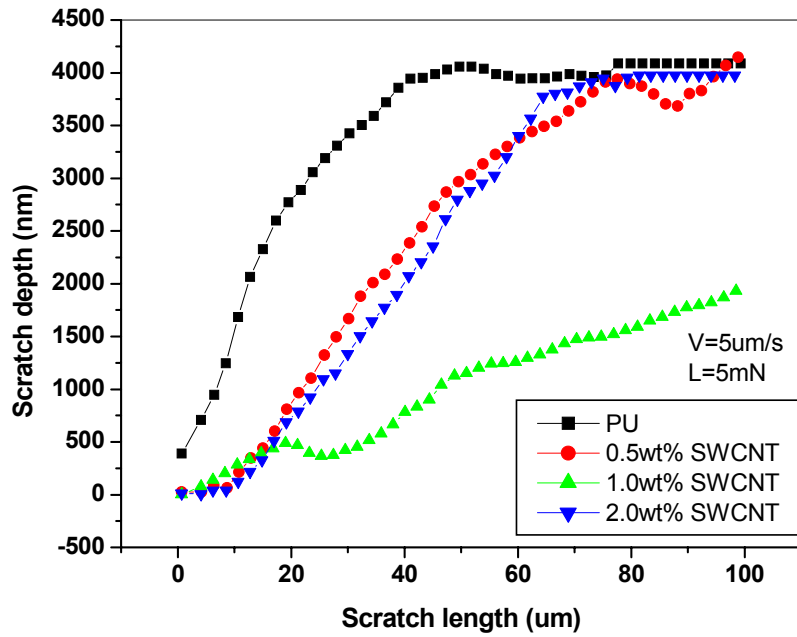


(a)

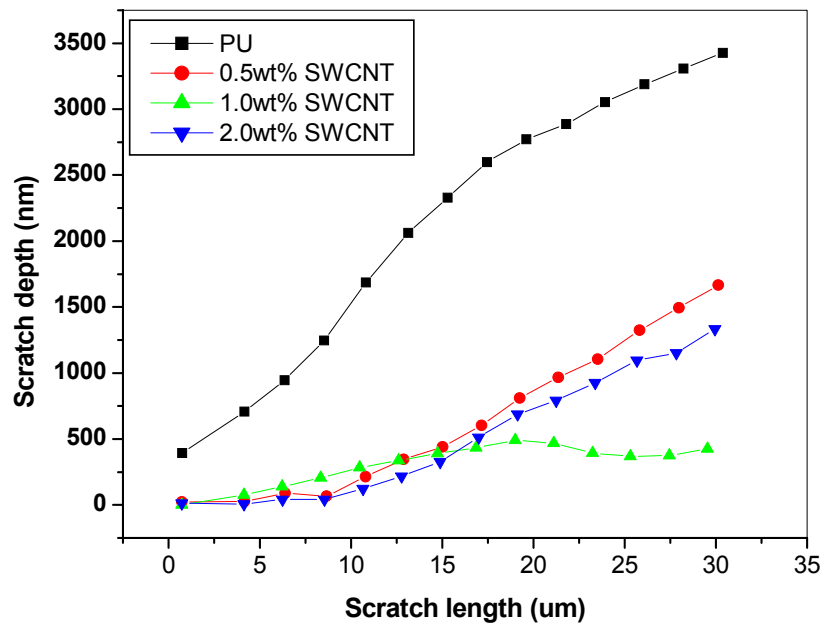


(b)

Figure 7.11: Nanoscratch depth profiles for PU and its MWCNT nanocomposites at 3 μm/s. (a) After 100 μm and (b) After 25 μm of scratch length

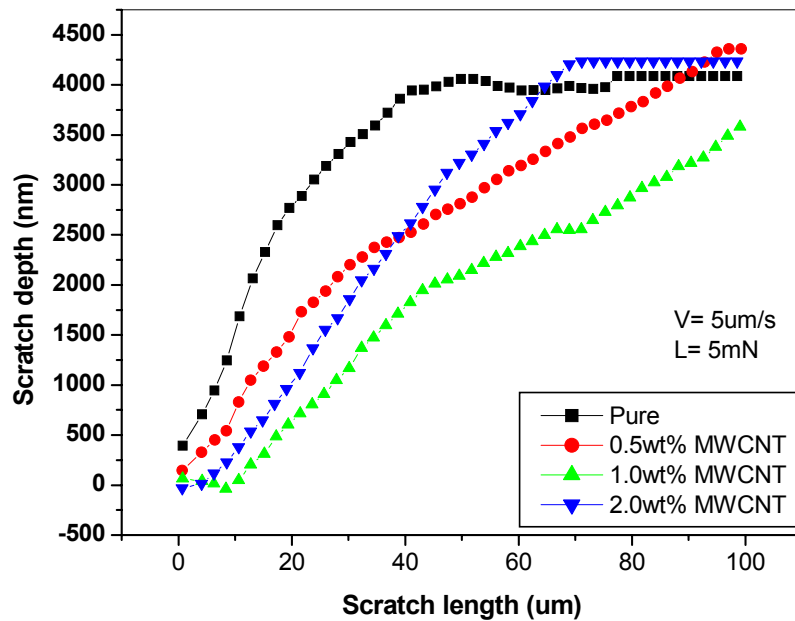


(a)



(b)

Figure 7.12: Nanoscratch depth profiles for PU and its SWCNT nanocomposites at 5 $\mu\text{m/s}$. (a) After 100 μm and (b) After 30 μm of scratch length



(a)

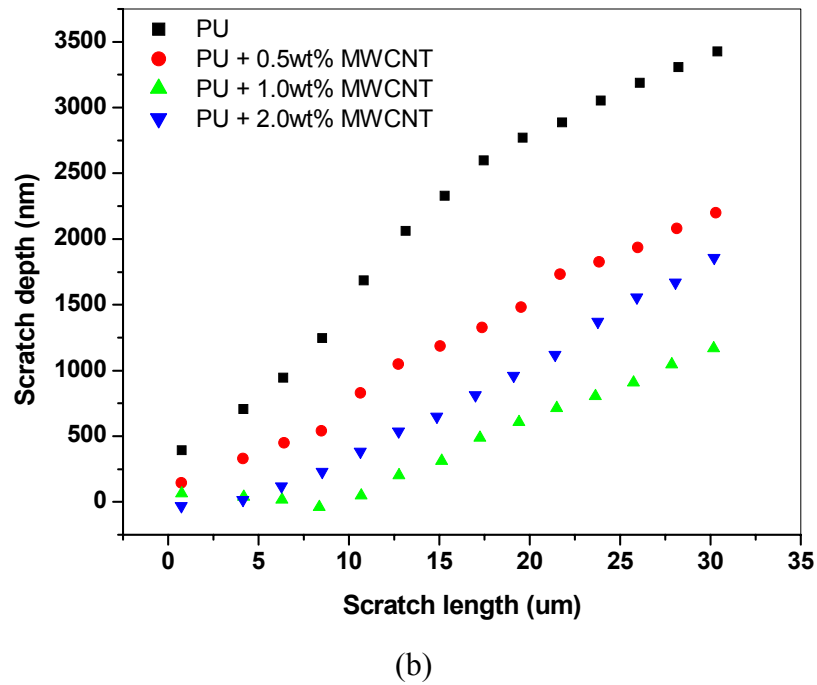


Figure 7.13: Nanoscratch depth profiles for PU and its MWCNT nanocomposites at 5 $\mu\text{m/s}$. (a) After 100 μm and (b) After 30 μm of scratch length

7.4.2 Relative scratch resistance

The relative scratch resistance as a function of CNT concentrations is shown in Figure 7.14. Introduction of CNT into the PU matrix increased in the surface hardness and enhanced the scratch resistance. Figure 7.14 shows that with only 1wt% of SWCNT in the PU the scratch resistance increased by more than 1.6 fold as compared to pure PU. Meanwhile with 1wt% of MWNT, the relative scratch resistance moderately increased and it was approximately by 0.6 fold as compared to the pure PU. As shown in scratch depth profile observation, the concentration of CNT more than 1wt% exhibits only a moderate improvement to the scratch resistant. There could be three main factors principally responsible for the enhancement: chemical bonding as contributed by homogeneous dispersion of CNTs in the PU matrix, nano-mechanical interlocking and non-bond interaction due to van der Waals and electrostatic forces [19]. Therefore, the combination of above three factors

contributes the strong interactions between CNTs and the PU matrix, thus strengthening the scratch performance of the composites. However, at high concentration, aggregation of CNTs occurs which could minimize the CNT and PU segment interactions.

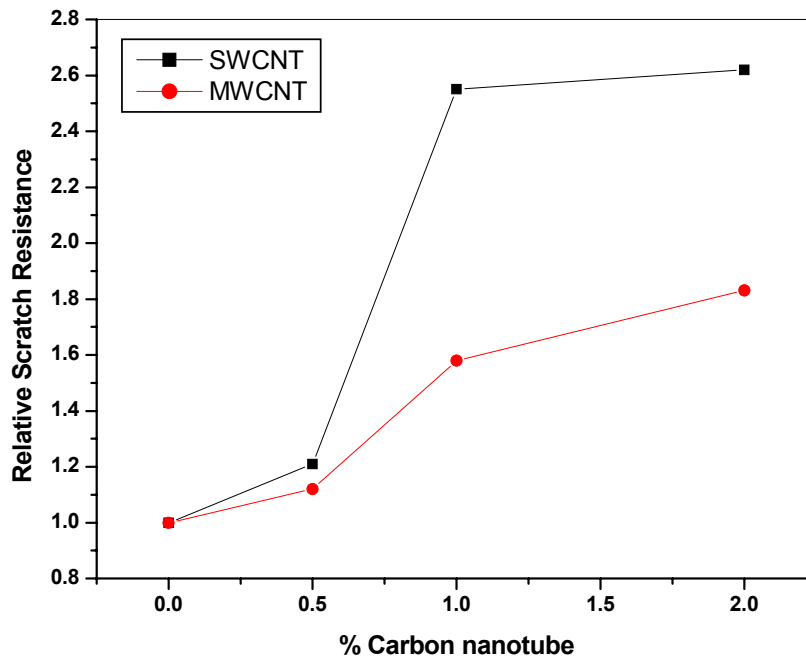


Figure 7.14: Relative scratch resistance as a function of SWCNT & MWCNT concentrations

7.5 Polyurethane with different hard segment contents

7.5.1 Scratch depth profile

Segmented PU is block copolymers with altering soft and hard blocks that, due to to structure differences, separate into two phases or domains. The degree of the hard segment phase plays a vital role in determining the solid-state properties of the multi-block coatings [20]. The hard domains serve as physical cross-link and act as high modulus fillers, whereas the soft phases provide extensibility [21-22]. The surface mechanical properties of pure PU prepared using different hard segment contents were also investigated. The scratch depth profiles with the different hard segment

contents of PU and different scratch velocities are shown in Figures 7.15 – 7.18. In Figure 7.15, with increasing the hard domain of PU, the scratch depths are dramatically reduced as the material shows strong dependent on the hard segments and become more resistant to scratching. As concentration of hard domain increased, the morphological of PU is changed from elastomer-like to semi-crystalline behaviour and this influences the performance of material to the scratch damages. The variation in microstructure and the effect on the surface mechanical behaviour of polymer especially in semi-crystalline material has been reported by Klapperich et al [23]. In addition, the increase in hard-segment is contributed by the increase of isocyanate ratio in PU. Generally, the increase in isocyanate ratio resulted in an increase of the crosslink density of PU. Thus, it is reduces the molecular mobility and restricts microphase separation [24]. At 25 μm of scratch length and 3 $\mu\text{m/s}$ in scratch velocity as shown in Figure 7.16, with increasing from 18% to 26%, 32% and 36% of the hard segment, the depth profiles were reduced from 3060 nm to 2620 nm (~440 nm), to 1773 nm (~1287nm) and to 821 nm (~2239nm), respectively. When increasing the velocity of the scratch, the PU surface is demonstrated very strong scratch resistance as shown in Figure 7.17 and the maximum depth delayed from 25 μm to 40 μm after initial start of scratch test. At 40 μm scratch length in Figure 7.18, the scratch depth was reduced from 3482 nm to 2279nm (for 26% hard segment), 1570nm (for 32% hard segment), and 638nm (36% hard segment), respectively. The effect of scratch velocity on the scratch behavior was discussed by Krupicka et al [25]. The main reason is due to the friction response which greatly reduced at the higher velocity of scratch. The decreasing in friction with increased velocity was suggested to be due to the reduction of plastic build-up in front of the scratch tips and thus, the resistance to penetration definitely improved.

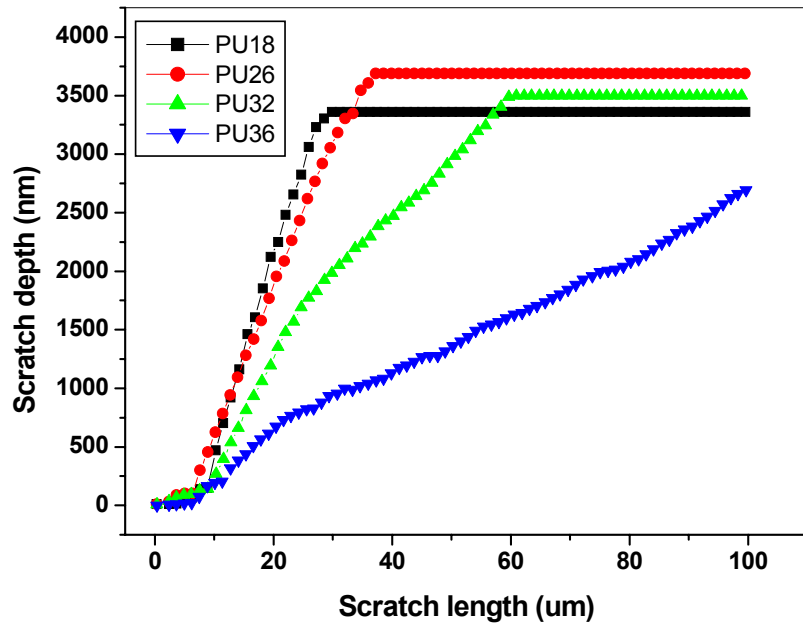


Figure 7.15: Nanoscratch depth profiles for PU with different hard segment contents at 3 μm/s

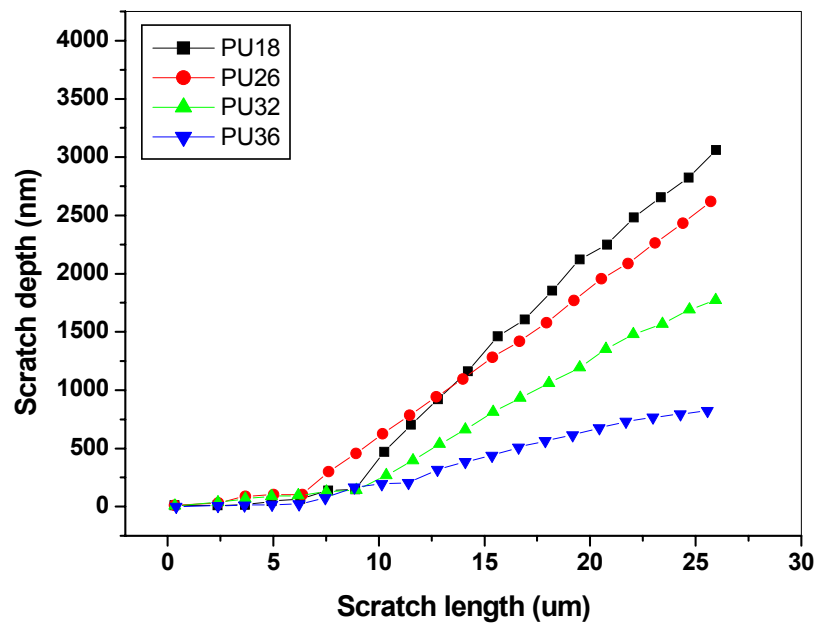


Figure 7.16: Nanoscratch depth profiles for PU with different hard segment contents at 3 μm/s after 25 μm scratch length

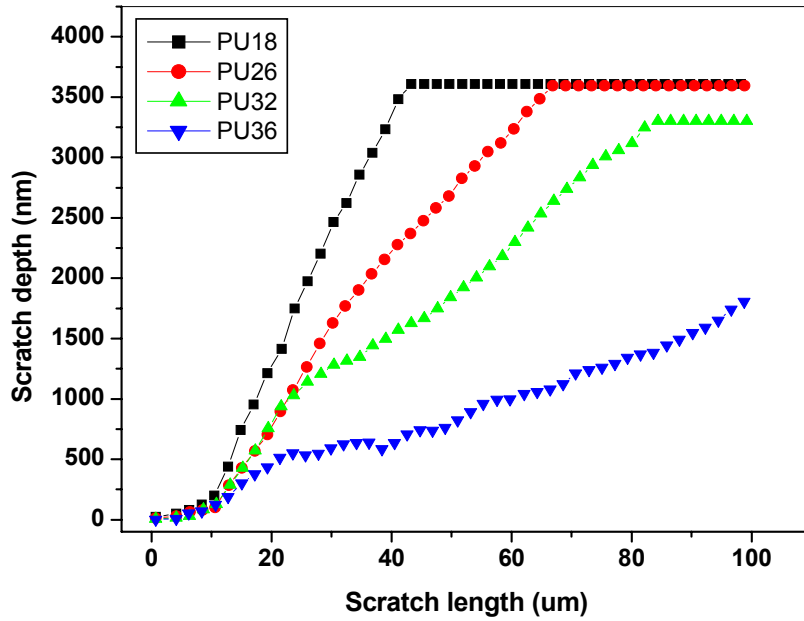


Figure 7.17: Nanoscratch depth profiles for PU with different hard segment contents at 5 μm/s

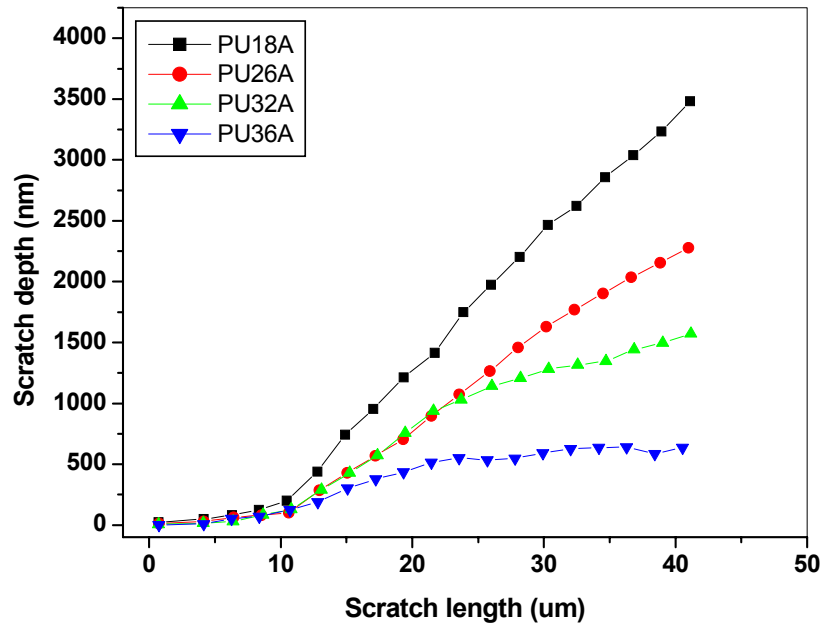


Figure 7.18: Nanoscratch depth profiles for PU with different hard segment contents at 5 μm/s after 40 μm scratch length

Conclusion

The scratch behaviour of polyurethane and its nanocomposites were studied. The scratch resistance exhibited a significant enhancement with incorporation of nanofillers by lowering the scratch depth as compared to the pure PU. Exfoliated PU nanocomposites showed greater improvement than intercalated counterpart in the PU clay nanocomposites. With 4wt% of GO, the scratch penetration of the PU shows a large reduction in depth with 73% from 2666nm to 712nm. It is clear that the addition of GO, the scratch resistance of the PU was dramatically improved. For PU-CNT nanocomposites, as expected, the scratch penetration exhibited greater resistance to nanoscratch as evident from the depth profiles at all percentages of SWCNTs compared to MWCNTs. It can be seen that the scratch depth dramatically reduced with only 1wt% of the loading level of the SWCNTs. The main reason could be due to the friction response which greatly reduced at the higher velocity of scratch. The decrease in friction with increased velocity was suggested to be a reason to the reduction of plastic build-up in front of the scratch tips and thus, the resistance to penetration definitely improved. With the study of different hard-segment content in PU, it can be said that the effect of nanofillers on the scratch behaviour of the PU is similar to increasing hard-segment content.

References

1. Wong, J.S.S., Sue, H.J., Zeng, K.Y., Li, R.K.Y., Mai, Y.W., *Act Mater.* 2004, 52, 431 – 443
2. Demirci, I., Gauthier, C., Schirrer, R., *Thin Solid Films*, 2005, 479, 207 - 215
3. Kajiyama, T., Tanaka, K., Takahara, A., *Macromolecules*, 1997, 30, 280
4. Brown, H.R., Russell, T.P., *Macromolecules*, 1996, 29, 798
5. Dasari, A., Yu, Z-Z., Mai, Y-W., *Act. Mat.* 2007, 55, 635 – 646

6. Kim, J.K., Sham, M.L., Wu, J.S., *Composites Part A*, 2001, 32A, 607
7. Dasari, A., Yu, Z-Z., Mai, Y-W., *Mater. Sci. Eng. R* 2009, 63, 31 – 80
8. Mathia, T.G., Lamy, B., *Wear*, 1986, 108, 385 – 399
9. Hutchings, I.M., *Tribology: Friction and Wear Engineering Materials*, Edward Arnold, London , 1992
10. Xia, J., Li, C.X., Dong, H., Bell, T., *J. Mater. Res.* 2004, 19, 291 – 299
11. LeBaron, P.C., Wang, Z., Pinnavaia, T.J., *Appl. Clay Sci.* 1999, 15, 11 – 19
12. Pinnavaia, T., Beall, G.W., (eds), *Polymer-Clay Nanocomposites*. Wiley, New York, 2000
13. Cai, D., Kamal, Y., Song, M., *Nanotechnology* 2009, 085712 (5pp)
14. Baughman, R.H., Zakhidov, A.A., de Heer, W.A., *Science* 2002, 297, 787 – 792
15. Ajayan, P.M., Schadler, L.S., Giannaris, S.C., Rubio, A., *Adv. Mater.* 2000, 12, 750 – 753
16. Schadler, L.S., Giannaris, S.C., Ajayan, P.M., *Appl. Phys. Lett.* 1998, 73, 3842 – 3844
17. Li, X., Gao, H., Scrivens, W.A., Fei, D., Xu, X., Sutton, M.A., Reynolds, A.P., Myrick, M.L., *Nanotechnology*, 2004, 15, 1416 – 1423
18. Dasari, A., Yu, Z-Z., Mai, Y-W., *Nanotechnology*, 2008, 19, 055708

19. Liao, K., Li, S., Appl. Phys. Lett. 2001, 79, 4225 – 4227
20. Cooper, S.L., Tobolsky, A.V., J Appl Polym Sci. 1996, 10, 1837 – 1844
21. Hepburn, C., Polymer Elastomers, 1982, London
22. Paul, P.J., Nair, M.G.R., Koshy, P., Idage, B.B., J Appl Polym Sci. 1999, 74, 706 – 721
23. Klapperich, C., Komvopoulos, K., Pruitt, L., ASME J. Tribol. 1999, 121, 394 – 402
24. Song, M., Hourston, D.J., Yao, K.J., Tay, J.K.H., Ansarifard, M.A., J. Appl. Polym. Sci. 2003, 90, 3239 – 3243
25. Krupička, A., Johansson, M., Hult, A., Prog Org Coat. 2003, 46, 32 – 48

Chapter 8

Conclusion & Future Work

8.1 Conclusion

Polymer nanocomposite has been a topic of interest in recent years due to their significant improvement in mechanical, thermal and barrier properties. However, in evaluating their properties, a precise device should be considered in order to obtain and understand the mechanical properties of polymer nanocomposite films or coatings. In the recent years, nanoindentation has been established as a standard method for probing mechanical properties of metal at submicron length scale and the application is increasingly being applied to polymeric materials. In this research, the mechanical properties of polyurethane nanocomposite films with three different types of nanofillers were studied by means of nanoindentation technique. Huge specific surface area of nanofillers dispersing in polymer matrix produces stronger interfacial interactions between the fillers and the polymer matrix. The interactions due to well dispersed nanofillers in the polymer matrix result in a significant improvement in the surface properties of polymer nanocomposites compared to the neat polymer.

The understanding of rheological behaviour of polyol/clay dispersion is essential in order to produce well dispersed nanofiller in the polyurethane matrix. The experiment results suggested that the interactions between polyol and clay either exfoliated or intercalated were occurred and influenced by the type of polyols, shearing rate and also the mixing temperature. The trifunctional polyol with 6000 produced a well dispersed mixture. With B30 clay, an exfoliated system was successfully prepared. The relationship between rheological data (flow behaviour index) for polyol/clay dispersions and the intercalated or exfoliated state of clay was established. A possible exfoliation mechanism was proposed. It was believed that the exfoliation of platelets could be achieved through a combination of molecular diffusivity, destabilization of clay layers, and the external and internal forces. For the CNT systems, the results indicated that the polyol/MWCNT

mixture produced a lower shear thinning behaviour compared to polyol/SWCNT mixture. Thus, the better dispersion was predicted using Herskel Bulkley model. In situ polymerisation is one of the methods for preparation of polymer nanocomposite. The viscosity study during the first stage of this process which is the mixing of polymer precursor or monomer and nanofiller is very crucial and the rheological data for polyol/clay and polyol/CNT dispersion is a good indicator of achieving the well dispersed nanofillers in the polyurethane. This could provide a convenient and efficient way to evaluate the final state of dispersion.

Surface mechanical properties of the PU nanocomposite films with three different nanofillers were evaluated by mean of nanoindentation. In the PU clay nanocomposites, the hardness and elastic modulus of PU significantly increased with increasing organoclay content. The improvement in these properties was determined by two factors: content of clay and formation structure of clay in the PU matrix. Exfoliated PU nanocomposites showed greater improvement than intercalated PU nanocomposites. For PU-Graphite oxide (GO) nanocomposites, incorporation of GO into PU matrix leads to a significant increase in hardness and modulus due to the physical crosslinks and chemical bonding. In PU-CNT nanocomposites, the advantages and uniqueness of using CNTs as reinforcing nanofillers to make PU nanocomposites are obvious especially in SWCNTs. Both the hardness and the modulus properties were improved. The study also suggested that the loading rate and the holding time are a crucial role in producing a good result of the hardness and the modulus in indentation test.

The bulk and subsurface creep behaviour of PU-organoclays was studied by conventional and indentation techniques. Indentation creep test at room temperature revealed an enhanced creep resistance of the subsurface of the PU nanocomposite films with addition of C20 and B30 organoclays. Meanwhile, for bulk properties of PU nanocomposites the increment in creep resistance obviously occurred in the exfoliated systems. However, with a higher percentage of the

organoclay in the intercalated systems, the significant increase in creep resistance also can be achieved. The exfoliated PU nanocomposites showed greater improvement than the intercalated PU nanocomposites. The study demonstrated that the creep resistance of the PU nanocomposites were greatly improved. In PU-GO nanocomposites, the presence of GO in the composites could offer resistance for the creep by introduction of good mechanical interlocking and the presence of obstacles to the motion of the matrix chains. It is noticed that the creep deformation (creep strain) of the PU matrix decreased with the incorporation of GO. As GO content increased to 4wt%, the creep resistance was only slightly improved. After 70s of creep time, the creep strain of 1wt% and 4wt% of GO were reduced to 236nm and 257nm, respectively. The increase in the creep resistance was contributed by the interaction of the PU matrix with GO. This could be the reason for the enhancement in creep strain in the PU-GO nanocomposites. In PU-CNT nanocomposites, the creep strain was reduced with increasing the weight percentage of CNTs in both SWCNT and MWCNT systems. This discrepancy can be explained by considering the possibility of aggregation of CNTs that always impair the performance of nanocomposites i.e reduced the shear stress between CNTs and the polyurethane matrix after passing of certain amount in concentrations. This indicates that the full beneficial effects of CNTs in the reduction of creep deformation should be optimising with the weight percentage of CNTs.

The scratch behaviour of the PU and its nanocomposite films was studied. The scratch resistances in all PU nanocomposites exhibited a good enhancement with the incorporation of nanofillers compared to the PU. Exfoliated clay/PU nanocomposites showed greater improvement than intercalated clay/PU nanocomposites. For the PU / GO (4wt%) nanocomposite, the scratch penetration showed a large reduction in depth by 73% from 2666nm to 712nm. It is clear that the addition of GO, the scratch resistance of PU was dramatically improved. For PU-CNT nanocomposites, as expected, the scratch penetration for the PU with SWCNTs exhibited greater resistance to nanoscratch as evident from the depth

profiles at all percentages of SWCNTs compared to MWCNTs. The scratch depth dramatically reduced with only 1wt% CNTs and the scratch velocity also affected the scratch behaviour. The main reason could be due to the friction response which greatly reduced at the higher velocity of scratch. The effect of adding nanofillers on the scratch behaviour of polyurethane is similar to increase in the hard-segment content in the PU matrix.

8.2 Future works

The polyurethane nanocomposites have been successfully prepared by in situ polymerization and the mechanical properties of these materials were investigated. Following the investigations described in this thesis, there are things that could be considered in the future.

1. It would be interesting to obtain the results under dynamical conditions in indentation experiments with temperature.
2. In order to understand the relationship of scratch resistance with hardness and modulus, it could be useful if the scratch damage images of soft materials can be obtained.
3. Indentation scratch model could be developed for understanding the scratch behaviour of polymer materials.

List of Publications

1. K. Yusoh, J.Jin, M.Song, *Subsurface mechanical properties of polyurethane/ organoclay nanocomposite thin films studied by nanoindentation*, **Prog. Org. Coat.** 2010, 67, 220 – 224
2. D. Cai, K. Yusoh, M. Song, *The mechanical properties and morphology of a graphite oxide nanoplatelet/polyurethane composites*, **Nanotechnology**, 2009, 20, 085712
3. K.Yusoh, M.Song, *Bulk and subsurface behaviour of polyurethane/organoclay nanocomposites*, **In progress**